ISBN 978-82-471-1430-8 (printed ver.)
ISBN 978-82-471-1431-5 (electronic ver.)
ISSN 1503-8181

Doctoral theses at NTNU, 2009:31

Kristine Nore

Hygrothermal performance of ventilated wooden cladding

Kristine Nore

Doctoral Thesis

NTNU
Norwegian University of
Science and Technology

NTNU
Norwegian University of
Science and Technology
Thesis for the degree of
philosophiae doctor
Faculty of Engineering Science and Technology
Department of Civil and Transport Engineering

Doctoral theses at NTNU, 2009:31

NTNU

NTNU
Norwegian University of
Science and Technology

Kristine Nore

Hygrothermal performance of ventilated wooden cladding

Thesis for the degree of philosophiae doctor

Trondheim, October 2009

Norwegian University of
Science and Technology
Faculty of Engineering Science and Technology
Department of Civil and Transport Engineering

NTNU
Norwegian University of
Science and Technology

NTNU
Norwegian University of Science and Technology

Thesis for the degree of philosophiae doctor

Faculty of Engineering Science and Technology
Department of Civil and Transport Engineering

ISBN 978-82-471-1430-8 (printed ver.)
ISBN 978-82-471-1431-5 (electronic ver.)
ISSN 1503-8181

Doctoral Theses at NTNU, 2009:31

Printed by Tapir Uttrykk

Hygrothermal performance of ventilated wooden cladding

Kristine Nore

Thesis submitted in partial fulfilment of the degree of Philosophiae Doctor (PhD) in Civil and Transport Engineering at the Faculty of Engineering Science and Technology, Department of Civil and Transport Engineering, Norwegian University of Science and Technology (NTNU)

Contact information:
Norwegian University of Science and Technology (NTNU)
Department of Civil and Transport Engineering
Høgskoleringen 7A, NO-7491 Trondheim, Norway
Telephone +47 73 59 46 40

Or

SINTEF Building and Infrastructure
NO-7465 Trondheim, Norway
Telephone +47 73 59 30 00

kristine.nore@gmail.com

ISBN Printed version: 978-82-471-1430-8
ISBN Electronic version: 978-82-471-1431-5

ISSN Doctoral thesis at NTNU 2009:31

Printed by Tapir Uttrykk, Trondheim, Norway 2009.

This PhD study has been carried out within the SINTEF research & development programme
"Climate 2000 – Building constructions in a more severe climate" (2000-2007)

http://tjenester.byggforsk.no/prosjekter/klima2000
www.sintef.no/byggforsk

To Lars, Kari & Helten

Acknowledgements

Doing a PhD has an analogy to the growth of high quality cladding wood. The roots must be placed in a medium providing the proper nutrition and water supply. As a juvenile one should stand sheltered below a screen of taller and stronger models. Organisms using photosynthesis grow into positions with the most light, but doing this requires strength and ingenuity. Wood grown at a high altitude becomes too brittle for construction purposes, but shows the increased durability as a cladding material. As a PhD research fellow at SINTEF Building and Infrastructure and Norwegian University of Science and Technology (NTNU) I am sincerely grateful for having been included in the team of building physicists. Their wisdom has provided an educational foundation and good growing conditions. I am especially grateful for the opportunity to go abroad and be enlightened by fellow building physics researchers. Now I am proud to deliver this thesis and present the building physical research challenges of ventilated wooden claddings.

This PhD study has been carried out within the SINTEF research & development programme "Climate 2000 – Building constructions in a more severe climate" (2000-2007), strategic institute project "Impact of climate change on the built environment". I gratefully acknowledge all construction industry partners and the Research Council of Norway (NFR reference no. 154002). Gratitude is also given to all my senior colleagues Terje, Kim, Tore, Einar and especially Berit who have kindly introduced me to the challenges of working life. Special thanks are given to Kathinka who always had time for editing and a talk, and to Egil, thanks for having your top floor available both physically and mentally. Life would be a lot harder without colleagues like you.

In the course of my study I enjoyed half a year abroad. Three months was at the Fraunhofer Institute for Building Physics (IBP) in Holzkrichen, Germany, especially thanks to Andreas Holm, Wolfgang Zillig and Kristin Lengsfeld. The interesting stay gave me a peek into the WUFI development. Not only did this stay lead to considerable professional growth; the charming co-workers and beautiful surroundings made the winter and spring of 2005 seem heavenly. In 2006, I was fortunate to be allowed to work in the Laboratory of Building Physics at Katholieke Universiteit Leuven, Belgium thanks to Professor Jan Carmeliet. This work intensive but pleasant environment provided some valuable insights into building physics research. Making the acquaintance of Professor Bert Blocken has been a key factor in my motivation. I have also had the pleasure of visiting Professor Carsten Rode at the Department of Civil Engineering, Technical University of Denmark.

I wish to thank my supervisor professor Jan Vincent Thue at the Department of Civil and Transport Engineering, NTNU for his invaluable assistance. He has provided room and direction for my individual growth. His guidance has been exceptional. I would also like to thank my co-supervisor Stig Geving at SINTEF Building and Infrastructure. I am also grateful for the assistance from Stewart Clark, senior adviser at NTNU for editing the main part of this thesis.

My Trondheim cohabitant, Alex has not only provided shelter but also coached me throughout in my writing process. I am profoundly grateful for your shielding and educational efforts. The people at the business garden in the Valley of Artists, where I have done most of my writing, have provided encouragement. Also thanks to TUKK, our work has increased my energy level. My family and friends have also contributed to have this PhD becoming one piece, with technical guidance, revision and child caring. Thank you for believing in me. Also, to our lost carpenter of Court, Ilstad, without you I would never have chosen the field of building physics. My family is my foundation. Thank you, Lars and Kari for being the joy of life and Jon Andreas for taking care of everything while I have been lost in my PhD. *Sono il suo schiavo!*

Oset, 25.10 2009

Kristine Nore

Summary

This PhD project contributes to more accurate design guidelines for high-performance building envelopes by analysis of hygrothermal performance of ventilated wooden cladding. Hygrothermal performance is defined by cladding temperature and moisture conditions, and subsequently by risk of degradation. Wood cladding is the most common façade material used in rural and residential areas in Norway. Historically, wooden cladding design varied in different regions in Norway. This was due to both climatic variations and the logistical distance to materials and craftspeople. The rebuilding of Norwegian houses in the 1950s followed central guidelines where local climate adaptation was often not evaluated. Nowadays we find some technical solutions that do not withstand all climate exposures. The demand for thermal comfort and also energy savings has changed hygrothermal condition of the building envelopes. In well-insulated wall assemblies, the cladding temperature is lower compared to traditional walls. Thus the drying out potential is smaller, and the risk of decay may be higher. The climate change scenario indicates a warmer and wetter future in Norway. Future buildings should be designed to endure harsher climate exposure than at present. Is there a need for refined climate differentiated design guidelines for building enclosures?

As part of the Norwegian research programme “Climate 2000”, varieties of wooden claddings have been investigated on a test house in Trondheim. The aim of this investigation was to increase our understanding of the relation between microclimatic conditions and the responding hygrothermal performance of wooden cladding, according to orientation, design of ventilation gap, wood material quality and surface treatment. The two test façades, facing east and west have different climate exposure. Hourly measurements of in total 250 sensors provide meteorological data; temperature, radiation, wind properties, relative humidity, and test house data; temperature, wooden moisture content, time of surface wetness, relative humidity in cavities and wind-driven rain (WDR). Four years have been analysed and recalculated by numerical simulation. The moderate climate of Trondheim provides thorough boundary conditions for hygrothermal analyses of building envelopes.

The WDR was measured in the cardinal directions in a free field and on each façade of the test house. Eight WDR gauges were mounted on the west facing wall with the highest amount of WDR. The WDR measurements are provided in a database on the web that is available for the validation of WDR simulations.

A statistical analysis investigated which climate parameters contributed most to the fluctuations of the moisture content in the wood. It was found that air temperature, global radiation and wind velocity were the three main parameters. WDR was the fourth most important parameter. WDR only defines moistening and not drying, which might be the reason for not being a determinate parameter for the fluctuations in the moisture content in the wood. The time of wetness was further investigated and compared to WDR. The surface wetness sensor measures describes periods with liquid water moistening more accurately and includes the period with free water on the surface after rain and by condensation.

The importance of the wind velocity led to a separate CFD study of the air flow in the cavities when including the bulk wind flow around the test house. The cavity flow is not measured at the test house. The CFD study resulted in a function describing the air change rate of the ventilated cavities dependent on wind velocity, wind direction and cavity opening. The function was tested in WUFI 1D calculations. The calculations showed good correlation with measured data when including air change rate in calculations of cavity temperature and RH.

It was intended to measure the moisture profile in the wood cladding with moisture pins, by measuring the electrical resistance in different depths, but these measurement results were not possible to interpret. However, the methodology might work, even on thin wood boards, if the set up is thoroughly calibrated prior to mounting.

The test house study shows the advantage of two-stage tightening, with a ventilated cavity behind the cladding. The cavity reduces the risk of moisture problems in wall assemblies; it serves as a safety valve, discharging excess moisture by drainage and ventilation. At the test house, with open fields around, it is shown that by having only a few millimetre cavity opening the cavity operates sufficiently. In a dry climate, where the wall will be mostly dry, the results indicate that a design with the cavity openings closed will give the driest wood cladding. No significant conclusion can be drawn regarding the surface treatment and material quality. Although the four year study shows some results, the service life of a wooden cladding might exceed a hundred years with correct design and maintenance.

The Voll measurements were used for validation in HAM simulations of wooden claddings. Models were defined for the separate wooden cladding with controlled outdoor and cavity climates, and with the complete wall assembly including the cavity ventilation. The model had good correlation to measurements and is a useful step towards calculating climate adaptation of wooden cladding. The climate influence and wall design can easily be altered and the hygrothermal performance defined. This enables simulations to find the best suited cladding to different climates. However, there is still a need to define the validity and range of action of the simulations. In any case HAM simulation tools provide a breakthrough in terms of geographically dependent façade designs.

The findings within this PhD project reveal that the current design recommendations on wood cladding provide sufficient performance. Wood cladding can still be promoted as a high-performance rain screen, also in harsh climates.

Table of Contents

List of papers

Wood cladding field study – Chapter 3

Paper I
Nore, K., Blocken, B., Jelle, B.P., Thue, J.V. and Carmeliet, J. (2007) A dataset of wind-driven rain measurements on a low-rise test building in Norway. *Building and Environment.* 42(5):2150-2165.

Paper II
Nore, K. and Thue, J.V. (2008) Evaluation of Moisture Pins for Measuring Moisture Variations in Wood Claddings. *Proceedings of the 8th Symposium on Building Physics in the Nordic Countries.* (Rode, C. ed.), Report R-189, Dept. of Civil Engineering, Technical University of Denmark, Kgs. Lyngby: 991-998

Analyses of the wood cladding field study – Chapter 4

Paper III
Nore, K., Thue, J.V. and Rydock, J.P. (2006) A comparison of time-of-wetness and wind-driven rain measurements on wooden cladding. *Proceedings of the 5th International Conference on Cold Climate - Heating, Ventilation and Air-Conditioning*, Moscow, Russia.

Paper IV
Nore, K., Lisø, K.R. and Thue J.V. (2006) Statistical analysis of wooden cladding moisture response to climate parameters. *Research in Building Physics and Building Engineering – Proceedings of the 3rd International Building Physics Conference* (Fazio, Ge, Rao & Desmarais eds), Taylor & Francis Group, London: 985-990.

Numerical simulation of ventilated façade with wooden claddings - Chapter 5

Paper V
Nore, K., Zillig, W. and Thue J.V. (2006) Climate adapted wooden cladding design – field investigation and numerical validation. *Research in Building Physics and Building Engineering – Proceedings of the 3rd International Building Physics Conference* (Fazio, Ge, Rao & Desmarais eds), Taylor & Francis Group, London: 387- 394.

Paper VI
Nore, K., Blocken, B., Carmeliet, J. and Thue, J.V. (2010) On CFD simulation of wind-induced airflow in narrow ventilated facade cavities: coupled and decoupled simulations and modelling limitations. Accepted for publication in *Building and Environment*, February 15, 2010

These papers will be referred to by their roman numbers.

My contributions

All papers have been written in collaboration with my supervisor, Professor Jan Vincent Thue, His careful guidance throughout my PhD study has directed me towards the most important fields in order to understand ventilated façades. He has let me prepare my work with increasing independence.

Paper I
This paper provides wind-driven rain (WDR) measurement data on a low-rise test building in an online database. The data can be used for validation of WDR models. The WDR amount on the building is analysed and quality assured. I helped to build the measurement set up, analysed the measurement data, designed the database and wrote rough drafts of the paper. *Bert Blocken* initiated the paper, was an active co-author and initiated the accuracy analysis. *Bjørn Petter Jelle* designed the test set up of the WDR measurements. *Jan Vincent Thue* and *Jan Carmelie*t supervised the process and contributed with their extensive experience within building physics.

Paper II
The idea of this paper came after repeated questions about the accuracy of wooden moisture pins. When our moisture profile measurements, based on moisture pins failed, a basis for a conference paper was given. The full paper was prepared in collaboration with *Jan Vincent Thue*.

Paper III
This paper analyses and discusses the time-of-wetness versus wind-driven rain measurements at the Voll test house. The surface-wetness measurements on facades include more liquid exposure, the period with liquid water on the façade after a rain incident and condensation. I did the data analyses and writing of the paper. *James Rydock* was involved in the discussion of the focus and presentation of the paper and quality assured the language. *Jan Vincent Thue* contributed with comments based on extensive experience within building physics.

Paper IV
This paper succeeded a course in statistics, evaluating the research at Voll after only one year of monitoring. The results show the influence of different meteorological parameters on the moisture content level of the wooden cladding. I did the analysis and has been the main author of the paper. *Kim Robert Lisø* discussed and refined the research idea and made the paper more stringent. *Jan Vincent Thue* contributed with his extensive experience within the field of building physics. Both secondary authors have contributed to the accomplishment of the paper by providing comments to successive rough drafts made by myself.

Paper V
This paper provides the first step of climate simulations of measured wooden cladding performance, its temperature and moisture conditions. The WUFI simulations were done during a research stay at Fraunhofer Institute für Baufysik in Holzkirchen, Germany in 2005. I wrote the paper based on WUFI simulations done in collaboration with *Wolfgang Zillig*. *Zillig* also assisted in the writing process. *Jan Vincent Thue* commented on the results and paper drafts.

Paper VI
The weakest link turned out to be defining the air flow in the cavity behind the cladding. A research stay was arranged in Leuven, Belgium, to collaborate with researchers using CFD in building physics on a daily basis. A comprehensive mesh was made of the idealized Voll test house. The full bulk flow around the building including the cavity were modelled in one simulation and compared to the usual decoupling of calculated surface pressures in a cavity flow model. This resulted in coupled and decoupled CFD simulations investigating the basis of air flow behind a narrow ventilated facade dependent on wind speed, surface pressure coefficients and cavity dimensions. B. Blocken supervised the CFD simulations, performed the validation studies of the realizable $k\varepsilon$- model.

Symbols and Abbreviations

Abbreviations

A	Alkyd based paint	
ACH	Air change rate	h^{-1}
B	Acryl based paint	
BDS	Building design sheets	
CFD	Computational fluid dynamics	
E	East	
F	Fast grown	
MC	Moisture content	% by weight
MTR	Moisture temperature response coefficient	-
NTNU	Norwegian University of Science and Technology	
RH	Relative humidity	%
S	Slow grown	
SINTEF BI	SINTEF Building and Infrastructure	
TOW	Time of wetness – surface moisture	h
W	West	
WDR	Wind-driven rain	mm/m^2

Symbols

θ	Wind direction	° from north
φ	Wind incidence angle, the angle between wind direction and the normal to the façade	°
U	Wind velocity	m/s
A	Area	m^2
c	Specific heat capacity	J/kgK
C_p	Wind pressure coefficient	-
d	depth	mm
h	Hour	
h_c	Surface heat transfer coefficient	W/m^2K
k_{TOW}	Coefficient to define the critical limit of TOW	-
M	Mass	kg
p_v	Water vapour pressure	Pa
QO	Global radiation – accumulated last hour	W/m^2
r	Short wave radiation on vertical wall	W/m^2
RR	Rain -increase in rain gauge last hour	mm
RT	Number of minutes precipitation last hour	#
T	Temperature	℃
U	Coefficient of heat transmission	$[W/m^2K]$
w	Wetness	h
β	Water vapour transfer coefficient	m/s
λ	Thermal conductivity	W/mK
μ	Water vapour resistance factor	-
ρ	Density	kg/m^3

Subscripts

2	2 metres height
10	10 metres height
AIR	Ambient outside air
B	Cladding back
C	Cladding inside
CAV	Cavity
CS	Cladding surface
FD	Full depth
L	Local
NMI	Norwegian Meteorological Institute
WB	Wind barrier

1 Introduction

"Wood is a traditional material providing a cultural heritage to humanity but at the same time, it is capable of huge flexibility when used intelligently and wisely to serve our modern society."

Stéphane Hameury (2006)

1.1 Principal objectives

The purpose of this thesis is to add scientific understanding to the Norwegian experience with the performance of wooden cladding. Wooden claddings have been the most common rain screen for residential building façades in Scandinavia for centuries. In 2006, Norway had 3.7 million buildings and 38 % of these, or 1.4 million, were residential buildings (Nordvik and Lisø 2004). Consequently, there is extensive Norwegian experience with wooden claddings. A century ago the Norwegian rough topography and the vast distances limited communication between craftsmen and the transport of materials. Over time, the best suited design was proven to withstand the local climate. Thus, wooden claddings were designed according to their ambient climate exposure. In recent times, improved infrastructure has provided more uniform cladding designs, although differences between new inland and coastal buildings remain. Geographically dependent climatic properties linked to material or performance properties, may to a large extent "replace" vanishing local craftsmanship knowledge (Lisø 2006). This project has been a part of the research & development programme "Climate 2000 – Building constructions in a more severe climate". The programme was initiated to investigate the impact of climate change on the built environment. Although standard technical solutions for all types of climates are appropriate, future buildings will have more stringent requirements regarding energy savings. In addition, climate change scenarios for Norway present us with a future with more precipitation and wind. Hence, climate differentiated performance requirements and solutions might lead to future building enclosure design with increased levels of reliability (Lisø 2006). However, does changes in cladding exposure due to climate change and improvements in building assemblies require adaptation of current wooden cladding designs?

By monitoring different wooden cladding designs it is possible to learn how climate exposure and design details relate to hygrothermal building enclosure performance. Hygrothermal performance is defined by cladding temperature and moisture conditions, and subsequently by risk of degradation. A test house investigation at Voll in Trondheim, Norway has been a main part of this PhD project, see Figure 1.1. Simulations of wooden claddings have been run according to design, ventilation rate and real climate exposures. Simulating the hygrothermal cladding performance is the most efficient and powerful tool in order to revitalize climate adapted wooden cladding design. However, simulation tools are yet to be developed to satisfactorily calculate complex building systems. This work is a step

towards a numerical approach in the development of geographically dependent climate considerations for wooden building enclosures. The issues discussed in this PhD project are:

- How does wooden cladding respond to its ambient climate?
- Is a cavity behind the wooden cladding necessary?
- How does the ventilation rate of the cavity influence the wooden cladding performance?
- What is the influence of wood quality and surface treatment?
- How can geographically dependent wooden cladding recommendations be obtained?
- Is wood a material for modern building assemblies?

Figure 1.1. The east and west facing facades of the test house, 14 test sections are presented on each side, with varied cavity opening design, growth quality and surface treatment.

1.2 Wooden claddings in a climate change perspective

In 1994 the United Nations Framework Convention on Climate Change presented its first article: ”A change of climate which is attributed directly or indirectly to human activity that alters the composition of the global atmosphere and which is in addition to natural climate variability observed over comparable time periods” (UNFCCC 1994). The Intergovernmental Panel on Climate Change has pinpointed the climate change more clearly: “Warming of the climate system is unequivocal. (…) Both bottom-up and top-down studies indicate that there is high agreement and much evidence of substantial economic potential for the mitigation of global greenhouse gas emissions over the coming decades“ (IPCC 2007). Increased storage of wood in constructions can be included in climate change mitigation. The forest absorbs CO_2, and by building houses of wood the CO_2 is stored in the building for decades. Norwegian architects have investigated the effect of exchanging biomass products like wood with mineral building materials in order to reduce CO_2 emissions. By increasing the use of wood-based materials and improvement production and waste treatment, one might save up to 1.1 million tonnes CO_2 annually in Norway (Berge and Stoknes 2004). The total Norwegian CO_2 discharge in 2007 was 55 million tonnes (SSB 2008).

During the last century homogeneous materials like concrete and steel, which are easy to calculate and include in large constructions, have been the main construction elements in structural engineering. The construction industry has been conservative and Norwegian legislation too strict to allow wood to enter larger buildings. Wood is flammable and biodeteriorable, other more “durable” materials have been preferred as structural and cladding materials. However, wood has always been the main structural and cladding element in rural areas, particularly on Norwegian farms and in residential houses. As the perspective of sustainable development has evolved, wood has regained its old fields of usage and also developed new ones. However, there is severe lack knowledge about how to include wood in larger constructions, especially in combination with other materials. “Multi story wooden

houses" was a project which concluded with an extensive collection of building design details for complex building structures (NBI 2003).

1.3 Outline of the Thesis

In order to fulfil the principal objective of this PhD project an extensive test house investigation and subsequent numerical simulations have been performed. The thesis includes five published, and one submitted paper. The papers are "satellites" of the research project, while the thesis includes a full presentation of the PhD project. The general context related to this thesis is presented in Chapter 2. It discusses the division of climates in geographical zones based on essential climate parameters, deals with the development, design and research of wooden claddings, and introduce numerical simulations. Chapter 3 presents the methodology of the test house study and measurement data on wooden claddings. Chapter 4 shows the analyses of the test house results. Chapter 5 gives the numerical simulations validated by the test house study. It also includes how numerical assessments can be pursued in the design of climatically adapted wooden claddings.

The Voll test house study was initiated in order to increase the understanding of the relation between microclimatic conditions and the responding performance of wooden claddings, according to façade orientation with different micro-climates, design of ventilation gap, surface treatment and material qualities. The methodology of the set up and measurements is presented for wind-driven rain (WDR) in Paper I. The means of measuring moisture content (MC) in wood is discussed in Paper II. Further methodology and data set analysis regarding liquid water influence on facades is described in Paper III, while Paper IV defines the most important weather parameters providing fluctuations in cladding MC.

Simulation tools can provide precise predictions of the wood cladding performance in different climates and Paper V uses the Voll measurements to validate a hygrothermal 1D model of wooden cladding in the commercial heat and moisture tool WUFI (Künzel 1995). The model was used to define hygrothermal performance of wooden cladding in four Norwegian climates. As a result of early findings in this PhD project, air flow simulations were initiated to increase the understanding of the two-step tightening principle and wooden cladding response. This work resulted in Paper VI, where the computational fluid dynamic (CFD) tool was the commercial Fluent (2008).

1.4 Limitations

The limitations of this PhD thesis are listed below. The limitations concerning the Voll test house study, choice of cladding and instrumentation, are described in Chapter 3.

- "Modern" wooden rain screens, often open jointed, are not considered. The test house has the wooden rain screen type; horizontal double folded cladding. The plane back side of this cladding provides ideal boundary conditions for air flow simulations. Horizontal double folded cladding is most commonly used along the weather-beaten coast of Norway.

- Only wood from spruce is considered in this work. Prior to the 19th century pine was mostly used for claddings in Norway, preferably heartwood, like in the Urnes stave church depicted in Figure 1.2. Then pine became a great export article and the best pinewood was sold outside Norway. At that time spruce became, and still is, a major source of wood for constructions and claddings. Alternative wood cladding materials are impregnated wood (pine) or wood with natural preservatives (for instance heartwood of pine or larch), or wood with special patina, like aspen. But hardwoods, like aspen, require different design due to larger material stresses.

- Untreated claddings are only briefly commented on in this thesis. Untreated wood is gaining popularity due to the limited amount of chemicals. However, by omitting surface treatment, the hygrothermal fluctuations increase, and the service life may be reduced. In addition the aesthetical considerations change.

- The test house is located in an open, exposed field in Trondheim. The placing provides a limited range of climate influences. However, during the four years of study, the cladding response in several climate types has been measured. For example heavy rain showers or dry, hot weather.

- The Voll test house is a low-rise building with a nearly perfect airtight wall assembly. Usually small failures give access to moisture penetration, like hot air leakage. High buildings have more openings and joints in the façade, which provides more weak points. Since 1997 the Plan and Building Act in Norway allows wooden structures in houses to exceed four floors.

- No durability tests are included in this study, earlier models and methods are used in the evaluation of hygrothermal performance.

- Few future recommendations of wooden cladding design are given. However, the method about how to obtain future recommendations is provided.

Figure 1.2. Urnes, the oldest existing stave church in Norway, built around 1100-1150. The carved wall staves are dated to 1050. Drawing by I.C. Dahl 1837.

2 Background

"Building physics is the cornerstone of designing, constructing, and operating high performance buildings, that is, buildings that are durable, comfortable, energy efficient, affordable and healthy."

www.buildingscience.com

Like in most sciences building physics has been developed through experience, monitoring and now also by the possibility of simulation. Prior to designing the building enclosure the prerequisites must be defined. The climate of the building site is of main importance for the choice of enclosure. This chapter defines climate exposure and classifications. It also presents the building enclosure, particularly the wooden cladding rain screens. The results of cladding experience and research on wooden cladding performance are provided. Finally an introduction is given to the numerical simulation of building enclosures with wooden cladding.

2.1 The climate exposure

One must know the preferred interior and the given exterior climates in order to determine what the building enclosure must provide in terms of comfort. There is great conformity in the interior climate preferences due to relatively narrow and equal comfort limits of people. However, the exterior climates are highly variable. The outer climate on our globe has extreme limits and has areas that have too hostile climates to consider normal building developments.

Different climates can be classified according to various climatic parameters, like precipitation amounts or temperature averages. For engineering purposes such categorization is useful when designing outdoor structures. Climate parameters may also be combined in indices providing more complete climatic definitions, for example WDR or moisture index (Cornick and Dalgliesh 2003). The degree of climate classification accuracy varies according to the design perspective and cost efficiency. In general, indices often provide sufficient background to settle a suitable design. But when introducing new materials, new range of applications or new wall systems, more exact investigations are required. Thresholds for wall assemblies may be set following experience, but more efficient wall performance analyses are the result of monitoring in the laboratory or in situ and simulation with hygrothermal models. This requires more accurate boundary limits than what are required by the standard engineering classifications. This section defines the Norwegian climate conditions and describes different climate classifications. Micro climate boundary conditions used for research and in simulations are discussed in Section 2.3, regarding the numerical assessment of wooden cladding.

2.1.1 Essential climate parameters

In a temperate climate any open-air exposed materials are subjected to climatic fluctuations; variations in relative humidity (RH) and temperature, liquid water from precipitation and condensation, frost, UV radiation and wind loads. These influences, either separately or combined, result in material stresses.

Temperature variations make materials swell or shrink. In addition UV radiation often degrades the material surfaces. A decayed surface may absorb more water, which in turn may enhance erosion, further degradation and reduced esthetical quality. The ambient air RH correlates with the RH of materials with open pores. Most building materials are porous. Winds increase the temperature variations, the water uptake or drying rate of exposed materials. Strong winds may also strain the façade providing additional tensioning to the materials. Frost is a challenge for some porous building materials. However, most wood species are not endangered by frost due to the small pores in the wood structure which insulate and reduce the freezing point below an obtainable level (Geving and Thue 2002).

In order to use climate adapted design, the climate exposure must be defined, and preferably classified. Climate influences are complex and simplifications are desired. Essential climate parameters are derived to differentiate design recommendations, which often are dependent on the material. Wood has no risk for frost damage, but masonry does. In Norway the climatic differentiation of wooden framed house designs are currently based on WDR loads, as presented in Table 2.1 (Kvande et al. 2007). The method to define annual WDR loads by using the synoptic meteorological data was developed by Rydock et al. (2005) and replaced the WDR map developed by Hoppestad (1955). Currently the collection of meteorological data is mostly served by automatic stations. Hourly data will provide the basis for future calculations of WDR loads according to EN 15927. Figure 2.1 illustrates moisture exposure of the building enclosure.

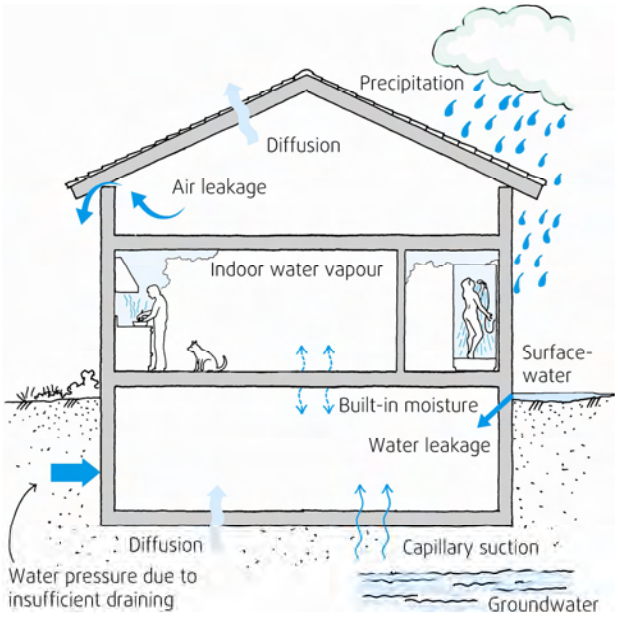

Figure 2.1. Moisture impact of a building enclosure.

Table 2.1. WDR impact classification of annual load in the direction with the highest load (Kvande et al. 2007).

WDR load	
Low	*< 200 mm*
Moderate	*200 – 400 mm*
High	*> 400 mm*

2.1.2 Spatial variation of climate exposure in Norway

The climate of Norway is extremely varied. The rugged topography is one reason for large local differences in temperatures, precipitation and wind velocities over short distances. The sheltered inland usually has cold stabile winters with snow, warm summers and wet autumns. The mountainous areas are dry and cold. The coastal parts of Norway have more intense rain showers and winds, but a more steady annual temperature due to the proximity to the ocean. The ocean current, the Gulf Stream, provides a regular warming and dominating winds from southwest. Thus, Norway has a milder climate compared to other regions on similar latitude.

A combination of temperature and moisture influence, in climate zone classification, is the risk for rot index. Scheffer (1971) presented an equation based on outdoor field tests of wood in ground contact in the USA. He found a correlation between the risk of rot and the climate parameters RH and temperature. He developed a method including these climate parameters in a risk for rot index. Calculated for Norwegian conditions the risk for rot index is presented in Figure 2.2. Wood does not rot equivalently with or without soil contact, but this is the best we have so far. Climate zones for plants, based on temperatures in the growth season, are defined within horticulture science (Redalen 2005). These maps resemble what is found in the Scheffer index and may be an interesting partner when developing this field. In North America a moisture index has been transferred from the climate zoning with agricultural aspects and related to building enclosures (Cornick and Dalgliesh 2003). The moisture index combines the independent wetting and drying potentials at weather stations. The index gives the potential of moisture-related problems in building envelopes. The strategy used in Norway at the time being is, as described in Section 2.1.1, is WDR. The amounts of WDR on the coast of Norway are quite significant, see Figure 2.3. Local differences, topography, terrain roughness and obstructions like vegetation, nearby buildings and such, are not accounted for in general climate zones.

Figure 2.2. Risk for rot map for Norway based on Scheffer's index (Lisø et al. 2006).

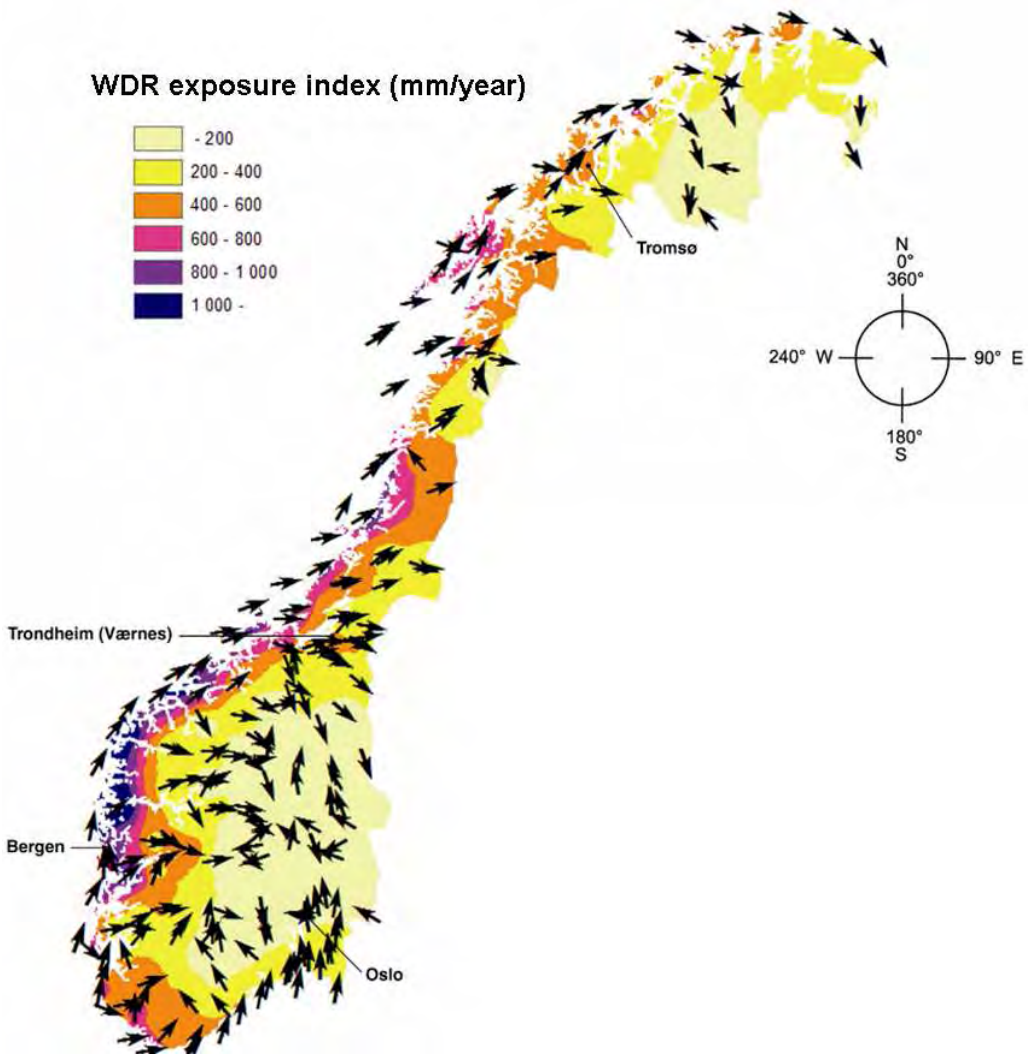

Figure 2.3. General WDR map for Norway (for the normal period 1961-1990). The arrow presents the wind direction that gives the highest WDR load (Lisø 2006).

2.2 Wooden cladding design

Wooden cladding has existed in timber rich areas for several centuries. Efficient board production was possible when the gate saw run by a water wheel was invented in the 16th century. Wooden cladding design has been developed and adapted to local climate conditions throughout the ages and wooden cladding has been and still is the most common façade material in suburban and rural areas of Norway. Consequently, there is considerable experience in this region with wooden cladding.

Traditionally large local design differences of wooden cladding were found in the country. This was due to major climatic variations and inconvenient infrastructure. In the 1860s the circle saw became conventional. With more cost effective production and further efficient and economic transport, more regional cladding productions evolved. Slowly but surely, the knowledge of wood and wooden cladding designs were not needed and consequently reduced. Some old buildings are still equipped with their original cladding, like the farmhouse and Søgne Church in Figure 2.4 a and b. The knowledge that can be extracted from old designs might be of interest to future climatic adapted wooden cladding design. Some knowledge and experience on wood and cladding design from the aged craftsmen and old buildings has been collected in Godal (1994).

a) ***b)***

Figure 2.4. a) Old farm house in Bardu with pine hartwood cladding exceeding one hundred years, the different climate exposure is seen in its colours. b) The church in Søgne, sanctified in 1640, still with its original cladding.

Experience data of more recent cladding design is collected in Kvande et al. (2007). The report is an evaluation of ventilated cladding experience at SINTEF Building and Infrastructure (SINTEF BI). The Building Design Sheets (BDS 2008) of SINTEF BI are generally meant to provide technical solutions that are valid for the entire country. They present drawings and descriptions for numerous building details to support the building industry. The Climate 2000 project pointed out the need for geographical and climate adapted design (Lisø 2006). Climate specific recommendations are now being included, but the designs and climatic boundaries must be studied further. However, with the extensive experience on wooden cladding, robust designs recommendations can be given for all parts of the country (Kvande et al. 2007).

2.2.1 The building enclosure

The building enclosure separates the interior and exterior environments of a building. The interior climate serves the resident; the outer shell protects from exterior climate fluctuations and the wall assembly facilitates indoor comfort. Building enclosures are designed in collaboration between the architect and the engineer. The best structural, aesthetic, durable and most user friendly solutions are sought. The durable and user friendly perspectives include the air, heat and moisture control of the building, aspects that are included in the field of building physics. The performance of the building enclosure system is dependent on the planning, the materials and their assembly, and the detailing of the building. Building enclosure performance is measured in indoor air quality, energy performance, durability and capability of the physical barrier to withstand exposure to the exterior climate.

In 1988 the European Union published the Construction Product Directive prescribing six essential requirements for building and civil engineering works: mechanical resistance and stability, fire safety, hygiene, health and environment, safety in use, noise protection and energy economy (Council Directive 89/106/EEC). These requirements should be satisfied during the intended service life of a construction. The Norwegian Plan and Building Act is currently being revised, but indications are that the principle of performance requirements which was introduced in Norway in 1997 will be sustained. Although no directives are given for the use of materials or structural dimensions, satisfactory performance must be documented prior to construction. The building codes in Canada and the United States also address minimum requirements for health and safety in an object based format.

In 2007 new building regulations were implemented in order to move towards the building energy performance requirements of the Kyoto Protocol (TEK 2007). TEK (2007) requires an air tight building enclosure. The building enclosure must be air tight in order to control the fresh air and exhaust ventilation. The total air change rate (ACH) by leakages is maximum 1.5 air changes per hour

in buildings exceeding two floors. Norwegian walls are usually designed with a vapour and wind barrier to be sufficiently air tight. The maximum U-value of outer walls is currently 0.18 W/(m^2K), which in Norway usually requires 250 mm mineral wool insulation. Most walls have 150 mm mineral wool, which fulfilled the former requirements.

Effective moisture control is vital in order to obtain satisfactory building enclosure performance. The design must endure wetting from precipitation and condensation. The moisture content (MC) of the materials must be kept to a minimum. Rapid drying of the excess liquid and vapour water is vital when the moisturizing stops. For wooden cladding it is important to keep the MC below the risk of biological growth, often set at 20 % MC.

During the last few decades building enclosure failures have occurred more frequently. SINTEF BI investigates several building failures every year, the inspections are logged in a building defect archive. As part of Climate 2000 this archive has been evaluated (Lisø et al. 2006). All process related building defect cases, from 1993 to 2002, 2423 in total, have been categorized. Process induced building defects are defined as "absence or reduction of presupposed capacity that is discovered after a construction project has been completed and taken over by the owner". Defects caused by normal wear and tear are not defined as building damage. Building defects occur because the actors involved have not succeeded in meeting the requirements in standards, methods or specifications. 76 % of the failures were related to moisture, as seen in Figure 2.5. Earlier, roofs were considered as the most problematic part of the building enclosure, but the study of Lisø et al. (2006) pointed out that the walls have failures more often (36 %) than roofs (22 %). Figure 2.6 shows the damage defect cases for outer wall assemblies. 32 % is due to precipitation and only 25 % is due to non-moisture sources. Similar experience has been recorded in British Colombia, Canada, with large amounts of low-rise building enclosure performance problems with buildings less than eight years old (Rousseau and Hazleden 1998).

In response to experienced failures, extensive research programmes have investigated the thresholds of wall systems in different climates. Wall performance studies are based on experiences, laboratory experiments, monitoring test houses and numerical simulations. Some projects are EDRA - Envelope Drying Rate Analysis (Hazleden 2001), MEWS - Moisture Management for Exterior Walls Systems (Beaulieu et al. 2002), Moisture proof timber frame walls (Andersen et al. 2002), ASHRAE 1091 - Development of Design Strategies for Rainscreen and Sheathing Membrane Performance in Wood Frame Walls (Straube et al. 2004) and Climate 2000 (Lisø and Kvande 2003). The findings of these projects are presented in the relevant context.

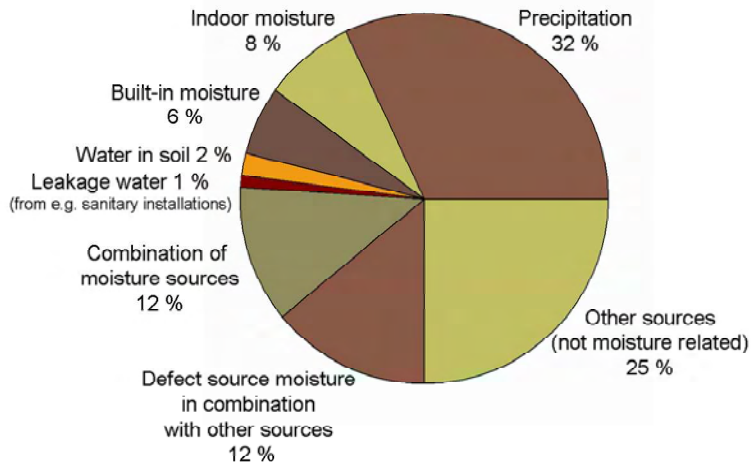

Figure 2.5. Building defect sources on outer wall assemblies (Sagen 2006).

2.2.2 Wall system: One-stage versus two-stage tightening

Building enclosures may be divided in one-stage or two-stage tightening. One-stage tightening wall systems include protection to exterior climate and providing indoor comfort in one compact wall structure. One-stage tightening wall systems are often considered the most economical wall assembly for larger buildings and buildings in warm latitudes. The two-stage tightening, illustrated in Figure 2.6, is also named ventilated screen type wall systems (VSWS) or pressure equalized rain screen (PER). The system is also known as “two lines of defence” and “ventilation drying”. The two-stage tightening is the prevailing design of low-rise residential building enclosures in Norway. Ventilated wooden cladding first appeared on the weather beaten western coast of Norway. To obtain durable wooden cladding that protected the logged walls, intermediary vertical battens were installed creating the cavity, on which the horizontal wooden boards were mounted. The WDR protection of the wall improved when this cavity behind the cladding was introduced. Double skin façades (DSF) is a third variety of enclosure systems. DSF has a deep cavity between the skin and the inner enclosure of the wall (0.2 - 2 m), typically constructed in glass. This cavity may include a ventilation system, sun shading, fire exits and more. DFS is not relevant to the objective of this thesis.

Compact wall systems perform satisfactorily in areas with limited precipitation. Wood and wood based products are often suitable within the wall assemblies, both for structural and cladding purposes. But wood is susceptible to rot which means that wood may be an indicator of the wall system performance; the wood is often the weakest link in terms of durability. Teasdale-St-Hilaire and Derome (2007) studied the behaviour of three wood based sheathings in compact wall assemblies with rain penetration loads simulated for the Montreal area. All sheathing materials were found to be durable with a standardized rate of failure.

LaCasse et al. (2003) investigated the drainage function of the cavity in the laboratory, and found that no water passed the “second line of defence”, the wind barrier. Even though no water was accumulated within the core of the wall assembly the evaporative drying effect was studied as a second part of the project. The cavity provided increased evaporative effect when limited amounts of water were to be dried out, compared to one-stage walls (Beaulieu et al. 2002). Bøhlerengen et al. (2008) presented malfunctioning façades with both one-stage and two-stage tightening. They accentuate the importance of understanding the two-stage tightening principles and how to provide better alternatives when traditional constructions have to be improved. Hazleden (2001) encourages the use of drainage cavities in future building enclosure systems in British Colombia.

Historically, the weather beaten façade was first protected with wooden cladding. The principle of two-stage tightening was defined in the 1960s (Birkeland 1963, Isaksen 1966). They thoroughly analysed the performance of two-stage tightening and rain water penetration. Though the principle is simple, it is still a highly relevant research topic in the pursuit of high-performance building enclosures. Kvande et al. (2007) discuss ventilated cladding in general and sum up principles, recommendations and Norwegian experience from several building defect cases regarding ventilated cladding. They presented performance requirements of the two-stage tightening of the wall:

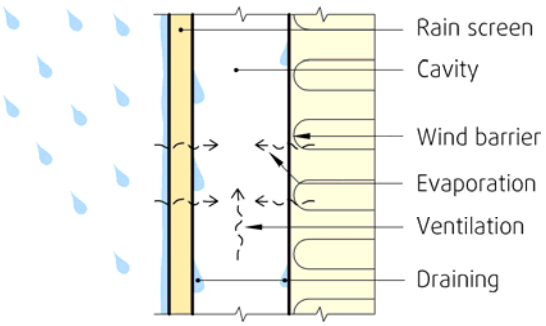

Figure 2.6. Two-stage protection of the wall, also showing impact of WDR. BDS 542.003.

The cladding should

- work as a rain screen in order to impede precipitation from reaching the wind barrier
- be a mechanical safeguard for the back wall
- endure climatic and mechanical exposure
- provide aestehtical qualities to the building

The wind barrier should

- prevent cold outdoor air entering the insulation layer and reducing its effect
- be an air tightening layer supplementing the indoor vapour barrier, hindering warm humid air from leaving the the building enclosure and possibly creating condence water traps
- drain water that managed to enter the construction
- serve as temporary cladding during building erection
- be vapour open so that built-in moisture or leakages can evaporate outwards

The ventilated cavity should

- separate the exterior rain screen from the wind barrier in order to prevent water transport into the wall by capillary suction or gravity
- drain water that has penetrated the rain screen
- allow drying of excess moisture in the internal parts of the wall assembly
- allow drying of the cladding on the reverse side
- equalize the pressure differences across the cladding to avoid water being forced through joints into the main wall assembly

2.2.3 The wood material

As mentioned, wood has been an important material throughout the ages in Norway. The quality of the wood is variable, but experience has shown how one can “read” the wood and use it within its limitations. The stem of trees is divided in heartwood and sapwood. Sapwood is the transport route of the living tree, while heartwood serves the structure and stabilizing. The heartwood is often filled with extractives, but this is not the case for spruce. Wood is anisotropic, with three main directions; longitudinal, radial and tangential, as indicated in Figure 2.7. The cambium part of the tree produces new cells both for the protective bark and the sapwood. The spruce trunk has distinct growth rings. The seasons are mirrored by in the earlywood and latewood; in the spring the cells are thin walled and have large capacity for water transport, whereas the summer latewood has more thick walled cells with structural support.

Until about fifty years ago wood quality was estimated by analysing the trunk, the growth ring distance, the heartwood share knots, and several other details. The wood quality was also assessed by observing the tree in the forest. The microscopic view of wood was not perceptible a hundred years ago. What they did know and study was the tree itself, its climatic conditions, growth place and form. Elowson et al. (2003) found no influence from geographical growth place or of the time of year of the cutting in their extensive study of moisture dynamics in wood. Ways of treating the tree to increase the resin content or to control whether it was mature were known by the logger and the craftsman, often the same person. He or she could pick trees depending on what material was needed, different wood provided specific properties. Knowledge of the woods was vital to select high quality timber. Some characteristics to ensure high quality wood both for durability and strength are found in Godal (2002):

- The young tree started growing under a screen of older trees
- Steady growth throughout the lifetime of the tree – best growth ring size is 1-2 mm
- Aged trees – gives the largest heartwood portion and the most dimension stable wood
- Large dimensions of the wood – preferably the log is more than 40 cm in the top
- Materials are taken from the bottom part of the log
- Straight growth provides lined fibres
- Limited amount of reaction wood – that is wood produced if the tree has to straighten up

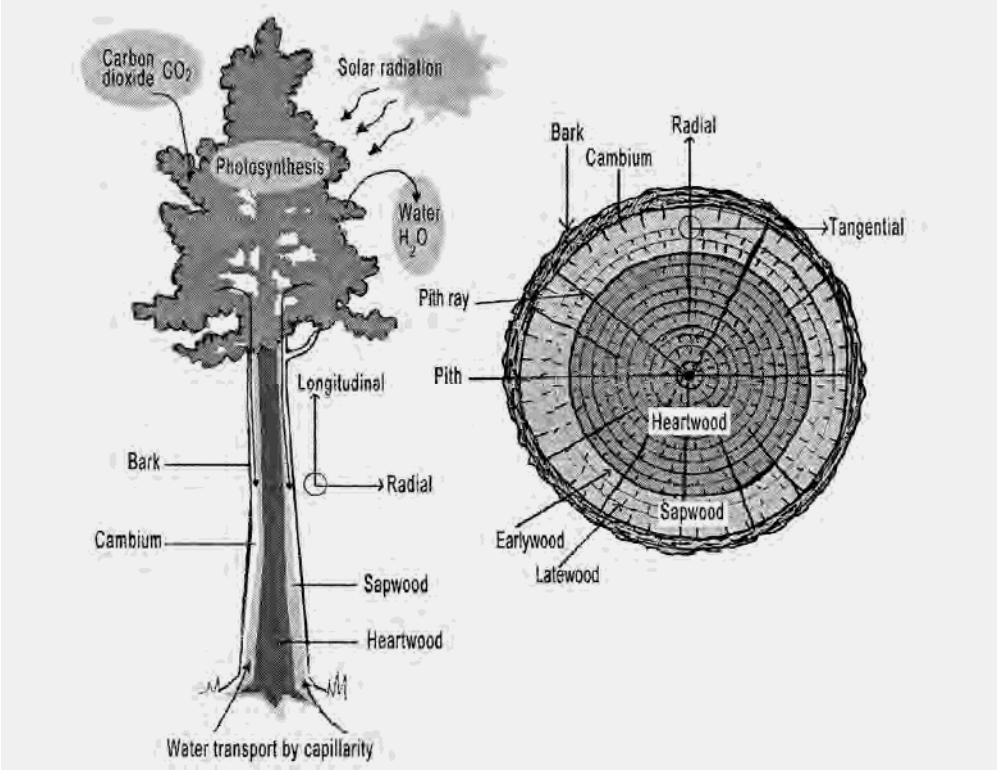

Figure 2.7. The living tree and the cross section of the tree trunk (Hameury 2006).

For cladding material the best wood was provided by spruce growing next to marshes or in mountain areas. In Norwegian the trees are called “sturegran” – meaning “moping” tree. They grow slowly providing dense wood, too brittle for construction planks, but durable for cladding boards (Godal 1994). The acidic conditions around the marsh must somehow provide good conditions for growing dense wood. Spruce is a sour wood, with pH of 4.5. This might also be helpful in the reducing the risk for biodeterioration. The logging machines used today are too efficient to include considerations of growth place and form during cutting. The time needed for choosing the best suited wood material probably paid off in increased durability.

Water and nutrients have been transported in the living tree through its cells and the pores connecting the cells. These water routes are also operative then when the wood is included in wall assemblies. However, the torus, the pore membrane in the lens pores of spruce, close when spruce dries. This is also the reason for the difficulty of impregnating spruce. The standard of solid wood panelling and cladding, NS-EN 14915 Annex B, points out that the wood used in cladding should not be fast absorbing. Elowson et al. (2003) characterize spruce to be “moisture insensitive”.

The microstructure of wood is illustrated in Figure 2.8. The wood colour is mainly due to the golden tint of the lignin. The density of wood depends on the ratio of solid cell wall and pore volume. The dry density of the cell wall is 1500 kg/m^3. The dry density of spruce is 300-640 kg/m^3. The volumetric shrinkage rate of spruce is 11.6 – 12 %. More dense wood gives a larger shrinkage rate. The anisotropy provides different shrinkage in the longitude, tangential and radial direction. The largest shrinkage is in the tangential direction, around 8 %, the radial direction has about 3.7 % and in the longitudinal direction up to 0.3 % shrinkage (FPT 28 2003). In general spruce shrinks 0.25 % across the fibres per % MC. Wood dimension changes introduce micro-cracks. A stable environment is preferred in order to reduce cracking. NS-EN 14915 provides properties of importance in building physics; water vapour resistance factor and thermal conductivity, according to density. These are listed in Table 2.2.

The natural durability of wood is low. Wood is an organic material that decomposes in its original environment. Moisture, nutriments, oxygen and temperature are needed to grow fungi. The conditions

for fungi growth are shown in Figure 2.9. Wood is prevented from the biodeterioration that takes place on the forests ground by averting bacteria and insect attacks with limited contact with the ground and keeping the influence of moisture to a minimum. Fungi grow when the wood has more than 20 % MC over a longer period of time, 8-10 hours. This moisture content in the wood is reached when the relative humidity is more than 75-80 % (Valbjørn 2003). Temperature is also an important parameter for growth of fungi in the wood. Temperatures between 5ºC and 40ºC give possible development of fungi. To get fungi growth the combination of moisture, temperature and oxygen is vital. Biodeterioration may therefore also be prevented when the wood is soaking wet.

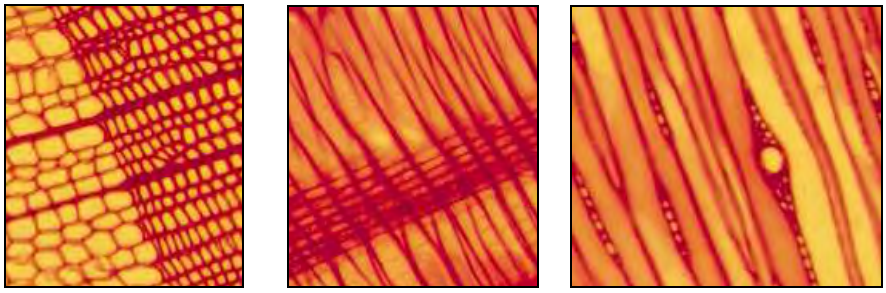

a) ***b)*** ***c)***

Figure 2.8 Microstructure of spruce a) cross-section of stem, earlywood and latewood b) radial section; a band of pith ray cells are seen on top of the traceide cells c) tangential section; pith ray cells are cut (FPT 28 2003).

Table 2.2. Water vapour resistance and thermal conductivity of softwoods at different densities (NS-EN 14951)

Density	*Water vapour resistance factor*	*Thermal conductivity*
δ	*μ*	*λ*
kg/m³	*-*	*W/mK*
300	*50*	*0.09*
400	*60*	*0.11*
500	*70*	*0.13*

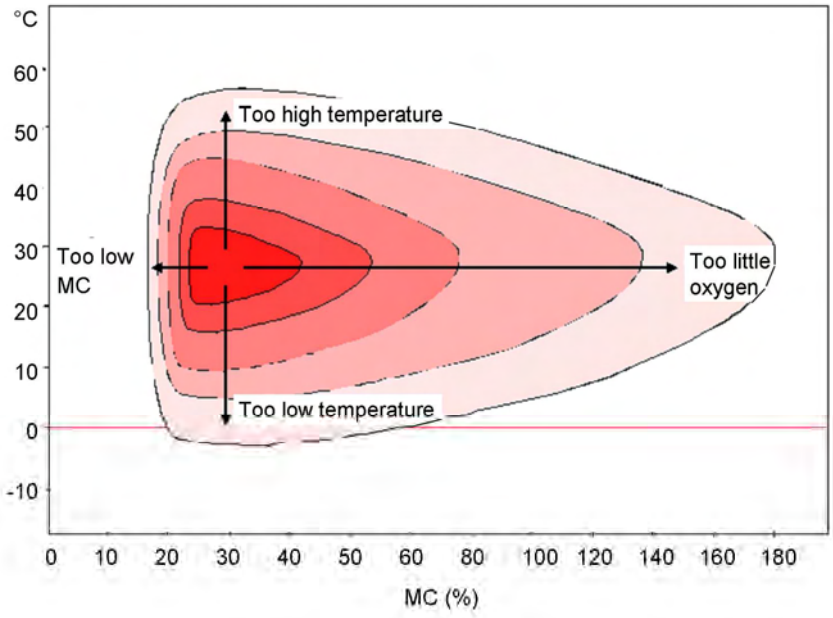

Figure 2.9 Decomposing hazard due to fungi in wood. Each fungi has its own hazard map. Deep red indicates the greatest danger of attack (Tronstad 2002).

2.2.4 The cladding board – production and quality

The dimensions and quality of the single boards are determined by the utilization of the log and with respect to durability. SN/TS 3186 holds the requirements of cladding board designs. The thickness ranges from 16 to 22 mm and width from 73 to 173 mm, dependent on the cladding type. The wooden structure has different material properties in the three main directions. Generally radial cuts are preferred, cut option c in Figure 2.10. Such boards keep the pith rays as reinforcement and not as water routes. In addition the dimension stability improves with equal shrinkage in all directions. The latewood is the most robust when it comes to weathering. The radial cut provides the most uniform spread of latewood. The drying might induce curving of the board. The reasons for curving is the arching due to uneven amounts of radial and tangential wood which shrink unevenly, curving due to unsymmetrical drying of the wood in the longitudinal direction and twisting due to the slope of the fibres within the board. is the preferred board, providing the least risk of arching and twisting and having no longitudinal curving. In Figure 2.10 cut option a has this highest risk of curving and twisting and cut option b has a high risk of longitudinal curving. However, the selection of cuts is most often based on getting the most out of each log, not increasing quality of the sawn board.

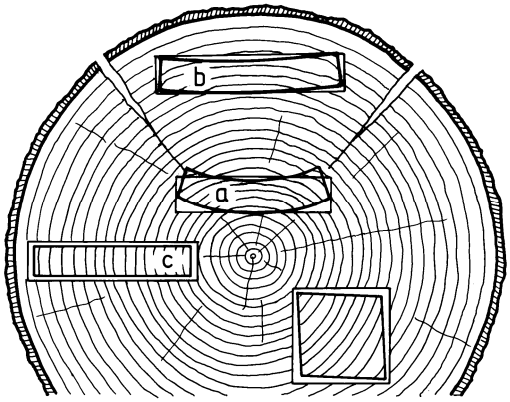

Figure 2.10 Sketch of different cutting options. Cut option c is the radial cut.

Wood is a fresh product and the cladding board quality is dependent on its treatment from the time of cutting to maintenance periods of the wall. NS-EN 14915 directs proper handling, properties, factory production control and marking of solid wood cladding. It points out that all machining, boring, planing etc. must be completed prior to preservative treatments. In Sweden a practice called the Kauna procedure promises a prolonging of the maintenance term of the surface treatment with 50 % (kauna.com). Thirteen action steps are included, the nine first are provided by the cladding supplier and the four last must be completed at the building site:

1. Choosing the right tree, the spruce is sorted by quality and marked with felling date
2. Careful handling to and within the saw mill and no wet storing
3. The planks are sawn within four weeks after felling
4. Drying to 16 % MC – drying starts within one day after sawing
5. Classification and dry storage
6. Boards are sawn by splitting the planks – profiles are applied
7. New sorting - Kauna is the highest classified planks
8. Primed within 60 hours after sawing – front, sides and ends
9. Packaging to hinder moisture penetration and marking for identification and traceability
10. Correct storage at the building site – preferably under a roof
11. Prime and paint new cut end wood
12. Nails level with the cladding board and mount the lower part of the panel at least 250 mm above the ground
13. Last paint layer at a proper time

2.2.5 Current best practice of wooden cladding in Norway

"The main importance is to preserve the exterior panels from having too high MC during longer periods" (Annex B in NS-EN 14915). The standard gives some general construction recommendations to increase durability of wooden cladding:

- Water traps must be avoided
- Panel ends should be cut in butt joint oblique for minimum gaps.
- Splashing from ground should be avoided by keeping a good distance
- Protective constructions should be used to protect the cladding from moisture absorption
- The construction must be ventilated with at least 22 mm free cavity behind the cladding

Several wooden cladding designs exist. Figure 2.11 shows the typical wooden façade of the inland area of Norway together with a design detail for this cladding. The most common and traditional Norwegian claddings are presented in Figure 2.12. The original function of the cladding was to protect and supplement the logged wall. In the inland areas the boards were mounted directly on the wall, hence vertical cladding. Along the coast cladding ventilation was necessary to protect the logged wall to WDR. A batten was placed vertically; following the cladding was oriented horizontally. This orientation was also beneficial in regard to maintenance, the lowest boards were mostly subjected to weathering and decayed planks could easily be exchanged.

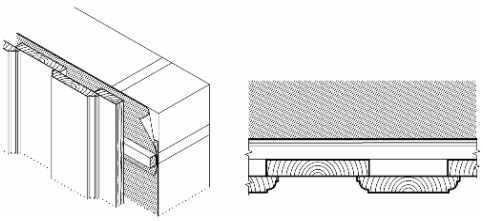

a)

b)

Figure 2.11.a) Typical vertical wooden cladding design. b) Profiled wooden cladding on an old farm house west of Oslo.

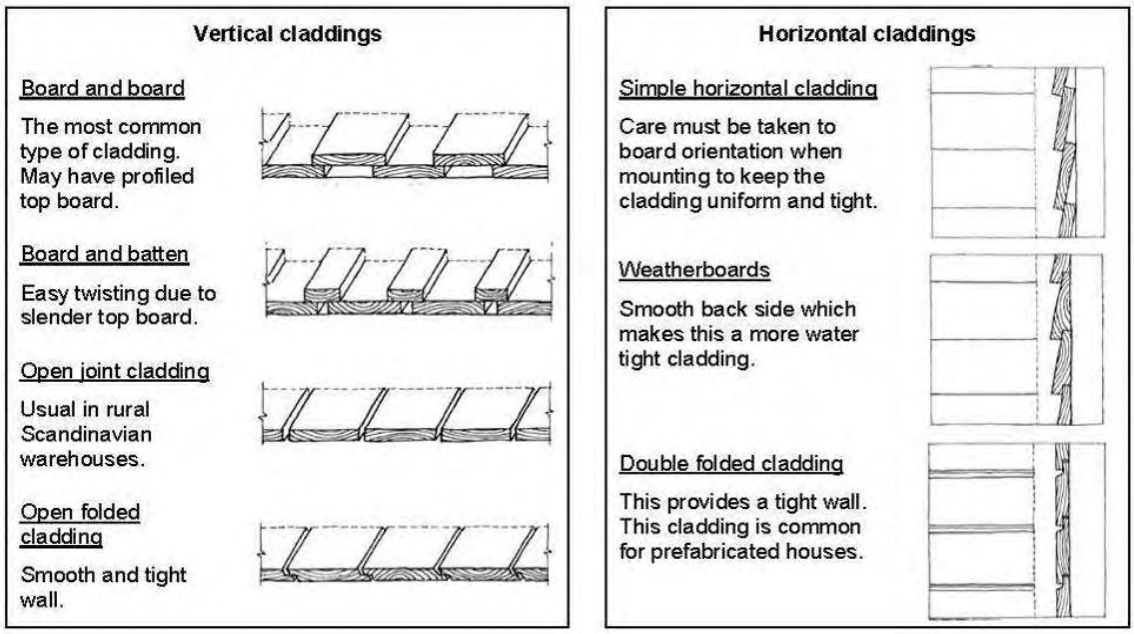

Figure 2.12. Vertical and horizontal cladding types (FPT 22 2002).

A drainage opening with at least 10 mm clearance to the water board is recommended (Edvardsen and Ramstad 2006). This gap serves both drainage and ventilation, and gives room for maintenance treatment of the end wood. Nevertheless, in the Norwegian inland many claddings are placed directly on the water board and the joints are sealed with paint. In some cases this design has lasted for more than a hundred years. Figure 2.13 a and b shows this detail with damage and repaired. Still, the ventilation opening is a more robust design.

The pith is the middle of the tree (see Figure 2.9). The side of the cladding board closest to the pith provides the best weather screen according to Godal (1994). Nicolajsen and Hansen (2000) also found that the orientation of the board must have the pith side facing towards the outdoor exposure. This is not a part of the BDS, this is seen in Figure 2.12. The pith side has the highest dimension stability and when mounting together the wall is levelled in all weather types even with the dimension changes of the wood. Cutting grooves on the back of the board also reduced cracking on the weather-beaten side. Nicolajsen and Hansen (2000) also found no difference in longitudinal orientation of the test boards. Godal (1994) states that the root end of vertical cladding boards should point upwards. This is in order to have the fibres that stand out pointing downwards. This is not taken into account when mounting cladding nowadays.

a) ***b)***

Figure 2.13. Detail of cladding placed directly on the water board. a) before and b) after fixing.

Wooden cladding decay often starts in areas differing from the uniform cladding, such as board ends, butt joints or overlaps (Hjort 1997). These areas often include mechanical fasteners which introduce micro cracks. Too short distances from nails or screws to board edges may cause splitting of the board. Minimum distances are given in NS 3470-1. Dense wood might have to be predrilled in order to avoid splitting. It is also important that the nail or screw is level with the surface of the cladding. In general one should not nail through more than one cladding board. Mounting recommendations are given in the BDS 542.101. The overlap of the boards should be at least 20-25 mm (Ramstad and Edvartsen 2006). The problem with rot in overlaps is mainly for vertical cladding, although it can be a problem of horizontal cladding as well. The capillary suction in the overlap area creates a "water trap". This type of rot is most common along the western coast of Norway (Aagaard 1992).

For the end wood at the lower part of the cladding SINTEF BI recommends a sloping cut (Kvande et al. 2007). The lowest part should face outwards to ensure that the water drips off in the far end of construction. Nore (2004) brings up some details that could have been functional, but some suggested design improvements are not yet cost effective. One example is planing grooves for draining in the overlap between boards (Holmgren 1945) or drip grooves on the lower board ends. Such details might be incorporated in the future with more efficient production equipment.

The recommendations for ground distance are 300 mm, but when the ground conditions do not create splashing and the roof overhangs are wide the distance may be reduced to 100 mm (Edvardsen and Ramstad 2006). Higher cladding should have water drained out for each storey height. Separate building design sheets are provided for flashings on parapets and flashings around openings within the façade for doors and windows (BDS 520.415). Also joints are treated separately in BDS 573.102. Outer wall defects are normally due to lack of sufficient ventilation and/or drainage, or inappropriate detailing such as flashings (Lisø and Kvande 2007). Figure 2.14 shows the details that often cause cladding damage. Thue (2008) summarize the common defects on wooden facades: unfavourable constructive solutions, lack of cavity, exposed end wood, leakages and lack of maintenance.

Constructive protection of details is often neglected. Instead engineers often rely on chemical treatment of the wood. However, relying on these treatments requires an effective maintenance management (Byg-erfa 81 09 15). Protective construction includes roof overhang and flashings that are designed to divert precipitation water away from the cladding. Rousseau and Hazleden (1998) report a survey of low-rise multi-unit wood frame residential buildings with building envelope defects in British Colombia. They found an invert correlation between the width of roof overhang and the percentage of walls with problems, see Figure 2.15. They also conclude that walls with limited amounts of details and well designed flashings are less vulnerable to building enclosure failures.

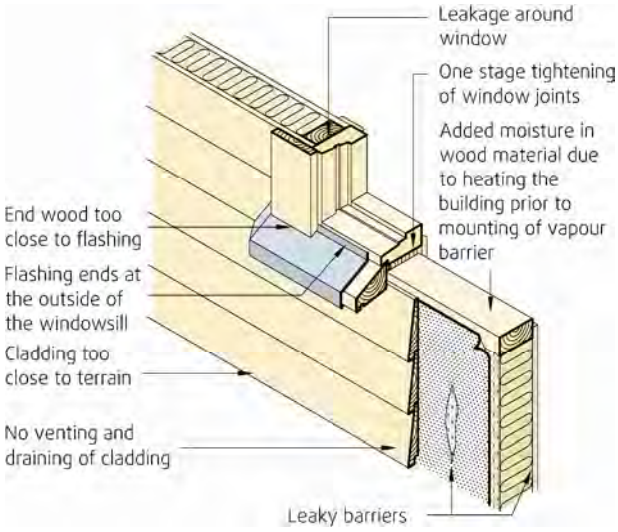

Figure 2.14. Defects causing damage to wooden cladding (Lisø and Kvande 2007).

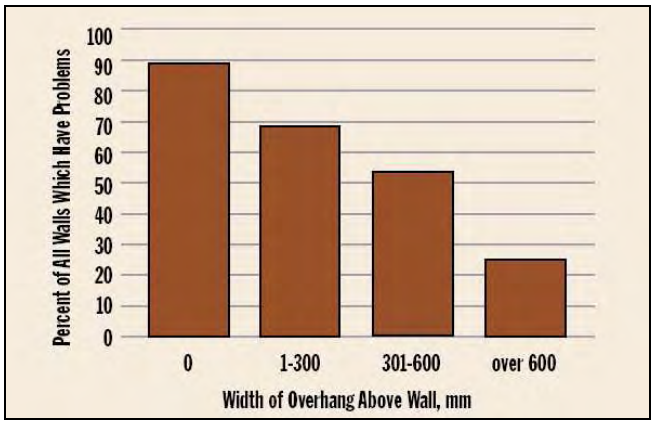

Figure 2.15. Degree of failures dependent on roof width of overhang (Rousseau and Hazleden 1998).

2.2.6 Design of the ventilation cavity

An extensive low-rise test house investigation on wooden cladding was carried out at Lista from 1987 and ten years ahead. Christensen (1999) reported that no difference was found for cladding with or without cavities. The project had somewhat random measurements, and trouble with lightening stopping the measurements and destroyed the temperature sensors. The ventilated cladding was detached from the wind barrier with a 48 mm batten, while the unventilated cladding was mounted directly to the wind barrier with no cavity in between. It was concluded that the non-ventilated cladding has lower MC for the south facing wall, but reverse for the north facing wall. When studying the graphs better conditions were generally found for the non-ventilated cladding except for the north facing wall in the winter period. The wall was insulated with 100 mm glass fibre wool, in addition to inner wood cladding, vapour barrier, and asphalt plate. The heat conduction should be considered substantial to the externally mounted wooden cladding without a ventilation gap, providing substantial drying of these cladding boards. This means that lower MC in the unventilated cladding boards is expected. However, the higher MC of unventilated versus the ventilated cladding at the north facing wall during the winter time is unexpected. This may be explained by the missing temperature correction. According to Apneseth and Hay (1992) a reading of 24 % MC at 0°C is actually 27.4 % MC when temperature corrected, and if the unventilated cladding is slightly heated e.g. 10°C, the reading should have been 25.6 % MC. This implies that an error of 2 % MC may be possible, which could be enough to reverse the trend, the basis for the conclusion. This shows the importance of temperature corrections. Also the drying out during the winter period is more limited at the north facing wall with almost no direct sunlight. The report also indicates icing on the north facing wall. The ice might dry and wet the north facing wall in the unventilated cladding sections. Icing is not seen at the south facing wall, probably due to sun heating and this may mainly explain the drying out of the south facing wall during the winter.

Johansson et al. (2000) could not find the cavity necessary, but notes that the test cladding had only been exposed for 5.5 years, which is a relatively short time period and the cladding was intact. Andersen et al. 2002 and Hansen et al. 2002 both show that wood cladding without a cavity had a slower moisture uptake and they concluded that walls without a cavity were not inferior, in terms of the moisture content behind the wind barrier, to the walls with a ventilated cavity. However, they emphasized that cavities always should be drained and that venting in order to equalize pressure differences might prove necessary at exposed sites. They also note the importance of having a well functioning vapour barrier in order to keep a dry wall. Gudum (2003) argues that a wooden cladding would not deteriorate if a cavity is missing, but the construction is more robust and less sensitive to the quality of the workmanship with the cavity included. Stang (2002) reports an investigation, both free field and in the laboratory, of wooden cladding with load-bearing lightweight concrete back walls. These walls are so called robust walls, often used for bathrooms etc. The results show that overpressure ventilation on the inside, combined with built in residual water gave critical conditions

for the wooden cladding. Both ventilated and unventilated cladding was examined and the conclusion was that outer cladding should be mounted in such a way that ventilation of the cavity is ensured. Fynholm et al. (2003) report an investigation on whether higher level of insulation influences the timber framed function in relation to moisture. The ventilation cavity of the wooden cladding is one of the parameters examined, in addition to construction design, moisture barrier and insulation thickness. The investigation was done in a hot-box experiment. No test build ups showed critical moisture content. Gudum (2003) investigated the influence of cavity ventilation with a Plexiglass cladding. She found that increasing the insulation thickness in the wall gives a tougher moisture load on the cladding. This is due to lower temperatures on the cladding, which leads to increased amount of condensation, which may also be a problem in ventilated façades. Cladding temperatures under the dew point temperature will give condensation. This can occur when a cladding is colder than the surrounding air for instance due to long wave radiation. Zillig (2003) found that the algal growth due to condensation is worst on the west- and north-facing walls. The walls facing south and east are sun warmed earlier, and the wall facing west had the most WDR. Walls with condensation may have algal growth, which demands free water, not like moulds that grow with high RH and temperatures above 5°C.

Nicolajsen A. (1989) presents an experimental investigation of ventilated outer walls and the influence of the wind pressure on the heat loss. She found no correlation between the wind velocity and the pressure loss of the ventilation cavity, and then also not on the heat loss. She also found no extra effect of the wind barrier as long as the vapour barrier was flawless.

The new European standard NS-EN 14915 includes the importance of ventilating wooden constructions with at least 22 mm free cavity behind wooden cladding. Kvande et al. (2007) present the recommendations of ventilation cavity design. On modern buildings it is experienced that unventilated wooden cladding may perform well in dry, inland situations. However, it is generally recommended to design wooden cladding with a ventilated cavity behind the cladding. Also the new insulation requirement makes this former design detail more risky due to less drying out potential with the lowered heat conductance through the wall. The cavity is usually 23 mm deep, determined on the size of the battens. Such cavity depth is sufficient in areas with low WDR impact, (see Table 2.1). In areas with moderate to high WDR impact, the cladding is mounted on furring strips and cross banded battens. Then the cavity depth is recommended increased to 54 mm. The furring strips ≥ 18 mm and the battens should be minimum 36 × 48 mm. It is debated whether this extensive cavity depth is necessary. In Canada, the drainage cavity width was tested according to ventilation rate, with 0 mm, 10 mm and 19 mm cavity depths. The widest cavity provided the best drying effect. Thus the depth of at least 19 mm is recommended behind wood based sheathing, Hazleden (2001). To hinder mouse and insects from getting into the reverse side of the cladding, the ventilation opening may be entirely of partly tightened with wood chocks or insect bands. The openings should be at least 4 mm (Geving et al. 2006). The bottom of the cladding should always be open, whereas the top must be open when the height of the wall is one storey height or more. When the wall is more than one storey high a wall break should be included to drain out excess water. Figures 2.16 and 2.17 illustrate building design details of wall breaks in Norway and in Canada respectively. The rain screen design is also displayed in the Canadian case.

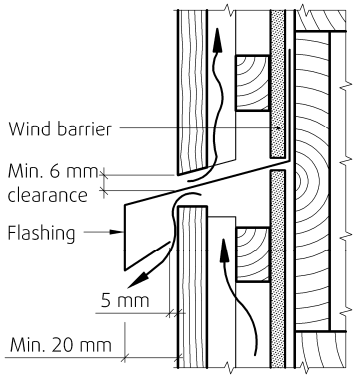

Figure 2.16. Design of a wall break (Kvande et al. 2007).

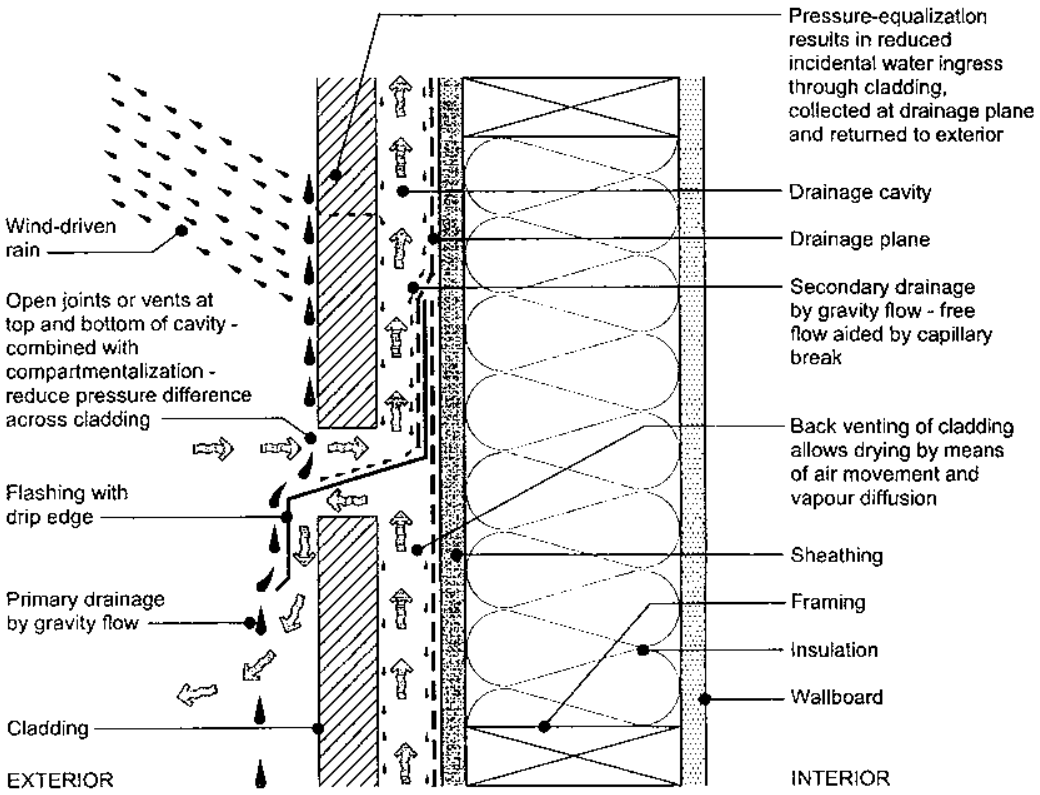

Figure 2.17. Construction of "pressure-equalized rain screen wall" which is included in the two-stage tightening wall system (Steffen 2000).

2.2.7 Surface treatment – preservative and cosmetic

When not considering constructive protection, surface treatment is the most important resistance for the wood against weather exposure Elowson et al. (2003). Surface treatment of cladding serves two objectives; it protects the surface from weathering and enables various appearances of the façade, like colour and texture. The treatments are divided in stain and paint. A mix is called "resistant stain" and is a common surface treatment in Norway. The main difference is the film depth, providing different degrees of transparency, and the durations between maintenance periods. Maintenance periods are usually within 2 to 15 years. When leaving the surface untreated the lignin of the wood is decomposed by light, mostly by the UV portion of light. Cellulose fibres are uncovered in the wooden surface and create a grey appearance. The fibres will prevent the cladding from deeper UV degradation, but the surface will not be protected from the ingress of water. The water fluctuations provide material stresses causing cracks and further degradation. Natural weathering provides an erosion of the wood surface of about 5-6 mm during one century in a constant southern Norwegian climate. In more exposed areas, the cladding may have to be changed every 20-25 years due to weathering (Jacobsen and Ånerud 2003). Surface treatment prevents water ingress and thereby weathering of the wood surface. A surface film must be water repellent but vapour open at the same time, allowing some water vapour to dry out.

Modern wood treatments are classified according to the binding agent used. Paint based on linseed oil or tar is not common for modern cladding. Special products of impregnated wood are available, but the use of these is limited too. One binding agent is alkyd, embodied by polyhydric alcohol and polyvalent acids in combination with vegetable aliphatic acid. Alkyd paints are dissolved in naphtha. The paint creates the film when the naphtha evaporates (FPT 23 2003). The paint film is flexible at first but turns brittle over time. Alkyds have small pores (Raknes 1985). The evaporating naphtha constitutes an environmental problem. In general, the authorities have decided to phase-out treatments dissolved in naphtha (2004/42/EF).

The transition from paint systems dissolved in naphtha to water is part of the approach towards sustainable development.Acryl binders consist of acryl polymers dispersed in water. The monomers and emulsifying agents determine the properties of the acryl coating. The water evaporates when the film settles. The temperature and RH during drying influence the acryl film properties. Acryl films are thermo elastic, which means that they are flexible and therefore compensate dimensional changes better than alkyd films. Alkyd films paints harden and cause crack formation faster than acryl films when ageing (Raknes 1985). This cracking may result in greater water absorption. The pores of the acryl film are larger than of alkyd paints, which to minor extent causes greater water uptake. Combinations of the two paint systems are also common. Generally, modern paints do not penetrate significantly into the wood. A primer is commonly required to provide the desired protective treatment and adhesion. The wood should be primed prior to any UV-radiation decomposing the surface to have the best adhesion of the paint. Primed cladding boards are available on the marked. One should also prime prior to mounting in any case, in order to treat the overlap part and reduce the risk of rot in this area (Raknes 1985). The paint producer recommends painting all six sides of the board to keep the cladding board dimension stable (Aagaard 1992). Hjort (1997) found a strong correlation between wood rot and surface treatment. The best wood panels had several layers, impregnate, primer and paint.

Untreated wood dries out 20 times faster in the tangential direction compared to the radial direction (Tronstad 2002). This might lead to reduced durability and critical moisture conditions at the board ends. End sealing by intrusion of primer, or impregnate oils for end treatments, and following surface coating is of great importance (Hjort 1997). Proper maintenance of the end wood is also essential. Maintenance treatments should be performed with the same painting type as the original surface treatment. Maintenance paint must be performed on a surface clean and free of aged fibres (BDS 742.301).

2.2.8 Wood cladding trends

Modern residential houses and larger buildings are more frequently using wood as a façade material not only in the countryside but also in Norwegian cities. As mentioned earlier the change in the Plan and Building Act in 1997 provided the possibility of enhanced wood usage in multi-storey buildings. The wood is often left untreated and/or combined with other materials. Larch (*Larix sibirica*) is often used, it is known for its large share of heartwood. New façade types, liken baluster facades are introduced. Untreated façades are used in several projects due to reduced maintenance, the environmental perspectives, cost efficiency and design possibilities. Earlier, untreated wooden cladding was predominantly used for outhouses, boathouses and shelters, not for more prestigious buildings. Larsen and Mattson (2003) provide some guidelines for successful design of untreated wooden facades. They recommend using 100 % heartwood and that the façade should be mostly flat without projecting details. Figure 2.18 shows a new built school with untreated cladding.

The possibilities within known design recommendations do not limit the inventiveness. Traditional experience and knowledge is often neglected in the design of many modern wooden façades. Several damage cases on modern designs have been reported to SINTEF BI. Open joint cladding is gaining popularity. The smooth wall gives a desired tactile style and the shadow effect caused by the sunlight appearance is precious for architects. Nevertheless the open cladding increases reliability on the wind barrier which must be upgraded according to its new climate exposure.

New building materials are frequently introduced to the market. New technologies, changing architectural styles and new user conditions are reasons for the great range of possible façade materials and designs. Combinations of wood and other products provide a vast amount of alternative façades. With this liberal view towards wooden façade design a link to the old wood knowledge might result in durability.

Figure 2.18. Nardo primary school, opened autumn 2008. The cladding has been exposed for one year. Notice the discolourization to the left of the large window. (Photo: Egil Rognvik)

2.3 Numerical assessment of wood cladding hygrothermal performance

2.3.1 HAM tools

Several numerical simulation tools can solve energy and mass conservation equations and are able to calculate heat, air and moisture in building enclosures. The early heat, air and moisture, HAM, models solved 1D steady state heat flow by conduction and water vapour flow by diffusion (Glaser 1958). Now more sophisticated models which comprise more transfer mechanisms are available. The energy balance considers the heat flow by conduction, radiation and convection. The mass balance includes moisture flow by vapour diffusion and convection, and liquid transfer. The mass balance for air includes air flows driven by natural, external or mechanical forces. The basic transfer phenomena are standardized in NS-EN 15026. Transient HAM tools within individual building components were developed through IEA ECBCS Annex 24 (Hens 2002). When including air flow modelling in the HAM response it is possible to calculate the interaction between the air and the boundary material. If moisture and air flow are included in the energy optimization of buildings this can also provide more exact moisture-related risk assessment.

IEA ECBCS Annex 41 was formed “to deepen the knowledge about the integrated heat, air and moisture transport processes when the whole building is considered” (Janssens 2008). The Annex compared and further developed HAM tools for including all building elements in simulations (Hens 2003). Specific exercises on the material properties, transfer models and coefficients, and internal and external climates were performed. The results of the common exercises showed a lack of consensus in the material data (Rode and Woloszyn 2008).

Woloszyn and Rode (2008) introduced the term “granularity” to define the precision of numerical models for building enclosures. Granularity refers to the spatial discretization, the size and dimension of the computational cells used in building simulation tools. The range is from very fine to fine,

intermediate and coarse grained models. The ratio depends on the process type. Some transfer models require high discretization, but this is of course also dependent on appropriate accuracy and computational efficiency. Differentiation is made between air flow and HAM modelling in defining the granularity for the simulations. In Paper VI the air flow of the test house building is modelled in CFD, having a very fine granularity definition. The heat and moisture modelling in this thesis is performed with WUFI 4.0 and 4.2, a 1D HAM simulation, but it may include ventilation of the cavity behind the wood cladding. This makes WUFI fit the intermediate granularity definition, but to the point of fine granularity.

One challenge is computational capacity. More efficient computers could improve the granularity of numerical simulations. However, this may not be the weakest link of HAM simulations for the time being. To ensure good balance between the many physical phenomena that interact with each other is the main challenge in HAM modelling (Janssens et al. 2008). The coupling of wind flow and building materials are especially important, which underlines the need for the development of boundary layer physics. The results of HAM simulations rely greatly on the input of constructional geometry, material data and boundary conditions.

2.3.2 Boundary conditions

HAM simulations use the micro climate, the ambient surface climate, as a boundary condition. The coupling from the micro to the macro climate is a separate field within meteorology. However, much research within atmospheric boundary layers, especially in urban areas, is done within building physics. Common meteorological parameters are often logged in the proximity of developed areas, but climate data is not always available. Design reference years of different climates exist. The downscaling from the meteorological data to the building enclosure exposure according to measurements of precipitation, temperature, cloudiness and so forth are often included in simulation tools. The boundary layer is defined to be the layer in distance to where 99 % of the free stream velocity is lost, and this is where the heat and mass transfer mainly takes place. The convective surface film transfer coefficients for heat and moisture define the HAM processes in the boundary layer.

WDR is one of the main direct moisture influence parameters on façades. WDR is the amount of rain through a vertical plane. WDR hits the façade and the wind pressure forces the water into cracks and details. The WDR distribution on a façade is determined by the six parameters: (1) building geometry (including the environment topology), (2) position on the building façade, (3) wind speed, (4) wind direction, (5) horizontal rainfall intensity and (6) horizontal raindrop-size distribution (Blocken and Carmeliet 2004). An overview of Norwegian WDR research and the WDR measurements for the Voll test house is given in Paper I. The WDR measurements are published in the online database. One paper has used the database for the validation of CFD modelling of WDR and found that WDR from oblique winds is challenging to predict (Akubu et al. 2008). Blocken and Carmeliet (2007) demonstrate how standard hourly values of meteorological data are too poor to be used in WDR calculations on building façades. They propose using a weighted averaging technique instead of the usual arithmetic averaging that is used on meteorological data today. By using the weighted averaging technique hourly data may contain enough information to calculate WDR on building façades. Catch-ratio charts define the WDR for different positions on the building façade. In order to define the correct catch-ratio on a façade, measurements, semi-empirical methods, like the WDR standard EN 15927-3 or CFD calculations may be used. The calculation of WDR on walls is still time consuming in numerical tools, and simplistic models are often conservative. A comparison between the three most pronounced methods are provided in Blocken et al. (2008 a, b, c).

Other moisture impacts are for high RH and condensation. The time of wetness (TOW) defines periods with liquid water on the façade surface. Drying is also an important part of the moisture performance. Evaporation is found to be the main drying process. HAM simulations of absorbing

façade materials are sensitive to the value of the vapour transfer coefficient (Janssens et al. 2007). Wood cladding has a low absorption coefficient on its treated side, but this changes with ageing.

The energy balance has parts that are quite accurate and parts that are more uncertain. The heat conduction measured in a hot box may also include radiation and some thermal or forced convection. Radiation models are also based on extensive research, but when considering boundary layers there are still major uncertainties. An improvement of the long wave radiation model is included in the WUFI model but this requires climate data that are often not available. The convective heat and vapour transfer coefficients (h_c and β) are linked, and their reliability depends on h_c.

The air flow within building simulations greatly affects the influence of moisture. Convective heat and mass transfer and also WDR are dependent on wind properties. Ideal air mixing is an assumption that produces predictions that may deviate substantially from measured data. The air velocity is often included in a simple way to the heat transfer coefficient. Blocken et al. (2008) point out weaknesses of the use of h_c, it is usually only defined for one point on the façade, even though it may vary across the façade between almost 0 and 6.

The cavity flow of a façade has been studied by several researchers, and it is proven to be complex. Andersen (2000) gives a review of the physics of a ventilated cavity and describes a calculation model for the estimation of airflow in ventilated cavities under different conditions. Several mathematical methods and computational programs have been developed to calculate the ventilation gap in two stage-tightening façades. However, Andersen (2000) did not find any adequate models. Piñon et al. (2004) state that the nature of the airflow within the cavities has yet to been developed and accepted.

2.3.3 Assessing material data for simulation input

Standards define the measuring procedure for most material properties needed for HAM simulations. Such as for thermal conductivity, specific heat capacity, radiation constants, sorortion curve, suction curve, surface roughness.

Annex 41 had a round-robin test of vapour permeability and hygroscopic adsorption/desorption on painted and unpainted gypsum boards. The different laboratories had large differences in their measurements. The differences were mostly linked to uncertainties around the measurement technique. Gypsum is rather tricky due to chemically bound water molecules that are easily dried at too high temperatures (Roels 2008).

Wooden cladding material properties are limited in the literature. Wood is an orthotropic material with large standard deviations, even within material samples of one single board. When applying paint, aspects like film thickness, number of layers and drying periods in between, climate during coating and drying preconditioning, workmanship and more, are also present.

2.3.4 Post processing - assessing risk for decay

The result of a HAM simulation is transient temperature and moisture conditions for the material studied. These results may be used directly to define and compare performance. However, for enhanced basis of comparison and understanding, post processing is often carried out to define the risk of mould, fungi or algae growth or other decay which may occur in a period of service life. Insects and bacteria also decompose wood.

First one must define the critical level fr the organism studied or the growth activity of different species mixed. An example of is shown in Figure 2.9. Critical level may only have RH or MC, but often temperature is included. Another important factor is the time, both for initiating growth and for

further growth. Some models even include the reduction of growth when the maximum growth is closing up (Ojanen et al. 2008).

In this work a simple model used to compare calculated cladding performance is used. An hourly moisture temperature response parameter (MTR) is deduced from Kumaran et al. (2002) in equation 2.1.

$$MTR = \sum_{i=1}^{h} (MC_{FD} - 20) * (T_{NMI} - 5) \qquad 2.1$$

for $MC > 20\ \%\ by\ weigth$ and $T > 5\ °C$

More advanced models are available on mould growth. Sedelbauer (2001) defines isopleths and plots the calculated surface moisture and temperatures values in a diagram. Values above the isopleth lines indicate the risk for mould growth. This model is included in WUFI Plus and WUFI Bio. Ojanen et al. (2008) calculate a more complex mould growth index which also takes into account the period of critical conditions. A simplified version of this calculation is used in the report on the Voll test house measurements Geving et al. (2006).

The models define the risk for growth and not the actual growth. Several uncertainties are present, most pronounced is the choice of critical level. For simulations the inaccuracy of the HAM model is also present. Much more research is required in this area.

3 Wood cladding test house study

The aim of the test house study is to increase our understanding of the relation between microclimatic conditions and hygrothermal response of the wooden cladding. This chapter describes the test house study objective and limitations, location and experimental set up, measurements details, sensor calibrations and material properties. Results from the test house study are presented in Chapter 4.

3.1 Test house study objective and limitations

An extensive wooden cladding investigation was initiated on a test house at the SINTEF BI and NTNU field station. The data collection ran over four years. The investigation aimed to describe the influence of;

- façade orientation; east or west,
- cavity behind cladding (rain screen),
- degree of cavity opening (ventilation rate),
- surface treatment (untreated or white alkyd and acryl paint),
- wood quality (fast and slow grown Norway Spruce),
- roof overhang
- variation over height and
- temperature relations.

In addition to the test variables listed above there are a number of factors that also may influence the wooden cladding moisture response. The following factors were recognised as potentially interesting, but were not included in the study in order to maintain a workable test matrix:

- surface treatment colour, pigmented paint was excluded. Most buildings are painted with pigmented paint in order to increase the cladding temperature to potentially kill fungi growth during the warm period. White paint is considered “worst case”.
- cladding board orientation, only horizontal cladding is tested
- ageing effect. Most research projects must be completed within a relatively short period of time. Some paint manufacturers have a twelve year guarantee. To investigate the development of the

paint and the wood MC up to maintenance level would provide insight according to for example service life analysis.

In order to analyse the parameters of interest, moisture content and temperatures were monitored in several cladding assemblies. The local- and microclimate was simultaneously recorded. The microclimate refers to the local atmospheric zone surrounding the cladding, in this case the climate around the test house building.

3.2 Test house location, surrounding topography and geometry

The field station Voll is located in an open field, 4 km southeast of the city centre of Trondheim. Located 10° 45'35'' E 63° 41'07''N, 127 m above sea level. Figure 3.1 shows an orthographic map of the Trondheim area and the location of the test station. The harsh climate on the coastal parts of Norway seldom provide shielding to buildings, apart from neighbouring buildings. Houses in the inland of Norway are more often shielded either by topography and/or surrounding vegetation. The climate of the test station is considered moderately harsh in relation to normal climate in Norway. Trondheim is somewhat shielded from the ocean by the Fosen peninsula and the hills of Bymarka. The worst climatic conditions, providing high moisture stresses to the building envelopes in Trondheim, are expected to occur when the wind is blowing from the ocean side, from southwest. This wind is often supplemented by precipitation.

An outline of the test station with its buildings is shown in Figure 3.2 a and b. Three buildings are located at the station; the main flat-roof test building, a small logging building and a sloped-roof rotating test building. The north-west corners of the buildings are indicated with A, B and C. The building façades of the fixed buildings A and B face the cardinal wind directions. The flat-roof test building A has test cladding on its east and west facing walls. It is a block-type building with dimensions LxBxH = 11.3 x 4.8 x 4.3 m³. The roof overhang length is 340 mm. The test station is secured with a hurdle fence. The meteorological masts D, E and F rise 0.3 m above this fence.

The test station is suitable for building physics field studies. It is situated in an open field, exposed to wind, WDR and solar radiation. This exposure gives stresses, moistening and degradation. In addition, the test station is located in a relative densely populated area. Figure 3.3 presents panoramic views of the surrounding terrain. The open field to the west and the south provides the most severe exposure of the building. The east facing side of the test house is somewhat shielded by the hill and the rotating test house, which blocks the morning sun radiation, as seen in Figure 3.3. This façade is also less exposed to WDR because the prevailing wind direction is south-west.

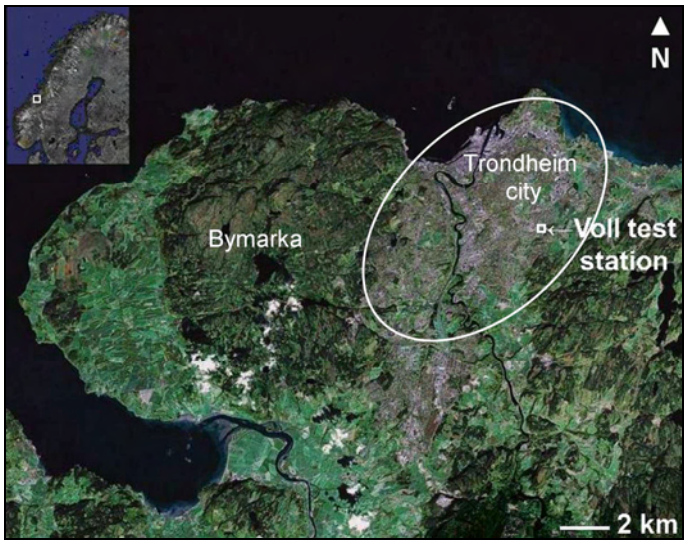

Figure. 3.1. Orthographic map of test station location in Trondheim. The mainland of Norway, defining the Trondheim map section, is in the upper left.

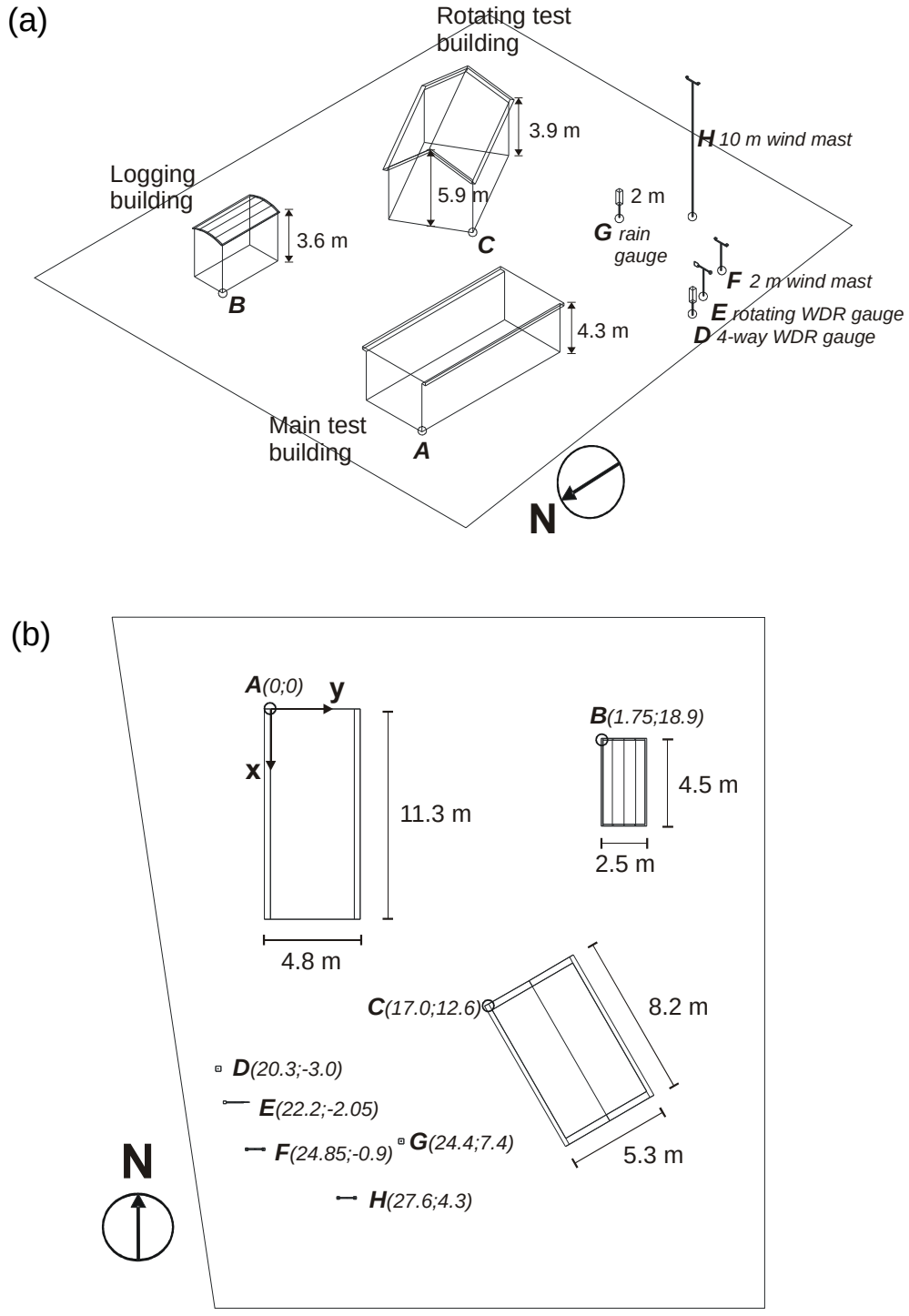

Figure. 3.2. The SINTEF BI and NTNU field station: (a) Perspective view and (b) top view with indication of the building dimensions and the location (x, y coordinates) of the buildings and measurement equipment relative to point A (north-west corner of the flat-roof test building) (in m).

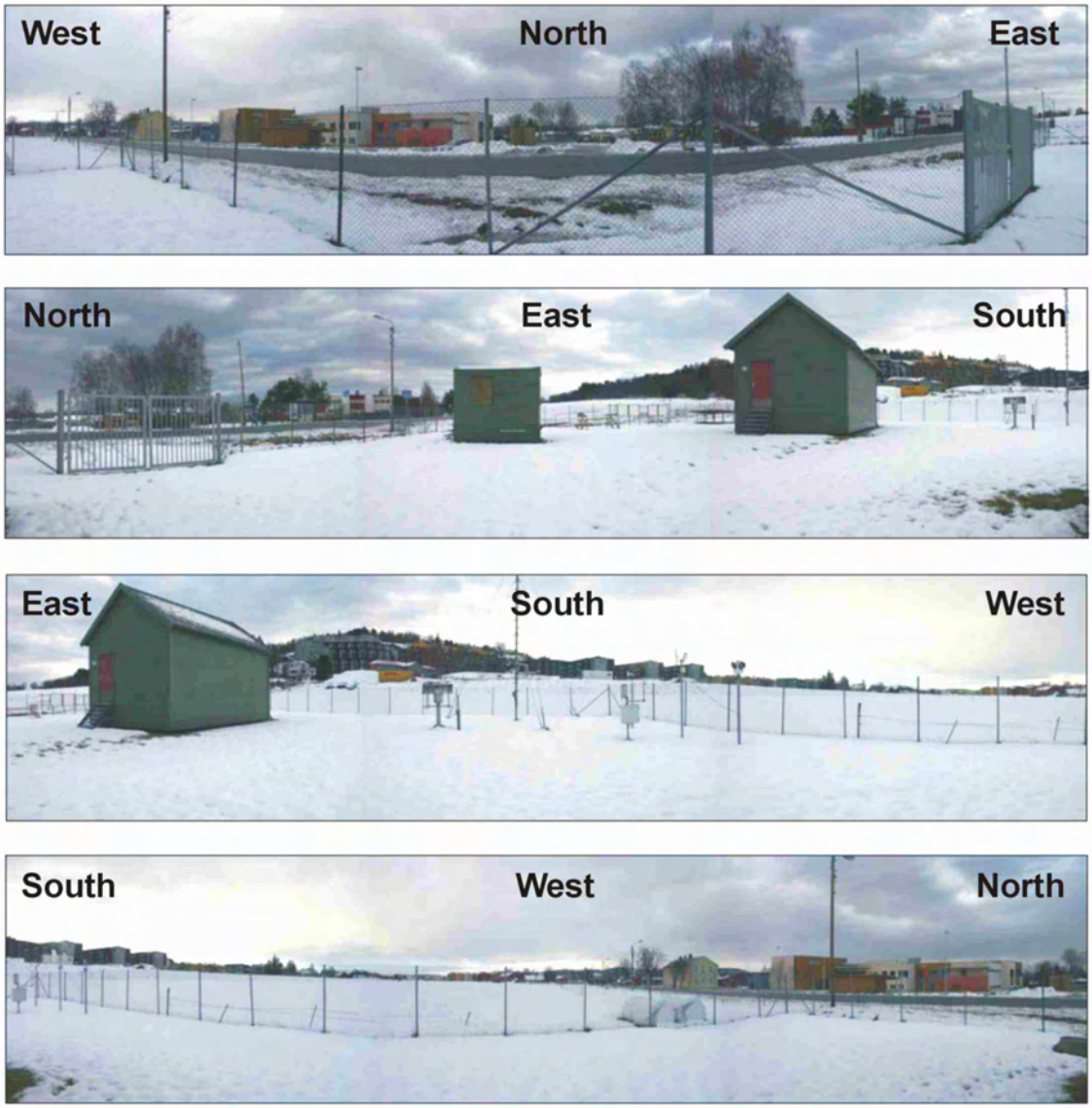

Figure 3.3. Panoramic photographs of the surrounding topography of the flat-roof test building for the cardinal directions.

3.3 Meteorological measurements

The Norwegian Meteorological Institute (NMI) runs an automatic weather station at the field station (station number: WMO 257). A 10 m mast is placed in point H in Figure 3.3, and a 1 m horizontal rain and snow gauge is placed in point G. The meteorological station measures the most common weather parameters by a Milos 500 Vaisala automatic weather station. Nine weather parameters are at present measured at the Voll weather station. The station has yearly inspections. Each sensor is sampled every second, but the storage rate is mainly averaged value every 10^{th} minute. Table 3.1 summarizes the meteorological parameters used in the cladding investigation, the meteorological abbreviations, sensor trade names and sensor height. Mostly hourly values are used for cladding response correlation analysis.

This cladding investigation also included three 2 m high meteorological masts. These masts have wind velocity and direction, WDR in the cardinal directions and one rotating WDR gauge. Temperature defines the energy level of masses. The air temperature, T_{NMI}, has a tolerance of ± 0.5°C, measured at inspections. Global radiation, QO_{NM}, is sun radiation incidence on a horizontal plate.

Table 3.1. Meteorological measurements used in the cladding analysis (from NMI). When data from the meteorological station is used the subtext $_{NMI}$ is added, except for the precipitation.

	Met. Abbr.	Unit	Sensor	Sensor trade name	Height of sensor (m)
T_{NMI}	TAM	℃	Air temperature – average last hour	Vaisala H DP 35D	2
	QO	W/m^2	Global radiation – accumulated last hour	Kipp & Zonen CG 1	2
	QL	W/m^2	Long wave radiation – accumulated last hour		
RH_{NMI}	UUM	%	Relative humidity – average last hour calculated from dew point temperature	Vaisala HDP 35D	2
θ_{NMI}	DM	°	Wind direction – average last hour	Vaisala WAV 151	10
U^{10}_{NMI}	FM	m/s	Wind velocity – average last hour	Vaisala WAA 151	10
	RT	#	Number of minutes precipitation last hour	Vaisala DRD 11A	2
	RR	mm	Increase in rain gauge last hour	Geonor	2
P_{NMI}	POM	Pa	Pressure - average last hour		2

NMI provides wind data in 10 m height. A heating element prevents the wind sensors from frost. Wind velocity is measured by a cup anemometer with a measurement range of 0.4-75 m/s and an accuracy of ± 0.17 m/s. The wind direction is measured by a wind vane with a starting threshold is < 0.4 m/s and resolution is 5.6°. The accuracy is better than ± 3° according to (Vaisala 2008). RH is measured by dew point temperature and then calculated (compared to air temperature. The tolerance of ± 2% is found at the last inspections. Pressure is measured with a tolerance of ± 0.2 hPa.

The test station has additional wind measurements 2 m in height, marked F in Figure 3.3. This is a Campbell Young 05103-5 Wind Monitor. The propeller is accurate within ± 2% and the wind vane is calibrated to have accuracy within ± 5°. The rotating WDR gauge, marked E in Figure 3.3 also records wind direction. The two do not always agree due to larger rotation inertia of the rotation WDR gauge. Figure 3.4 depicts the 2 m wind masts. When studying the wind profile approaching the test building the 2 m wind measurements are vital. This profile is used in CFD simulations performed in Chapter 5.

The precipitation gauge of NMI, G in Figure 3.2, uses weight to record quantity of precipitation in millimetre water equivalent. This gauge includes a heating element to include precipitation in solid state; snow, hail and sleet. A blend of methanol, ethylene glycol and oil is added in the precipitation measurement container to prevent evaporation. The accuracy is within ± 0.5%. Precipitation measurement equipment is also added as a part of the cladding investigation. Both normal precipitation, free field WDR and WDR reaching the wall is measured. Here liquid water is measured by a tipping bowl system, see Figure 3.6. Calibrations of these tipping bowls have been carried out by infusion, see Figure 3.5 b. The tipping bowls have been calibrated twice during the four year measurement period. An error analysis of the tipping bowl system is included in Paper I. The minutes with precipitations are registered and referred to as RT. This parameter allows accurate definition of the rain intensity when dividing precipitation amount on minutes the time it occurred. This parameter is used in WDR simulations validated with the Voll measurements (Akubu et al. 2008).

WDR is measured as quantity of rain through a vertical plane, mm/m^2 or l/ m^2. It is a complex parameter, depending on the precipitation amount, wind velocity and wind direction in addition to surrounding terrain, obstructions and building geometry. However, it is the most direct parameter to describe the moisture load on the walls. Two WDR free field gauges are mounted at the test station; situated at points D and E in Figure 3.2. The rotation WDR gauge is shown in Figure 3.4, and the gauge measuring WDR in the cardinal directions is shown in Figure 3.5 a. Figure 3.5 b shows the wall WDR gauges with the infusion set measuring accuracy. Paper I thoroughly describes the WDR measurement set up. There has been a problem with ice in the tipping bowls, see Figure 3.6 a and b. This error might occur whenever the air temperature sinks below 0°C. WDR measurement data are filtered according to this criterion; removing WDR registrations when the temperature is below 0°C. WDR may be calculated from the meteorological parameters precipitation, wind velocity and wind direction.

Figure 3.4. Wind measurements, the propeller measures wind velocity (m/s) and the two vanes measure wind direction (in degrees). The rotating WDR gauge at the back measures WDR in the main wind direction.

a) ***b)***

Figure 3.5. s a) Free field WDR gauge in the cardinal directions with a normal precipitation gauge on top, and b) WDR gauges on the test house wall. This also shows the accuracy investigation by infusion bags.

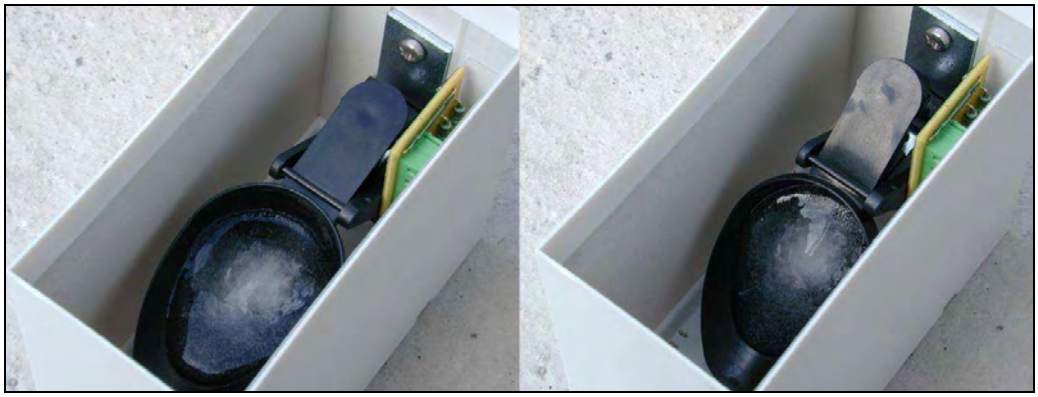

a) ***b)***

Figure 3.6. WDR tipping bowl a) ice in bowl and b) tipped bowl due to the weight of the ice. The ice prevents the bowl being emptied.

3.4 Wall sectioning and instrumentation of test house cladding

The methodology of recording hygrothermal cladding performance by MC and temperature was developed in the 1980s (Iván 1993).

3.4.1 Experimental set-up

The east and west façades of the test house are clad with nearly identical claddings in 14 full height test sections on each side. The following parameters are varied: growth rate of wood, surface coating and ventilation gap opening.

The test house has a steel frame with interchangeable wall and roof elements. The wall elements are insulated timber frames with an internal 12 mm chipboard, 0.2 mm polyethylene vapour barrier, 150 mm mineral wool insulation, 12 mm gypsum wind barrier, 23 mm cavity and a 19 mm wooden cladding as the rain screen (shown in Figure 3.9). The U-value of the external wall is approximately 0.29 W/(m^2K). The interior air temperature is monitored to be 20°C.

Overviews of the test sections are given in Figure 3.7 and Figure 3.8, where the location of the WDR rain gauges is also seen. Letter codes define variant type and placing of measurement sensors in these Figures. The following codes are used:

M	moisture content sensor
T	temperature sensor
RH	relative humidity sensor in the cavity
w	surface wetness sensor
A	painted with an alkyd (oil based) painting
B	painted with an acryl (water based) painting

When no paint type code is given, the cladding is left untreated. Numbers 0, 4 and 23 indicate cavity openings in mm: 0 = no opening, 4 = small opening and 23 mm = full opening. A number in front of sensor type indicates that the profile is measured as shown MC_L in Figure 3.9 b.

Figure 3.7. West-facing wall of the test house. Letter codes indicate design, material qualities and instrumentation of the different sections. 8 WDR gauges are mounted on this façade.

Figure 3.8. East facing wall of the test house. Letter codes correspond to Figure 3.7.

Details of the cladding boards, test section assembly and location of sensors are shown in Figure 3.9 a-c. The test claddings are horizontally fixed boards of Norway spruce (*Picea abies L. Karst*). The wood claddings (rain screens) are assembled by a series of boards fixed to support battens, designed to allow uninterrupted drainage and ventilation of the gap behind the cladding (see Figure 3.9 c). The double fold, the planing in upper and lower part of the panel boards, provides a flat back side. Two identical test sections are mounted on the east facing side, E1S and E2S.

The timber was cut, sawn and planed in summer 2003 and the test cladding sections were erected in September/October 2003. An initial phase with trials and errors was needed prior to the official start of cladding measurements on January 1st 2004. This initial period explains why the MC of the test cladding starts out at different values.

The experimental investigation includes a total of 102 moisture sensors, 94 temperature sensors, 6 RH sensors, 3 normal precipitation meters, 16 WDR gauges, 3 wind direction sensors, 2 wind velocity sensors and 1 radiation sensor. The most heavily instrumented façade is the weather-beaten west facing wall of the test building. All data are collected on an hourly basis, as a result of 5 sec, 1-minute or 10-minute instant values or sums, which are averaged or summed over each hour.

The cladding surface treatments are either an oil dilutable alkyd painting (Trade name: Drygolin Extrem Oljedekkbeis, “A” in Figures 3.7 and 3.8) or a water dispersed acrylic/alkyd painting (Trade name: Jotun Demidekk Optimal, “B” in Figures 3.7 and 3.8). At first all cladding boards were treated with a primer, based on penetration alkyd oils and reinforced with zinkoktoat (Production name: Jotun Visir). The first paint layer was applied in laboratory climate (50 % RH and 22°C). The last paint layer was applied after the cladding was mounted and covered the screw fixation points. The surface treatments were performed by a professional painter. Three test sections were left untreated. All painted sections are white, which gives the least absorption and emission of radiation. This also provides the most stable cladding MC.

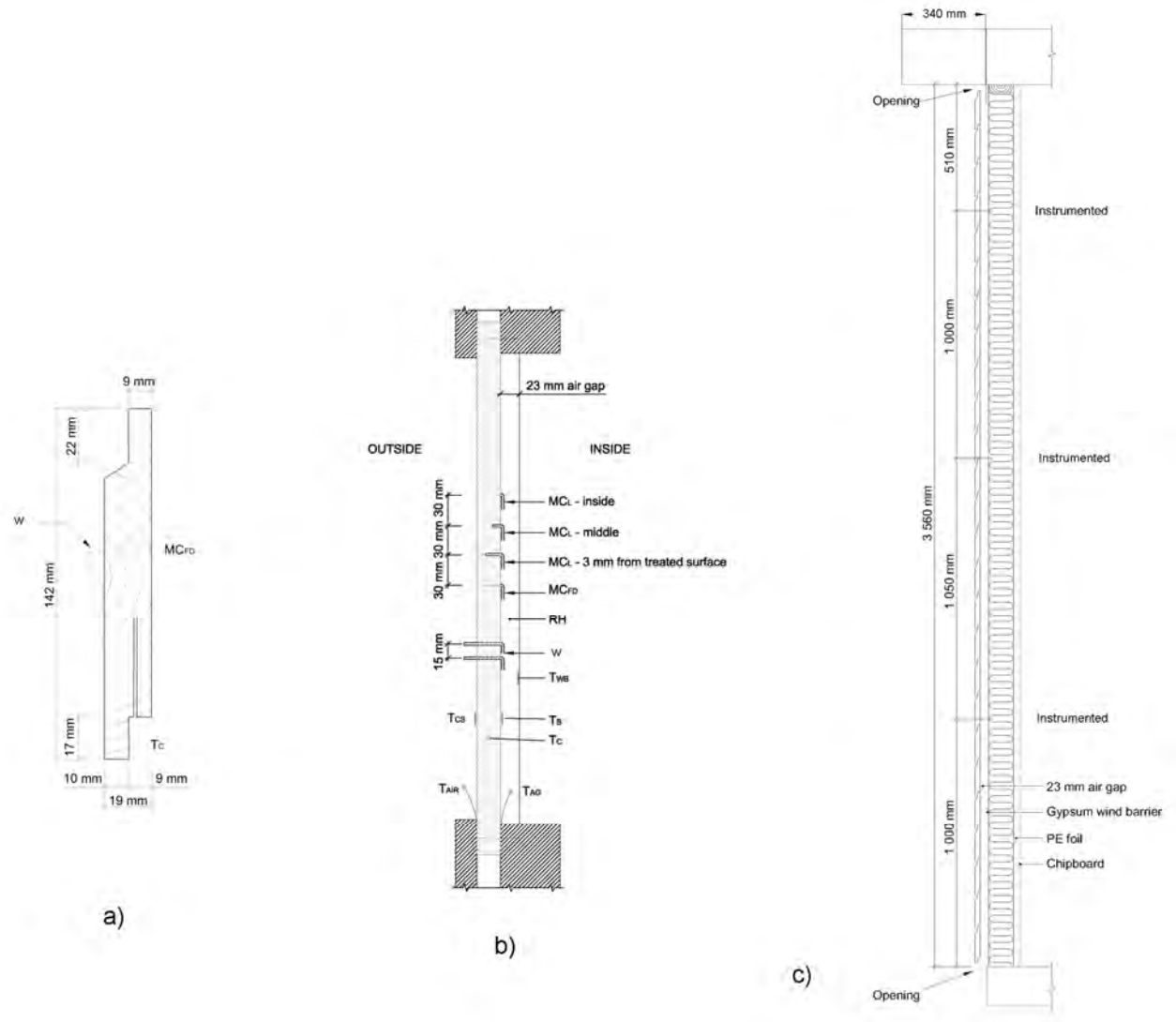

Figure 3.9. Details of test sections and claddings.
a) Vertical section of cladding board with temperature, MC and w sensor.
b) Horizontal section of test cladding, location of temperature, MC, w and RH sensors.
c) Vertical section of full cladding test section showing wall assembly and instrumentation heights.

3.4.2 Measurement sensors

RH is measured in the cavities behind the cladding with a Vaisala HMP233 sensor. RH sensor 1 was moved from measuring the test house indoor climate and mounted in section W3S in March 2004. Four additional RH sensors, 2-5, were supplied in January 2005. The five sensors were mounted in the test sections E1N, E3N, W1N, W2S and W2N, shown in Figure 3.10 and in Figures 3.7 and 3.8. All RH sensors have been mounted in the middle of each section. The RH sensors were calibrated when mounted. A new calibration was made in March 2008. The sensors were conditioned in a climate chamber and correlated to the reference RH sensor of SINTEF BI. A falling drift was detected, 9.8 % for RH sensor 1 and 3.4 % for RH sensors 2-5. The RH_{CAV} measurements are linearly corrected for this drift by interpolation.

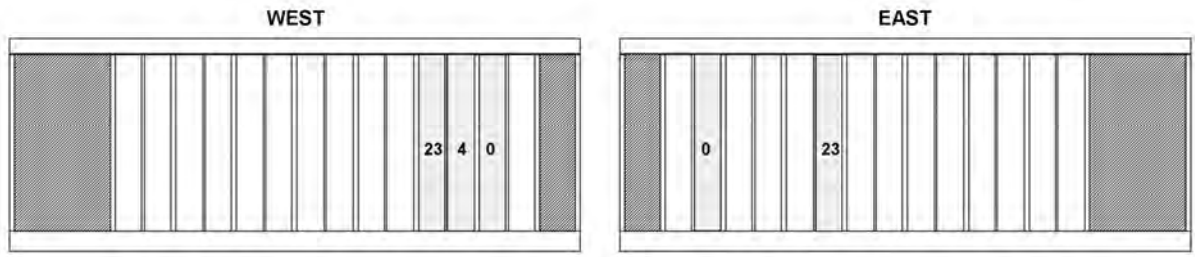

Figure 3.10. The sections with RH measurements.

The wetness on the façade is measured by mounting moisture pins directly on the cladding surface, w in Figures 3.8 and 3.9. The w sensors were mounted after the primer and first paint layer were applied. The last paint layer ensured surface contact. Heat shrinkable tubing protects the sensors from cladding contact in the bushing. The sensor is shown in Figure 3.11. Paper III discusses TOW measurements in comparison to WDR. TOW is defined as the hours that the MC is measured higher than the MC in the wood. A refinement of the TOW sensor is done in this thesis, TOW is defined below a critical limit, see Equation 3.1. Defining the limit k_{TOW} should be done to correspond to the registered WDR and calculated condensation. The critical level of TOW is defined for the west facing side; $k_{TOW} = 1$, and east facing side; $k_{TOW} = -3$.

$$TOW = w + k_{TOW} \geq MC_{FD} \qquad 3.1$$

The wood MC is defined as the weight of moisture (water) per dry weight of the material. In this project wood MC is measured by the electrical resistance between two steel pins. The measurements are adjusted according to wood species and temperature. The accuracy of the moisture pins measurements has been a point of discussion. Standards ASTM D 4444-92 and NT BUILD 302 both present the relative error of moisture pins within 7-25 % MC range, after temperature and species are corrected, to be 7 % in a 95 % confidence interval (0.5 – 2 % MC). Values outside this range have larger tolerance. Measuring the wood moisture profile, as intended by the MC sensors at different depths (see Figure 3.9 b), was not possible in coated wood cladding. The wood cladding boards are too slim and the surface treatment interferes with the electrical resistance measurements. Paper II addresses the accuracy of the MC sensor and the moisture profile measurements in this project. The variation measured within each MC sensor is more precise. These variations are used in the trend analysis in Section 4.4.

The test cladding has temperature sensors in the cladding, on the cladding surfaces and in the air close to the surface. The latter is shielded by tinfoil, as shown in Figure 3.9 b. The temperature sensors were mounted after the primer and first paint layer were applied. The last paint layer also coated the temperature sensors; see Figure 3.11 b. Temperatures are measured by a compensation cable and thermo element copper/constantan, type T. The temperature measurement accuracy is ± 0.5°C in the temperature range [-59 to 93 °C].

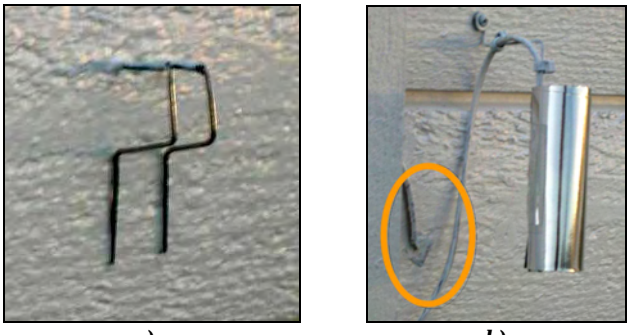

a) ***b)***

Figure 3.11.a) Wetness sensor, w, mounted on the cladding. b) Temperature sensors on the cladding surface T_{cs} (in oval frame) and proximity air measurement T_{AIR} (shielded in tinfoil).

3.4.3 Improvements of future test house instrumentation

After a project is finished there is a tendency to discover how the test set up could have been improved. The planning of the cladding investigation was completed prior to this PhD project. Improvements of the test house set up could have been:

- Randomizing the test section placing on each wall orientation, to get more independent results. In building physics WDR research illustrates different wall exposures. Most WDR is found on the corners and edges on buildings, known as "corner effects". This gives dependency on wall section placing, and it could have been minimized quite easily.
- Testing of methodology on moisture profile measurements. The moisture transport in the wooden cladding was indented to be monitored, this was proven not to work, this cost some extra effort to instrument and redundant measurement data have been stored throughout the four test years. See Paper II.
- Air flow monitoring by pressure gauges or hot wire instrument would have provided valuable data.

3.5 Material properties

This section describes the material origin and properties. The material properties are needed to analyse and calculate HAM transport of wood cladding.

3.5.1 Wood origin and selection of boards for instrumentation

Wood origin is a point of discussion regarding the large deviation within this organic material. In order to reduce the sources of deviation some precautions have been taken. The wood was cut in the spring 2003. Each cladding board is carefully marked with tree of origin. The trees were growing in a known place. The timber is sawn at Aavatsmark Saw in the county Nord-Trøndelag and planed in Spongdal, in Trondheim municipality. The information on wood origin is not utilized in this work.

The same plank was used for several instrumented boards in order to diminish measurement errors. That is four planks in total; one slow and one fast grown on the east and west facing walls. The plank was split, planed, treated (primer and first paint layer) and cut in test board length. The mean length of cladding board is 585 mm, with standard deviation 0.6 mm. Original planks exceeded five metres, giving about 16 test boards for each plank. Boards with failures such as visible amounts of wood resin or twigs were discarded.

3.5.2 Density

For each of the 60 test cladding boards selected for instrumentation; weight, length and MC were measured. The mass, m, was measured on a scale with 0.01 gram tolerance and the volume, V, was measured by multiplying the end section area and the board length. The MC of the cladding boards was measured by electrical resistance, following NS-EN 13183-2. The average dry densities of the instrumented cladding boards are presented in Table 3.2.

Table 3.2. Densities and standard deviation of the instrumented boards in the cladding investigation.

	Fast grown		Slow grown	
	West	East	West	East
Density (kg/m^3)	377 *	374	438	469
Standard deviation	14.5 *	12.0	13.9	25.0

*Measured gravimetric in October 2006 then with density 398 kg/m^3 and standard deviation 19.0.

In October 2006 the instrumented boards of section W6N, with fast grown wood, were taken down to perform a gravimetric check. The gradient measurements of the moisture pins were analysed as described in Paper II, by NS-EN 13183-1. The density was found to be 398 kg/m^3, almost 6 above the first measurement. This method has a more exact volume measurement due to lowering the wood pieces in water on a weight scale and also more exact MC measurement, also by weight. The density is probably underestimated for the slow grown wood as well.

3.5.3 Sorption curves

In HAM calculations the correct moisture capacity of the cladding must be known. The sorption curve of the wood provides this information. Sorption refers to the action of either absorption or adsorption, and is the equilibrium MC different RH. The difference between sorption and desorption is called hysteresis. Sorption is measured according to NS-EN ISO 12571. Desorption is not measured in this work.

Two cladding test boards of each growth rate were measured. Standard deviations for the measurements were 0.1 for slow grown wood and 0.4 for fast grown wood. Figure 3.12 shows the measurements and three sorption curves from the literature. Densities and temperatures during measurement in this and comparable work are given in Table 3.3. The measurements from this work are higher than the earlier measured sorption curves, but within an acceptable range. Slow grown was slightly higher than fast grown wood.

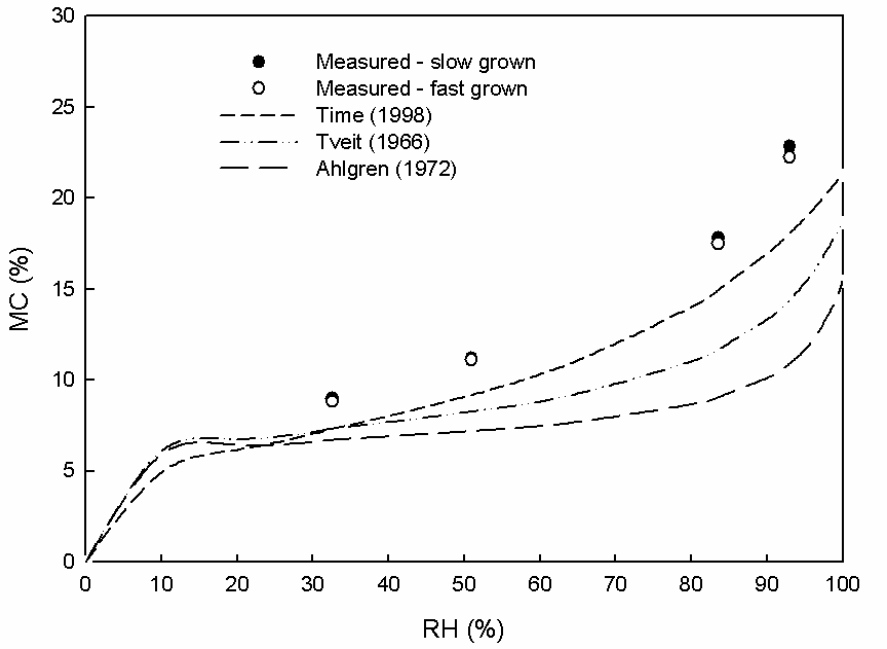

Figure 3.12. Sorption curves of Norway Spruce (Picea abies).

Table 3.3. Densities and temperatures during sorption measurements, corresponding to Figure 3.13.

	Tveit (1966)	Ahlgren (1972)	Time (1998)	This work; Fast grown	This work; Slow grown
Density (kg/m^3)	410	420	390	375	454
Temperature (°C)	25	20	26	23	23

3.5.4 Diffusion resistance factor

The water vapour diffusion resistance of the paint layer is needed for HAM calculations. This is measured in accordance with the standard NS-EN ISO 12572 (2001). Figure 3.13 shows the measured mean values of this analysis. The test samples were retrieved from boards of test sections W2N, W3S, W4S and W4N in 2006 after three years of ageing. The S_d values are as expected, highest for the oil based paint; 2.8 m (st.dev. 0.23 m) and water based paint; 1.6 m (st.dev. 0.15 m). Untreated wood is 0.18 m.

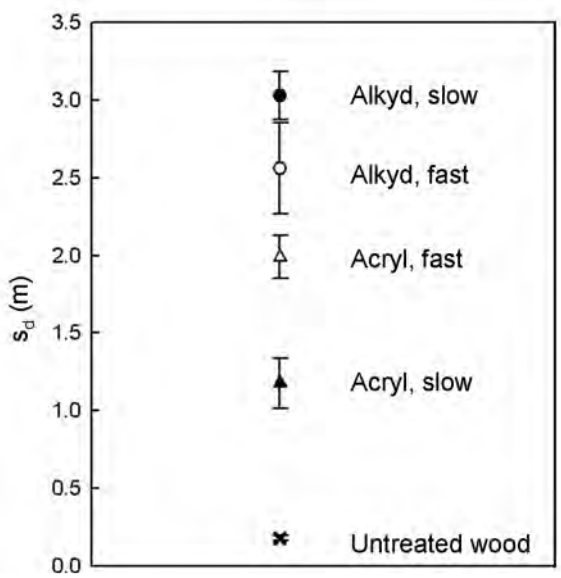

Figure 3.13. Measured mean s_d values of alkyd and acryl based paint on slow and fast grown spruce with error bars showing the standard deviation.

4 Analyses of Voll test house data

This chapter presents the analyses of the measured data from the Voll test house. The measurement methodology is described in Chapter 3. Four years of monitoring (2004-2007) are analysed. A description of the ambient test house climate is given in Section 4.1. Three main analyses are performed on the measurement data in this chapter. First in Section 4.2, all sensors are included in analyses of the entire measurement period by yearly and monthly averages. Section 4.3 gives a closer look at one wet and one dry week in order to study the hourly correlation of climate data and cladding MC response. In Section 4.4 MC trends of four day periods with uniform weather types are used to analyse the different cladding parameters. The papers relevant for this analysis chapter are Paper III and Paper IV. Additional papers using Voll data measurements are summarized in Appendix 3. The conclusions from all publications from the test cladding at Voll are presented in Section 4.5.

4.1 Climate in the measurement period

The measured climate at the Voll station is described in this section. Table 4.1 states the normal, the yearly and total mean values for precipitation, T_{NMI} and RH_{NMI} for the four test years. The normal is from the period 1961-1990. The mean temperature of the measurement years generally exceeds the normal by 2°C. The latitude of Trondheim gives long winter nights and long summer days, providing a strongly seasonal climate, usually with snow covered winters and warm summers. This is reflected in the monthly temperatures in Figure 4.1. Normal precipitation of Trondheim is 885 mm/year, which means that 2004, 2006 and 2007 were wet. The correlation between RH_{NMI} and precipitation is 0.68, this is seen in Figure 4.1. Generally Trondheim has dryer spring periods, with less precipitation and lower RH_{NMI} compared to the autumn periods.

Table 4.1. Yearly mean values of T_{NMI}, RH_{NMI}, and the precipitation sum. The normal values are included. Total and standard deviations for the measurement period are also calculated.

	T_{NMI} (℃)	RH_{NMI} (%)	Precipitation (mm)
Normal (1961-1991)	4.1	-	885
2004	6.2	71.9	982
2005	6.3	73.1	829
2006	6.9	71.0	1000
2007	6.0	74.1	1277
2004-2007 mean	6.3	72.5	4088
St.dev.	7.2	14.6	-

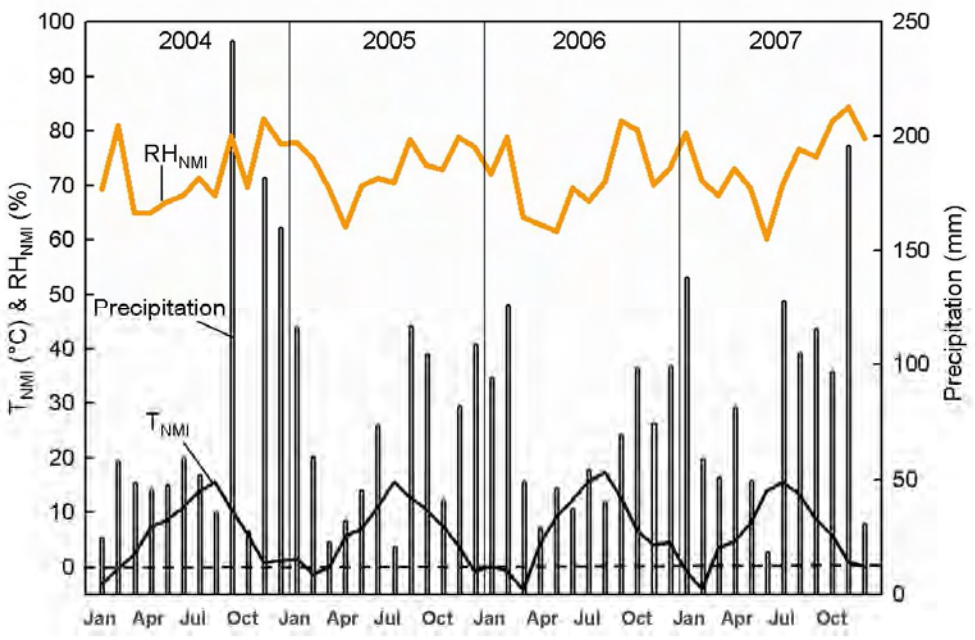

Figure 4.1. Monthly mean values of T_{NMI} (°C), RH_{NMI} (%) and normal precipitation (mm) in the measurement period.

Figure 4.2 shows the frequency of the wind velocity in total and for hours with rain. The mean wind velocity at 10 m height is 2.6 m/s in the measurement period. The mean wind velocity for wind with rain is 3.1 m/s. Figure 4.3 shows the wind rose, describing the frequency of wind in each wind direction. The wind is mainly blowing from southwest. Few winds come from north and southeast. This might be partly due to shielding from the hill and the trees in these directions, as seen in the panorama view in Figure 3.2. Wind, and wind and rain combined, are shown by the solid lines in Figure 4.3. 26.7 % of the hours in the four test years had rain. When there is rain the wind has a minor shift to the west, the wind with rain comes on average from the southwest, 225°. The wind influence is greater on the west facing side, which is mostly upwind; whereas the east facing wall is usually in the wake, as seen in Figure 4.3.

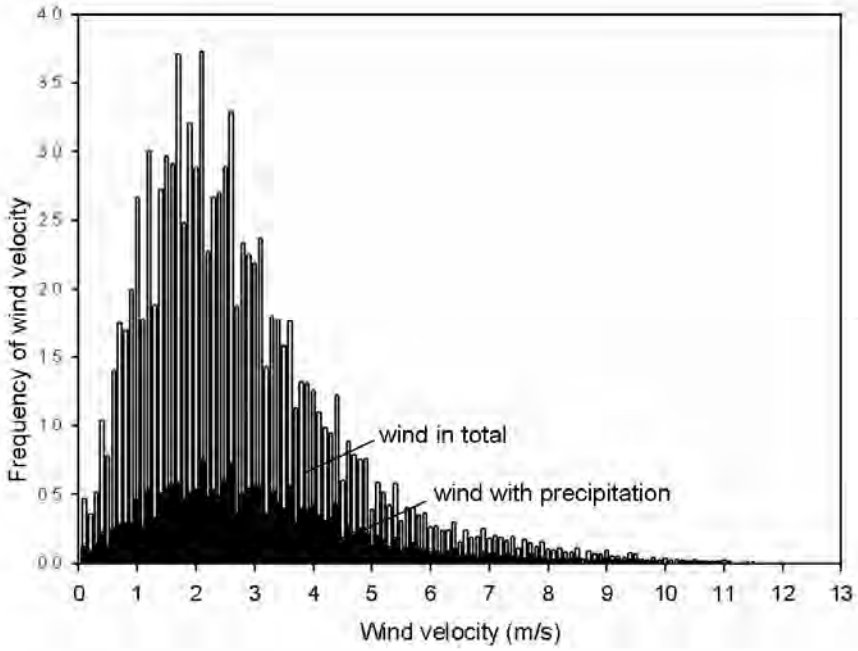

Figure 4.2. Frequency of wind velocity in total and only wind in combination with precipitation.

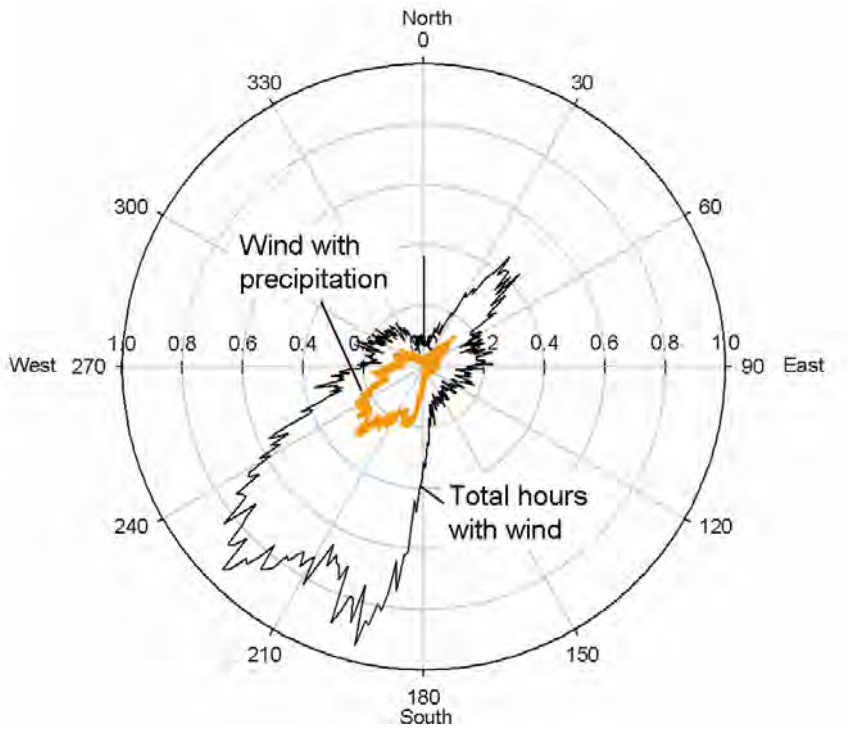

Figure 4.3. Wind rose showing frequency of wind direction in the measurement period 2004-2007. The black line represents the total hours and the orange line represents number of hours with precipitation.

4.1.1 WDR and TOW

Wind-driven rain (WDR) is considered a major reason for cladding deterioration. WDR provides liquid water on the cladding surface, which enables capillary transport into the wood substrate. WDR has been carefully monitored in this project. The WDR measurements at Voll are fully described in Paper I. Table 4.2 and Figure 4.4 show the accumulated free field WDR data in the four cardinal directions for each year. The yearly values of WDR data in the four cardinal directions reveal that almost half of the total fallen precipitation has a western wind drift. About 1/5 has a southern wind drift. The east oriented wall receives small amounts of WDR. An s-form in Figure 4.4 shows that midsummer often has the lowest WDR amounts, and an increase of WDR is found in the autumn periods. Large amounts of WDR are found in the winter periods. Periods with temperatures below zero are filtered out, but recorded WDR might be drifted snow melting in the warm weather following a cold period or snow which may also occur with warmer air temperatures.

Table 4.2. Yearly avereage values of precipitation and free field WDR (mm) in the measurement period.

	Precipitation	WDR-west	WDR-south	WDR-north	WDR-east
2004	982	544	263	71	16
2005	829	520	188	103	19
2006	1000	420	199	78	54
2007	1277	540	235	97	27
2004-2007 total	4088	2024	885	349	116

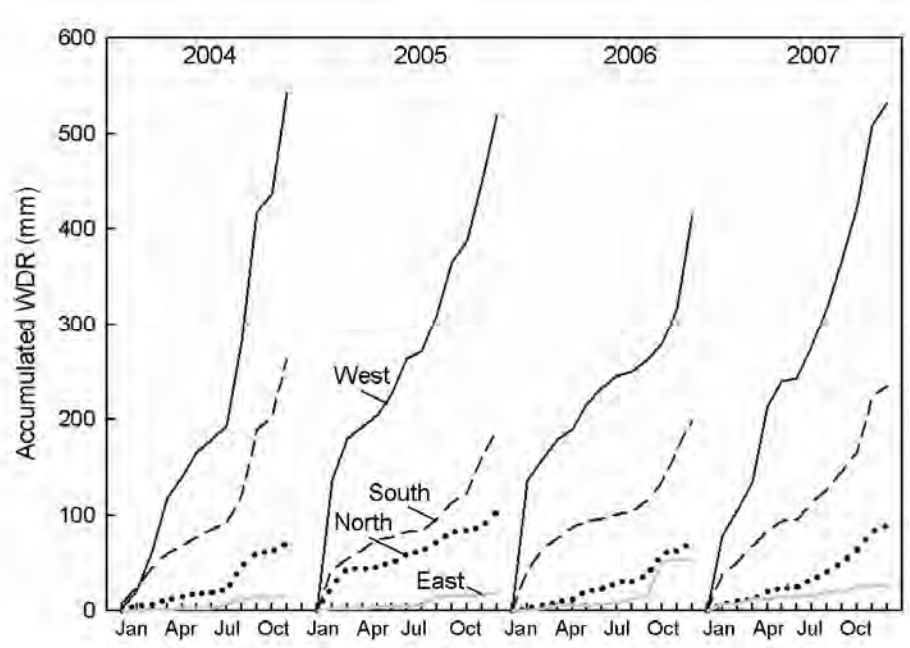

Figure 4.4. Accumulated WDR in the free field gauges for each year in the measurement period.

The WDR catch on the test house walls is presented in Figure 4.5. The WDR catch ratio is defined as the WDR distribution across the façade: the ratio of WDR to horizontal rainfall. The figure presents the total amount of WDR for the four year measurement period. The figure shows higher WDR catch on the edges and that the roof overhang shields the upper gauges. One WDR spell is thoroughly described in Section 4.4. Paper I analyses one WDR spell. When analysing each WDR spell respectively the catch ratio is often more pronounced, with lower amounts below the roof overhang and even higher values towards the edges and corners of the house.

Figure 4.6 presents the hours of liquid water measured on the cladding surface, TOW. Some correlation to normal precipitation is clear on the west facing wall. The east facing side has a large number of hours with TOW compared to the west facing wall. There may be several reasons for this. TOW is calculated by the hour the surface moisture exceeds the critical limit of the wood moisture. The critical limit is difficult to define for the dry east facing wall. Paper III explains the calculation of TOW and compares it to hours with calculated condensation. The east facing side has a larger number of hours with condensation due to less sun radiation. In addition the wetness sensor may not work in periods with temperatures below zero. However, TOW does define the hours of moistening compared to drying, regarding liquid water influence on the wall surface.

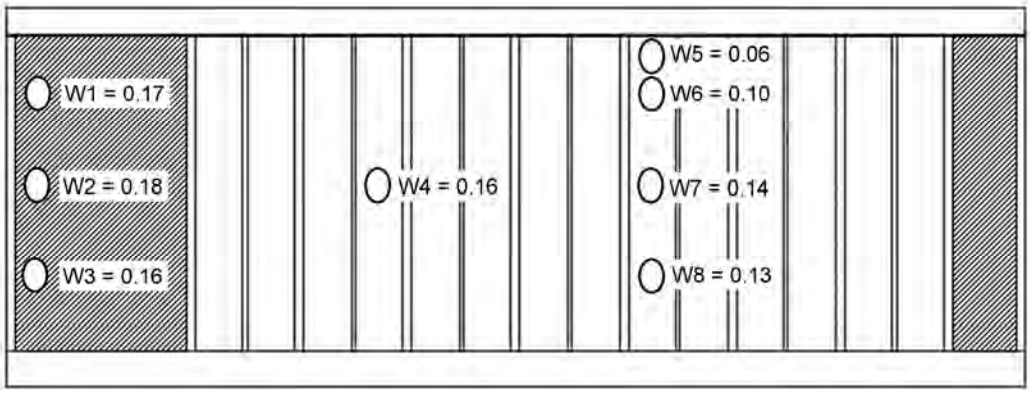

Figure 4.5. Catch ratio of WDR on the west facing test house wall. Total in measurement period 2004-2007. The wall facing south has 0.09, facing east has 0.00 and facing north has 0.01.

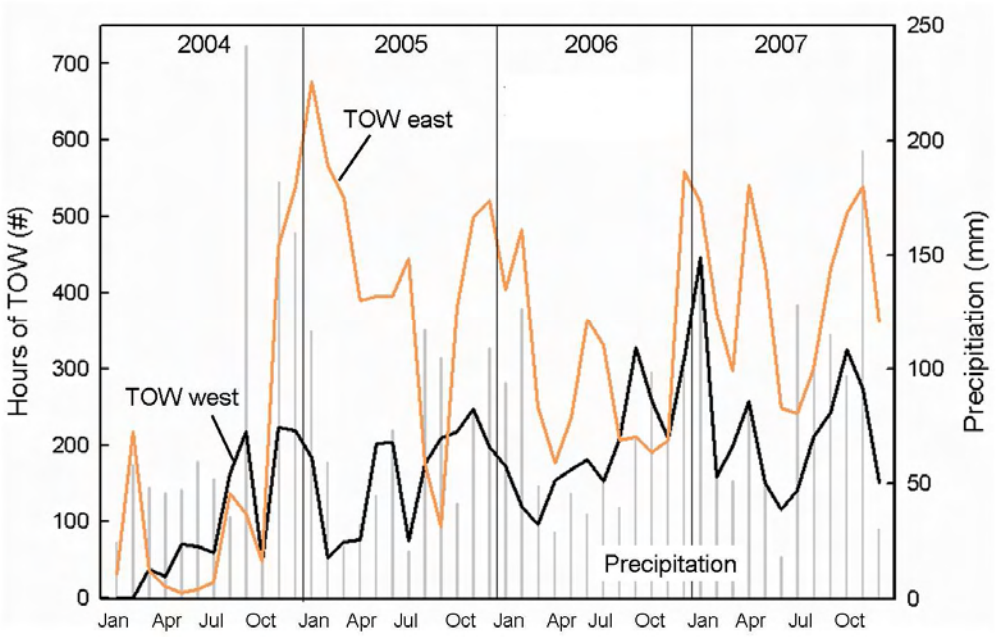

Figure 4.6. Measured TOW on the east and west facing sides of the test house and precipitation.

4.1.2 Temperature, radiation and water vapour content in air

The micro climate refers to the climate within 10 cm distance from the surface of the cladding. In this project the rain screen is mostly ventilated, resulting in an additional micro climate of importance in the wall assembly, the climate of the cavity.

The yearly averages of global radiation, QO_{NMI}, T_{NMI} and T_{CS} on the east and west facing sides are shown in Figure 4.7. The close relation between QO_{NMI} and T_{NMI} is easily observed. When looking closely one can see that QO_{NMI} and T_{CSE} correlate and T_{NMI} and T_{CSW} correlate. This is most evident in the data from November-December 2006. The east facing side is to a certain degree shielded from weather influence, except for the QO_{NMI}, especially in the winter period. The hill southeast of the test station is a sunshield for the east facing wall, the sun does not get to the east facing cladding, except for in the morning. Table 4.3 shows the corresponding yearly mean values to Figure 4.7. The temperatures are below the mean air temperature on the east facing wall and above on the west facing wall.

Table 4.3. Yearly mean values of T_{NMI} (°C), global radiation, QO_{NMI}, (W/m^2) and T_{CS} at the east and west facing sides. Lower temperature sesors of the equal cladding sections W3S and E4S are displayed.

	QO (W/m^2)	T_{NMI} (℃)	T_{CSW} (℃)	T_{CSE} (℃)
2004	89.1	6.2	6.5	6.1
2005	84.4	6.3	6.6	6.2
2006	91.9	6.9	7.3	6.6
2007	83.0	6.0	6.2	6.0
2004-2007 mean	87.1	6.3	6.6	6.2
St.dev.	154.6	7.2	8.1	8.1

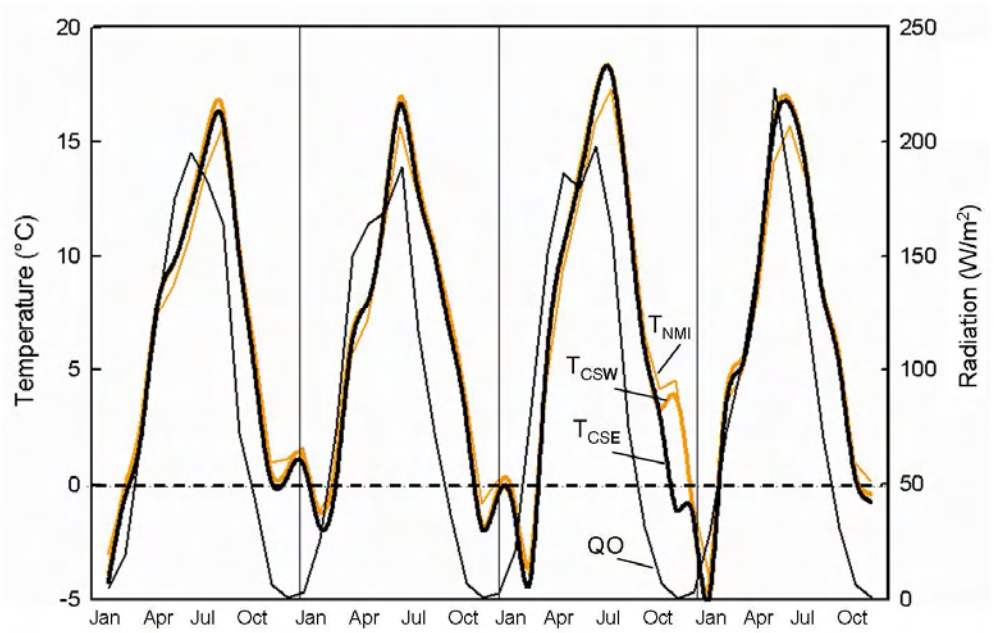

Figure 4.7. Monthly mean value of T_{NMI} (°C), global radiation, QO_{NMI}, (W/m^2) measured on a horizontal plane and surface temperatures on east, and west facing sides, T_{CSE} and T_{CSW}, (°C).

RH sensors were mounted in order to monitor the climate in the cavities. Five cavities had RH sensors in May 2005, Figure 4.8 shows which. Table 4.4 gives yearly values of the RH_{NMI} and RH_{CAV}. The trends of the RH fluctuation are seen in the monthly mean values in Figure 4.9 for the west and east facing claddings. The RH_{CAV} sensors on the east facing wall shut down in the period April to June 2005. The RH in the cavities is generally lower than in the outside air, but it follows the RH_{NMI} fluctuations. The highest RH_{CAV}, in mean yearly values, is found on the west facing side, in the cavity without ventilation. This location exceeds the RH_{NMI} in the winter periods. The lowest RH_{CAV} values are found for the fully ventilated cavity on the east facing side. The highest RH_{CAV} is in the closed cavity on the weather-beaten west facing side, where no moisture is ventilated out. The difference between the 4 and 23 mm on the west facing side is small, so is the difference between the two cavities, 0 and 23 mm on the east facing side.

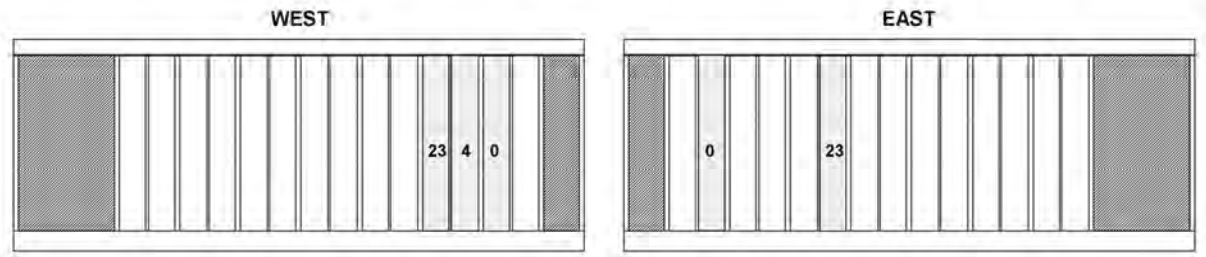

Figure 4.8. The sections with RH sensors. The numbers are indicating cavity opening(mm).

Table 4.4. Yearly mean values of RH_{NMI} and RH_{CAV} (%) in the air and in the cavities with no opening, *0 mm, some opening, 4 mm, and full opening, 23 mm on the east and west facing sides. Cladding sections W1N, W2S, W2N, E1N and E3N holds RH sensors.*

	RH_{NMI}	RH_{CAV} west 0 mm	RH_{CAV} west 4 mm	RH_{CAV} west 23 mm	RH_{CAV} east 0 mm	RH_{CAV} east 23 mm
2005	73.1	71.5	66.4	64.9	-	-
2006	71.0	72.7	65.9	64.8	63.9	63.1
2007	74.1	81.1	71.7	69.8	67.8	66.6
2004-2007 mean	72.5	70.8	68.0	66.5	62.7	61.8
St.dev.	14.6	10.5	10.7	11.3	15.7	17.5

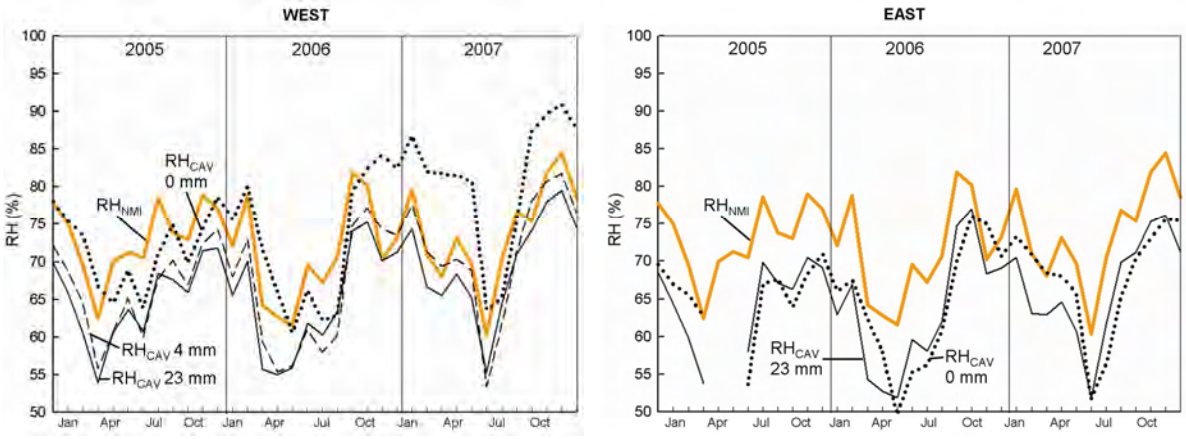

Figure 4.9. Monthly mean value of RH_{NMI} and RH_{CAV} (%) in the cavities with no opening, 0 mm, some opening, 4 mm, and full opening, 23 mm, on the east and west facing sides.

By including the temperature the water vapour pressure (p_v) can be calculated. The temperature used is the cavity temperature in the neighbouring section, but this is corrected according to T_B in the two cavities. The calculated p_v gives more accurate data about whether a moistening or drying is taking place, see Equation 4.1.

$$p_{v,\,NMI} < p_{v,\,CAV} = \text{moistening} \qquad 4.1$$
$$p_{v,\,NMI} > p_{v,\,CAV} = \text{drying}$$

Table 4.5 presents the average $p_{v,\,NMI}$ and $p_{v,\,CAV}$. The highest total p_v is for the outside air. This is as expected, when no moisture is added from inside the test house. Figure 4.10 presents $\Delta p_v = p_{v,\,NMI} - p_{v,\,CAV}$. The west with 0 mm cavity opening has is moistened. For the west facing side the 23 mm, fully ventilated, cladding has the highest drying potential. The cavity with 4 mm cavity opening responds almost as well as the fully ventilated cavity. This is the opposite for the east facing wall where the closed cavity has the best drying potential.

Table 4.5. Yearly mean values of p_v (Pa) in the air and in the cavities with no opening, 4 mm opening and full opening on the west facing side. Slow grown wood with oil base paint (A).

Section		W1N	W2S	W2N	E1N	E3N
	p_v NMI	p_v - west 0 mm	p_v – west 4 mm	p_v - west 23 mm	p_v - east 0 mm	p_v - east 23 mm
2005	788	753	735	814	-	-
2006	838	808	801	887	759	768
2007	785	794	775	901	744	744
2005-2007 mean	804	785	770	867	752	756

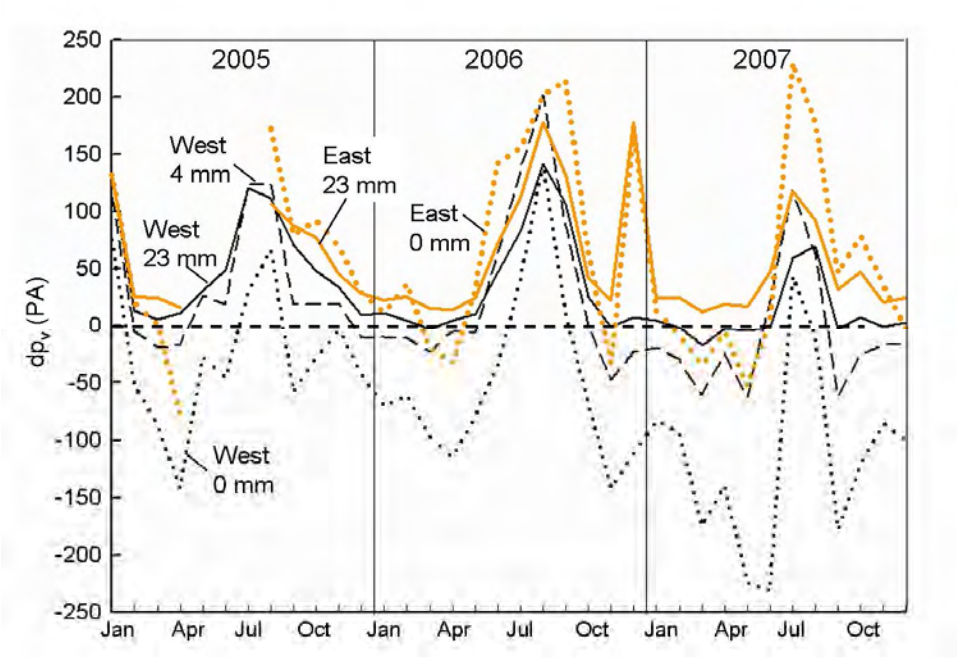

Figure 4.10. Monthly mean value of vapour pressure diference, Δp_v, (Pa) indicating a drying potential of the cavities with the different openings and façade orientation.

4.2 Analyses of averages

Analyses of wood performance are often based on the MC. Yearly averages provide an overview of the measurement data and its trends. The yearly averages of the Voll data are compared to understand the difference of the cladding; orientation, cavity influence, degree of ventilation, surface treatment, wood quality and the difference in height of cladding. The yearly averaged temperatures are included when clarifying. The averaged data are presented in three ways:

1. Total average of the measurement period, MC or ΔMC, is compared for the various configurations. This parameter includes all test sections. ΔMC is given in Equation 4.2 and Table 4.6.

$$\Delta MC = \sum_{i=1}^{i} \frac{\left(MC_{X1,i} - MC_{X2,i}\right)}{i} \qquad i = year \qquad 4.2$$

Table 4.6. Parameters used to calculate ΔMC_X in Equation 4.1.

	X1	X2
ΔMC_{Orient}	West	East
ΔMC_{MQ}	Slow grown	Fast grown
$\Delta MC_{high\text{-}low}$	High on wall	Low on wall

2. The yearly mean values are compared for equal cladding sections in a table. The total average and its standard deviation are also included. Appendix 1 gives every yearly and total averaged value of the four measurement years.

3. Graphical displays of the test sections presented in point two, showing the monthly mean MC and T values of the 48 measurement months. This graph expands on the development in the measurement period by including the seasonal variations.

The micro climate across the wall is not uniform. The set up of the test sections were not randomized according to wall placing, as mentioned in Section 3.5. When studying Figures 3.7 and 3.8, showing the wall set ups, a clear division in the two paint types is found. The other cladding parameters are apparently well spread. This dispersion must be taken into account when analysing.

Some MC sensors have suffered short circuiting. Data with errors are removed from the dataset; the faulty data sets are presented in Table 4.7. Even if only one measurement month has an error the entire year is removed in order to analyse the full year cycles.

Two identical claddings are mounted on the east facing wall, the identical sections are marked in Figure 4.11 and Figure 4.12 shows their yearly average values of MC and T_B. The variation of the MC sensors indicates the error of these sensors; it has a span up to 2 % MC. The reason for the discrepancy of the MC sensors may be due to the distance between the cladding sections giving the different climates, to the material properties or to the general measurement error. The accuracy of the MC sensors is discussed in Paper II. The two instrumented cladding boards at the lower and the two cladding boards at the upper part of the wall are from the same initial board, as described in Section 3.5, so the differences due material properties are limited. The temperature measurements are very accurate; with all four data plots in Figure 4.12 are on top of each other. Figure 4.12 also gives an impression of the negative correlation of cladding MC and T_B. Low temperatures hinder biological growth when the MC is high and with high temperature the MC is below the critical limit. This is an advantage for exposed wood claddings in temperate climates.

Table 4.7. Removed data with errors. Section numer refers to numbers in Figures 3.7 and 3.8.

Section	Data removed	Annotation
E3N-d	2004	
E4S-d	2004	
E5S-u	2004	
E6S-d	2005, 2006, 2007	Cavity removed, cord torn
W1S-u	2004	
W2N-d	2005, 2006, 2007	
W6N-d	2006, 2007	Gravimetric control
W6N-d	2006, 2007	Gravimetric control

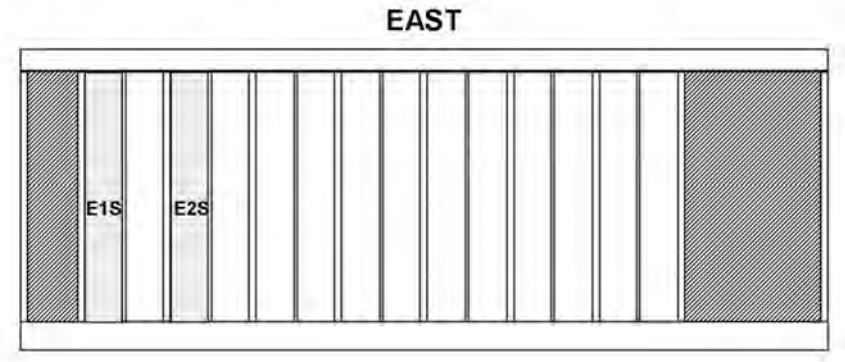

Figure 4.11. The test sections with identical configuration.

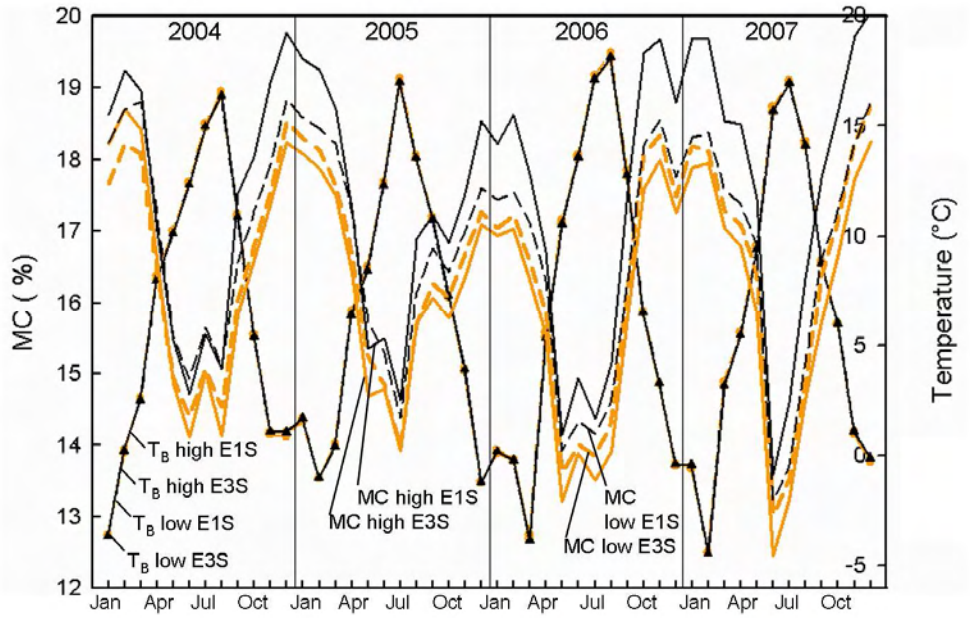

Figure 4.12. Two identical cladding sections facing east, E1S and E2S, are mounted for sensor control. The claddings have fast grown wood with alkyd paint (A).

The total trend in the measurement period is presented in Table 4.8, with the yearly averaged values of all test sections, except for the untreated claddings. $T_B > T_{NMI}$. About 0.2 % higher wall temperature is logical because of the shielded sensor location, on the inside of the cladding boards, and due the heat transfer from the house. An increase in the MC is seen in the four measurement years. This is either a result of the aging process or of a stabilization of the cladding boards. Knowing the rapid MC response of wood it is likely to believe that this trend corresponds to ageing. The author knows no equivalent extensive free field wood cladding investigation, with detailed monitoring for as many years. In this regard these results are unique and may also reveal results on the ageing process, also according to cladding design. However, this is not the main objective of this analysis and ageing is sparsely commented in the following sections.

Table 4.8. Yearly mean of T_{NMI}, T_B (℃) and MC (%) values of all surface treated test sections.

Average	T_{NMI} (℃)	T_B (℃)	MC (%)
2004	6.2	6.4	18.9
2005	6.3	6.5	19.2
2006	6.9	7.0	20.0
2007	6.0	6.2	20.9

4.2.1 The influence of test wall orientation

The climate on the east and west facing walls is quite different. Section 4.1 describes the different climatic exposures. The most distinct difference is found for the meteorological parameters; radiation, WDR and wind influence.

ΔMC_{Orient} is presented in Table 4.9. The MC of the surface treated cladding is generally lower for the east facing side. The MC on the west facing side is 1.8 % higher compared to the east facing side. This is not the case concerning the untreated cladding, the east facing side exceeds the west facing untreated cladding with 0.53 % MC. Alkyd paint has higher MC compared to acryl paint for the specific orientations. Alkyd paint is more impermeable with smaller pores than acryl paint, as mentioned in Section 2.2.7. This means the acryl paint may have a more rapid response to RH, which might be the reason for less difference between east and west. Considering the ventilation rate the largest difference between the east and west facing sides is for the cladding with 4 mm cavity opening, 3.16 % MC. Fast grown wood has a larger difference than the slow grown wood. One explanation might be that the slow grown wood responds slower to moisture influence. The lower part of the wall has a larger difference than the upper part of the wall. This difference is probably explained by the roof overhang shielding, and having less water running high on the wall. This reduces the liquid moisture impact on the upper part of the wall in both orientations. The mean T_B on the west facing side is 6.7°C, and 6.5°C on the east facing side for all sensors in the total measurement period. The east facing wall receives less solar radiation, and is partly shielded from long wave heat loss due to some surrounding buildings.

Figure 4.13 has four test sections that show the differences between the façade orientations; treated and untreated, facing east and west. Tables 4.10 and 4.11 present the yearly averages of MC and T_B for the same test sections. The T_B shows a trend of higher temperatures on the west facing side for the untreated cladding. This is not found for the treated surfaces, where both orientations are equal. This might be due to the higher heat absorption factor of untreated wood surface. The standard deviation is somewhat higher for the west facing side. The west side reaches higher maximum temperatures due to solar radiation.

Figure 4.14 shows the seasonal difference of the cladding response in the respective orientations. Untreated cladding has larger fluctuations than treated cladding, but still the east facing wall is more stable throughout the measurement period. This is also reflected in the standard deviation values in Table 4.11, higher for the west facing sections relatively to the corresponding east facing claddings.

Concerning the ageing effect; the amplitudes of the yearly fluctuations increase, as marked by thin lines in Figure 4.14. This is most evident for untreated cladding, especially when not regarding the high value of the west facing untreated cladding in November and December 2004. The increasing amplitude is probably due to micro cracking in the wood, allowing higher moisture uptake and faster drying. Surface treatment is designed partly to suppress wood cracking.

Table 4.9. ΔMC_{Orient} values describing the difference of the west facing / east facing side in MC %.

Total of treated	Untreated	A Alkyd	B Acryl	Cavity opening 0 mm	Cavity opening 4 mm	Cavity opening 23 mm	H Fast grown	S Slow grown	Low	Up
1.82	-0.53	2.51	1.24	2.49	3.16	0.29	2.12	1.17	2.43	1.65

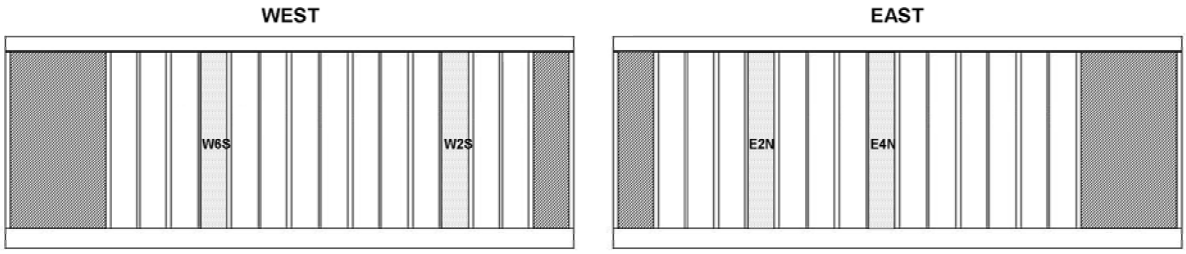

Figure 4.13. The sections chosen to show the difference between orientations.

Table 4.10. Yearly mean values of MC (%) cladding sections facing east and west. Lower part sensors of sections have slow grown wood, with 4 mm cavity opening and coated with alkyd paint (A) or untreated. The monthly averages of the same sections are graphically displayed in Figure 4.14.

Section	W2S	E2N	W6S	E4N
	West	East	West untreated	East Untreated
2004	18.0	17.1	18.7	17.8
2005	17.4	17.4	16.7	18.0
2006	17.3	17.4	16.3	17.9
2007	19.0	17.5	17.8	18.0
2004-2007 mean	17.9	17.4	17.4	17.9
St.dev.	2.7	1.9	4.6	3.4

Table 4.11. Yearly mean values of T_B (°C) cladding sections corresponding to Table 4.10.

Section	W2S	E2N	W6S	E4N
	West	East	West untreated	East Untreated
2004	6.5	6.6	7.2	6.8
2005	6.6	6.6	7.6	6.8
2006	7.2	6.9	8.9	7.2
2007	6.1	6.4	7.8	6.7
2004-2007 mean	6.6	6.6	7.9	6.9
St.dev.	7. 8	7.7	9.4	8.2

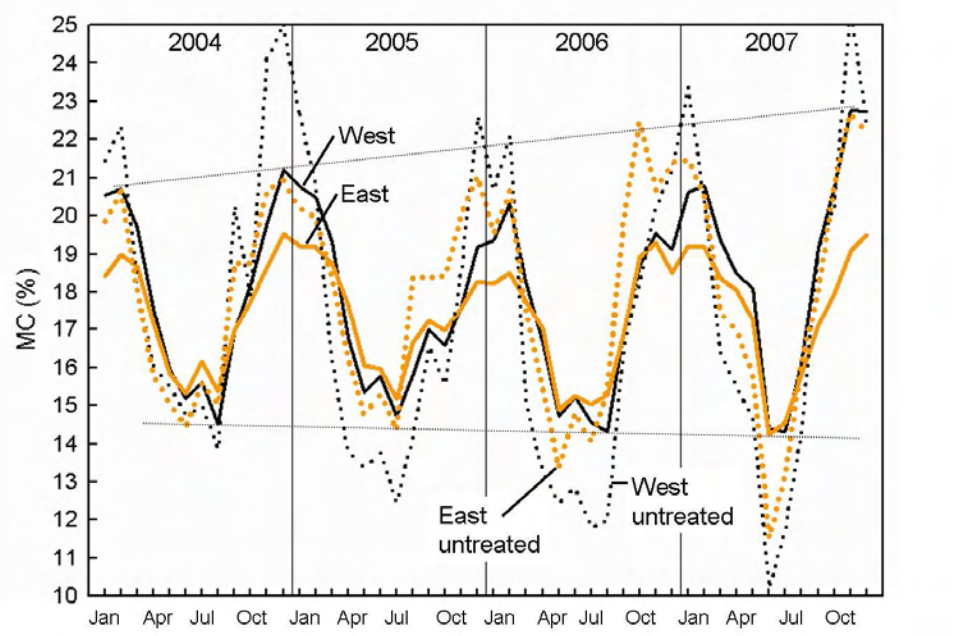

Figure 4.14. Monthly mean values of MC (%) on cladding facing east and west. The lower sensors of section W2S and E2N with slow grown wood, untreated or coated with alkyd paint (A) and with 4 mm cavity opening are displayed. The thin lines show the increasing amplitude. The yearly mean values are given in Table 4.11.

4.2.2 Cavity or Not?

In May 2005 the cavities were omitted at two sections, E6S and W5N, and the wooden cladding was mounted directly to the gypsum wind barrier. The sections have fast grown spruce and are coated with acrylic paint (B). The E6S lower MC sensor suffered a short circuit directly after the configuration change. The limited amount of data is not enough to calculate ΔMC.

Figure 4.15 shows the test sections with omitted cavities and cavities with 23 mm opening, full ventilation, with the same design parameters. Tables 4.12 and 4.13 show the mean T_B and MC in these sections. The temperatures of the cladding without cavity are higher; this is due to the higher heat flux from the wall. As mentioned in Chapter 2, an increased insulation thickness will reduce this heat flux through the wall. In sections with cavities this heat is removed by ventilation.

The upper sensors without cavity have low MC, especially during the winter time. Less of the sky is visible when peeking from the upper part of the wall, resulting in less long wave heat radiation lost and consequently higher temperatures.

Figure 4.16 shows the monthly mean readings corresponding to Tables 4.12 and 4.13. The graph shows the developing MC trend. For the cladding without cavity the MC of the west facing lower part is higher and increasing throughout the measurement period. This is due to the removal of the drainage and ventilation of the cavity. Directly mounted wooden claddings on the wind barrier get water traps. Shrinking and swelling of the wood gradually creates these water traps, where liquid water is stored and capillary soaked up into the wood over a period of time. The wind barrier and the insulation will also be moistened if the water is not dried out. The east facing wall has lower influence of liquid moisture, so this cladding stays dry also without cavity. But the results show the need for the cavity behind the cladding.

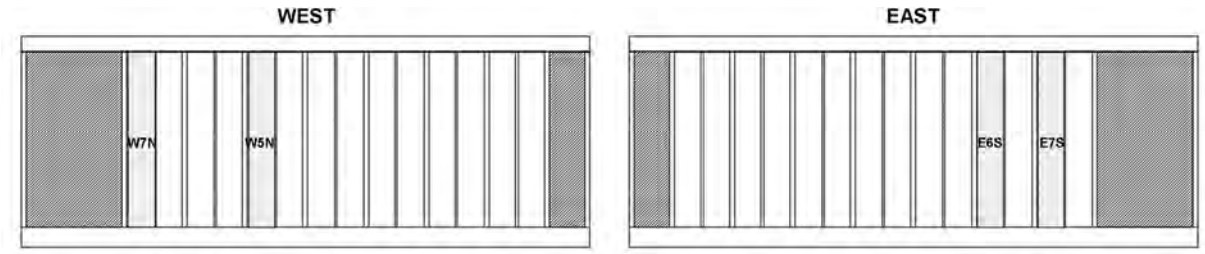

Figure 4.15. The sections compared with and without cavity. In sections W5N and E6S the cavity is omitted.

Table 4.12. Yearly mean values of cladding temperature T_B (°C) of cladding with no cavity (2005-07) and cavity with full ventilation (23 mm). Corresponds to Table 4.13. Grey numbers shows measured values of the sections with ventilation (2004)

Section	W5N-d	W7N-d	W5N-u	W7N-u	E6S-u	E7S-u
Location	West low	West low	West up	West up	East up	East up
Cavity?	No	Yes	No	Yes	No	Yes
Cavity opening	-	23 mm	-	23 mm	-	23 mm
2004	6.1	6.0	6.5	6.3	6.3	6.2
2005	6.2	6.0	6.6	6.3	6.3	6.1
2006	6.9	6.7	7.2	7.0	6.7	6.4
2007	4.9	4.6	6.2	4.9	6.1	4.8
2004-2007 mean	6.3	6.1	6.6	6.4	6.4	6.1
St.dev.	7.8	7.6	7.8	7.7	7.8	7.8

Table 4.13. Yearly mean values of MC (%) of cladding with no cavity after May 2005 and cavity with full ventilation (23 mm) on east and west facing side. Corresponds to Figure 4.16 and Table 4.12. Grey numbers shows measured values of the sections with ventilation (2004).

Section	W5N-d	W7N-d	W5N-u	W7N-u	E6S-u	E7S-u
Location	West low	West low	West up	West up	East up	East up
Cavity?	No	Yes	No	Yes	No	Yes
Cavity opening	-	23 mm	-	23 mm	-	23 mm
2004	18.5	18.7	18.3	18.2	17.5	17.6
2005	16.4	17.4	17.4	18.1	17.3	17.6
2006	18.0	17.8	16.9	17.7	16.9	17.3
2007	21.2	19.4	17.8	18.9	17.3	18.1
2004-2007 mean	18.5	18.3	17.6	18.2	17.3	17.7
St.dev.	3.6	2.9	2.4	2.6	1.8	2.2

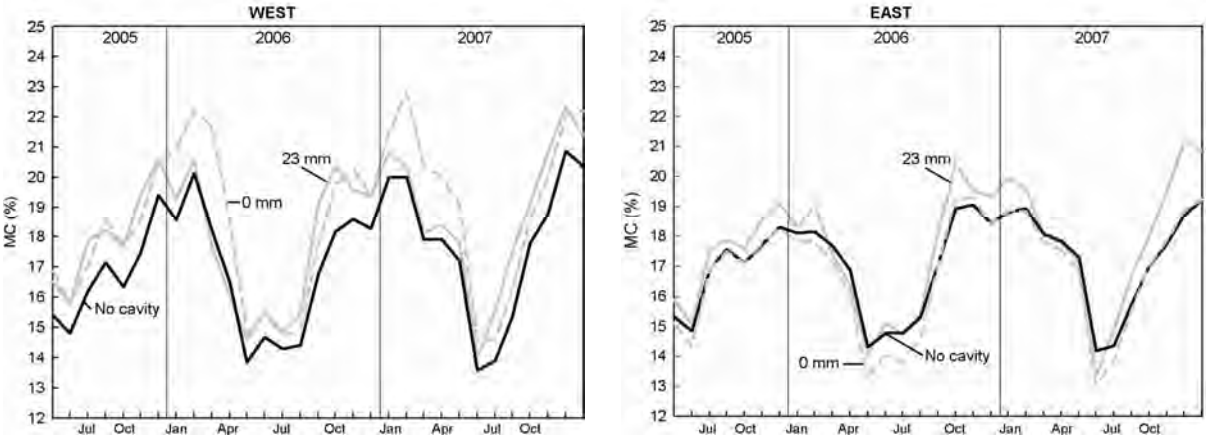

Figure 4.16. Monthly mean values of MC (%) on cladding with and without cavity on the west facing side. The claddings with cavity is shown with 23 mm, and closed 0 mm, opening. The cavity was removed in May 2005. Upper sensors on sections with fast grown wood with acrylic (B) paint are used. Corresponds to Tables 4.12 and 4.13.

4.2.3 Ventilation rate

The ventilation rate of the two-stage tightening wall assemblies varies. The ventilation rate is determined by the cavity design; the openings in the lower and upper ends, and type of convection; forced, by wind influence, or natural, by thermal buoyancy. Convection is not measured at the Voll test house. Forced convection is not influencing the closed cavities, given that these are tight, as assumed. Wind is unpredictable due to turbulence. In the boundary layer the wind velocities are low and rapidly shifting. Paper VI shows CFD calculations of steady state air flow determined by wind influence.

The test house measurements do suggest the best performing ventilation gap. Table 4.14 shows the total of all cladding sections except for the untreated ones. The results of ventilation rates on the east and west facing sides are opposite. The west facing side has the lowest MC with full cavity opening, while the east facing side has the lowest MC with no cavity opening. A higher temperature is registered in the closed cavities, because heat from inside the test house is not ventilated out. Figure 4.17 shows the section chosen to compare ventilation rate. Tables 4.15 and Figure 4.18 support the conclusions above. The partly ventilated cladding (4 mm cavity opening) is performing almost similar to the fully ventilated cladding. These results improve the results presented in Nore et al. (2005), regarding the ventilation effect. The weather-beaten west facing side performs best with cavity ventilation, slightly improved with full cavity opening (23 mm). The shielded east facing cladding wall performs best with closed cavities.

Table 4.14. Total average values of MC (%) and T_B (°C) on all cladding with the different ventilation rates. Two decimal places are included in the temperatures to see the correct span.

Cavity opening	MC west	MC East	T_B West	T_B east
0 mm	18.8	16.6	6.56	6.51
4 mm	18.2	16.8	6.47	6.37
23 mm	18.0	17.6	6.54	6.38

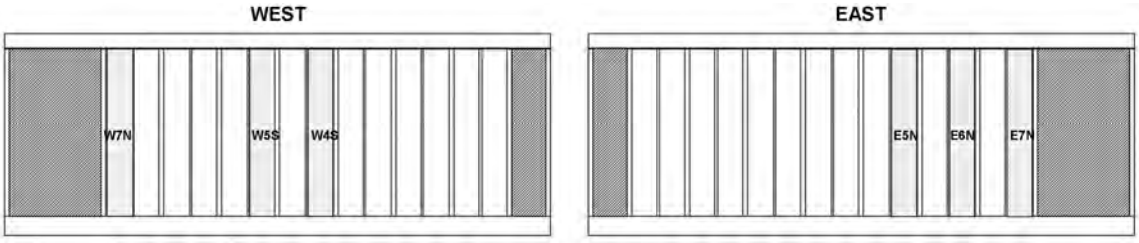

Figure 4.17. The sections compared for the ventilation study.

Table 4.15. Yearly mean values of MC (%) of claddings with no ventilation, 0 mm, a little cavity opening, 4 mm, and cavity with full ventilation, 23 mm. Corresponds to Figure 4.18.

Section	W4S	W5S	W7S	E5N	E6N	E7N
Orientation	West	West	West	East	East	East
Cavity opening	0 mm	4 mm	23 mm	0 mm	4 mm	23 mm
2004	19.9	18.6	18.0	18.1	17.5	17.7
2005	17.7	16.8	16.9	16.5	17.0	17.0
2006	17.7	17.4	17.0	16.0	16.8	17.4
2007	19.8	18.7	18.0	17.0	17.4	18.2
2004-2007 mean	18.8	17.9	17.5	16.9	17.2	17.6
St.dev.	3.3	2.8	2.3	2.3	1.9	2.1

a)

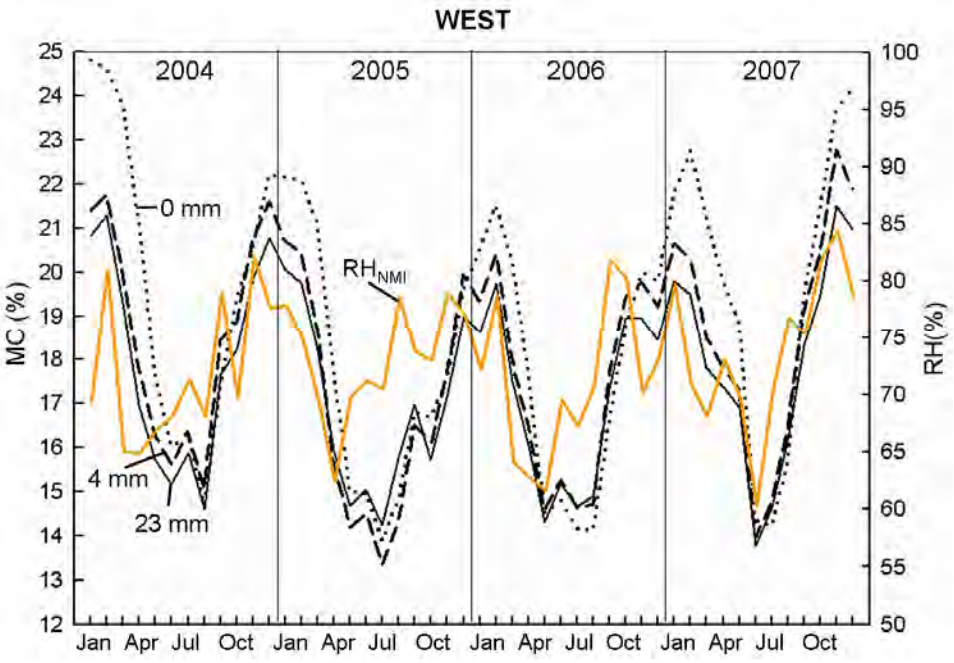

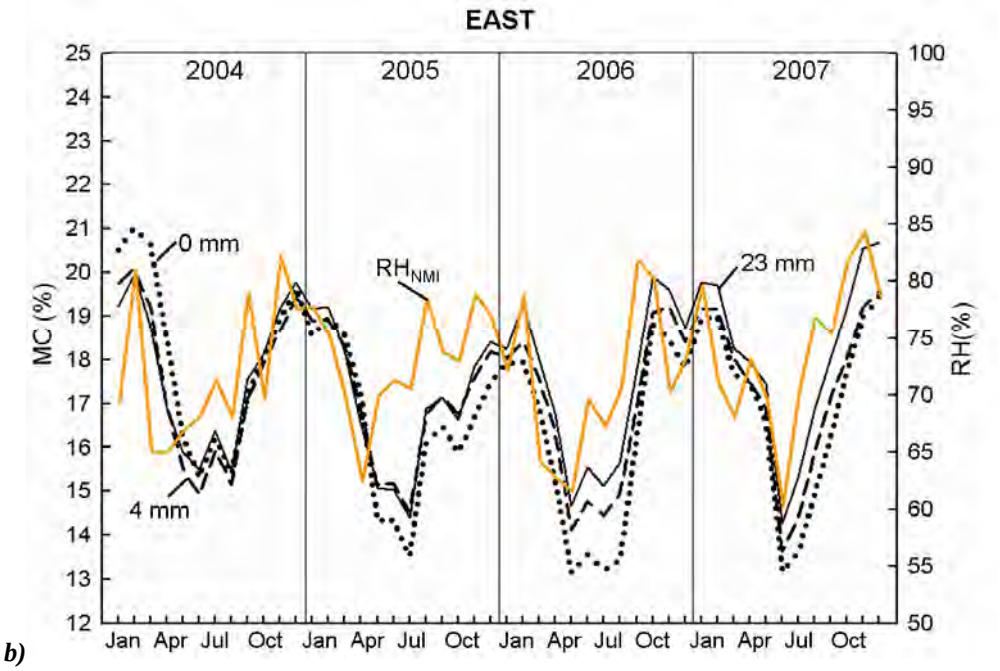

b)

Figure 4.18. Monthly mean values of MC (%) on cladding with different ventilation rates, a) west facing side and b) east facing side. The lower sensors on sections with slow grown wood and acryl (B) paint are used. RH_{NMI} (%) is included to show the correlation. Table 4.15 corresponds to this figure.

4.2.4 Surface treatment

Surface treatment is applied for protective and esthetical reasons. Two aspects limit the surface treatment analysis. The parting of the two paint types on the wall, as mentioned earlier may mean that wall location response is measured and not surface treatment influence. The other aspect is, as mentioned in Paper II, that the surface treatment may influence the electrical resistance measurements. The two paint types may even influence the electrical resistance MC measurements differently. Anyhow the analysis provides results as expected.

Table 4.16 gives the overall picture of the MC response of surface treated cladding. In total the untreated claddings have a lower mean MC than the treated on the west facing wall, but highest on the east facing wall. Differences between treated and untreated surfaces are shown in Section 4.3.1. Table 4.10 initially shows the influence of orientation, but also the MC trend of treated and untreated claddings. The MC amplitude of the fluctuations is larger for untreated cladding than treated cladding. This is also apparent in the larger standard deviation of untreated cladding in Table 4.17. This result is expected since one reason for applying surface treatment is to stabilize the MC to reduce cracking. The difference between the alkyd, A, and the acryl, B, is small, but alkyd has the lowest MC on the east facing wall and acryl on the west facing wall. The same was found by Johansen (2007), also studying the Voll data.

Figure 4.19 shows sections analysed according to surface treatment. The results given in Figure 4.20 and Table 4.17 further propose that alkyd paint (A) gives the best performance, the lowest MC, on weather-beaten claddings. For claddings with modest climatic exposure, like the east facing side, the acryl paint (B) may perform better, even better than untreated cladding.

Untreated cladding has the most rapid response to climate exposure, as earlier stated. In Trondheim the hours of drying exceed the hours of moistening. Due to the rapid response the untreated claddings have longer dry periods compared to the treated claddings; this is one reason for the lower MC.

As time passes the surface treatment erodes. In weather-beaten areas the surface treatment may lose its function after short period of time. The Lista house had maintenance painting 6 years after the original painting. The original paint layer was almost totally dissipated (Ivan 1993). When the surface treatment dissipates the cladding response approach the untreated cladding response.

Table 4.16. Total average values of MC (%) on all cladding with the different surface treatments.

	West	East
Untreated	17.1	17.5
A - alkyd	18.4	16.9
B – acryl	18.2	17.1

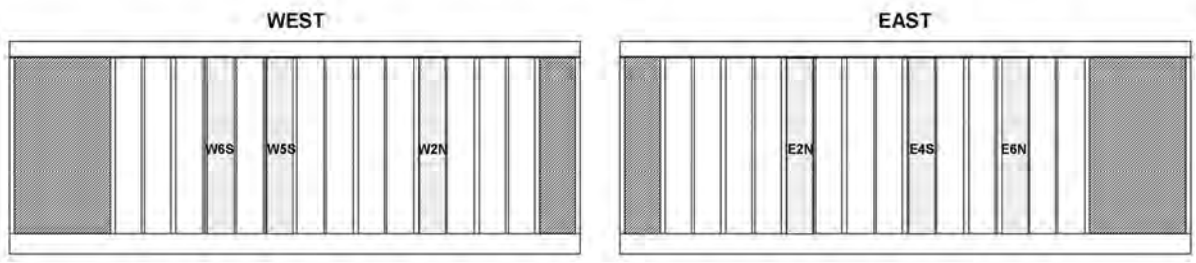

Figure 4.19. The cavities compared for the surface treatment study.

Table 4.17. Yearly mean values of MC (%) on cladding with different surface treatment. Slow grown wood and high sensors are used. Test sections correspond to Figure 4.19.

Section	W2N	E2N	W5S	E6N	W6S	E4S
Orientation Surface treatment	West A	East A	West B	East B	West Untreated	East Untreated
2004	18.4	17.2	18.6	16.5	17.6	17.8
2005	18.2	17.3	18.2	16.4	16.7	18.0
2006	17.7	16.9	17.8	16.0	14.6	17.9
2007	18.4	17.4	18.8	16.5	16.6	18.0
2004-2007 mean	18.3	17.2	18.3	16.3	16.6	17.9
St.dev.	2.1	1.9	2.3	1.9	4.0	3.4

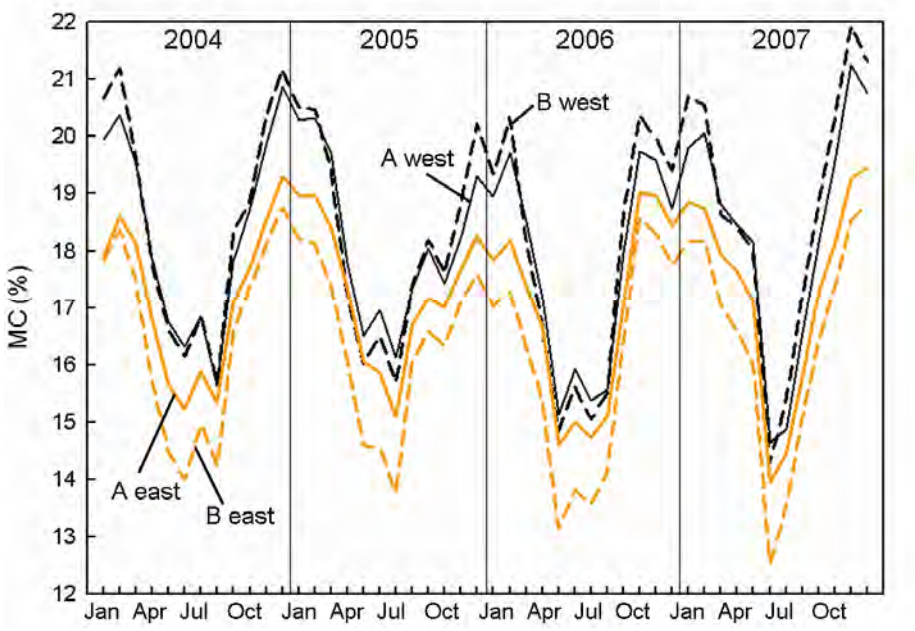

Figure 4.20. Monthly mean values of MC (%) on cladding with different surface treatment. Slow grown wood and upper sensors are used. Table 4.17 corresponds to this figure.

4.2.5 Material quality – fast or slow grown wood

The material quality parameter has not as explicit differences in MC as found for the other design parameters. A weakness in the Voll test house set up is the lack of differentiation between the two densities in the MC calibration curves. Less wood substrate gives higher resistance, this in turn might give too dry MC measurements. However the larger amount of wood substrate in slow grown wood provides larger microscopic contact surface, which may also store more water. This is also discussed in Paper II.

ΔMC_{MQ} is the difference of slow grown – fast grown wood, seen in Table 4.18. ΔMC_{MQ} gives in total only a difference in the total treated cladding of 0.16 % MC, which is very low. The only parameter that may be distinguished in regard to the material quality is the different ventilation rates. No cavity opening gives highest MC in slow grown wood, whereas the full opening gives the highest MC in the fast grown wood. This might mean that slow grown wood, without the possibility to dry out on the back side, stores more moisture than fast grown wood.

A closer look at fast and slow grown wood, is done for the sections displayed in Figure 4.21. Slow grown treated surfaces has a higher mean MC than fast grown treated claddings, as given in Table 4.19. The difference is most distinct for the unventilated sections with a total difference of 20.0 – 18.6 = 1.4 % MC. Untreated wood shows the opposite, with higher MC for the fast grown wood on the west facing side. The standard deviations show no clear trend in material quality. The graph in Figure 4.22 elaborates on the yearly average values. No clear trends are found. Both Table 4.19 and Figure 4.22 show higher MC of slow grown treated wood. But when studying the months of the measurement period no trends are perceptual.

Table 4.18. ΔMC_{MQ} values describing the difference of the slow grown – fast grown wood in percent.

Total of treated	Untreated	A Alkyd	B Acryl	Cavity opening 0 mm	Cavity opening 4 mm	Cavity opening 23 mm	East facing	West facing	Low	Up
0.16	-0.11	0.25	0.01	0.51	0.40	-0.29	0.19	0.13	0.11	0.20

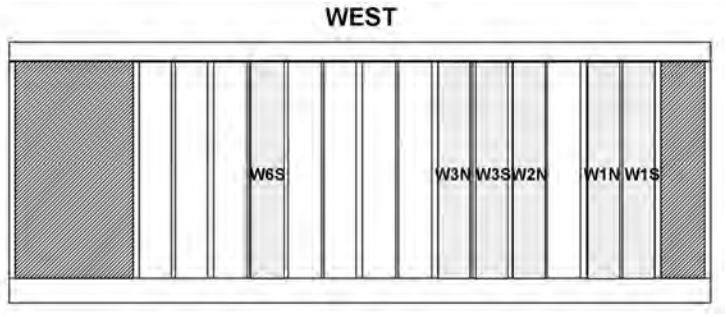

Figure 4.21. The cavities compared for the material quality study.

Table 4.19. Yearly mean values of MC (%) on cladding with different material qualities; fast and slow grown wood. Different ventilation rates and surface treatments are shown. Corresponds to figure 4.22.

Section	W1S-u	W1N-u	W3S-u	W2N-u	W3N-u	W6S-u
Growth rate	Fast	Slow	Fast	Slow	Fast	Slow
Cavity opening	0 mm	0 mm	23 mm	23 mm	4 mm	4 mm
Surface treatment	A	A	A	A	Untreated	Untreated
2004	16.2	19.7	17.7	18.1	18.0	17.6
2005	19.7	19.9	17.6	18.1	17.5	16.7
2006	18.7	19.4	17.1	17.5	16.3	14.6
2007	20.0	20.9	18.2	18.3	17.6	16.6
2004-2007 mean	18.6	20.0	17.7	18.0	17.4	16.6
St.dev.	2.7	2.6	2.4	2.2	4.7	4.0

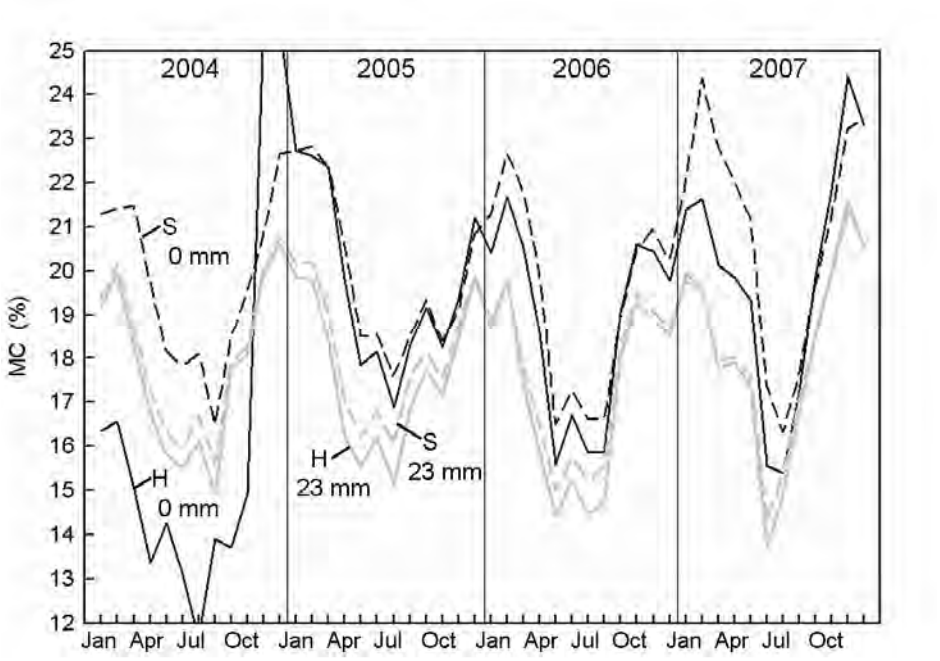

Figure 4.22. Monthly mean values of MC (%) on cladding with different material qualities; fast and slow grown wood. Full cavity opening, 23 mm, and no cavity opening, 0 mm. High sensors on west facing cladding with alkyd paint (A) are displayed. Table 4.19 corresponds to this figure.

4.2.6 Lower versus upper part of cladding – variation with the height of wall

Figure 4.12 at the start of this section, shows the difference of high and low measurements on the identical sections facing east. No trend is found for the MC. This graph shows the sensitivity of the MC data, and how careful one should be in concluding about direct MC measurements. $\Delta MC_{High\text{-}Low}$ is the upper wall MC minus the lower wall MC in one section, is presented in Table 4.20. It shows almost no difference in the total treated surfaces of upper and lower end. Most significant is the difference within the orientation, with 0.5 % MC. The total $\Delta MC_{High\text{-}Low}$ in each orientation is opposite, suggesting that in total the upper part of the wall is wetter on the west facing side and contrary on the east facing side. But, the ΔMC_{Orient} gave a larger difference of the high part, indicating in total larger MC on the lower end boards with 2.4 % MC and the higher boards with 1.7 % MC, see Table 4.9.

An interesting aspect in $\Delta MC_{High\text{-}Low}$ is the difference in the upper and lower parts with regard to the ventilation rate. The higher MC in the upper part of the cladding when the cavity is closed is evident, with 0.6 % MC. This is opposite when the ventilation gap is fully ventilated. This trend is elaborated on in Tables 4.21 and 4.22 and Figure 4.24. The reason for the higher MC for the upper cladding boards, when the ventilation gap is closed, is probably an internal natural convection transporting moisture from the lower cladding boards to the cladding boards in the upper part of the cladding. The higher temperature in the upper part, see Table 4.22, supports this theory, although this also may also be due to the higher emission of long wave radiation at the lower part during night time. With no outdoor air in the cavity the temperature may increase further. In addition the warmer air in the upper part allows more moisture in the air. This moisture precipitates on its way down in the internal cycle.

Table 4.20. $\Delta MC_{High\text{-}Low}$ values describing the difference of the slow grown – fast grown wood in MC %.

Total of treated	Untreated	A Alkyd	B Acryl	Cavity opening 0 mm	Cavity opening 4 mm	Cavity opening 23 mm	H Fast grown	S Slow grown	East facing	West facing
0.06	-0.34	0.74	0.19	0.59	-0.19	-0.26	0.07	0.06	-0.20	0.34

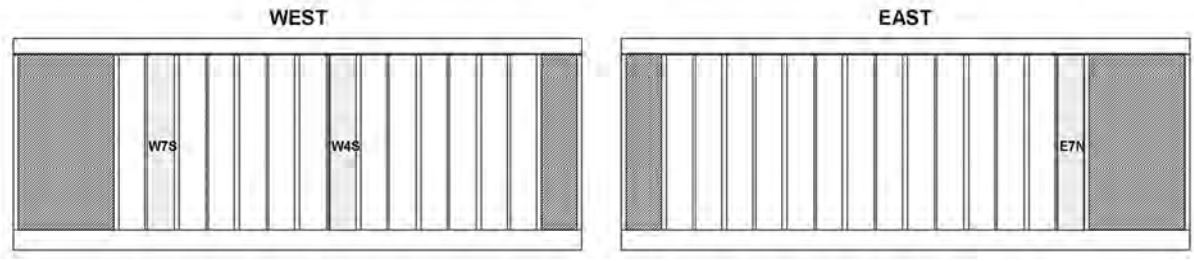

Figure 4.23. The sections compared for variation over the wall height.

Table 4.21. Yearly mean values of MC (%) on upper and lower part of cladding.

Section	W4S-d	W4S-u	W7S-d	W7S-u	E7N-d	E7N-u
Wall location	Low	Up	Low	Up	Low	Up
Cavity opening	0 mm	0 mm	23 mm	23 mm	23 mm	23 mm
2004	19.9	20.0	18.0	18.4	17.7	16.8
2005	17.7	18.8	16.9	18.1	17.0	16.9
2006	17.7	18.3	17.0	17.4	17.4	16.5
2007	19.8	19.2	18.0	18.6	18.2	17.2
2004-2007 mean	18.8	19.2	17.5	18.1	17.6	16.9
St.dev.	3.3	2.4	2.3	2.1	2.1	2.0

Table 4.22. Yearly mean values of cladding temperature, T_B (°C).

Section	W4S-d	W4S-u	W7S-d	W7S-u	E7N-d	E7N-u
Wall location	Low	Up	Low	Up	Low	Up
Cavity opening	0 mm	0 mm	23 mm	23 mm	23 mm	23 mm
2004	6.1	6.4	4.9	6.4	6.3	6.4
2005	6.3	6.5	4.9	6.3	6.3	6.4
2006	6.9	7.2	6.6	7.0	6.6	6.8
2007	4.9	6.1	4.5	4.9	6.0	6.1
2004-2007 mean	6.3	6.6	6.0	6.4	6.3	6.4
St.dev.	7.8	7.8	7.7	7.7	7.9	7.8

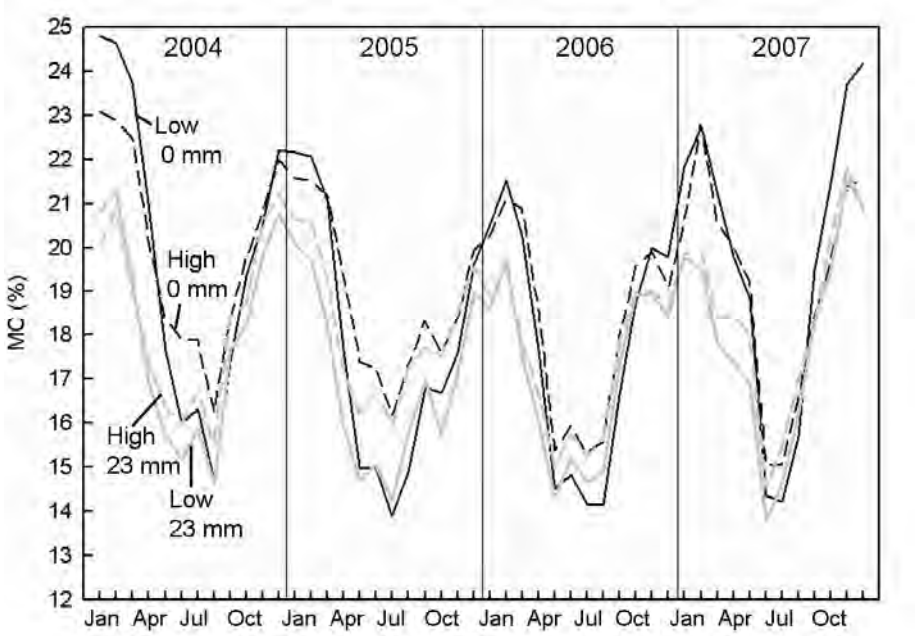

Figure 4.24. Monthly mean values of MC (%) on higher and lower part of the wall. West facing claddings with acryl paint (B) are displayed with full cavity opening, 23 mm, and no cavity opening, 0 mm. Table 4.21 and 4.22 corresponds to this Figure.

4.2.7 Profiles

When initiating the project one task was to monitor temperature and MC distribution in the cladding board. With transient measurement one could also get the temperature and MC gradients. See Figure 3.9 for sensor placing at different cladding depths. Regarding the moisture gradient measurements they did not turn out as expected. This is described in Paper II.

The temperature gradient is valid, but due to only minor temperature differences when studying the effect on an overall basis, a graphical presentation is not possible. Studying the tempertures in Table 4.23 shows a decrease in the temperature close to the back wall and outwards, except for the T_{CS} and T_{AIR}. The cladding surface is locally heated due to its heat absorption from solar radiation and cooled due to long wave emission. Figure 4.25 shows the $\Delta T = T_{NMI} - T_{wall}$. The T_{WB} is most stable and the T_{CS} is the temperature with the highest amplitude.

Table 4.23. Yearly mean values of temperatures, (°C).

Section	W3S-u	W3S-u	W3S-u	W3S-u	W3S-u	W3S-u	TTM
	T_{WB}	T_{CAV}	T_B	T_C	T_{CS}	T_{AIR}	T_{NMI}
2004	7.3	7.2	7.0	6.7	6.9	6.8	6.2
2005	7.4	7.3	7.1	6.8	6.9	6.9	6.3
2006	8.0	7.9	7.8	7.5	7.6	7.6	6.9
2007	6.9	6.8	6.6	6.4	6.4	6.6	6.0
2004-2007 mean	7.4	7.3	7.1	6.9	6.9	7.0	6.3
St.dev.	7.4	7.5	7.6	8.0	7.7	7.8	7.2

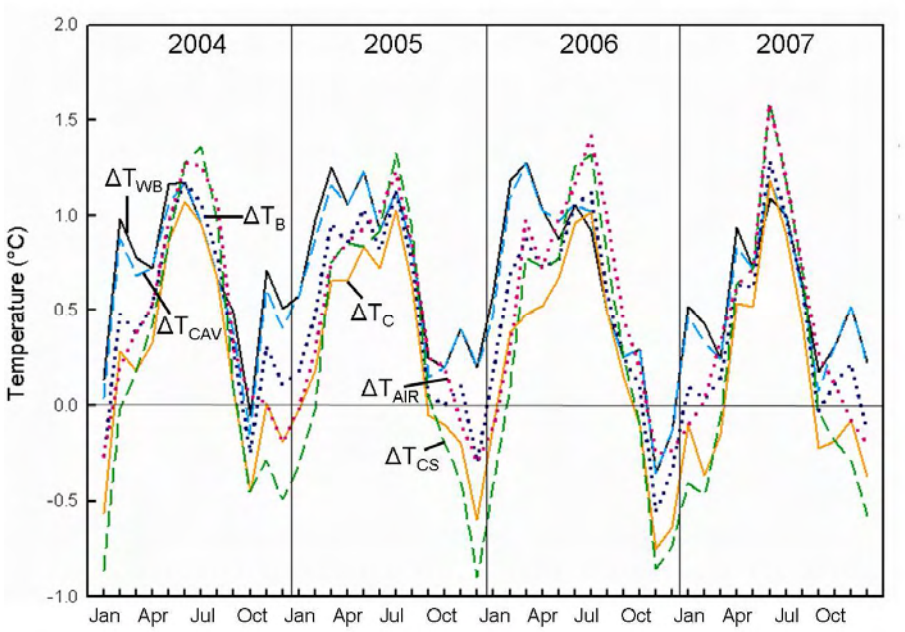

Figure 4.25. Monthly mean values of ΔT (°C), showing the temperature profile through the cladding. Upper sensors of the west facing claddings with alkyd paint (A) are displayed.

4.3 Closer look – wet and dry weeks

In order to study details in the vast data set, an investigation of the hourly data is carried out on one wet and one dry week. This clarifies the relation between climate parameters and cladding MC on a short term basis. At first the general climate is described for the two weeks, following the radiation and temperature response of the cladding, and last, the micro climate concerning moisture and cladding moisture response, is analysed.

As stated earlier the MC sensors have errors. However, when directly comparing MC response to the corresponding climate, the measurements are reliable. The two weeks are selected within the autumn period, which is considered to have the toughest moisture impact throughout the year. The dry week is not completely dry; one entire week without rain is not feasible to find for Trondheim. The wet week is in the period September 11th to 17th 2005 and the dry week is September 23rd to 29th 2005. The same cladding is presented in the wet and dry weeks.

Figure 4.26 shows T_{NMI}, RH_{NMI} and precipitation of the two chosen weeks. The wet week has 56.7 mm normal precipitation and the dry week has 4.3 mm. The total duration of rain was 2070 minutes for the wet week and 641 minutes for the dry week. The dry week has an average T_{NMI} of 7.8°C and an average RH_{NMI} of 80 %. The wet week has an average T_{NMI} of 12.0°C and 61 % RH_{NMI}. The larger RH_{NMI} fluctuations in the dry week are natural when the heated air during daytime is not supplied with moisture, thus reaches a lower RH_{NMI}.

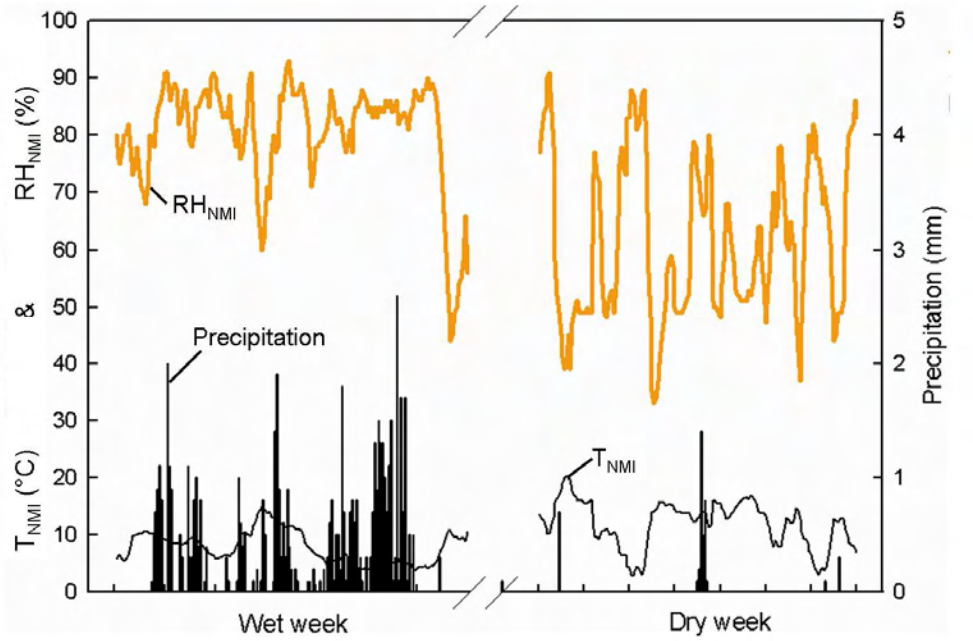

Figure 4.26. Hourly values of T_{NMI} (°C), RH_{NMI} (%) and normal precipitation (mm).

4.3.1 Radiation and temperatures

Figure 4.27 shows the T_{NMI} and the global radiation, QO_{NMI}. When studying the cladding surface, T_{CS}, facing east and west the dependency on both T_{NMI} and QO_{NMI} is discovered. During the nights, the bottom of temperature curves, the T_{CS} follows T_{NMI}. At day time, especially when the sun is shining like during the dry week, the T_{CS} peak follows the QO peak. The east facing wall reaches the T_{CS} peak earlier than the west T_{CS}. In early mornings, when the west facing side is shaded, the east facing side receives some solar radiation. The sun disappears around noon from the east facing side, so it cools down faster than the west facing side.

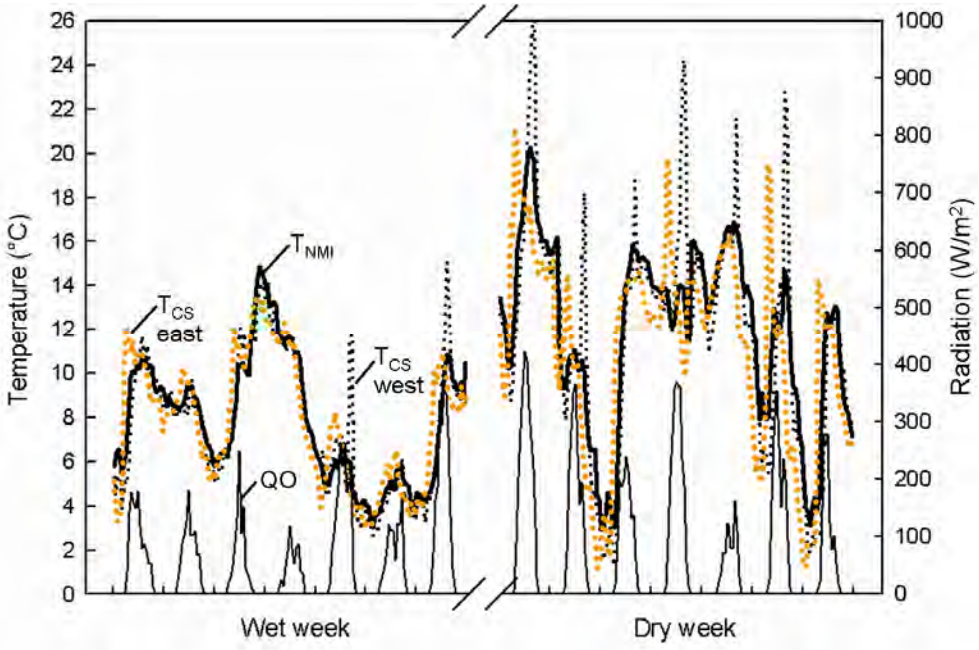

Figure 4.27. Hourly values of T_{NMI}, T_{CS}, T_{CS} on the east and west facing sides and the global radiation, QO. The surface tempeartures are measured on sections W3S and E4S and the lower part sensor is read.

The rapid temperature response is also visible in Figure 4.28, showing one day of each chosen week. The temperatures in the depth of the cladding design follow each other closely (Figure 3.9 shows sensor placing). A decreasing temperature is found from the T_{WB} to the T_{AIRr}, due to heat flux from the inside of the test house. But one exception is cladding surface temperature T_{CS}, like in Section 4.2.7, that exceeds the other cladding temperatures for the dry week, due to the solar radiation and low heat conductance of the wood.

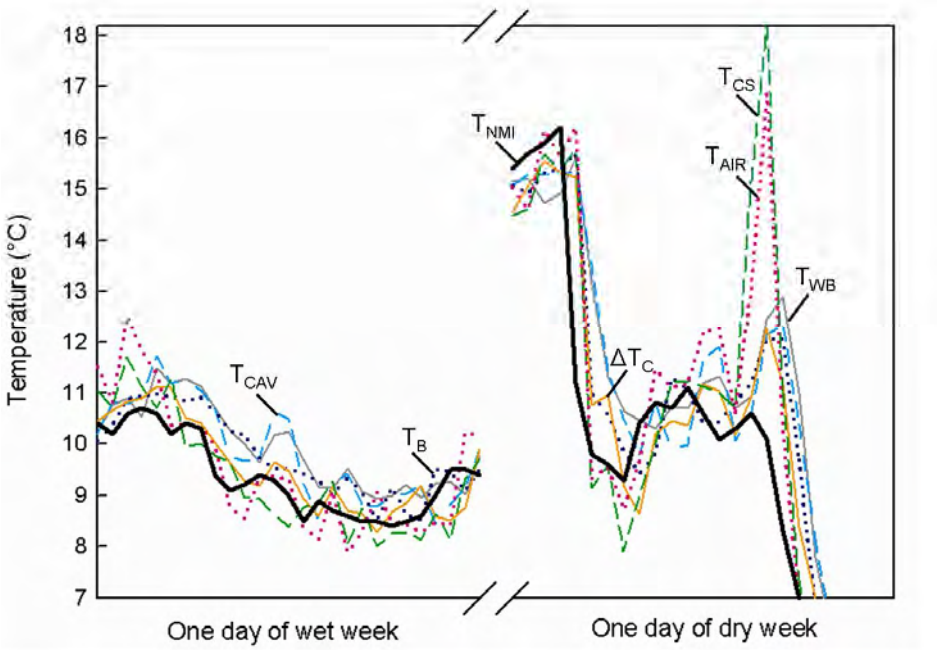

Figure 4.28. Hourly values of temperatures over the cladding at one measurement point for the two days. Temperatures are shown from 12 a.m. each day. Temperatures and sensors are equivalent to Figure 4.27.

4.3.2 Wind and WDR

The wind properties for the two weeks are given in Figure 4.29. The mean wind velocity in the wet week was 3.4. m/s and 3.1 m/s in the dry week, at 10 metres height. At 2 metres height it was 2.1 m/s for the wet week and 2.2 m/s for the dry week. The wind direction is mainly southwest (227.5°) for the wet week and southwest south (202.5°) for the dry week. The wind direction for wind with rain in the wet week is 230°. This is equivalent to the main wind directions during the total measurement period; the wind is turning west when wind is accompanied by precipitation. The rapid wind fluctuations are found in hourly wind data. When the line is vertically across the graph window the wind has turned from 360° to a low degree or contrary.

For the wet week the free field WDR measurements had 36.2 mm in the west facing WDR gauge, 64 % of the normal rain, and the south oriented gauge received 8.2 mm, 14 % of the total rain, see Figure 4.30. When WDR hits the façade the amount of WDR is presented in Figure 4.23. The west oriented façade receives 11.4 mm in the centre of the wall (W7), which is about 1/3 of the free field WDR. The short rain incident during the dry week also gives some WDR on the test house. The figure also shows TOW, each hour with registered TOW is marked. For the wet week 87 hours of TOW is registered on the west facing wall and 4 hours on the east facing wall. For the dry week 29 hours are registered on the western wall and 19 hours on the eastern wall.

Figure 4.32 gives the catch ratio on the test house walls for the wet week. The usual pattern for WDR spells on façades with wind normal on the façade is not seen. The roof overhang somewhat shields the upper gauges, the gauge mounted almost directly below the roof overhang (W5) barely receives WDR. The mid-wall has more WDR than the edge. This is due to the oblique wind to the façade; 270° – 130° = 40°. WDR with oblique winds is analysed and attempted simulated in Akubu et al. (2008).

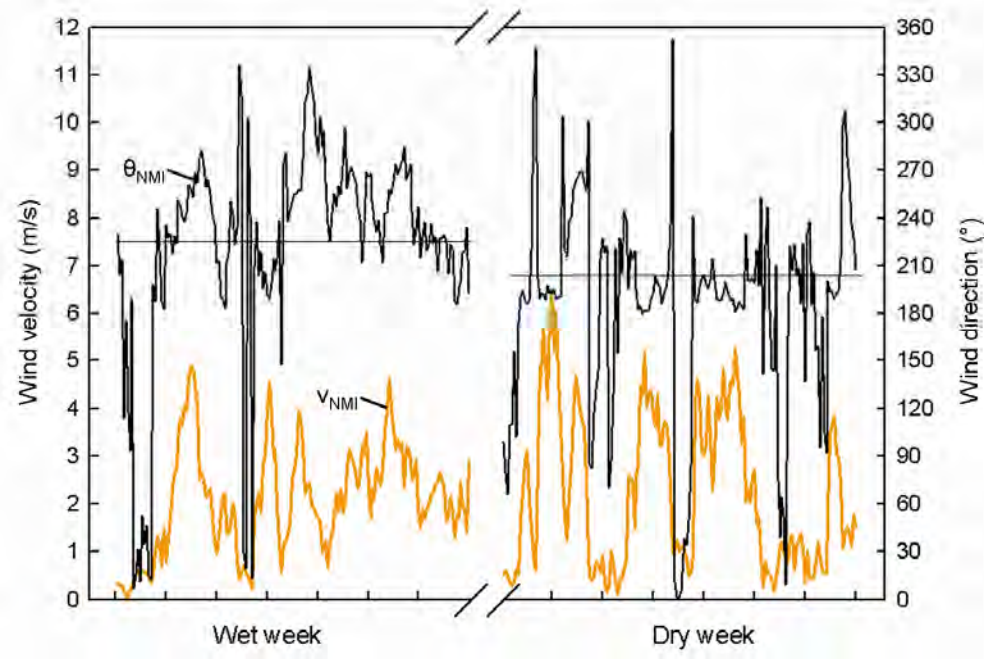

Figure 4.29. Hourly values of wind velocity (m/s) and wind direction (°) in 10 m height.

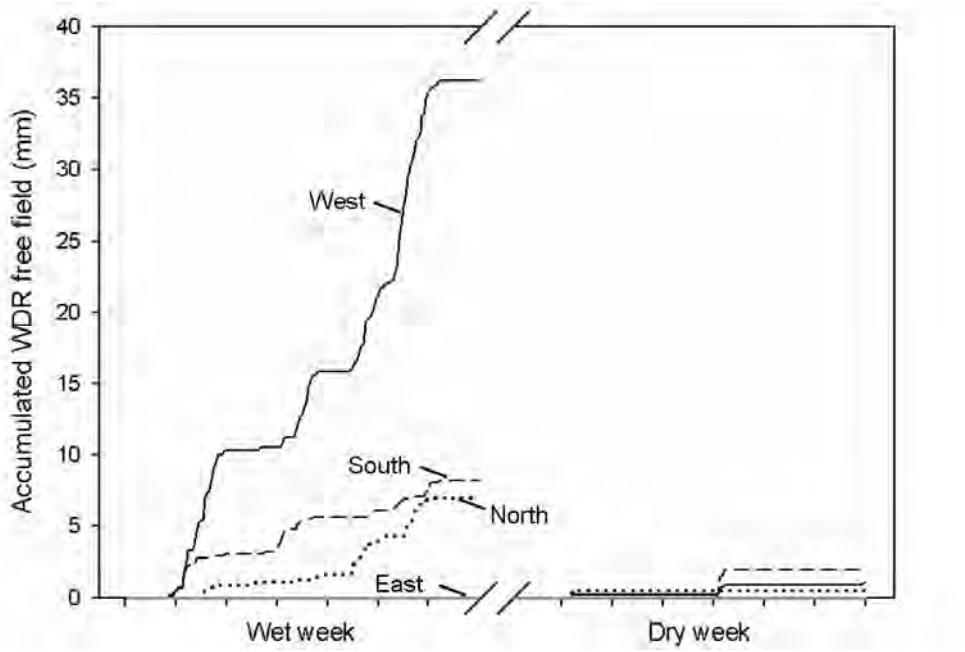

Figure 4.30. Hourly values of accumulated WDR measured in the free field gauge shown in Figure 3.5a.

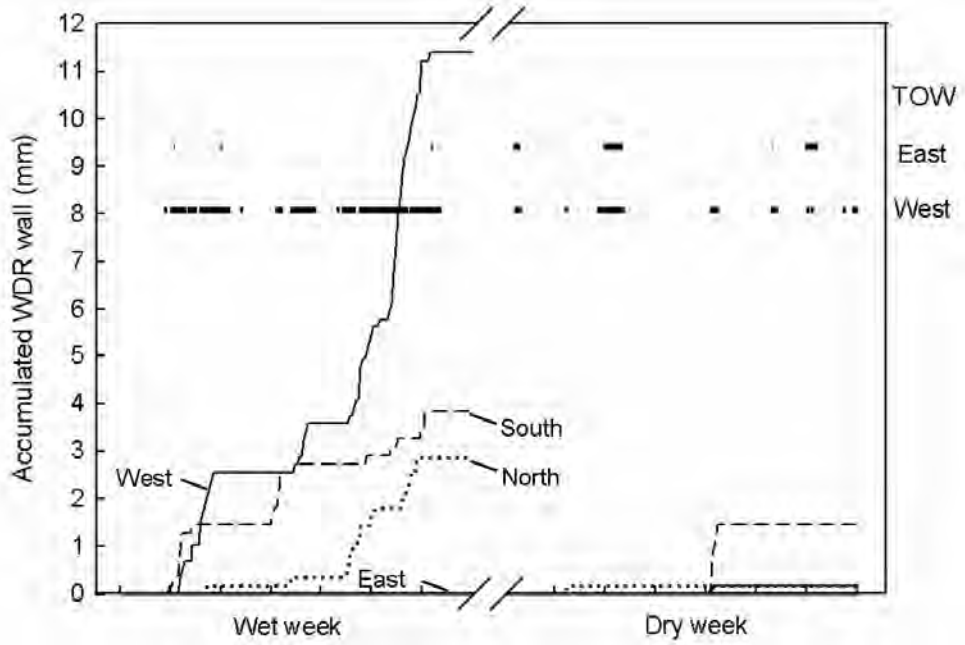

Figure 4.31. Accumulated WDR measured on wall with TOW for east and west facing walls.

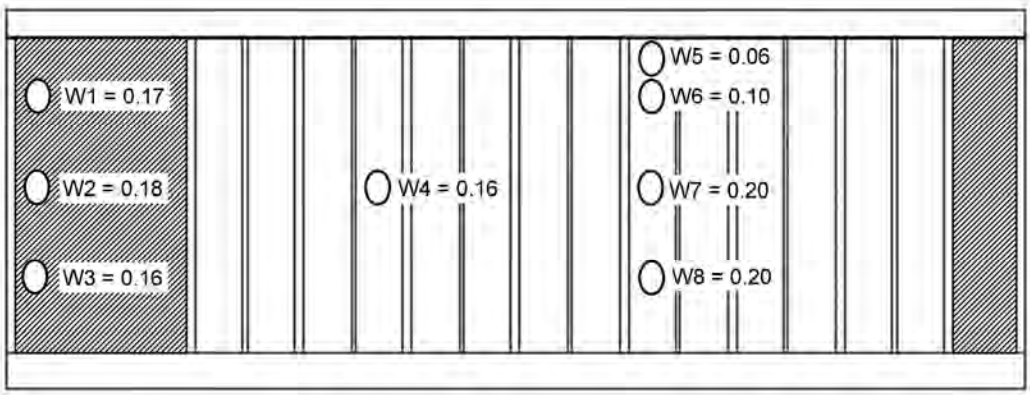

Figure 4.32. Catch ratio of WDR to show the dispersion on test house wall for the wet weeks.

The wall facing south has 0.07, facing east has 0.00 and facing north has 0.05.

4.3.3 Water vapour in cavity air

Figure 4.33 shows the RH_{CAV} and RH_{NMI}. The 23 mm, fully ventilated, cavity on the west facing side, has the lowest RH_{CAV} for both weeks. The east facing side is opposite; the fully ventilated cavity has a higher RH_{CAV} than the closed cavity. The dry week has lower RH_{CAV} in the fully ventilated cavity on both sides. The RH_{CAV} with 23 mm has the highest amplitudes, but the tops of the curves, which are during night-time does not increase like RH_{NMI}. This might be due to less ventilation during night-time because the thermal buoyancy decreases.

Vapour pressure includes the cavity temperature, and gives a more exact climate description of the water vapour content in the air. Figure 4.34 shows the state of the p_v for the west facing wall. This picture is more accurate regarding the moisture influence on the cladding. The full cavity opening does not perform best during the rainy week. However, it has clearly the lowest $p_{V,CAV}$ when the sun is shining. Figure 4.34 should show the correlation of the Δp_v, defined in Section 4.1.2, and the MC of the corresponding claddings. It is clear that when the air includes more moisture the MC is increasing and contrary decreasing.

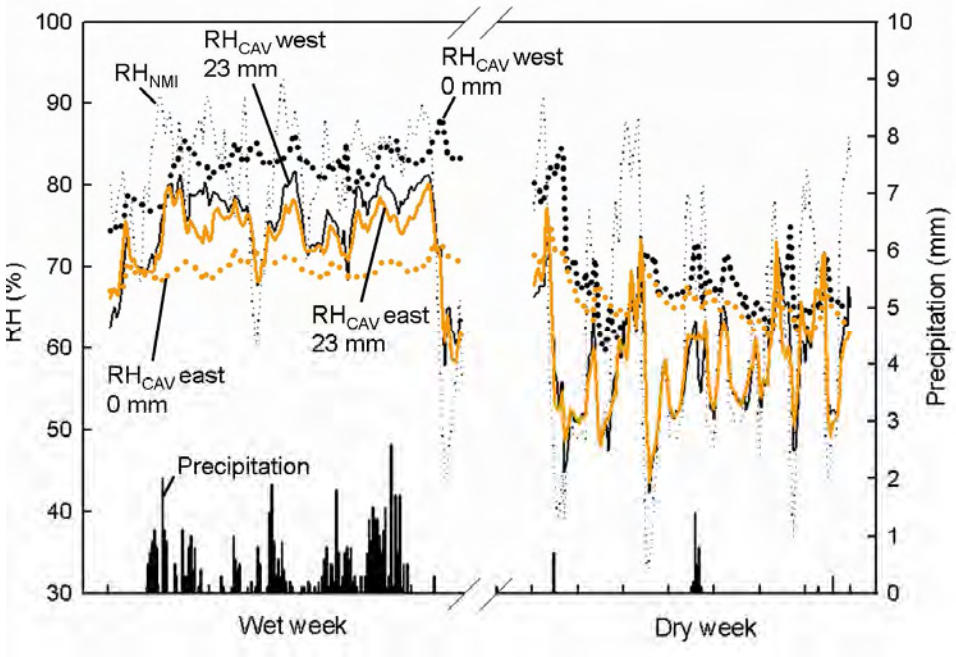

Figure 4.33. Hourly values of RH_{NMI} and RH_{CAV} (%) in the cavities with no and full cavity opening, on the east and west facing sides. Normal precipitation is also shown.

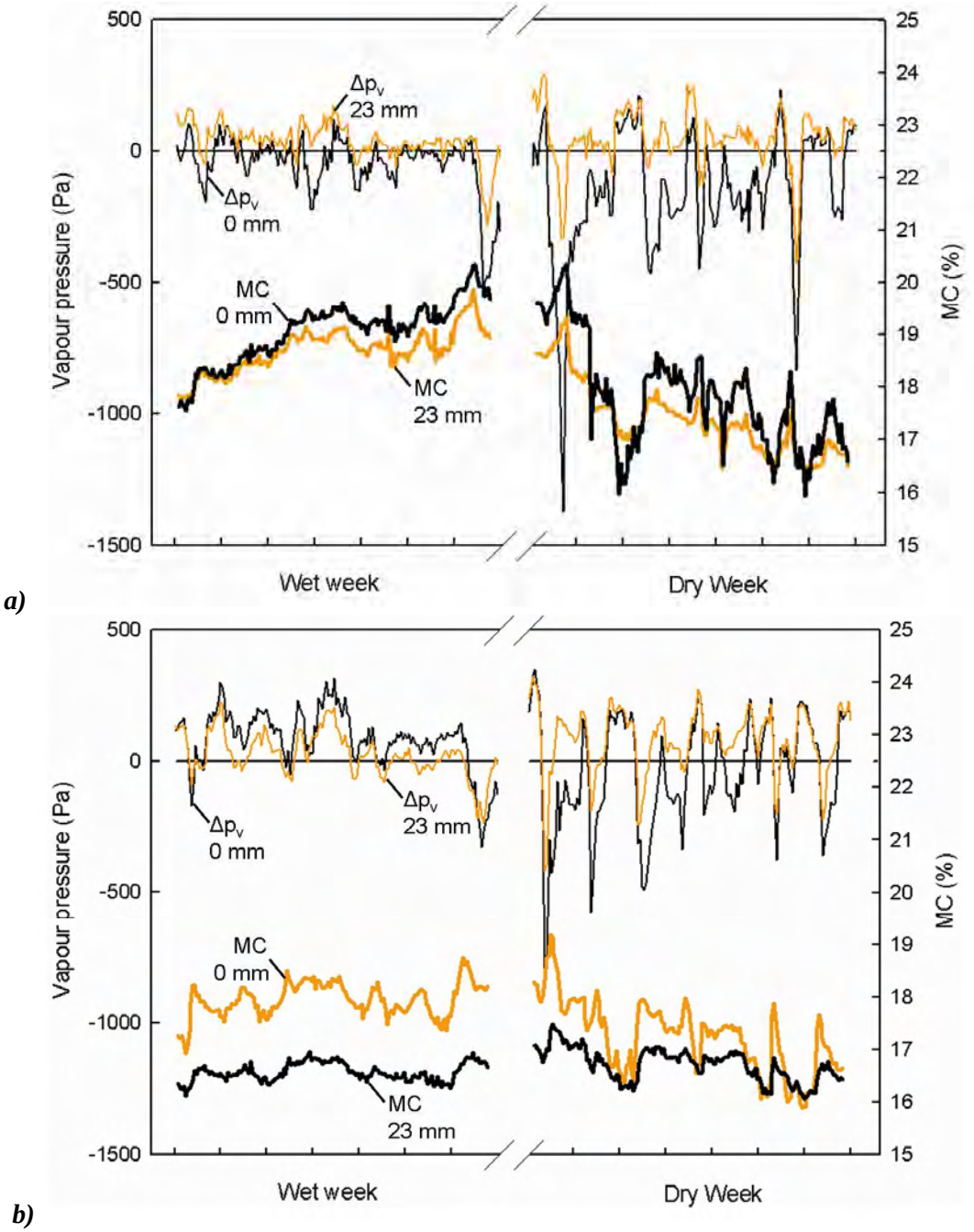

Figure 4.34. Hourly values of vapour pressure difference, Δp_v (Pa), between the ambient air and the cavities, with no and full ventilation on the a) west facing side and b) east facing side. The correlation is seen in the steep moistening when Δp_v is negative and the contrary drying when Δp_v is positive.

Wall response

The cladding without cavity has a slower response in the moistening period, as observed in Figure 4.35. This is obvious since only one side is susceptible to moisture. Figure 4.36 presents the picture of the cladding moistening and drying. The graph shows that the moistening is most rapid for the fully ventilated cavity, which is ventilated with moist air during the rainy week. During the dry week the opposite trend is seen. This graph correlates with the vapour pressure p_v in Figure 4.34.

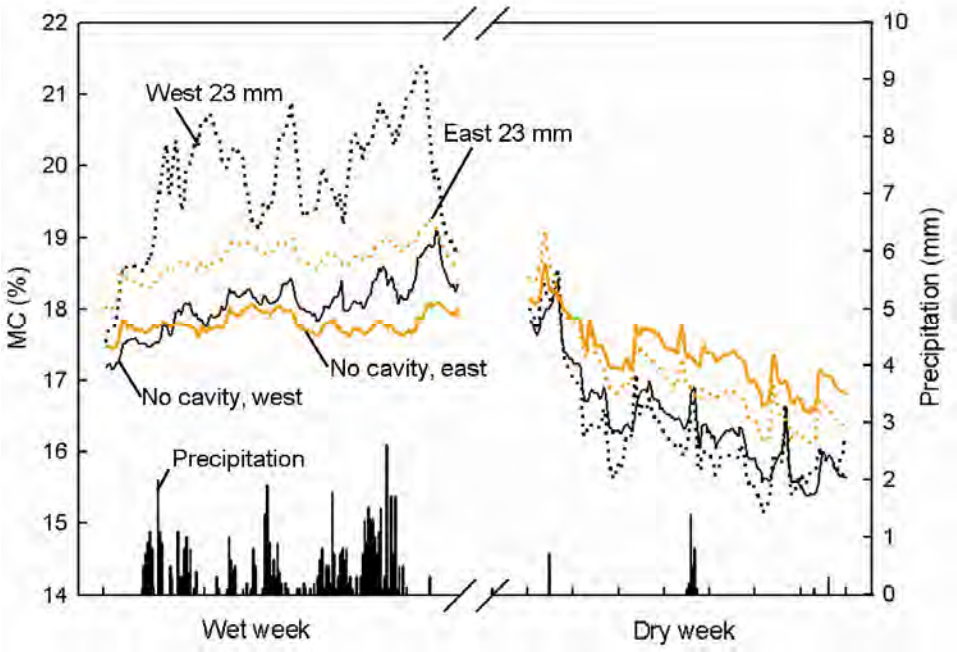

Figure 4.35. Hourly values of MC (%) on cladding with and without cavity. The cladding with cavity has full ventilation opening. Upper sensors on sections with fast grown wood with acryl (B) paint are used.

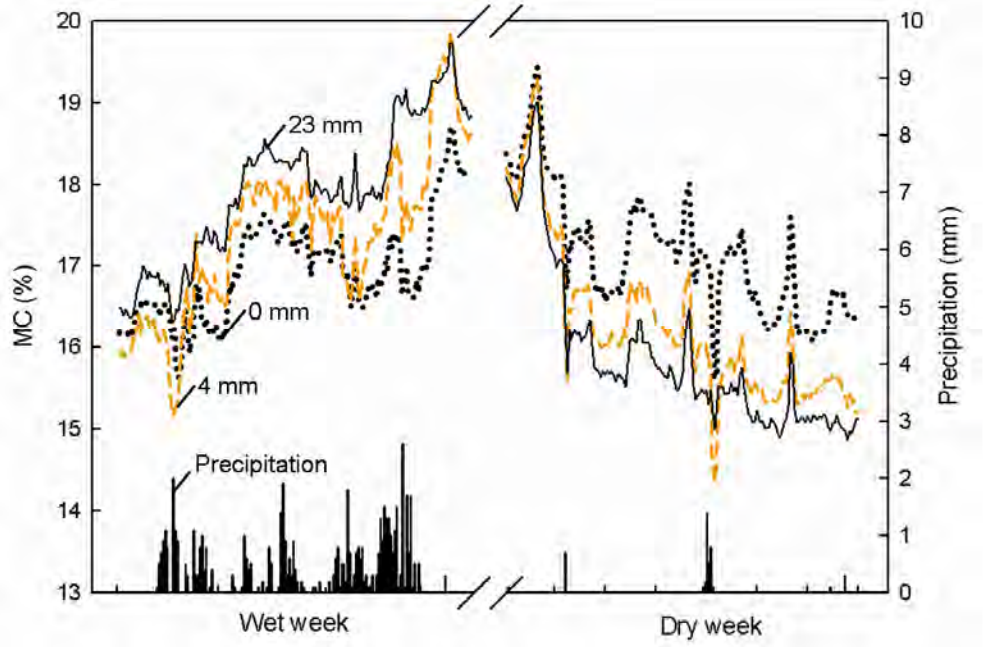

Figure 4.36. Hourly values of MC (%) on cladding with different ventilation rates. Lower sensors on sections with slow grown wood and acryl (B) paint are used.

4.4 Multiple four-day trends

When analysing wood MC there is a risk of sequential errors due to the measurement inaccuracy. A discussion of the accuracy of the MC sensors is given in Paper II. In order to avoid this error the data trend is an improved analysis; the measurement value becomes insignificant, only its variation is of importance. The trend indicates the rate of moistening or drying, and is a form of variance analysis. The advantage of extracting uniform weather periods is the possibility to differentiate between drying and moistening. The two processes have different sorption rates because the drying starts from a saturated surface. However no such differences are found in this analysis. This analysis studies the MC trends according to the design parameters; orientation, surface treatment, degree of ventilation, wood quality and the difference in the height of the cladding, similar to the average analyses in Section 4.2.

Four-day periods with uniform weather are chosen from the measurement data set. The 24 hour fluctuations are included in this analysis. The periods chosen include all periods of the year, but no periods with averaged T_{NMI} below zero. The cladding response at low temperature periods is of less importance due to the reduced risk of decay. The MC trends is the degree of slope, the x in the linear regression equation, $y = a + xb$. The climate data is averaged or summed to indicate the general climate type. Table 4.24 shows the periods chosen, with the corresponding climate and the trend values for no and full ventilation of the cavity. The periods are sorted according to RH_{NMI}, which gave the best fit for dividing the moistening and drying periods. Moistening and drying periods are analysed respectively. As seen in Table 4.24, the moistening periods include periods with rain, TOW and high RH_{NMI}. Drying out periods have somewhat warmer and windier weather.

The values of this trend analysis might improve when adding data of the cladding state prior to each four day period. But how to include such and “history” parameter is not figured. When analysing the data, the trends are averaged and compared for each parameter. The standard deviation defines the data span. Each cladding design parameter is presented in Figure 4.37.

Figure 4.37a shows the difference in the trends according to orientations. The west facing wall has a higher moisture impact compared to the east facing side, naturally giving a higher moistening influence on the west facing wall. The data span is less on the east facing wall. This is expected when the rain hitting this façade is minimal – the wind is usually giving WDR at the west facing façade. The mean value of the drying rate is slightly greater for the east facing side, indicating more efficient drying than the west facing wall. This could be because the east facing wall has limited moisture amounts to dry out.

Figure 4.37b presents the average trend values of treated and untreated claddings. Surface treatments are applied to prevent moisture soaking into the wood and the desired response is evident; the data span is greater for the untreated cladding, that is both moistening and drying out is more rapid on untreated cladding.

The ventilation rates have trends showing moisture response as expected, see Figure 4.37c. The fully ventilated cavity has the most rapid moistening and drying. This is elaborated on by the wind influence of the wood cladding MC in Figure 4.38, showing the corresponding wind velocity and trends of the fully ventilated cavity. The fitted lines show a correlation of the trends, that is the moistening and drying rate increase with increasing wind velocity.

Comparing the cladding with different growth rates reveals a slight increase in both moisture uptake and drying for fast grown wood, see Figure 4.37d. But as discussed in Section 4.2.6, the reason for the difference is not easy to define. Comparing the surface treatments does also not give a definite trend, see Figure 4.37e.

The difference over the height of the wall is given in Figure 4.37f. It shows faster moistening at the lower versus the upper part. This is equal to what is registered earlier; the lower part has a higher moisture impact. The upper part is somewhat shielded by the roof overhang.

A concluding remark is that the findings of this analysis are similar to the previous analyses, but this analysis is better regarding the level error in the MC sensors.

Table 4.24. Trend periods chosen from the measurement dataset (2004 – 2007). Climate data and trends for no or full ventilation on the west facing side is shown. The periods are sorted according to RH_{NMI}. The shaded area in the midle of the measurement periods separates moistening and drying periods and includes the summed precipitation and average values for the drying and moistening.

	Precipitation	T_{NMI}	RH_{NMI}	U^{10}_{NMI}	Trend	Trend
	Sum	Average	Average	Average	No Ventilation	Full Ventilation
Period	Mm	℃	%	m/s	0 mm	23 mm
2-5/9/06	27.7	12.6	84.4	3.1	1.2	1.7
11-14/9/04	36.4	9.3	83.8	2.1	0.3	0.3
20-23/6/05	26.8	13.6	83.3	1.5	0.6	1.2
20-23/9/04	87.1	10.5	82.8	3.1	1.3	1.6
16-19/6/06	9.7	13.8	82.1	1.5	0.6	1.5
5-8/9/04	44.6	11	81.9	3.1	1.3	1.2
19-22/7/05	4.7	14.5	80.7	2.1	0.7	1
1-4/5/07	1.6	6.1	80.2	1.9	0.1	0.5
26-29/6/05	14.3	9.2	80	3.1	1.2	0.9
16-19/9/06	4.3	12.6	77.6	1.1	0.4	0.6
7-10/6/05	9.7	8.5	77.5	3.4	0.8	1
13-16/6/04	26.1	8.7	77	4.4	1.1	1
13-16/5/05	10.2	4.4	74.8	2.8	0.4	0.4
13-16/5/06	11.1	4.4	74.3	3.5	0.8	0.8
19-21/4/06	4.8	3.3	73.4	2.4	0.1	0.3
4-7/5/05	10.9	4	71.8	2.2	0.4	0.7
↑ Moistening	330	9.2	79.1	2.6	0.7	0.9
↓ Drying	80.5	11.7	58.2	2.9	-0.7	-0.9
4-7/11/06	33.2	4.3	79.9	4.3	0.3	-0.4
22-25/8/05	11.1	14.4	74	2.9	-0.7	-0.9
18-21/8/06	4.9	16.9	73.7	1.5	0.1	0.1
25-28/5/06	4.5	7.8	66.8	2.7	0	-0.1
1-4/8/06	7.2	19	66.5	1.9	-0.3	-0.7
27-30/4/06	6.5	7.5	60.1	2.9	0	0.1
20-23/11/06	3.6	4.4	59.7	3.3	-0.4	-0.3
14-17/2/06	0	0	56.6	4.7	-1.6	-2.6
10-13/6/06	4.7	17.3	54.6	1.9	-1.6	-1.6
20-23/7/06	4.4	16.4	53.5	1.7	-0.9	-1
28/4-1/5/05	0.4	9.6	50.9	2.9	-1.2	-1
2-5/7/07	0	20.6	48.3	3	-1.3	-1.4
31/3-3/4/04	0	7.1	47	3.4	-1.1	-1.6
3-6/5/06	0	14.9	41.8	4	-1	-0.3
5-8/5/06	0	16	39.7	2.5	-1.4	-1.4

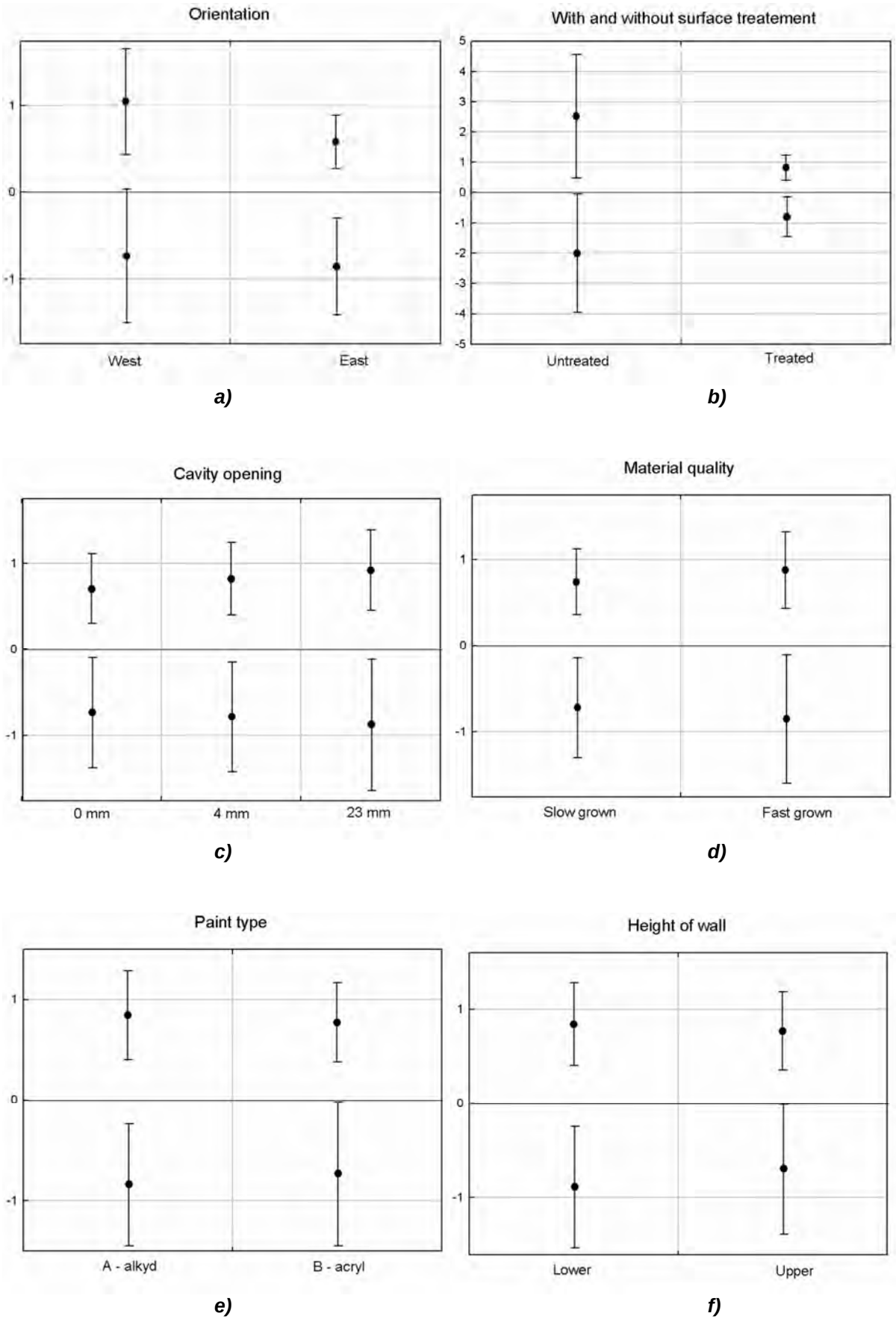

Figure 4.37. Comparing trends according to cladding parameters. The values above zero gives moistening rate and the values below is drying. Mean trend (dot) and the standard deviation (span) is shown.

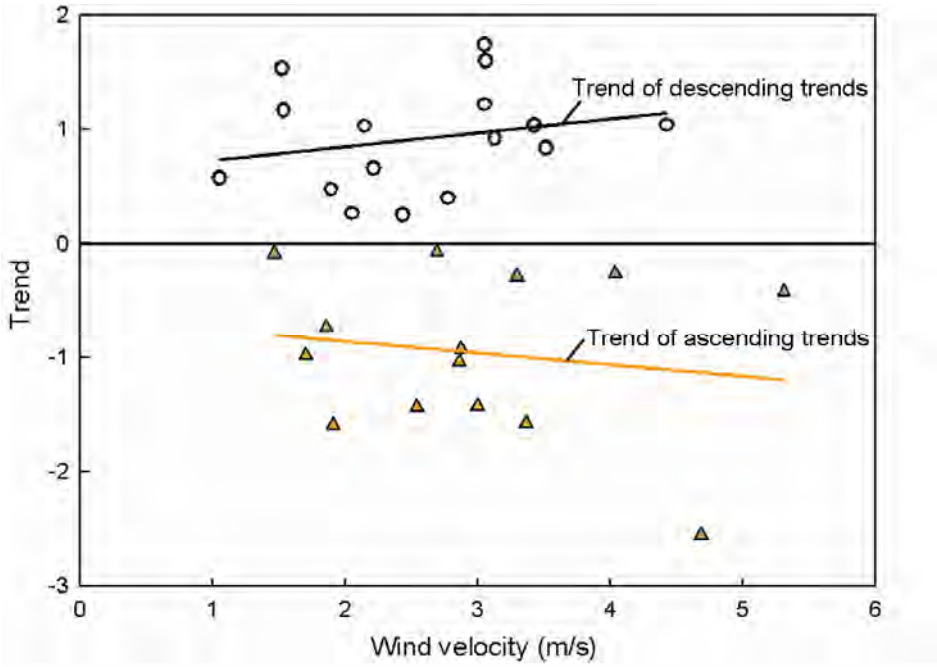

Figure 4.38. Correlation of vind velocity, U^{10}_{NMI}, and trends of moistening and drying of the fully ventilated cladding (23 mm).

4.5 Conclusions from Voll measurements

The overall conclusions of all publications based on Voll data and this chapter, are presented and are shortly summarized below. The wood cladding response to ambient climate has been measured by temperature and MC in the test house cladding. The performance of the wood cladding is clearly different on the two opposite facing walls at Voll, indicating that it might even be appropriate to differentiate cladding design on differently oriented walls in the same building.

The analysis used to analyse the moisture performance is based on studying climate exposure, cladding temperature and MC respectively. No post processing is carried out to define risk of rot or such. For the time being such analysis needs MC data with low error. To avoid escalation of such errors the most advanced analysis performed is the trend analysis. Trend does not take the average value into account, only the development of the value. Trend may be best way to differentiate similar studies using wood MC.

Paper IV presents an analysis of the cladding response time lag to the climate influence. The wood MC has a rapid response to the ambient climate variation. In the hourly data, a one hour time lag gave the best data fit. The response is most rapid when the cladding is untreated and ventilated. Paper IV also defined the most important climate parameters using the direct meteorological measurements; T_{NMI}, QO_{NMI} and U^{10}_{NMI}. The fact that wind turns out as a top three parameter was surprising and lead to an intensified investigation of the wind influence of ventilated cavities resulting in Paper VI.

The wood cladding design element study revealed that the difference in the micro climate between the east and west facing walls is distinct, with the main difference within the radiation, wind and WDR properties. This gave different response on the two opposite oriented walls. Lauter and Time (2005) also pointed out this as the major difference of the different cladding design parameters.

The need for a ventilated cavity is shown, most clearly in Section 4.2.2. Adding up the experiences without cavity gives a clear recommendation to include the cavity whenever water may be present and there is a risk of decay, which probably is a possibility on all external applications.
The function as a capillary break and liquid water drainage of the wall is additional to the ventilation effect of the cladding. Fully ventilated cavities perform well when the weather influence is severe, as for the west facing side at Voll. When fully ventilating the cladding on east facing side the effect reverse; moistening the cladding, probably with warmer, humid air. This is why closing the cavity is sound in less exposed locations.

Untreated wood reacts more rapidly to climate exposure compared to treated wood. Acryl paint (B) performs best on the east facing wall (Johansen 2007 and Section 4.2.4). This means that acryl paint may be used in less severe climates. The alkyd based paint performed best on the west facing wall.

The difference of the wood quality, slow and fast grown wood is not easy to interpret when the MC sensors are not calibrated according to density. The only distinction made is the higher standard deviation of the fast grown wood (Section 4.2.5 and Lauter and Time 2005).

The roof overhang shields the upper cladding boards. The upper instrumented boards have slightly higher temperature and lower MC average and standard deviation. Small variations are found in the temperatures measured over the cladding depth.

5 Numerical simulation of hygrothermal performance of ventilated wooden claddings

Hygrothermal performance, transient temperature and moisture conditions, can be calculated with numerical HAM simulations. When the calculated hygrothermal performance is validated with measured values, the understanding of building physical challenges increase. The challenges with building physical simulation tools are to apply the correct material and geometrical data, transfer coefficients and appropriate physical transfer models. The great advantage of HAM simulations is the low cost of calculations with modified designs or different climate conditions, compared to field or laboratory studies. A change in climate conditions may represent a new geographical location or a climate change scenario.

This chapter includes three simulations; (I) the solitary wood cladding, (II) CFD of the wind-induced bulk and cavity air flow at the test house, and (III) full simulations of the wall assembly with cavity ventilation. The simulation of the wood cladding (I, see section 5.1) is done by using outer climate and cavity climate as input. Only painted cladding is calculated. The cavity air flow (II) resulting from an entire bulk air flow around a low-rise house is calculated in CFD. This study is described in full in Paper VI. The simulation of the original Voll test house configuration is presented in this section 5.2. An equation is deducted to calculate the ACH from wind speed, wind direction and cavity depth of the ventilated wall. The full wall assembly simulation (III, see section 5.3) includes the cavity air change rate (ACH) calculated from the equation given in (II). The ACH is derived from the CFD results. Finally, this model is altered to calculate hygrothermal performance with increased insulation thickness and different climate exposures. Paper V was a first attempt on a simplified simulation of cladding performance in different climates. WUFI 4.2 Pro (2008), a 1D numerical software, is used for hygrothermal simulations and Fluent 6.3.26 (2008) is used for the CFD simulation.

WUFI is commercial software designed to calculate realistic hygrothermal processes. It is a numerical simulation tool which includes coupled heat and moisture transport. Three moisture transport mechanisms are included: vapour diffusion, surface diffusion and capillary conduction, with vapour pressure, RH and capillary tension as the respective driving forces. In order to use WUFI in research, direct control can be taken, i.e. by defining separate climate files or by defining separate material layers like the paint layer. Wood is a material with large variations and the material properties are not easy to measure or find in the literature, at least not in the capillary region. The capillary region is often neglected, and the sorption curve is extended to include this transport process as well. In this analysis the capillary coefficients are defined for the wood cladding, to improve the simulation results. The wood reaction to variation in climate exposure is quick, especially in the outer millimetres (Time 1998). This is not easy to calculate by hourly time steps. One limit in WUFI is that the material input does not admit temperature dependent sorption curves. Another challenge is that the moisture history (i.e. the hysteresis effect) of the material is not taken into account, for example whether a material is drying or whether moisture is redistributed after a WDR incident.

5.1 Hygrothermal simulation of wooden cladding

This section describes a wooden cladding model, and its validation against the five cavities instrumented with RH sensors for the year 2006. The same exercise was done in Paper V, but at that time the measurement data did not include RH measurements in any cavities.

1.1 Model and input

In order to calculate hygrothermal conditions in wooden cladding the input data must be well defined. The input data is the climate data, material data and transfer coefficients. By simulating wooden cladding alone, these parameters can be controlled. Figure 5.1 a and b show the test sections calculated and the sensors used to define climate input and measure test cladding validation data. The climates are measured close to the cladding board on both sides.

In WUFI a climate file can be used as input by defining:

- the liquid/rain load on the vertical exterior surface in [l/m²h or mm]
- the solar radiation on the vertical exterior surface in [W/m²]
- the temperature of the exterior air [°C]
- the relative humidity of the exterior air [-]
- the temperature of the interior air [°C]
- the relative humidity of the interior air [-]
- the barometric pressure [hPa].

a)

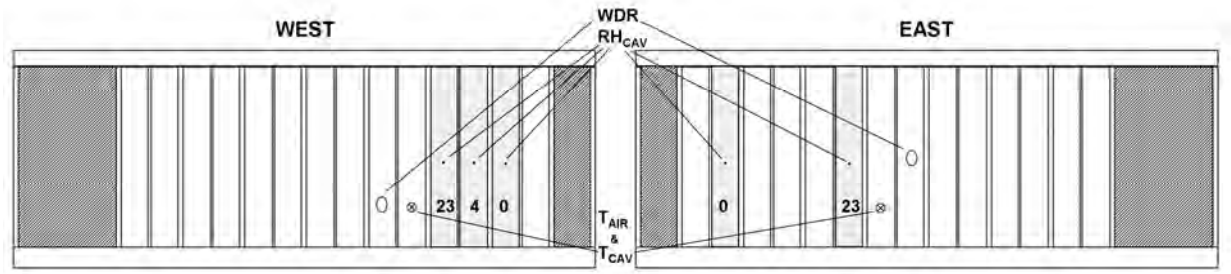

b)

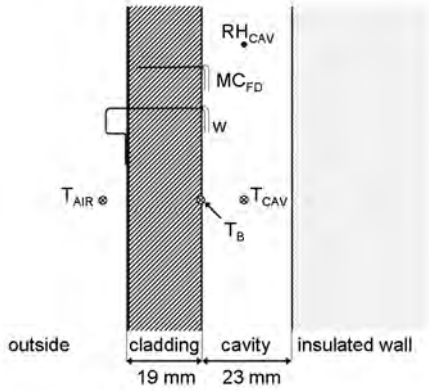

Figure 5.1.a) The test sections and sensors used for validation of the cladding model. The test sections have slow grown wood (S) and alkyd paint (A). b) Vertical section of the wooden test cladding with the test sensors that provide input and validation data.

The liquid water influence on the test cladding is defined both by measured WDR and TOW. Primarily the measured WDR amount on the wall defines the liquid water influence. Additionally when TOW is registered in hours without WDR influence, the wall moisture is set to 0.1 mm, equivalent to a thin water film. With less surface liquid water WUFI does not include it in the calculation. TOW is defined in Equation 3.1.

The shortwave radiation, r, is calculated for the two test walls, see Figure 5.2 a. r includes direct and diffuse radiation calculated by a program written by Geving (1995). Input was T_{NMI}, QO_{NMI}, $U^{10}{}_{NMI}$, and data to define the solar azimuth. Unfortunately the calculation crashed in the autumn, after this the measured global radiation is used, as seen in Figure 5.2 b and c. The average radiation incidence on the west facing side is 31.3 W/m^2 and 33.5 W/m^2 on the east facing side. This is not entirely correct as the east facing wall should have the least radiation incidence due to the shading from the hill and the neighbour test house. Topography is not included in the radiation calculation. The albedo of the ground which defines much of the diffuse radiation, changes according to the season, with grass or snow cover. This is also not taken into account when defining short wave radiation.

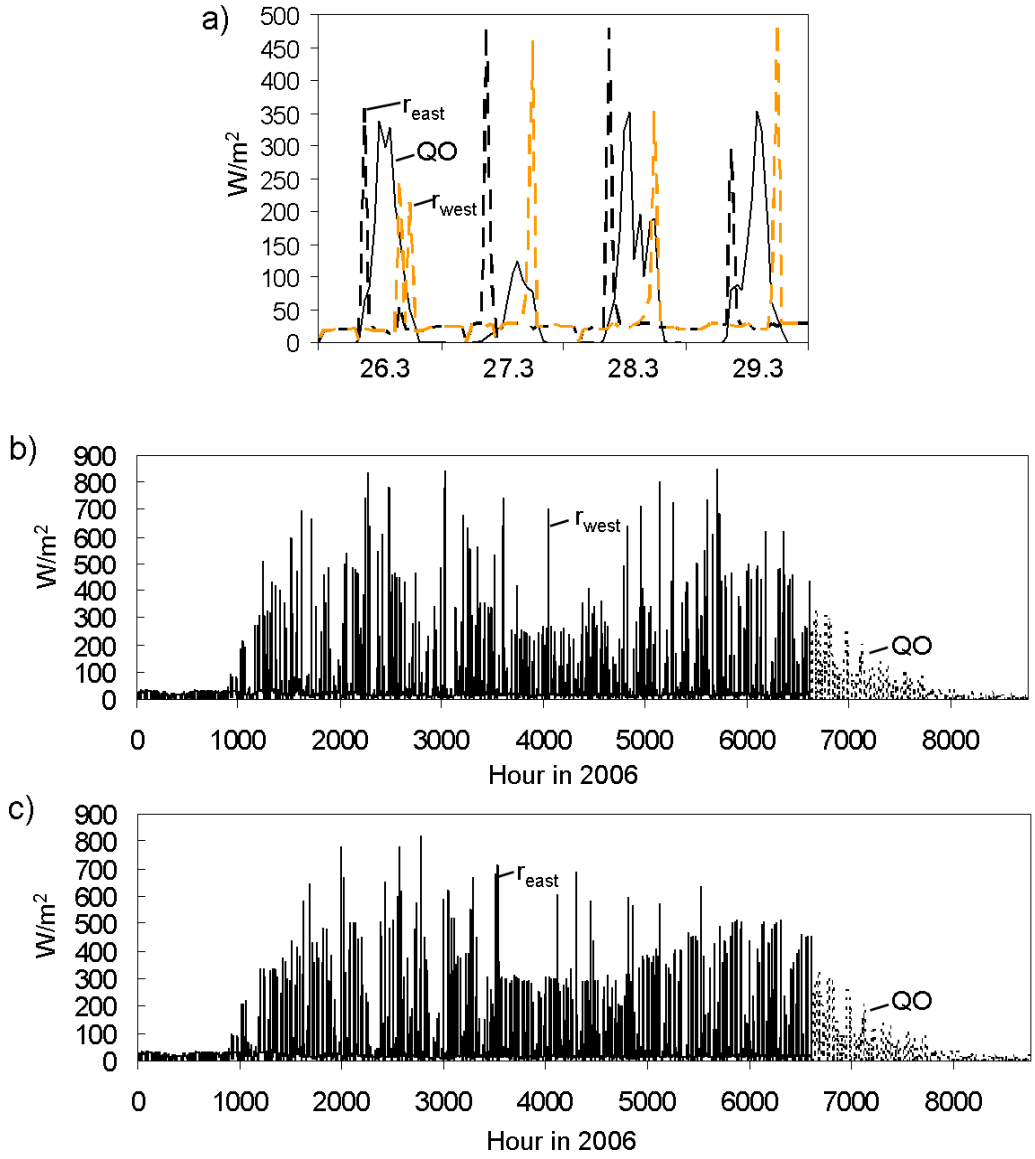

Figure 5.2. Radiation calculated on the west and east facing walls for 2006. a) Four days showing the 24 hour short wave radiation incidence, calculated for east and west facing wall and measured. b) Short wave radiation on the west facing wall and c) short wave radiation on the east facing wall.

The exterior temperature T_{AIR} is measured near the cladding surface in neighbouring sections on both walls, as shown in Figure 5.1a. T_{CAV} is also measured in the neighbouring section, but corrected with the T_B difference of the section calculated and the section measured. The RH_{AIR}, that is RH of the exterior air close to the cladding surface, is calculated from the meteorological measurements and the T_{AIR}, as given in Equation 5.1. The barometric pressure is taken directly from the meteorological measurements.

$$RH_{AIR} = \left(\frac{p_{sat,TTM}}{p_{sat,T_{Air}}} \right) \left(\frac{RH_{NMI}}{100} \right) \qquad 5.1$$

To validate the model with the surface treatment inserted as an s_d value was not successful. Hence, the liquid transport properties have been included by adding the paint layer modelled as a separate material layer. This was also done in Paper V. To avoid large steps in element size of the numerical grid, the paint layer is inserted with 1 mm thickness; the resulting s_d-values are correctly scaled. The real thickness is ~0.1 mm. The input values of the material properties for the cladding and paint layer are shown in Tables 5.1 and 5.2. The initial moisture content is defined according to its measured values in the start of the simulation. The surface transfer coefficients used are shown in Table 5.3. The rain water absorbance coefficient in WUFI takes into account the reduced surface water amount due to rain splashing on the facade. However, the rain absorption coefficient is set to 1 in this work. This coefficient is of less importance for wooden cladding, since the capillary absorption through the paint is limited as long as the paint is intact. More important is the definition of wet or dry surface.

Table 5.1. Material properties for the test cladding.

MATERIAL PROPERTY	UNIT				REFERENCE
Density	kg/m^3	470			Measured, Section 3.5.2
Porosity	m^3/m^3	0.75			Støre Valen (1998)
Specific heat capacity	kJ/kgK	1600			EN 12524
Thermal heat conductivity	W/mK	RH 0 0.98	λ 0.125 0.320		EN 12524
Water vapour diffusion resistance factor		RH 0 0.3 0.6 0.7	μ 130 130 47 32		EN 12524 20% is added because the density was 390 kg/m^3
Liquid diffusivity coefficients	m^2/s	RH 10 80	D_{WS} 1E-12 1E-10	D_{WW} 1E-12 1E-10	Støre Valen (1998)
Sorption isotherm at 23 ℃	%	RH 0 33 51 84 90 95 100	u 0.0 42.0 52.5 84.0 107.3 126.0 370.0		Measured, Section 3.5.3

Table 5.2. Material properties for the paint layer.

MATERIAL PROPERTY	UNIT			REFERENCE
Density	kg/m^3	130		Paper V
Porosity	m^3/m^3	0.08		Støre Valen (1998)
Specific heat capacity	kJ/kgK	230		Paper V
Thermal heat conductivity	W/mK	RH 0	λ 2300	Støre Valen (1998)
Water vapour diffusion resistance factor		RH 0 70 90	μ 5000 2800 1800	Støre Valen (1998) and measured s_d at RH = 70%
Liquid diffusivity coefficients	m^2/s	RH 15 45	D_{WS} 1E-15 1.3E-10	D_{WW} 1E-15 5E-13	Støre Valen (1998)
Sorption isotherm at 23 ℃	%	RH 20 40 60 70 80 85 90 95 97	u 2.0 3.0 6.0 10.0 15.5 21.0 31.0 53.0 72.0	Støre Valen (1998)

Table 5.3. Surface transfer coefficients.

SURFACE TRANSFER COEFFICIENT	UNIT	CLADDING BOARD MODEL
Heat resistance outer wall	m^2K/W	0.588
Heat resistance inner wall	m^2K/W	0.125
Solar radiation absorbance	W/m^2	0.30
Long wave emissivity	W/m^2	0.95
Rain water absorbance coefficient	-	1

5.1.2 Results

Figure 5.3 presents measured MC_{FD} versus calculated MC_{WUFI}, as the total MC of the cladding boards. The correlation between MC_{FD} and MC_{WUFI} are shown in Table 5.4, showing the best correlation, 0.94, is with the fully ventilated (23 mm) west facing cladding. This implies that hygrothermal performance in wood cladding can be calculated relatively accurately. When using only WDR as surface water input data, omitting the TOW data, the result is shown in Figure 5.3a. MC_{WUFI} does not reach measured MC_{FD} when only using WDR as a liquid water boundary condition.

There are several reasons for the deviation between measured and calculated results. One reason for the discrepancy between measured and calculated values is the difficulty of defining the surface wetness of the outer wall. The wetness sensor does not work in periods below 0°C. It does not detect rime which may cause the WUFI calculations to be too low, as seen in the first part of all graphs. Another deviation is that the two wood claddings sections with no cavity ventilation and 4 mm opening, are close to the corners of the test house, see Figure 5.1.a. The wind flow increases near the corners. This may increase the drying rate in these sections, which might explain the lower MC measured in the autumn for these sections. At last the fluctuations are larger on a daily basis for the measured MC data. This might be due to the liquid transport coefficient which is difficult to measure and correctly imply in simulations.

However, the calculations show that the model does predict the cladding MC fairly good. This cladding model is used in the further studies when including the full wall assembly.

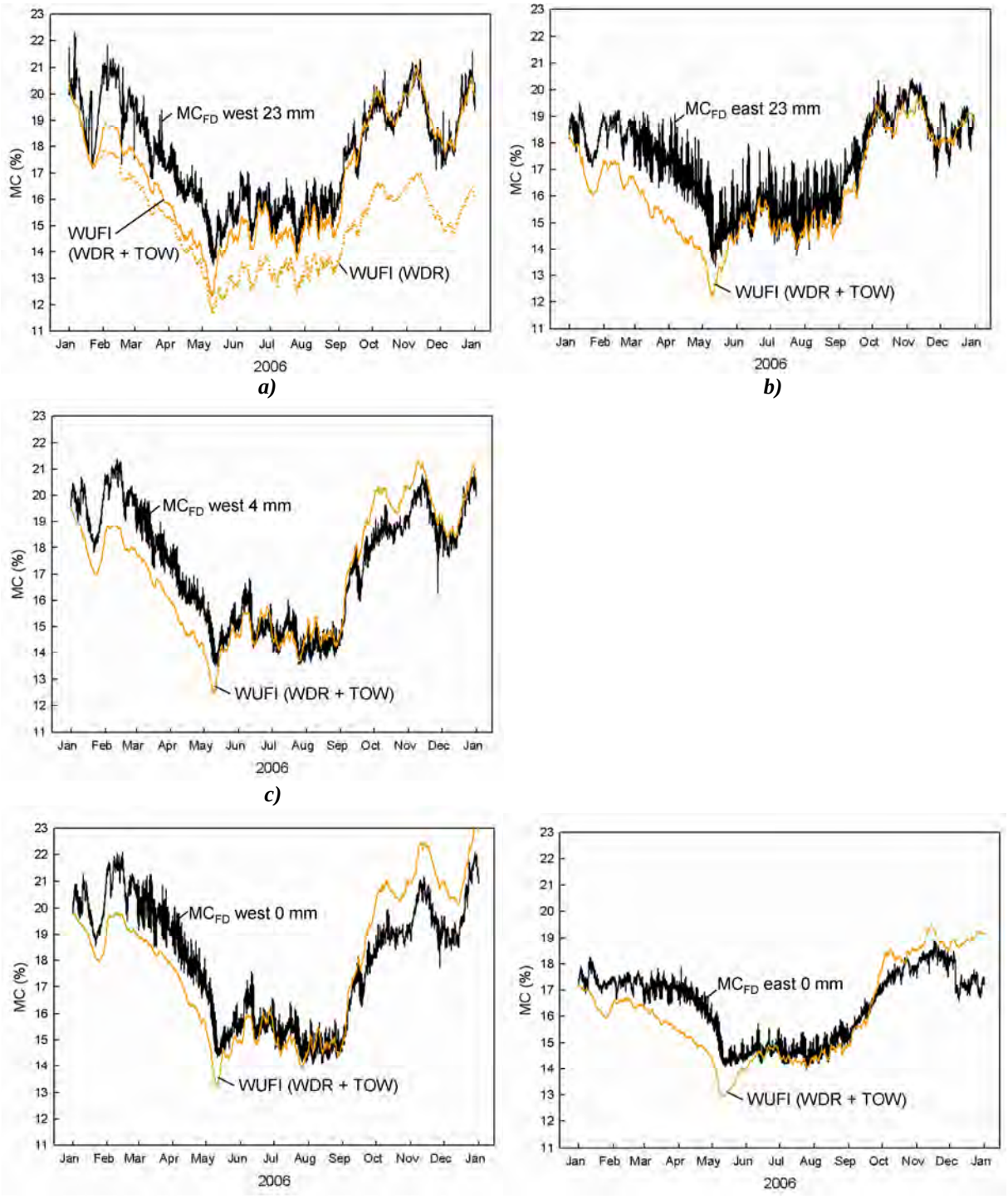

Figure 5.3 Measurement and calculation results of the cavities with RH sensors installed. a) Test section with fully ventilated cavity facing west. MC_{WUFI} is shown simulated with surface liquid from WDR and TOW or WDR only. b) Fully ventilated, 23 mm, facing east, c) 4 mm cavity opening facing west, d) No cavity opening facing west and e) no cavity opening facing east.

Table 5.4. Correlation coefficients for the MC_{FD} and calculated cladding MC_{WUFI}.

Section	Corr
East 0 mm	0.86
East 23 mm	0.88
West 0 mm	0.88
West 4 mm	0.89
West 23 mm	0.94

5.2 Modelling cavity air flow

When calculating the hygrothermal behaviour of the full wall assembly, the cavity ventilation should be included. The air flow around the Voll test house and in the cavity has been studied by CFD modelling. Paper VI describes the coupled and decoupled CFD simulations done on the test house and the CFD validation studies. For the study in Paper VI the foundation of the Voll house went all the way down to the ground, which is most common. The test house however, is supported by posts, as seen in Figure 5.4 and in the picture in Figure 1.1. The original test house build up with air flow underneath is used in the CFD simulations in this section.

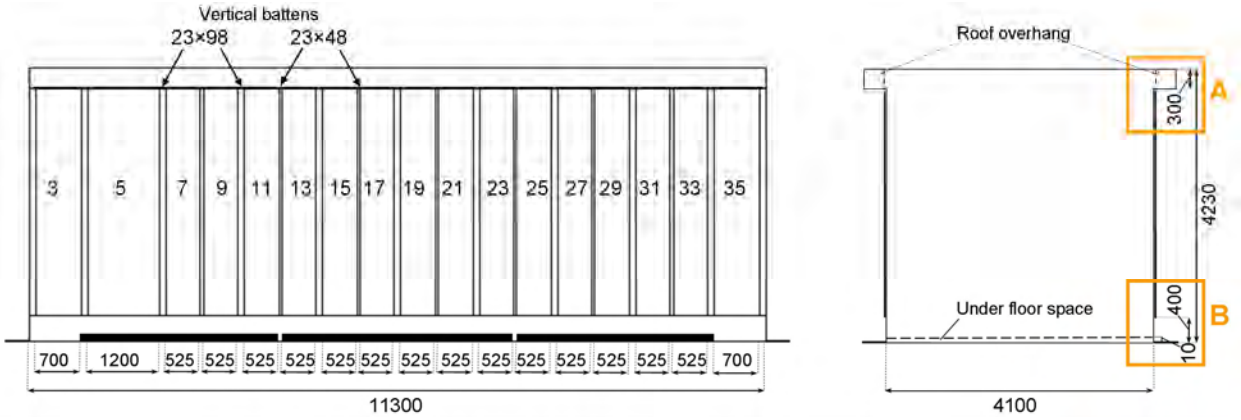

Figure 5.4 Set up of the Voll test house for CFD simulations of the test house including the air flow underneath.

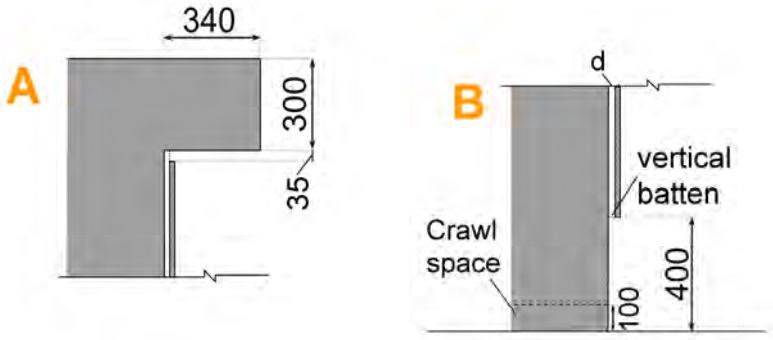

Figure 5.5. Detailed cross sections of the test house, as outlined in Figure 5.4. a) top with roof overhang b) bottom of test house.

Figure 5.6 show the air speed in the cavity according to wind direction. One can see that there is mostly downwards flow, but it also has a lateral component. This lateral is more pronounced as the wind becomes more parallel to the facade. The flow is quite complex, more than expected. This reveals the need for thorough CFD studies of cavity flow including the bulk flow of test buildings. The flow is less pronounced in thesis simulation compared to the flow calculate in Paper VI. This is due to the opening underneath the building serving as an outlet for the built up pressure.

Figure 5.7 show the air change rate and pressure difference over the cavity according to wind direction. As expected, there is a correlation between the pressure difference and air change rate. Paper VI holds a discussion on the simplified decoupled calculation compared to the full bulk CFD model shown here. It is shown that extracting surface pressures and implementing them in a cavity model overestimates the ACH because factors like the lateral wind flow are not included.

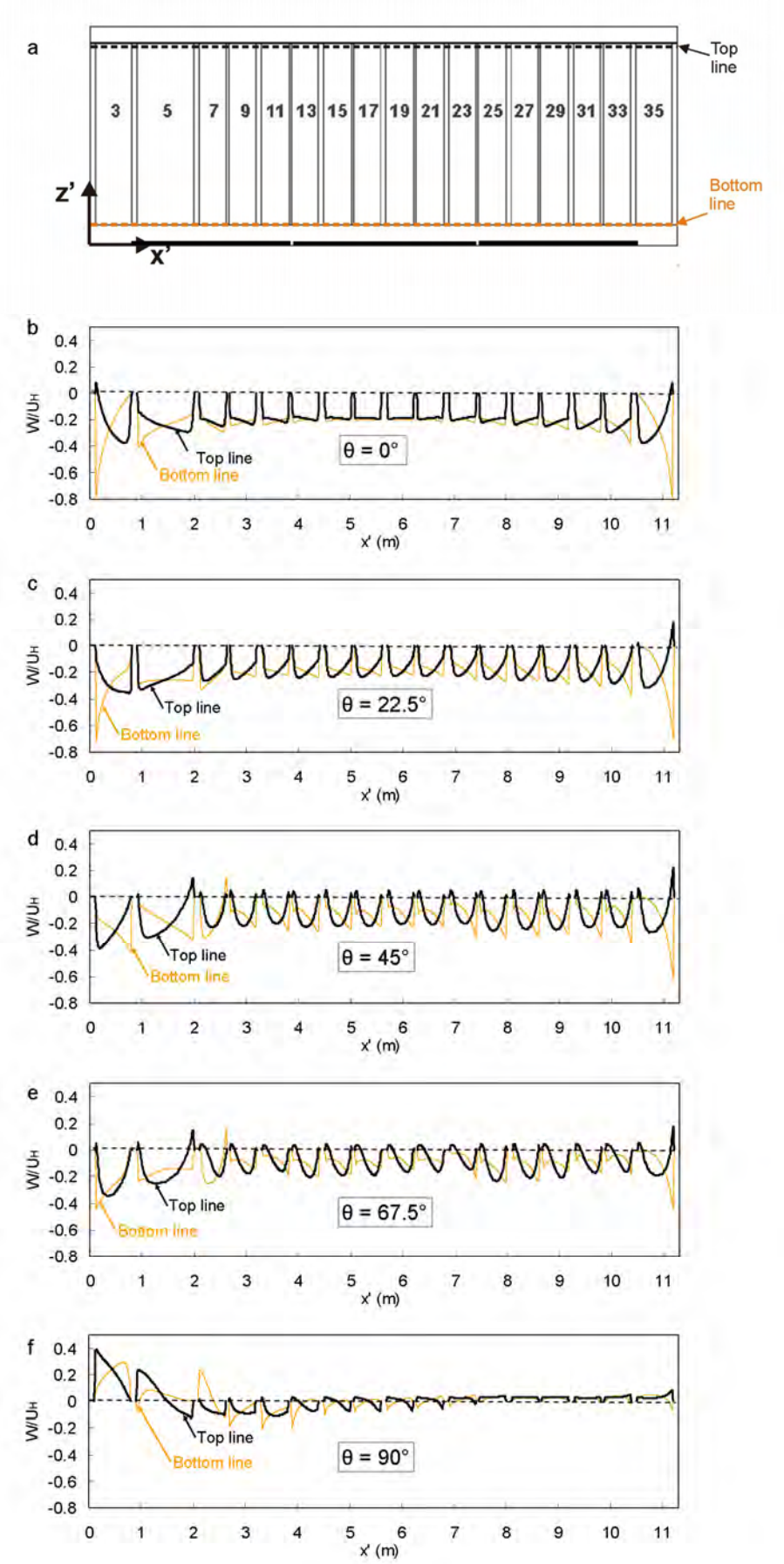

Figure 5.6. Air speed ratio and direction in top and bottom of cavities according to wind direction. a) Outline of the test house. b)-f) air flow with wind direction 0°, 22.5°, 45°, 67.5° and 90° towards the facade.

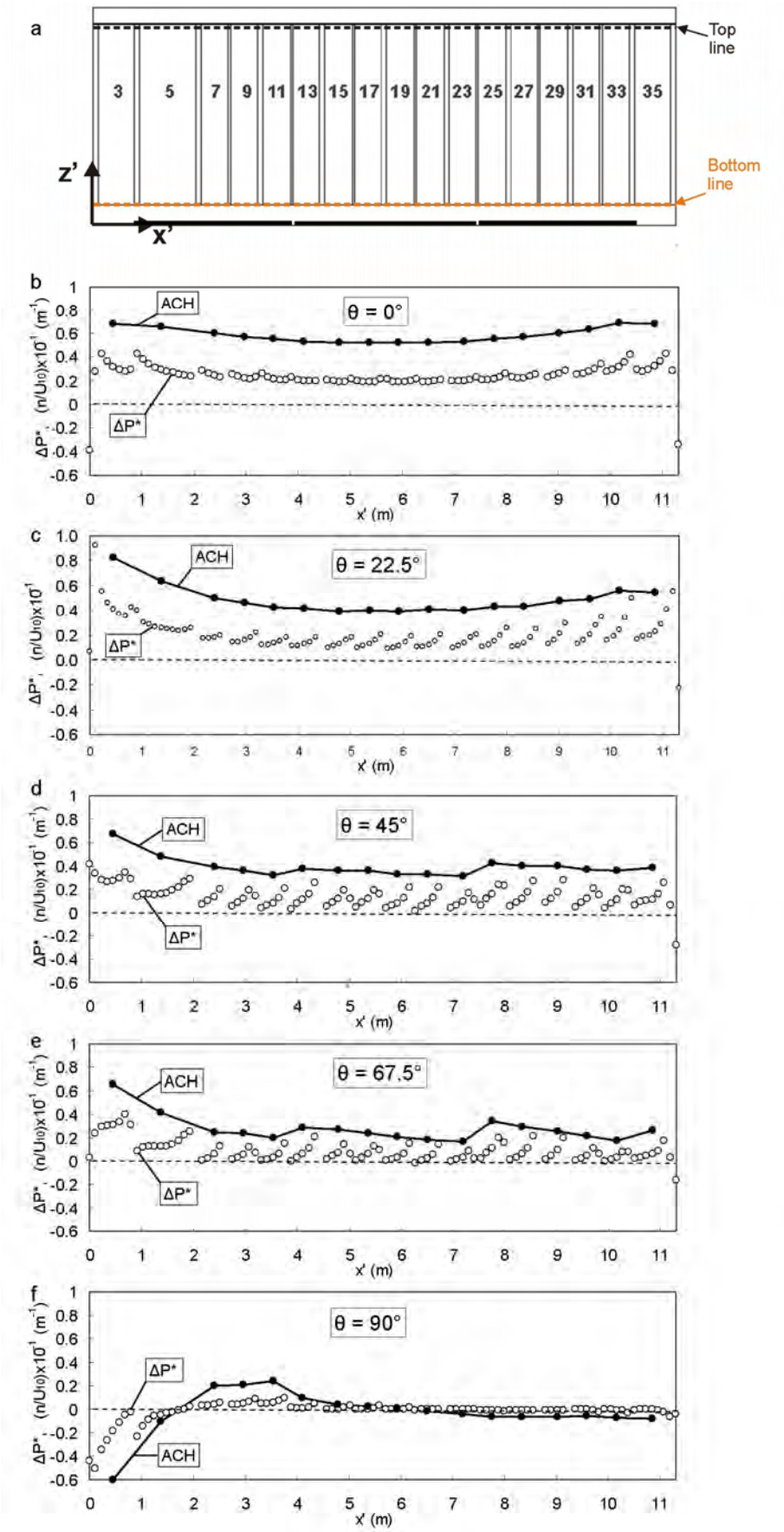

Figure 5.7. Air change rate and pressure difference (pressure along top line – pressure along bottom line) of the cavities according to wind direction. a) Outline of the test house. b)-f) air flow with wind direction 0°, 22.5°, 45°, 67.5° and 90° towards the facade.

A function is deducted from the results, which defines the ACH (1/h) of the cavities at the Voll test house, based on U^{10}_{NMI}, θ_{NMI}, and cavity depth, d, see Equation 5.2. Turbulent flow in the cavities is assumed. Note: The equation is only valid for the Voll building. The generalized equation is given in paper VI. A small ventilation rate is assumed at all times, when Equation 5.2 gives ACH = 0, ACH is set to 10 h^{-1}. This function is used when calculating the ACH in the full wall assembly. The buoyancy counteracts the air flow due to wind pressure. Thermal buoyancy is not included.

$$ACH = 10^{-5} \times U_{10} \left(-5d^2 + 365d\right) [\cos\theta]^{1.1} \qquad 5.2$$

Figure 5.8 show the calculated ACH from five days in August in 2006. The ACH ranges from 10 to almost 4000 in extreme windy weather, but is limited to 600 in order to avoid convergence errors in further calculations.

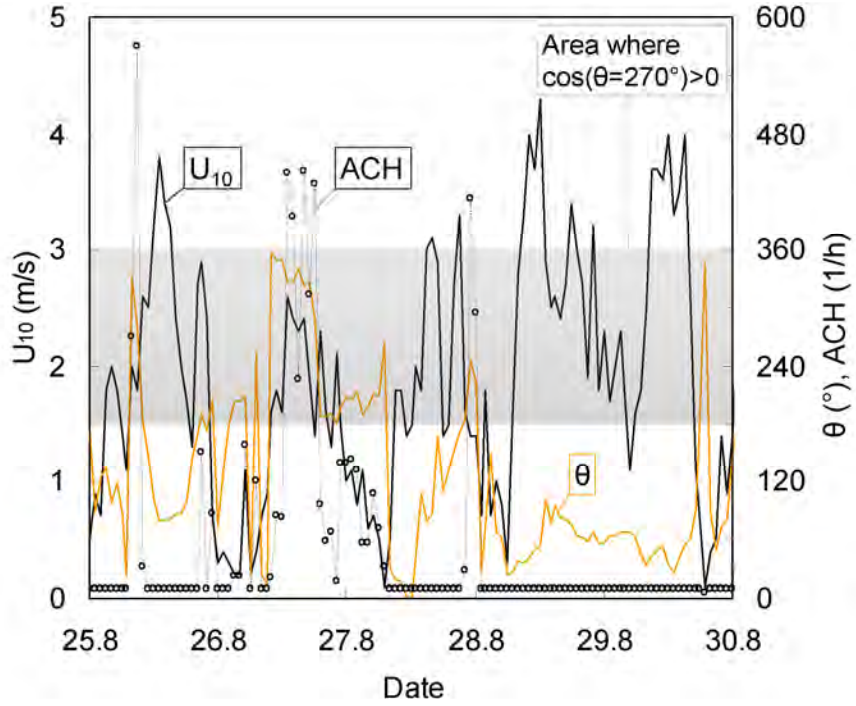

Figure 5.8. Air change rate (ACH) calculated from equation 5.2, from wind velocity and wind direction for the west facing side (θ=270°) and 23 mm cavity opening. The grey area shows the angle span (180-360°) where ACH is calculated.

5.3 Numerical simulation of the wall assembly

The full wall assembly is displayed in Figure 3.9.c. This section comprises a validation study of the ACH calculation in WUFI; measured (section 2WN) versus calculated RH_{CAV}, and the full wall assembly cladding MC is calculated for increased insulation thickness and for the climates in Oslo, Bergen, Trondheim and Tromsø.

5.3.1 Model and input

WUFI 4.2 is used in for calculation of the full wall assembly. A model including the cavity air flow gives a good basis for hygrothermal wood cladding performance analysis. Material properties of the full wall assembly are given in Table 5.5, except for the cladding and the paint layer, which is presented earlier. The material property for the cavity air depends on whether the cavity is ventilated or not. In these simulations the vapour concentration in air was limited to 1.25 kg/m^3, which is plenty, but this was needed to stop WUFI from convergence errors during calculations.

Table 5.5. Material properties for the full wall assembly used in WUFI calculations.

Material	Thickness mm	Density kg/m^3	s_d-value m	λ W/mK	Heat.cap. J/kgK	μ -
Air gap – not ventilated	23	0	0.1	0.155	1000	0.01
Air gap – ventilated	23			0.155		0.51
Gypsum board	12	850	1	0.20**	850	
Insulation	150/200/250	60	2.6	0.04**	850	
PE foil	1*	130	87	1.65	2200	
Chipboard	12	595	20.6	0.13**	1500	

* To avoid large steps in element size of the numerical grid, the layer is inserted with 1 mm thickness, the resulting s_d-values are correctly scaled. The real thickness of the PE-foil is 0.2 mm.
** Conductivity is dependent on the moisture content of the material. The conductivity for dry conditions is given.

5.3.2 ACH – validation

The full wall assembly model includes the cavity ventilation. Figure 5.9 shows the measured RH_{NMI} and RH_{CAV} for the studied cladding section. The RH_{CAV} is generally below the RH_{NMI} due to the cladding shelter from precipitation. To validate the calculated ACH, the RH_{CAV} is compared with and without the calculated ACH, as presented in Figure 5.10. The simulations with ACH improve the calculated RH_{CAV} values significantly. A simulation is also run for the steady ACH of n = 50 h^{-1}. The resulting correlation coefficients of all calculations are presented in Table 5.6. The simulation without ventilation has a high and rather stable RH_{CAV}. The wind dependency is probably the main factor determining the ACH on the east facing side, giving the good correlation 0.86. Thermal buoyancy is most effective on the west facing facade, acting in the opposite direction of the cavity wind flow and limiting the ACH. The fit is improved by setting the ACH to a constant of n = 50 h^{-1}, giving a correlation coefficient of 0.88.

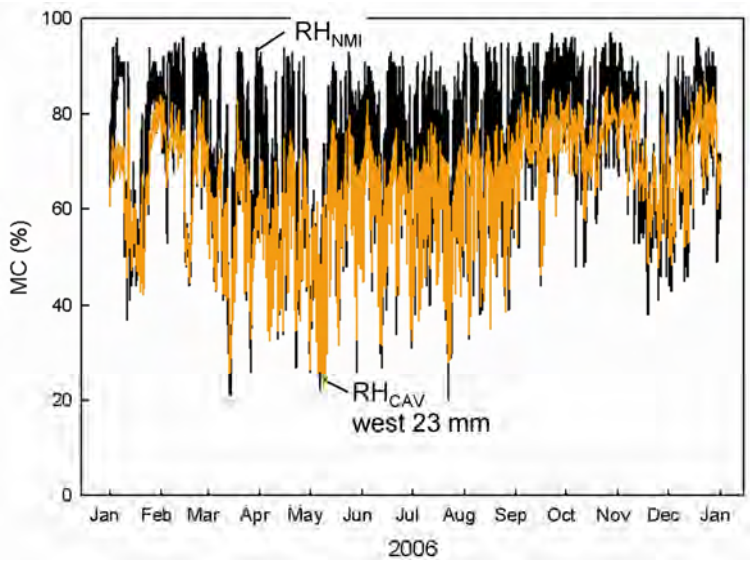

Figure 5.9. The RH_{NMI} and RH_{CAV} measured in 2006, corresponding to Figure 4.9a that shows the monthly means values for the entire measurement period.

Table 5.6. Correlation coefficients of the RH_{NMI} and RH_{CAV} for the simulations of the full wall assembly.

	West 4 mm	West 23 mm	East 23 mm
ACH	0.60	0.86	0.86
n = 50 h^{-1}	0.60	0.88	0.78
No ACH	0.46	0.44	0.48

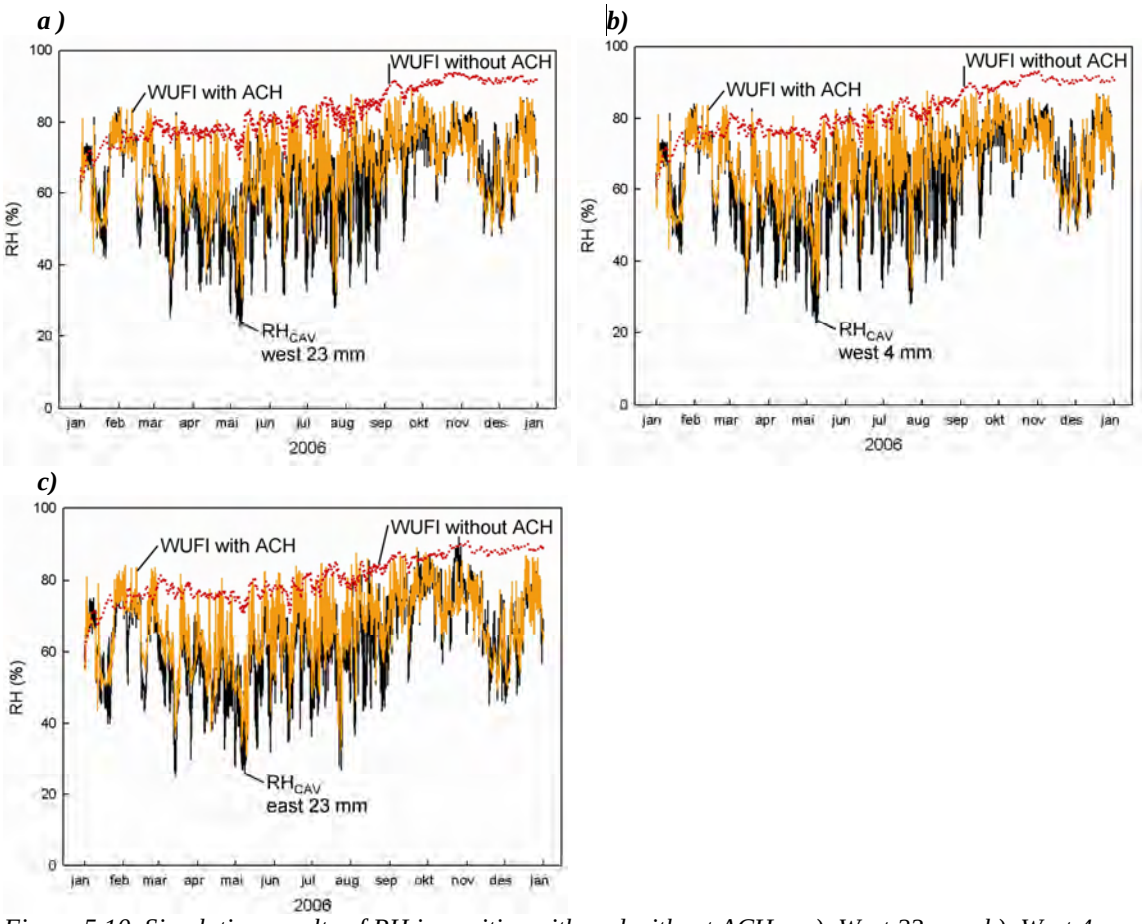

Figure 5.10. Simulation results of RH in cavities with and without ACH. a) West 23 mm b) West 4 mm and c) East 23 mm.

5.3.3 Cladding MC in the complete wall assembly

The model of the full wall assembly shows a good agreement when the ventilation of the cavity is taken into account. Figure 5.11 shows the transient simulation results with and without cavity ventilation of the 23 mm cavity opening. The fit is improved for the west facing side, the correlation increased from 0.94 to 0.95, see Figure 5.10.a. The east facing side has bad fit the first six months, probably due to the faulty input data on radiation incidence on this wall, see Figure 5.10.b. However, the correlation increased for the east facing side as well, from 0.88 to 0.90.

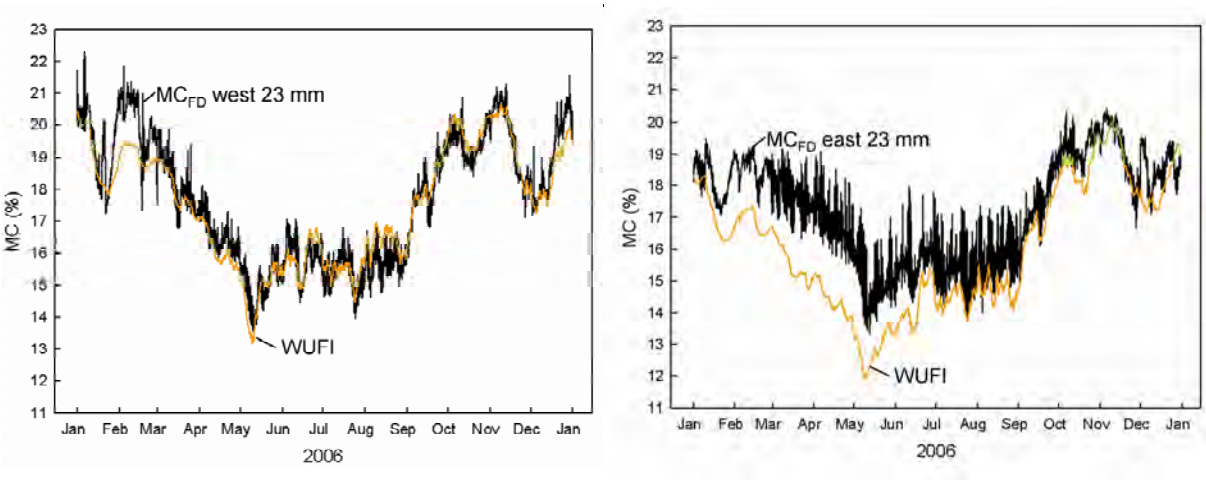

a) ***b)***

Figure 5.11. The measured and calculated MC when including the ACH in the full wall assembly. a) on the west facing side and b) on the east facing side.

5.3.4 Modelling wooden cladding in other Norwegian climates and with different insulation thickness

The model has been used for comparison of the hygrothermal cladding performance in four Norwegian cities, equal to the simulations performed in Paper V, Oslo, Bergen, Trondheim and Tromsø. These cities have climate data from MDRY years, which is chosen reference years selected as described by Geving and Torgersen (1997). The facade orientation is set towards the prevailing wind direction. One year is calculated and the same initial conditions are used in all cases. To improve the basis for comparison the moisture temperature response coefficient (MTR) is calculated as defined in Section 2.3.4. The calculated MTR values are shown in Table 5.7. With more insulation in the wall assembly the risk for rot, defined by increasing MTR, is slightly higher. This is also seen as the higher MC in Figure 5.12. This is due to the lower heat flux from the inside of the wall construction. Bergen has by far the greatest risk for rot potential. This fits with the Norwegian Scheffer index as shown in Figure 2.2. Tromsø has the lowest risk for decay according to the calculated MTR without ventilation (ACH) in the cavity. However, with cavity ventilation the MTR is lowest for the Oslo climate.

Table 5.7. MTR calculated for cavities with and without ACH and with 200 or 250 mm insulation.

	ACH 200 mm	ACH 250 mm	No ACH 250 mm
Tromsø	501	583	2081
Trondheim	117	253	11617
Bergen	2081	2744	56944
Oslo	77	203	4389

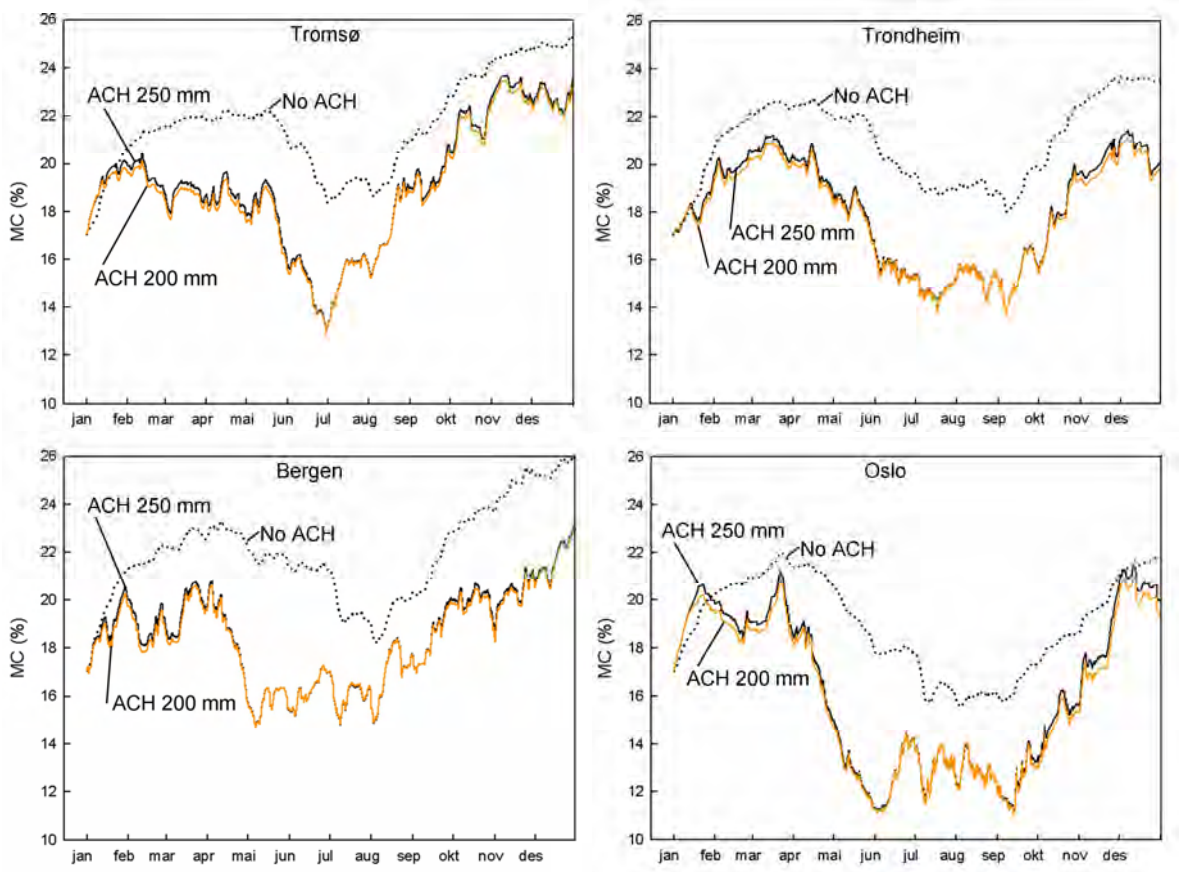

Figure 5.12. Comparison of hygrothermal wood cladding performance with MDRY years, with and without cavity ventilation and with 200 mm or 250 mm insulation for Tromsø, Trondheim, Bergen and Oslo.

In the future the Norwegian climate, with impact from climate change, is predicted to move towards the Bergen climate. This thesis does not hold durability considerations, but we do know that higher MTR does mean faster degradation. The critical limits of degradation are not defined for MTR. Anyways, with good design wood cladding endures more than 50 years in Bergen, which means that wooden cladding can still be promoted as a high-performance rain screen, also in harsh climates.

Calculating hygrothermal conditions in ventilated wooden facades may be done relatively accurate, but this is very time-consuming and does not improve wooden cladding design significant, as shown in this analysis of hygrothermal behaviour in four Norwegian cities. However, within the field of building physics this work is promising. Cavity ventilation can be calculated and define more accurate hygrothermal conditions. At the time being the lack of air flow characteristics is the first unsettled boundary condition which should be further explored.

6 General discussion and conclusions

6.1 Discussion

This PhD project was motivated by the following question: Does changes in cladding exposure due to climate change and improvements in building assemblies require adaptation of current wooden cladding designs? Today, the majority of Norwegian suburban and rural residential houses have wooden cladding. The common design principle is two-stage tightening, which is separating the rain screen and the main wall assembly with a cavity which is usually ventilated. In this thesis, the hygrothermal response, the temperature and moisture level, of different wooden cladding designs has been investigated experimentally and by numerical simulations to see if wooden claddings still provide robust façades in the future, or if adaptations are required.

Several climate indices try to link ambient climate exposure and material properties or design to for example the risk of damage by rot or frost. The functions defining these indices use logged meteorological parameters like precipitation, WDR amounts or temperature ratios of a specific geographical area. However, the hygrothermal response is complex and may not be sufficiently defined by a simplified index. For example in Paper IV it was found that when analysing the MC fluctuations in the claddings, the largest correspondence was with variations in temperature, radiation and wind velocity. The wind acts two ways; as a force pushing water onto and into wall assemblies, but also beneficially, by increasing the drying rate of the wall. In Norway today, cladding design recommendations are to increase the cavity depth according to the WDR amount in the location. This index (i.e. the WDR amount) does not take the drying effect of wind into account. Hygrothermal numerical simulation tools can relatively accurate model cladding performance with different designs and climate exposures (Paper V and Chapter 5). Paper VI describes the CFD model that simulates air flow around the building and in the cavity according to wind influence. By including cavity ventilation hygrothermal performance (HAM) calculations of wooden cladding are improved. This is shown in Chapter 5. However, for the time being the gain of wooden cladding design based on complex HAM simulations is minor. Although the modelling has not yet come to a stage where it can efficiently support cladding design, it is a step towards a numerical approach in the development of geographically dependent climate considerations for wooden building enclosures. There is little doubt that simulations will be of major importance in building research and industry in the future.

As pointed out earlier, current Norwegian cladding design recommendations prescribe to increase the cavity depth with increasing WDR amount. For a heavily exposed area like Bergen this implies a cavity depth of 54 mm for horizontal wood cladding (Kvande et al. 2007). As this thesis pointed out both experimentally and numerically, the hygrothermal response of cladding is not only dependent on the exposure to water, but also to the drying conditions, in particular the airflow around the building. Questions may therefore be raised if an increased cavity depth beyond 23 mm would improve the performance of the cladding, given that the cavity is ventilated.

6.2 Conclusions

The test house measurements were designed to investigate the difference of several cladding parameters. **The main findings of the experimental investigation at the Voll test house are:**

1. Data sets of extensive WDR measurements for the most weather-beaten wall are published online for model validation (Paper I).

2. There are difficulties in interpreting readings from electrical resistance wooden MC sensors in different depths in the cladding. This makes these sensors unsuitable for determining moisture profile in wooden cladding (Paper II).

3. There has been found a correlation between WDR and TOW measurements. This supports the use of TOW measurements as an enhanced wetness measurement sensor for painted wooden surfaces (Paper III).

4. The MC fluctuations in the claddings were more correlated with the variations in temperature, radiation and wind velocity, than with variations in precipitation, WDR and wind direction (Paper IV).

5. A cavity behind the wooden cladding is necessary. When the cavity was omitted the MC on the weather-beaten west facing wall increased. Due to the limited liquid water exposure on the east facing wall, this cladding dried out, probably because of the heat from inside the house. It should be noted that these results were obtained with 150 mm of mineral wool insulation, while current requirements are 250 mm. In the latter case a lower heat flux can assist the drying (Chapter 4).

6. The orientation of the test facades had the greatest influence on the hygrothermal response. With an open, ventilated, cavity, the west facing cladding had the best performance. The east facing side had the best hygrothermal performance with a closed, non-ventilated, cavity (Chapter 4).

7. Full cavity opening (23 mm) did not improve the cladding conditions on the west facing cladding significantly compared to a smaller (4 mm) opening (Chapter 4).

8. Untreated cladding responds more quickly to climate exposure, providing a hygrothermal response with larger MC fluctuations compared to surface treated claddings (Chapter 4).

9. The surface treatments, alkyd or acryl paint, did not show a significant different hygrothermal performance (Chapter 4).

10. The material qualities, fast or slow grown wood, did not show a significant different hygrothermal performance (Chapter 4).

11. Trend should be considered as an analysis tool in order to reduce the level of errors of the measurements (Chapter 4).

Hygrothermal numerical simulations in combination with CFD provide an analytical tool to model cladding performance with different designs and climate exposures. A model of the Voll cladding including the wall assembly has been build and validated. **The main findings of the numerical simulations are:**

1. Hygrothermal numerical simulation tools can relatively accurate model cladding performance with different designs and climate exposures (Paper V and Chapter 5)

2. CFD was used to model the air flow at Voll. A function was derived to calculate the cavity air change rate (ACH) from wind direction, speed and cavity depth or wind speed, surface pressure difference coefficient and cavity dimensions (chapter 5 and Paper VI).

3. With enhanced wall insulation the risk of decay increases, because a lower heat flux can assist the drying (Chapter 5).

4. The highest risk of cladding degradation calculated with recorded climate data for a geographical area in Norway was, as expected, in Bergen (Chapter 5).

The importance of a ventilated cavity increases due to rougher climate exposure and buildings with improved insulation. However, it appears that the current recommended wooden cladding design still is satisfactorily robust (Chapter 5).

6.3 Recommendations for further work

The findings presented in this thesis are a step towards a greater understanding of wooden claddings. Further development is needed before a numerical approach can support cladding design with graphically dependent climate adaptation. Among the remaining tasks are:

1. Further validation and investigation of range of action of numerical hygrothermal models.

2. More studies on hygrothermal performance for future climate scenarios and increased levels of thermal insulation.

3. Enhanced CFD studies of cavity air characteristics with wind induced flow and thermal buoyancy.

4. To improve downscaling of climate parameters. Local climates have large variations. A parameter study of effects of influencing elements like buildings, vegetation and surrounding topography is requested to increase the knowledge on façade climate impact.

5. Studies to relate indices (such as e.g. MTR value) derived from hygrothermal simulations to acceptable or unacceptable risk of decay for external wood cladding.

Figure 6.1. Sound ground beam protected with wooden cladding in more than 100 years.

References

Aagaard P.K. (1992) Wood – decomposing and maintenance. In Norwegian. Research and development Jotun A/S, BK Grafiske A.S. Sandefjord

Abuku M., Blocken B., Nore K., Thue J.V., Carmeliet J. and Roels S. (2009). On the validity of numerical wind-driven rain simulation on a rectangular low-rise building under various oblique winds. *Building and Environment* 44(3): 621-632.

Andersen K. T. (2000) Ventilated cavities in wall structures – a theoretical analysis. In Danish. By og Byg Dokumentation 001, Danish Building Research Institute (SBI), Hørsholm, Denmark.

Andersen K. T., Fynholm P., Hansen M. H. and Nikolajsen A. (2002). Moisture proof timber frame walls – moisture content in superinsulated timber frame walls. In Danish. Danish Building Research Institute (SBI). Documentation 025. Hørsholm, Denmark.

ASTM D 4444-92 (2003) Standard Test Methods for Use and Calibration of Hand-Held Moisture Meters. American Society for Testing and Materials, ASTM International, West Conshohocken, PA, United States.

BDS 2008. Building design sheets. In Norwegian. SINTEF Building and Infrastructure, Oslo, Norway.
BDS 520.415 Flashings for precipitation. Tightening to outer exposure. (2004)
BDS 542.003 Two-step tightening to WDR exposure on facades. Ventilated claddings and joints. (2005)
BDS 542.101 Vertical wooden claddings. Exterior claddings. (1998)
BDS 573.102 Horizontal wooden claddings. Exterior claddings. (2000)
BDS 742.301 Maintenance of exterior wood cladding. (1993)

Beaulieu P., Cornick S.M., Dalgliesh W.A., Djebbar R., Kumaran M.K., Lacasse M.A., Lackey J., Maref W., Mukhopadhyaya P., Nofal M., Normandin N., Nicholis M., O'Connor T., Quirt J.D., Rousseau M.Z., Said M.N., Swinton M.C., Tariku F. and van Reenen D. (2002) Final Report from Task 8 of MEWS Project – Hygrothermal Response of Exterior Wall Systems to Climate Loading: Methodology and Interpretation of Results for Stucco, EIFS, Masonry and Siding Clad Wood-Frame Walls. IRC-RR-118. National Research Council, Ottawa, Canada.

Berge B. and Stoknes S. (2004) Reduction of climate impact from the construction industry – by increased use of wood and other biomass. Preproject 1: Active substitute effect by increased use of wood in new-built houses. NAL | EXOBOX http://www.arkitektur.no/?nid=146289&pid0=155001 Dec. 18th 2008.

Birkeland Ø. (1963) *Rain Penetration Investigations: a summary of the findings of CIB Working Commission on Rain Penetration.* Norwegian Building Research Institute. Oslo

Blocken B. and Carmeliet J. (2004) A review of wind-driven rain research in building science. *Journal of Wind Engineering and Industrial Aerodynamics* 92(13): 1079-1130.

Blocken B and Carmeliet J. (2005). On the validity of the cosine projection in wind-driven rain calculations on buildings. *Building and Environment*. 41(9):1182-1189.

Blocken B. and Carmeliet. J. (2007) On the errors associated with the use of hourly data in wind-driven rain calculations on building façades. *Atmospheric Environment* 41(11): 2335-2343.

Blocken B., Roels S. and Carmeliet J. (2007) A combined CFD_HAM approach for wind-driven rain on building façades. *Journal of Wind Engineering and Industrial Aerodynamics*. 95(7):585-607

Blocken B., Defraeye T., Neale A., Derome D. and Carmeliet J (2008) High-resolution CFD simulations of forced convective heat transfer coefficients at exterior building surfaces. *Proceedings of the 8th Symposium on Building Physics in the Nordic Countries*, (C. Rode ed.) Report R-189, Dept. of Civil Engineering, Technical University of Denmark, pp. 261-268.

Bøhlerengen T., Rolstad A., Gustavsen A., Einstabland H. and Meløysund V. (2008) Tightening against rain and wind for facades – experiences from practise. *Proceedings of the 8th Symposium on Building Physics in the Nordic Countries.* (Rode, C. ed.), Report R-189, Dept. of Civil Engineering, Technical University of Denmark, Kgs. Lyngby: pp. 761:768.

Byg-erfa 81 09 15. Use wood right. Building technical experience transfer. Ballerup Denmark

Christensen H. (1999). Rot defects in wooden claddings. [In Norwegian] Project report 248, Norwegian Building Research Institute, Oslo, Norway.

Cornick S. and Dalgliesh W.A. (2003) A Moisture Index *to Characterize Climates for Building Envelope Design, Journal* of thermal environment and Scientific Design Vol 27, No 2 – October 2003, Sage Publications, Canada, pp. 151-177

Council Directive 89/106/EEC of 21 December 1988. ec.europa.eu/enterprise/construction/internal/cpd/cpd.htm. Dec. 18th 2008.

Edvartsen K.I. and Ramstad T. (2006) Handbook 53 – Wooden houses. Norwegian Building Research Institute, Oslo

Elowson T., Bergstöm M. and Hämäläinen M. 2003. Moisture Dynamics in Norway Spruce and Scots Pine during Outdoor Exposure in Relation to Different Surface Treatments and Handling Conditions. *Holzforschung* 57(2): 219-227.

EN 15927-3 (2008) Hygrothermal performance of buildings – climatic data – part 3: calculation of a driving rain index for vertical surfaces from hourly wind and rain data.

Fluent Inc (2000). Fluent 6.3 User's Guide. Lebanon.

FPT 22 (2002) Exterior wooden cladding. Wood Focus Norway, Oslo.
FPT 23 (2003) Surface treatment of exterior cladding. Wood Focus Norway, Oslo.
FPT 28 (2003). Focus on wood - Spruce, Wood Focus Norway, Oslo.

Geving S. and Thue J.V. (2002) Handbok 50 – Moisture in buildings. In Norwegian Building Research Institute, Oslo, Norway.

Geving S. (1995). Collection and analysis of climate data for moisture calculations. Work report 3 – Moisture in building materials and constructions. Department of Building and Construction Engineering, Norwegian Institute of Technology, Trondheim, Norway.

Geving S., Erichsen T.H., Nore K. and Time B. (2006) Hygrothermal conditions in wooden claddings – Test house measurements. Project report 407. Oslo: Norwegian Building Research Institute.

Geving S. & Torgersen S. E. (1997) *Climate data for moisture calculations. Reference years for 12 locations in Norway.* In Norwegian. Project report 227. Oslo: Norwegian Building Research Institute.

Glaser H. (1958) Temperatur und Dampfdruckverlauf in einer homogene Wand bei Feuchteausscheidung. In German Kältetechnik 1958b, 11, 12 pp. 358–362, 386–390.

Godal J.B. (1994) Wood for roofing and cladding. In Norwegian. Landbruksforlaget, Oslo. 1994.

Godal J.B. (2002) Wood for logging and framework – old houses tell about use of material. In Norwegian. 2. ed. Landbruksforlaget. Oslo, Norway.

Gudum C. (2003) Moisture transport and convection in building envelopes – ventilation in light weight outer walls. PhD thesis, Technical University of Denmark, Copenhagen, Denmark.

Gustavson M. (1999) Design of woden facades. In Swedish. Kontenta 9911047, Trätek, Stockholm, Sweden.

Hameury S. (2006) The hygrothermal Inertia of Massive Timber Constructions. Doctoral Thesis. Royal Institute of Technology Architecture and the Built Environment. Stockholm, Sweden.

Hansen .M.H., Nicolajsen A. and Stang B.D. (2002). On the influence of cavity ventilation on moisture content in timber frame walls. *Proceedings of the 6th Symposium on Building Physics in the Nordic Countries* (Editors: Gustavsen A. and Thue J. V.,), Norwegian University of Science and Technology (NTNU), Trondheim, Norway.

Hazleden D. 2001. Envelope drying rates analysis – Final report. Canada Mortgage and Housing Corporation.

Hens H. (2002) Technical Synthesis Report on Heat, Air and Moisture Transfer in Highly Insulated Building Envelopes. *UK, Faber Maunsell Ltd.*

Hens H. (2003) Proposal for a new Annex. 17 p. (accepted by the EXCO as Annex 41 in the fall meeting of 2003)

Hjort S. 1997 Moisture balance in Painted Wood Panelling. Doctoral thesis. Chalmers University of Technology, Göteborg, Sweden.

Holmgren J. (1945) Husbygging – bind 3. H. Aschehoug & co. Oslo. Chapters 1 and 21.

Hoppestad S. (1955) Driving rain in Norway. In Norwegian. Report 13. Norwegian Building Research Institute, Oslo

IPCC (2007) Climate Change 2007: Synthesis Report - Summary for Policymakers. An Assessment of the Intergovernmental Panel on Climate Change approved in detail at IPCC Plenary XXVII, 12th -17th November, Valencia, Spain.

Isaksen T. (1966) Rain penetration in joints. Reprint 119. Norwegian Building Research Institute. Oslo

Iván P. (1993) Rot defects in wooden cladding – Test house at Lista. National Institute of Technologies. In Norwegian. NTNF project, NR BA 400.420.216. Oslo, Norway.

Janssens A., Gode C., De Paepe M, Wolonszyn M. and Sasic-Kalaglsidis A. (2008) From EMPD to CFP – overview of different approaches for Heat Air and Moisture modelling in IEA Annex 41. Annex 41 Closing seminar. Copenhagen June 19th 2008.

Janssen H., Blocken B., Roels S. and Carmeliet J. (2007) Wind-driven rain as a boundary condition for HAM simulations: Analysis of simplified modelling approaches. *Building and Environment* 42(4): 1555-1567.

Johansen Ø. S. 2007 *Stochastic analyse of rot potential of house cladding.* In Norwegian. Master's Thesis. Norwegian University of Science and Technology (NTNU). Trondheim, Norway.

Johansson I., Fjellström P-A., Lindberg L. and Englund F. (2000) The impact of constructive details on wooden claddings. In Swedish. Trätek, Stockholm

Kauna.com. Dec. 18th 2008.

Künzel H. M. (1995) Simultaneous Heat and Moisture Transport in Building Components, One- and two-dimensional calculation using simple parameters. Dissertation Universität Stuttgart, Germany.

Kvande T., Lisø K. R. and Time B. (2007). Ventilated claddings. In Norwegian. Report 2, SINTEF Building and Infrastructure. Oslo, Norway.

Lauter P. and Time B. (2005) A method to assess the effects of climate and material parameters on the moisture conditions of a wooden façade. *Proceedings of the 7th Symposium on Building Physics in the Nordic Countries.* (Editor: Jóhannesson, G.) Reykjavik, Iceland. pp. 749-756

Lacasse M.A., O'Connor T.J., Nunes S. and Beaulieu P. 2003. Final Report from Task 6 of MEWS Project Experimental - Assessment of Water Penetration and Entry into Wood-Frame Wall Specimens. IRC-RR-133 National Research Council, Ottawa, Canada.

Larsen K.E and Mattson J. (2003) Untreated wooden claddings. In Norwegian. Norwegian Institute of Wood Technology, Oslo.

Lisø K.R. Kvande T. and Thue J.V (2003) Building enclosure performance in a more severe climate. *Proceedings of the 2nd International Building Physics Conference* (Editors: Carmeliet et al) Leuven, Belgium September 2003 pp. 309-319.

Lisø K. R (2006) Building envelope performance assessments in harsh climates Doctoral Thesis. NTNU 2006:185. Department of Civil and Transport Engineering. Trondheim

Lisø K. R., Kvande T. and Thue J.V. (2006a). Learning from experience – an analysis of process induced building effects in Norway. *Proceedings of the 3rd. International Building Physics Conference* (Editors: Fazio, Ge, Rao and Desmarais) Montreal Canada. pp. 425-432.

Lisø K.R. Hygen H.O., Kvande T. and Thue J.V (2006b) Decay potential in wood structures using climate data. Building Research & Information. 34(6):546-551.

Lisø K. R. and Kvande T. (2007) Climate adaptation of buildings. In Norwegan. Norwegian Building Research Institute Oslo.

NBI (2003) Multi storey wooden houses - Handbook 51. In Norwegian. Norwegian Building Research Institute Oslo.

Nicolajsen A. (1989) Ventilated outer walls - the wind influence on the heat loss (in Danish). Building Development Council. Copenhagen, Denmark.

Nicolajsen A. and Hansen M.H. (2000). Moisture conditions in timber claddings (in Danish). Danish Building Research Institute. SBI Report 310. Hørsholm, Denmark.

Nordvik V. and Lisø, K. R. (2004) A primer on the building economics of climate change, in Will Hughes (ed.) Construction Management and Economics 22: 765-775.

Nore K. (2004). Performance design of wooden cladding. Note 61. Norwegian Building Research Institute. Trondheim, Norway.

Nore K., Thue J.V., Time,B. and Rognvik E. (2005) Ventilated wooden claddings - A field investigation, *Proceedings of the 7th Symposium on Building Physics in the Nordic Countries.* (Editor: Jóhannesson, G.), the Icelandic Building Research Institute, Reykjavik Iceland, 617-624

NS 3470-1:1999/A1:2008 Timber structures - Design rules - Part 1: Common rules

NS-EN 13183-1 (2002) Moisture content of a piece of sawn timber - Part 1: Determination by oven dry method (Corrigendum AC:2003 incorporated)

NS-EN 13183-2 (2002) Moisture content of a piece of sawn timber - Part 2: Estimation by electrical resistance method (Corrigendum AC:2003 incorporated)

NS-EN 14915 (2006) Solid wood panelling and cladding - Characteristics, evaluation of conformity and marking

NS-EN 15026 (2007) Hygrothermal performance of building components and building elements - Assessment of moisture transfer by numerical simulation

NS-EN ISO 12571 (2000) Hygrothermal performance of building materials and products - Determination of hygroscopic sorption properties (ISO 12571:2000)

NS-EN ISO 12572 (2001) Hygrothermal performance of building materials and products - Determination of water vapour transmission properties (ISO 12572:2001)

NT BUILD 302 Building materials, wood: Moisture content. Approved 1986-09. Helsingfors Finland.

Ojanen T, Peuhkuri R. and Viitanen H. (2008) Assessment of the risk of mould growth in buildings using numerical simulation. *Proceedings in Building Physics Conference in honour of Prof. Hugo Hens*, (editors; S. Roels, G. Vermeir, D. Saelens), Laboratory of Building Physics, Catholic University Leuven, Leuven, Belgium. pp. 77-84

Piñon J.P., Davidovic D., Burnett E. and Srebric J. (2004) The Air Characteristics of Ventilated Cavities in Screen-Type Enclosure Wall Systems (RP-1091). ASHRAE.

Raknes E. (1985) Rot in exterior cladding, internal report. In Norwegian. Norwegian Institute of Wood Technology, Oslo

Redalen G. (2005). The Norwegian Horticultural Society list of species. (Hageselskapets Sortsliste, [In Norwegian]. 10th ed. Oslo, 2006

Rode C. and Woloszyn M. (2008) Common Exercises in Whole Building HAM Modelling. *IEA ECBCS. Annex 41 Closing seminar*. Copenhagen June 19th 2008.

Roels S. (2008) Experimental analysis of moisture buffering. IEA ECBCS. Annex 41 MOIST_ENG Subtask 2. ?

Rousseau J. and Hazleden D. (1998) Survey of Building Envelope Failures in the Coastal Climate of British Columbia. Canada. Mortgage and Housing Corporation.

Rydock J.P., Lisø K.R., Førland E.J., Nore, K. and Thue J.V. (2005). A driving rain exposure index for Norway. *Building and Environment* 40(11): 1450-1458.

Sagen V. (2004) Building damage related to climate - causes, extent and preventive actions. Master's thesis NTNU

Scheffer, T.C. (1971) A Climate Index for Estimating Potential for Decay in Wood Structures above Ground. *Forest Product Journal* 21:25-31.

Sedlbauer K. (2001) Prediction of mould fungus formation on the surface of and inside building components. University of Stuttgart, Fraunhofer Institute for Building Physics, Doctoral thesis. Stuttgart, Germany.

Straube J., VanStraaten R., Burnett E., and Schumacher C. (2004) Review of Literature and Theory. Report #1. ASHRAE 1091 – Development of Design Strategies for Rainscreen and Sheathing Membrane Performance in Wood Frame Walls. Building Engineering Group. University of Waterloo.

SN/TS 3186 (2008) Solid softwood cladding for exterior use

SSB (2008) http://www.ssb.no/vis/emner/01/04/10/klimagassn/main.html Nov 28th. 2008

Stang B.D. (2002) Moisture conditions in timber frame walls with load-bearing back walls. [In Danish]. By og Byg Documentation 033. Hørsholm, Denmark

Steffen M. (2000) Moisture and Wood-Frame Buildings – Building performance Series No. 1. Canadian Wood Council. Ottawa, Ontario, Canada.

Støre Valen, M. (1998) Moisture transfer in organic coatings on porous materials : the influence of varying environmental conditions. Doctoral Thesis. NTNU 1998:86. Department of Civil and Transport Engineering. Trondheim

Teasdale-St-Hilaire A., Derome D. (2007) Comparison of experimental and numerical results of wood-frame wall assemblies wetted by simulated wind-driven rain infiltration. Energy and Buildings, 39 (11): 1131-1139

TEK 2007. Norwegian building regulations. Minestry of Local Government and Regional Development. Oslo.

Thue J.V. (2008) Wooden facades: Building physical concerns. In "Dressed in wood" (editors: Hakonsen F and Larsen K.E.). In Norwegian. Gaidaros Forlag, Trondheim, Norway.

Time B. (1998) Hygroscopic Moisture Transport in Wood. Doctoral Thesis. NTNU 1998:20. Department of Civil and Transport Engineering. Trondheim

Tronstad S. (2002) Wood and moisture – from producer to consumer. In Norwegian. Teknisk småskrift 35, Norwegian Institute of Wood Technology, Oslo

UNFCCC (1994) United Nations Framework Convention and Climate Change (UNFCCC). Article 1

Vaisala (2008) Technical data. Instrument guidelines.

Valbjørn O. (2003) Examinations and evaluation of moisture and mould in buildings. In Danish. Danish Building and Urban Research, Hørsholm.

WUFI 4.2 Pro (2008) Institut für Bauphysik, Fraunhofer. Holzkrichen, Germany.

Zillig W., Holm A. and Künzel H.M. (2003) Condensation on façades – influence of construction type and orientation. *Proceedings of the 2nd International Building Physics Conference* (Editors: Carmeliet et al) Leuven, Belgium September 2003 Leuven, Belgium September 2003 pp. 437-445.

Complementary work carried out as part of the PhD study

I. **Nore**, K. (2004) Performance design of wooden cladding. *Note 61. Norwegian Building Research Institute.* Trondheim, Norway.

II. **Nore**, K., Thue, J.V., Time, B. & Rognvik, E. (2005) Ventilated wooden claddings - A field investigation, *Proceedings of the 7th Symposium on Building Physics in the Nordic Countries.* (Jóhannesson, G. (ed.)), the Icelandic Building Research Institute, Reykjavik Iceland, 617-624

III. Rydock, J.P., Lisø, K.R., Førland E.J., **Nore**, K. and Thue, J.V. 2005. A driving rain exposure index for Norway. *Building and Environment* 40(11): 1450-1458.

IV. Geving, S., Erichsen, T. H., **Nore**, K., Time, B. (2006). Hygrothermal conditions in wooden claddings. *Oslo: Norwegian Building Research Institute.* 93 p. NBI-report 220 2006; 407

V. Abuku, M., Blocken, B., **Nore**, K., Thue, J.V., Carmeliet, J., Roels, S. (2009). On the validity of numerical wind-driven rain simulation on a rectangular low-rise building under various oblique winds. *Building and Environment* 44(3): 621-632

VI **Nore** K., Blocken B, Carmeliet J & Thue J.V. (2008) CFD study of air flow in cavities in ventilated facades. Proceedings in Building Physics Conference in honour of Profesor Hugo Hens. (editors; S. Roels, G. Vermeir, D. Saelens), Laboratory of Building Physics, Catholic University Leuven, Leuven, Belgium. pp. 25-28. ISBN: 978-90-5682-99

Paper I: A dataset of wind-driven rain measurements on a low-rise test building in Norway

Is reprinted with kind permission from Elsevier, sciencedirect.com

Available online at www.sciencedirect.com
ScienceDirect
Building and Environment 42 (2007) 2150–2165
BUILDING AND ENVIRONMENT
www.elsevier.com/locate/buildenv

A dataset of wind-driven rain measurements on a low-rise test building in Norway

Kristine Nore[a,b,*], Bert Blocken[c,d], Bjørn Petter Jelle[a], Jan Vincent Thue[b], Jan Carmeliet[c,d]

[a]SINTEF Byggforsk, 7465 Trondheim, Norway
[b]Department of Civil and Transport Engineering, Norwegian University of Science and Technology (NTNU), Høgskoleringen 7A, 7491 Trondheim, Norway
[c]Laboratory of Building Physics, Department of Civil Engineering, Katholieke Universiteit Leuven, Kasteelpark Arenberg 40, 3001 Leuven, Belgium
[d]Unit Building Physics and Systems, Faculty of Building and Architecture, Technical University Eindhoven, P.O. Box 513, 5600 MB Eindhoven, The Netherlands

Received 2 February 2006; received in revised form 10 March 2006; accepted 10 April 2006

Abstract

Semi-empirical models and especially numerical simulation models based on Computational Fluid Dynamics (CFD) are increasingly being used to calculate wind-driven rain (WDR) on building facades. The development, verification and validation of these models require accurate and complete WDR measurement datasets. Although many WDR measurement campaigns have been conducted in the past, few reports of these contain enough information for model development and model validation. This paper presents a complete dataset of WDR measurements for a low-rise test building in Trondheim, Norway. It contains a detailed description of the building, its surroundings and the meteorological station, as well as WDR measurements in free-field conditions and on the building facades, measurements of wind speed, wind direction, horizontal rainfall intensity, temperature, relative humidity and error estimates for the WDR measurements. The paper also provides the link to a website from which the full set of data can be downloaded.

Keywords: Wind-driven rain; Driving rain; Air flow; Raindrop; Building facade; Measurement dataset; Field station; Experimental; CFD; Validation; Accuracy; Error; Tipping mechanism

1. Introduction

The combination of wind and rain results in wind-driven rain (WDR). WDR is one of the most important moisture sources for building facades. The intensity of WDR that reaches a building is an essential boundary condition for the hygrothermal analysis of building facades using, for example, Heat–Air–Moisture transfer models. However, characterising WDR is very complex. The intensity of WDR reaching a building facade is strongly dependent on the following six parameters: (1) building geometry (including the environment topology), (2) position on the building facade, (3) wind speed, (4) wind direction, (5) horizontal rainfall intensity and (6) horizontal raindrop-size distribution. The horizontal rainfall intensity is the intensity of rainfall through a horizontal plane (as measured by a traditional rain gauge with a horizontal aperture). The horizontal raindrop-size distribution is defined in a similar way, keeping in mind that it has been reported that the horizontal raindrop-size distribution is different from the raindrop-size distribution in a volume of air [1]. The last four parameters are highly variable in both space and time. As a result, WDR is also strongly dependent on space and time.

Three categories of methods to determine WDR intensities on buildings can be distinguished: measurements, semi-empirical models and numerical simulation models based on Computational Fluid Dynamics (CFD). A review of each of these methods was recently provided [1]. Since the start of WDR research in Building Physics in 1936, measurements have been the primary method used in WDR studies. However, WDR measurements are

*Corresponding author. SINTEF Byggforsk, 7465 Trondheim, Norway. Tel.: +47 73 59 33 90; fax: +47 73 59 33 80.
E-mail address: Kristine.Nore@SINTEF.no (K. Nore).

0360-1323/$ - see front matter © 2006 Elsevier Ltd. All rights reserved.
doi:10.1016/j.buildenv.2006.04.003

time-consuming, expensive and, most importantly, not generally available at meteorological stations. For this reason, researchers established semi-empirical models and, more recently, numerical simulation models to calculate WDR on building facades [1–15]. Despite new modelling advances, WDR measurements remain indispensable for the development, verification and validation of these models. The most widely used semi-empirical model is an analytical WDR relationship where WDR intensity is proportional to the product of the wind speed normal to the wall and the horizontal rainfall intensity [1–5]. The proportionality factor is called the WDR coefficient. WDR coefficients are typically determined based on WDR measurements on buildings. Numerical simulation models comprise the calculation of the wind-flow pattern around the building with a CFD code, the calculation of the motion of raindrops in the flow pattern and the determination of the intensity of WDR based on the configuration of the raindrop trajectories [7–15]. Although CFD is a very powerful tool, its use of a turbulence model to solve the Reynolds-averaged Navier–Stokes equations in turn requires the validation of this turbulence model. Validation should be performed for a wide range of building configurations by systematically comparing the numerical results of the WDR intensity with the corresponding WDR measurements. Also here, accurate WDR measurements are indispensable.

Although many WDR measurement campaigns have been conducted in the past, few have presented these results in a form that is suitable for model development and validation. Blocken and Carmeliet [16] state that an adequate experimental WDR dataset should comprise and/or be accompanied by the following information: (1) a detailed description of the building site and the building geometry; (2) a detailed description of the measurement set-up; (3) measurements of the reference wind speed, the reference wind direction and the horizontal rainfall intensity (i.e. the rainfall intensity through a horizontal plane) that have been conducted near the building site and in "free-field" conditions, i.e. at a position that is not significantly influenced by the presence of the building; (4) WDR measurements at the facade(s) with a sufficiently high resolution in space and time and (5) error estimates for the WDR measurements. To our knowledge, only two experimental datasets that satisfy at least four of these requirements have been made available to the research community: (1) the WDR data by the Unit Building Physics and Systems, Technical University of Eindhoven (TU/e), The Netherlands [12] and (2) the WDR data by the Laboratory of Building Physics, Katholieke Universiteit Leuven (K.U.Leuven), Belgium [16]. Both datasets can be downloaded from the internet: ⟨http://sts.bwk.tue.nl/drivingrain/, http://www.kuleuven.be/bwf/projects/WDRdatabase⟩.
The first dataset contains no specific information about WDR measurement errors, but the associated errors can be estimated following the procedure outlined in [16,17]. Both datasets are valuable for model development and model validation, but they have a common disadvantage, at least for early validation studies. The TU/e dataset concerns a high-rise building in a complex city environment [12] which geometry can complicate the interpretation and use of these data. The K.U.Leuven dataset concerns a low-rise building of complex geometry in a suburban environment with trees in the vicinity of the building [16]. The authors of the latter dataset explicitly state that, while their dataset is useful for model development and validation in this complex case, basic validation studies would definitely benefit from WDR datasets for buildings of simpler geometry and with less complex surroundings.

This paper presents such a dataset, established at the field station of the SINTEF Byggforsk and the Norwegian University of Science and Technology (NTNU) at Voll, in Trondheim, Norway, in the framework of the *Climate 2000* project [18]. This dataset is different from the two existing datasets in that it concerns a block-type low-rise building, and it comprises free-field WDR measurements and an error analysis for the tipping-bowl registration mechanism. In Section 2 of this paper, the historical background of WDR measurements in Norway is briefly described. Section 3 describes the building geometry, the surrounding topography, the measurement equipment and the accuracy of the WDR measurements. A selection of measurement results and the URL of the website from which the entire dataset can be downloaded are provided in Section 4.

2. Historical background

Norway is a country with an unusually long coastline compared with its land area. Therefore, it is not surprising that the cradle of WDR research in Building Physics was situated in Norway. The first WDR measurements on buildings were carried out by Holmgren [19] in 1937 at the former Norwegian Institute of Technology, NTH (now NTNU). Later, Holmgren's work was continued by Hoppestad [2] at the Norwegian Building Research Institute (NBI) that is integrated in SINTEF Byggforsk since January 2006. He conducted measurements of free-field WDR from 1951 to 1953 at four weather stations: Oslo (Blindern), Bergen (Fredriksberg), Trondheim (Voll, Strinda area) and Tromsø (Langnes). WDR coming from the main wind directions, i.e. north, south, east and west, was collected. The measurements from the four weather stations were used to establish a semi-empirical relationship between WDR and the influencing parameters wind speed and horizontal rainfall intensity. This correlation was then employed to calculate WDR amounts using data from 70 weather stations distributed throughout Norway and to construct WDR maps for Norway.

Isaksen [20] reported free-field WDR measurements made in Bergen by the NBI for a period of nearly 15 years, from 1951 to 1965. Later, in 1967, some WDR measurements were made on a 27 m tall building in Bergen. WDR intensities up to 21.6 mm/h over 10 min and up to

15 mm/h over 1 h were registered. The measurements were continued in the 1970s. After that period, no reports of on-site WDR research on buildings in Norway are known to the authors.

Norwegian WDR research has recently been taken up again as part of the R&D program *Climate 2000*, which investigates the impact of future climate scenarios on the built environment in Norway [18]. Within this framework and to support research concerning the wood cladding facades of the test house, WDR measurements are being conducted at the field station, as reported by Nore et al. [21]. Lately a new semi-empirical model for expressing WDR exposure has been developed based on synoptic weather data of the last 30 years [6], i.e. data containing measurements and observations made three or four times a day to provide an overall view of the weather during these intervals. Norway has mostly synoptic weather recordings, not hourly as required by the main procedure in the pre-standard for WDR assessment [5]. Nevertheless, it has been shown that the results from this model correlate well to those from the pre-standard model [22].

In this paper, the WDR measurement set-up and the data, as developed and obtained in the framework of the *Climate 2000* project, are presented and discussed.

3. Measurement set-up

3.1. Description of the building geometry and the surrounding topography

The field station is located in Trondheim, Longitude 10°27′14″ and Latitude 69°24′49″, at 129 m above sea level. Fig. 1 illustrates the location of the test site and the surrounding environment. Three buildings are located at the station (Fig. 2a and b): the main flat-roof test building, a small logging building and a sloped-roof rotating test building. The north-west corners of the buildings are indicated with A, B and C. The building facades of the

Fig. 1. Topographic map of the surrounding environment of Voll field station. Contours are given at height intervals of 1 m (© Trondheim kommune 2005).

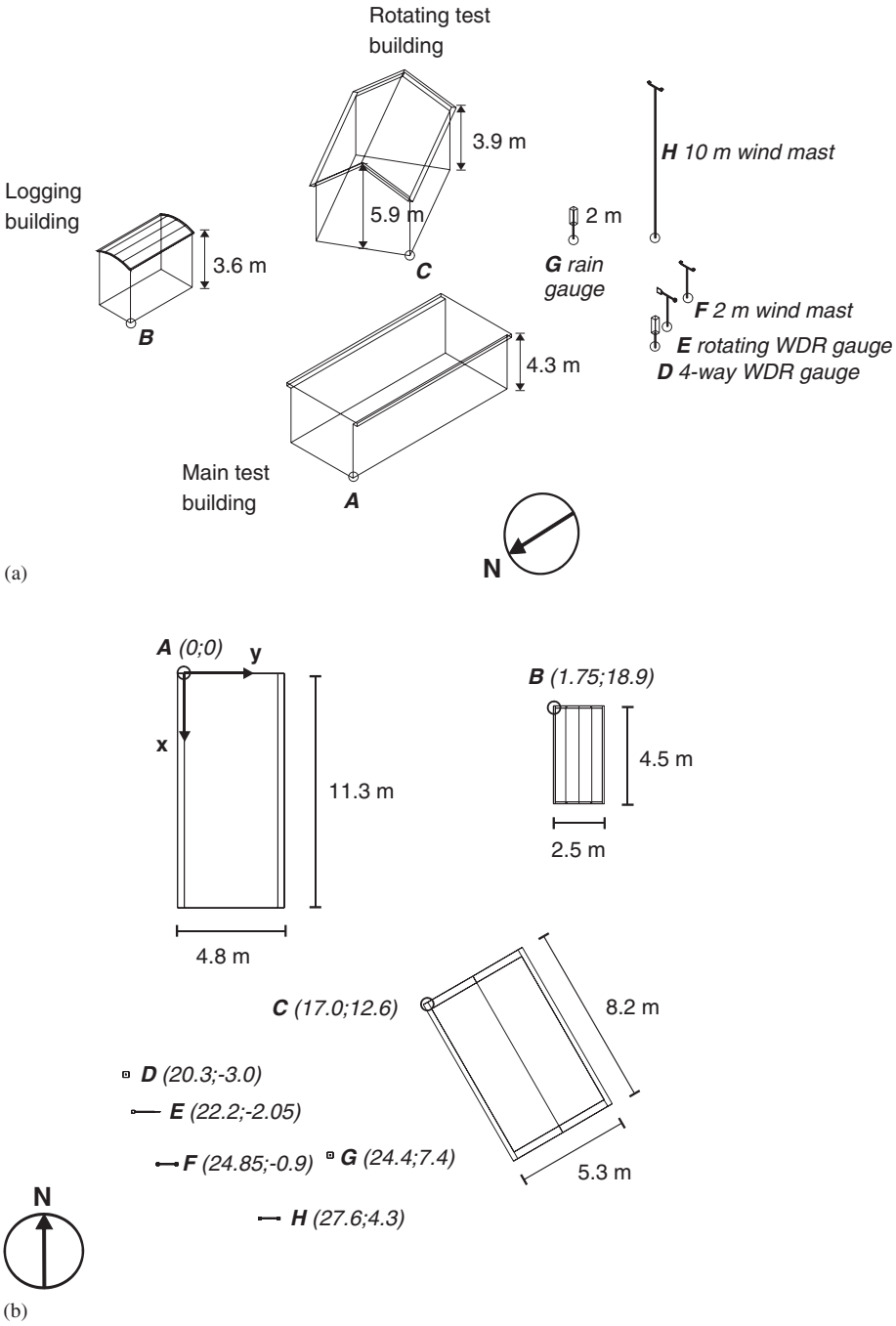

Fig. 2. Field station of SINTEF Byggforsk and NTNU: (a) perspective view and (b) top view with indication of the building dimensions and the location (x, y co-ordinates) of the buildings and measurement equipment relative to point A (north-west corner of the flat-roof test building) (in m).

fixed buildings A and B face the cardinal wind directions. The flat-roof test building A is considered in this study. It is a block-type building with dimensions $L \times B \times H = 11.3 \times 4.8 \times 4.3\,m^3$. Fig. 3 shows the building facades, the facade dimensions and the positions of the WDR gauges. The length of the roof overhang on the west and east-facing side is 340 mm, while the north and south-facing side have no roof overhang. Fig. 4 presents panoramic views of the surrounding terrain, for the cardinal wind directions. The field station as a whole, i.e. comprising the three test buildings, is very exposed to WDR in almost all directions. Only in the wind-direction sector WNW to ENE (interval 300°–70°, in degrees clockwise from north), distant obstructions such as low-rise buildings and trees can provide some shielding from wind and WDR. The flat-roof test building itself is very exposed to WDR (see Fig. 5) in the sector SSE to WNW (interval 150°–300°), moderately exposed in the wind-direction sector WNW to ENE (interval 300°–70°) and partly sheltered in the wind-direction sector ENE to SSE (interval 70°–150°), due to the presence of the other two test buildings B and C in this sector.

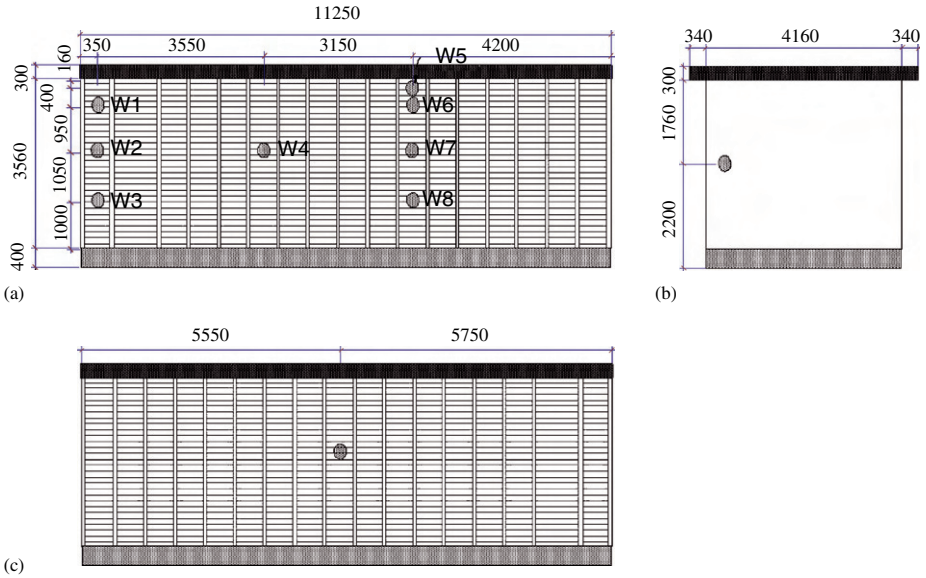

Fig. 3. Dimensions of test house (in mm) and the positions of the wind-driven rain gauges on the facades: (a) west-facing wall; (b) north-facing wall. The north and south-facing walls have the same position of the wind-driven rain gauge: (c) east-facing wall

Fig. 4.Photographs of the surrounding topography of the flat-roof test building for the cardinal directions.

3.2. Measurement equipment

The field station is equipped with instruments to measure the wind speed, wind direction, precipitation, free WDR, air temperature and relative humidity as well as detailed temperature and moisture content measurements in the facades themselves. The measurement equipment relevant for the WDR dataset

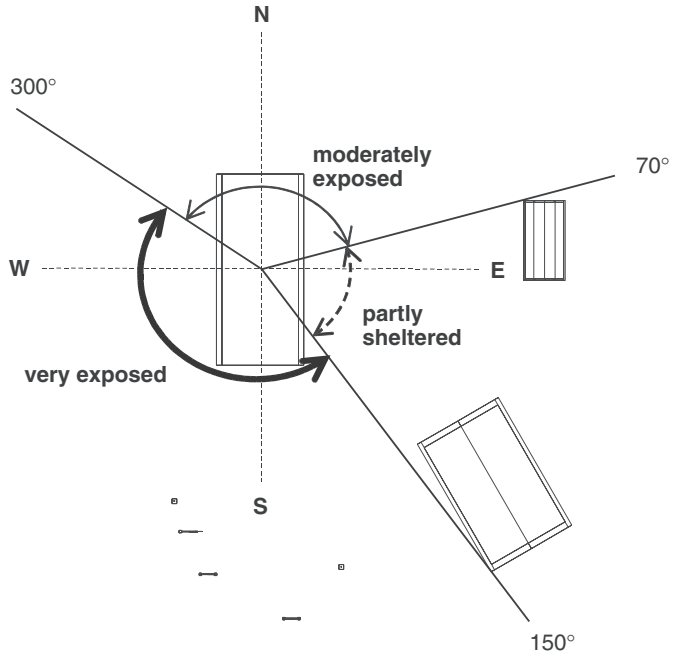

Fig. 5. Exposure of the main test building on the station to wind and wind-driven rain.

is described below. All data are gathered on an hourly basis (as a result of 1-min or 10-min values that are averaged or summed over each hour).

3.2.1. Wind speed and wind direction

Wind speed U (m/s) and wind direction φ (degrees clockwise from north) are measured at two locations at the site: on top of a 10 m meteorological mast (U_{10} and φ_{10}) and on top of a 2 m mast (U_2 and φ_2) (indicated by H and F in Fig. 2). A cup anemometer (at 10 m) and a wind propeller (at 2 m) are used to measure the wind speed and wind vanes are used to measure the wind direction. Both masts are located south of the test building and in the "very exposed" sector as indicated in Figs. 2 and 5. Generally, it is nearly impossible to position wind and rain measurement equipment at a test building site in such a way that "free-field" measurements are obtained for all wind directions. Free-field measurements mean that the measurements are taken in such a way that they are not disturbed by the presence of nearby buildings A, B or C or other obstructions on the test site. In the present situation, for wind directions in the interval from N to E (interval [0°, 90°]), the measurement equipment on top of the 2 m wind mast F is situated in the wake of the buildings and is therefore disturbed. For wind directions in the interval [180°, 270°], an upstream disturbance of the wind-flow pattern by the buildings can be present. CFD simulations for a low-rise building however have indicated that this disturbance is most pronounced close to the building and that it almost disappears at a distance of about two times the building height H from the building facade [16]. In the present situation where the height of test building A is 4.3 m, the upstream disturbance of building A on the wind measurements can be considered to be negligible. However, for wind from SW, building C creates a disturbance for the wind instruments and also for the rain gauge G.

3.2.2. Precipitation

Two precipitation gauges were installed to measure horizontal rainfall: D and G. One of these is located on top of the four-way free-field WDR gauge (Figs. 2a,b, 6a,b), described below. It contains a tipping-bowl mechanism to register the collected amount of rainwater. The tipping-bowl mechanism is similar to the well-known tipping-bucket mechanism. Fig. 7 illustrates the tipping bowl and its dimensions. The tipping bowl gives a signal (a tip) whenever the bowl is filled with water. It is designed to have a nominal 0.2 mm/tip, which is equal to 0.2 L of precipitation per m^2 horizontal surface. The second precipitation gauge G uses a balance with heating and can measure hail and snow. This gauge is property of the Norwegian Meteorological Institute (met.no). It is equipped with a wind shield to reduce the wind error in precipitation measurements. The wind shield consists of a set of pendent metal bars positioned around the gauge in order to suppress the upward wind-velocity component near the rim of the gauge that can be responsible for the wind error.

3.2.3. Free wind-driven rain

Two free-standing WDR gauges were installed to measure the oncoming WDR: a fixed gauge D with four apertures facing the cardinal directions (Figs. 2a,b, 6a,b) and a rotating gauge E that is always facing the wind thanks to a wind vane (Figs. 2a,b, 6c). The former collects the fractions of the free WDR coming from the different wind-direction sectors, while the latter collects all free WDR. Both gauges are positioned at 2 m height above ground. The rim of the free-standing WDR gauges is made of HDPE. The size of the rim and the collection area is the same for all these gauges.

Note that frost is a problem for the free-standing WDR gauges since no heater is included. When the water in the tipping bowl freezes, the measurements are not valid.

3.2.4. Wind-driven rain on the building facades

The wall-mounted WDR gauges (Fig. 8) used in this research were designed by the National Swedish Institute for Building Research [23]. The collection plate is made of aluminium and its catch area is 0.0314 m^2 (inner diameter = 0.2 m). The gauge design and dimensions are shown in Fig. 8. A modification was made to the original gauge design [23] so that the collected rainwater is led into the tipping-bowl mechanism placed inside the test house. This way, frost problems for the wall-mounted gauges are avoided and the evaporation of rainwater from the bowl is less variable due to the lower temperature and relative humidity fluctuations inside the test house. WDR is measured at 11 positions on the building facades, as shown

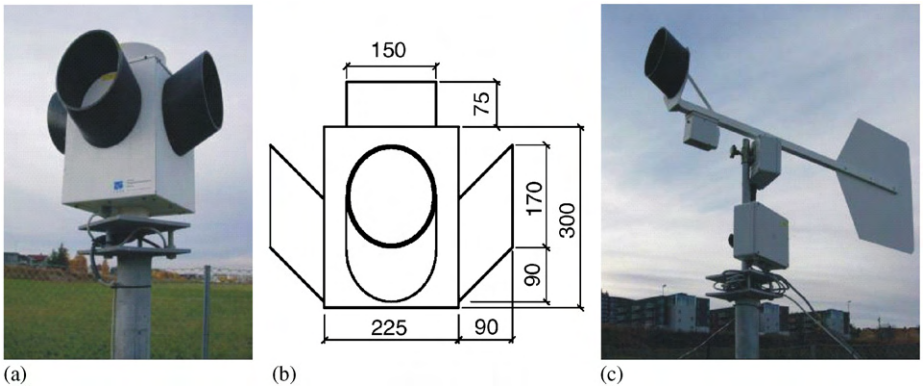

Fig. 6. Free-standing wind-driven rain gauges: (a) fixed four-way gauge "D" to measure the free-field wind-driven rain coming from the cardinal directions; (b) dimensions of the fixed free-standing gauge in mm; and (c) rotating free-standing wind-driven rain gauge "E" that is always facing the wind by a vane.

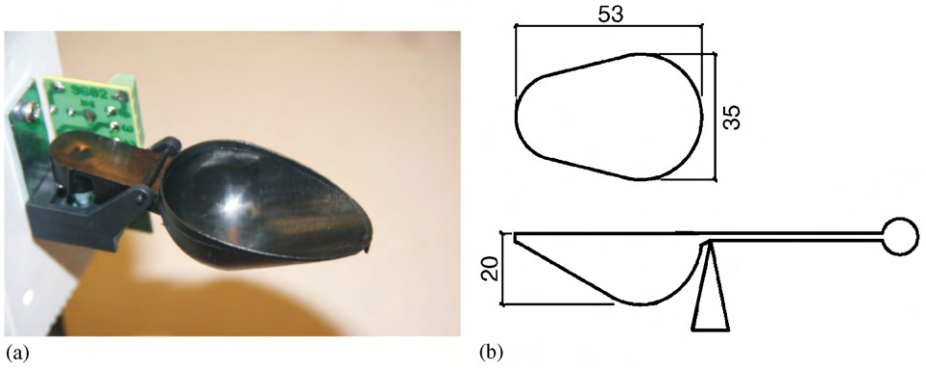

Fig. 7. Tipping-bowl system used to measure the collected rain water by the gauges: (a) photograph; (b) dimensions in mm. Average maximum content before tip of bowl: 6.3 ml.

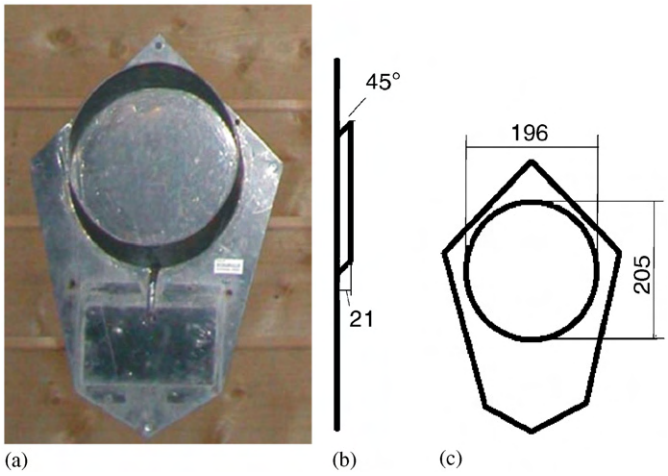

Fig. 8. Wall-mounted wind-driven rain gauge: (a) photograph; (b) side view; and (c) front view. The dimensions are given in mm.

in Fig. 3. The west-facing facade, which is the long facade with most WDR exposure, is equipped with eight WDR gauges, in order to capture the distribution of WDR across this facade. The other facades each hold one WDR gauge. As all tipping bowls have not exactly the same content capacity, all bowls were calibrated before use.

For the tipping bowls of each of the wall-mounted gauges, Table 1 holds the amount of collected WDR needed to yield one tip. The average value of WDR needed to fill the bowl completely is 0.182 mm, i.e. 0.182 L per m^2 of wall surface.

3.2.5. *Air temperature and relative humidity*

Measurements of air temperature and relative humidity are made by a thermocouple and relative humidity sensor at a height of 2 m on the 10 m high wind mast H (Fig. 2). They are needed for the indication and/or assessment of measurement errors by frost and by undercooling condensation at the gauge surfaces. The thermocouples were calibrated beforehand in thermo-liquid baths and the relative humidity sensors were calibrated using saturated salt solutions in a thermally stable environment.

3.3. *Measurement accuracy for wind-driven rain*

Earlier research [16,17,24] has indicated that errors in WDR measurements can be very large and significantly more important than errors in standard measurements of

Table 1
Amount of collected rainwater needed to yield one tip, for the tipping bowls of the wall-mounted WDR gauges

WDR gauge	W1	W2	W3	W4	W5	W6	W7	W8	S	E	N
mm of WDR per tip	0.198	0.179	0.174	0.173	0.202	0.203	0.170	0.185	0.182	0.158	0.179

wind speed, wind direction and horizontal rainfall intensity. Therefore it is important to address WDR measurement errors in detail.

3.3.1. Error sources

Information on the accuracy of WDR measurements in the literature is limited. Høgberg et al. [24] conducted a WDR gauge intercomparison study and noted serious discrepancies between the readings of different gauges. Blocken and Carmeliet [17] identified five possible error sources in WDR measurements: (1) evaporation of adhesion water from the gauge collection area (and from the inner side of the draining tube)—error E_{AW}; (2) evaporative losses from the reservoir (in this case: the tipping bowl)—error E_{EVAP}; (3) splashing of drops from the collection area at impact—error E_{SP}; (4) undercooling condensation on the gauge collection area—error E_{UC} and (5) wind errors due to the disturbance of the wind-flow pattern and the raindrop trajectories by the gauge body itself—error E_{WIND}. These authors performed an error analysis for WDR gauges and provided guidelines for WDR gauge design and for WDR error assessment. Adhesion water refers to water that sticks to the gauge surface and does not directly run off into the reservoir. As such it can evaporate during rain but especially during the dry period after the end of a rain spell. In [16,17], adhesion-water evaporation was mentioned to be one of the main error sources. However, these authors did not use tipping bowls but a fixed reservoir the content of which was measured by pressure gauges (height of water column in the reservoir). Tipping bowl and fixed reservoirs both have advantages and disadvantages [16]. Note that the use of a tipping-bucket or tipping-bowl mechanism can introduce additional errors that have to be taken into account. These errors are: (1) the error caused by the rest water that remains in the bowl at the end of a spell. Because a tip is only given when the bowl is completely filled, this amount of water is not registered for this spell. If it does not evaporate before the start of the next spell, it will be added to this new spell—error E_{RW}; (2) the error due to loss of incoming water running by and not collected by the bowl due to its brief vertical position during the tip—error E_{TIP}. In this paper, the existing procedure of analysing errors in WDR measurements is extended to include these errors.

3.3.2. Error analysis

The error analysis should be somewhat different depending on the way in which the WDR water is registered. The wall-mounted WDR gauges at the test building have tipping bowls that are located inside the building, while the free-field WDR measurements have tipping bowls that are located outside and that are exposed to more variable climate conditions (e.g. frost). As a result, some of the errors are different. The present error analysis focuses on the wall-mounted gauges with tipping bowls located inside.

Not all seven possible errors mentioned above are easy to estimate. Two errors will not be analysed in detail because of their complexity and the limited amount of knowledge about their occurrence: the splashing and the wind errors. In order to have splashing, the wind speed U_{10} must be high and even then it can only occur for sufficiently large raindrops [17]. Measurement data should be handled with care when the measured wind speed U_{10} (at the top of the 10 m mast) is higher than 10 m/s. This has occurred for only 3 h from January 2004 to May 2005 at Voll field station. At least in all other periods, splashing can be considered to be absent. Due to the disturbance of the wind field around the collection area of the WDR gauge, wind errors can occur [17]. These errors are hard to quantify and should be estimated by CFD simulations. They might be important for WDR measurements taken while the wind direction is quite oblique to the wall (e.g. 60–90° from the normal to the wall under study). When interpreting the measurement data one should be aware of the possibility for this error.

The other five errors are summarised in Table 2 and are discussed below. Note that absolute errors in WDR measurements are expressed in mm (equal to litre per square metre), same unit as for horizontal rainfall amounts. In the case of WDR however, the unit mm refers to the thickness of an equivalent water layer on a vertical surface instead of on a horizontal surface.

Following the procedure in [17], for the current WDR gauge with a collection area of 0.0314 m^2, spraying tests on the WDR gauges were conducted in the laboratory at SINTEF Byggforsk to determine the amount of adhesion water at the aluminium surface. A maximum value of 2 g on the collection area was measured, which is equal to 0.06 mm (calculated by dividing by the gauge area). This value is very close to those found from other adhesion-water spraying tests on different materials [17]. Adhesion water is also stored in the tube leading from the WDR gauge to the tipping bowl inside the house. In order to reduce this error, the length of the tube is reduced by placing the tipping bowls at the inside of the wall directly behind the WDR gauge at the outside. The amount of adhesion water in the tube was measured to be 0.2 g. The actual error due to adhesion-water evaporation depends on the type of the rain events. Adhesion water will evaporate

Table 2
Estimates for five different errors associated with wall-mounted wind-driven rain measurements with tipping bowls inside the test building

Error type	Symbol	Quantity in grams for the gauge area	Quantity in mm of WDR (L/m^2)	Frequency of occurrence
Adhesion-water evaporation	E_{AW}	2.2	0.070	During but especially after a WDR spell
Evaporation from tipping bowl	E_{EVAP}	0.016 (per hour)	0.0005 (per hour)	Assumed to be constant in time given indoor conditions
Undercooling condensation	E_{UC}	0–1.2	0–0.038	Rarely, dependent on climate and wall conditions
Rest water	E_{RW}	6.3	0.2	At the end or beginning of a spell
Collection loss during tip	E_{TIP}	0.067	0.002	At each tip

during but especially after a WDR spell. It can be estimated by using the procedure suggested in [17] by assuming that total adhesion-water evaporation occurs when it does not rain for 1 h. Note that the relative adhesion-water-evaporation error will become smaller as the cumulative collected WDR amount increases.

The evaporation from the tipping bowl, located inside the house, at 20 °C and at a relative humidity of 50% was measured to be 0.016 g/h, corresponding to 0.0005 mm/h. This value is very low, mainly due to the fact that the bowl is fit into a tight box with only two small openings.

Undercooling condensation on the WDR gauge collection area can be calculated based on the meteorological data and on the surface temperatures that are registered for the wooden cladding surface. One can assume that the surface temperature of the gauge collection area is equal to the surface temperature of the wooden cladding due to the large contact area of the wall gauge. The amount of condensation has been calculated and is, for each hour, included in the dataset. The maximum condensation amount for 1 h during the year 2004 is 1.2 g, corresponding to 0.038 mm. It is important to note that condensation is quite limited during rain events, because of the generally high cloudiness factor that limits radiation losses to the sky. Only for 3 h in 2004, undercooling condensation occurs during rainfall. The amounts are 0.14 (April), 0.01 and 0.03 g (November) which are very small values.

The maximum rest water error is the content of the tipping bowl; i.e. 6.3 g, corresponding to 0.2 mm, which is the highest value given in Table 1.

When the bowl tips, it briefly stops collecting water and incoming water is lost. A conservative estimate of this error, based on on-site measurements during WDR, is about 0.067 g/tip, corresponding to 0.002 mm/tip.

Table 2 summarises these errors and might give the impression that the rest water error is the most important error. However, the frequency of occurrence of the different errors has to be taken into account. A rain event is defined here as a period where rain can be interspersed by dry periods, such period can last from 1 h to several days. For a rain event, one is generally interested in the error in the accumulated amount of WDR for this rain event. Then the frequency of occurrence of every error is a follows:

- The adhesion-water evaporation error occurs after every break (dry period) in the rain event (worst-case scenario).
- Evaporation from the tipping bowl occurs continuously.
- Undercooling condensation occurs at discrete moments (hours) in time.
- The rest-water error can strictly occur during every hour, but focusing on the WDR amounts for the entire rain event it occurs only once as positive and negative errors from one hour to the next balance out during the rain event.
- The tip error occurs at every tip of the bowl.

A conservative estimate of the error in the WDR measurement at the end of the rain event is made by:

- Summing the errors E_{AW} during the rain event (assuming the worst-case scenario).
- Summing the evaporation errors E_{EVAP} for every hour in the rain event.
- Summing the condensation errors E_{UC} for every hour in the rain event.
- Extracting the combination of rest-water error E_{RW} and tip error E_{TIP} from Eq. (1) or from Fig. 9:

$$e_{BOWL} = \frac{E_{RW} + nE_{TIP}}{nV_{BOWL}}, \quad (1)$$

where e_{BOWL} is the relative error associated with the tipping-bowl registration mechanism, n is the number of tips, V_{BOWL} is the content of the bowls (in grams of water) and E_{RW} and E_{TIP} are also expressed in grams. Fig. 9 shows this error as a function of the number of tips (0.2 mm/tip) and as a function of the accumulated rainwater collected (mm). The total error E_{TOT} is the combination of all errors. Examples of total error estimates will be provided in the next section together with the measurement results.

Note that due to the presence of adhesion water at the gauge surface and due to the filling of the tipping bowl

there is always a delayed registration of WDR. This delay will be less important as the WDR intensity—and thus the number of tips within a certain time interval—increases.

4. Measurement results

The measurements were started in January 2004. The year 2004 had a total precipitation amount that is somewhat higher compared to a normal year in Trondheim. While yearly average precipitation is 855 mm (from the last reference 30-year period 1961–1990), 2004 had 985 mm. First, the wind and rain climatology at the field station is briefly described. Next, the measurement results for two selected rain events are presented: a rain event with rain mainly carried by westerly winds and a rain event with rain mainly carried by wind from south-west. The rain events were selected for temperatures significantly above 0 °C to exclude the possibility of snow registration instead of rain.

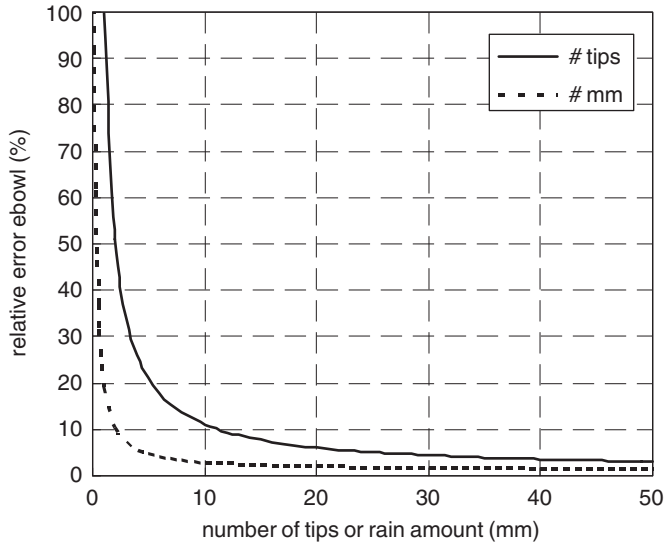

Fig. 9. Relative error in the wind-driven rain measurements associated with the tipping-bowl registration mechanism for the wall-mounted gauges, as a function of the number tips and as a function of the accumulated wind-driven rain collected (in mm).

4.1. Wind and precipitation climatology

The wind, precipitation and temperature conditions recorded at Voll during 2004 are shown in Figs. 10 and 11. The precipitation, wind and temperature measurements were obtained by the Meteorological Institute (met.no) at the field station. The year 2004 was characterised by a relatively dry first part of the year followed by wet autumn and winter months (including snow) (Fig. 10). Note that Fig. 10 displays weekly values while Fig. 11 has been obtained based on hourly values. Fig. 11 shows that the prevailing wind direction is south-south-west (SSW). The wind rose was constructed based on data from the cup anemometer and wind vane at the top of the 10 m mast. The frequency of occurrence of wind speed higher than 5 m/s is relatively low. More information about the co-occurrence of wind and rain in Norway has been provided by Rydock et al. [6].

4.2. Results for two selected rain events

4.2.1. Rain event June 13–16, 2004

Fig. 12 shows the measurement results of the rain event of June 13–16, 2004. Fig. 12a illustrates the wind direction measured at both 2 and 10 m height, the wind speed at both heights and the horizontal rainfall amount measured by the gauge of the Meteorological Institute G at the field station (Fig. 2). Both the set of wind-direction values and the set of wind-speed values are very closely correlated because the approaching wind is not disturbed by the presence of the

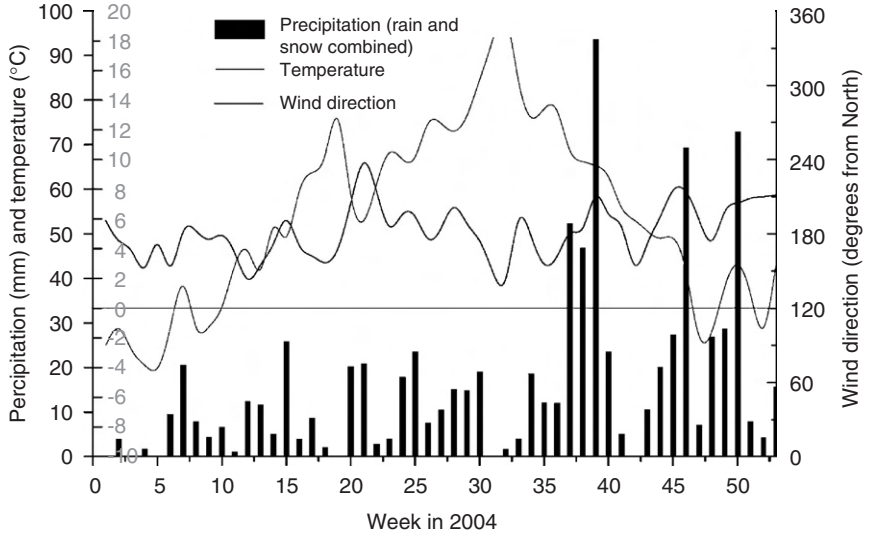

Fig. 10. Weekly values of precipitation, temperature and wind direction recorded at Voll in 2004.

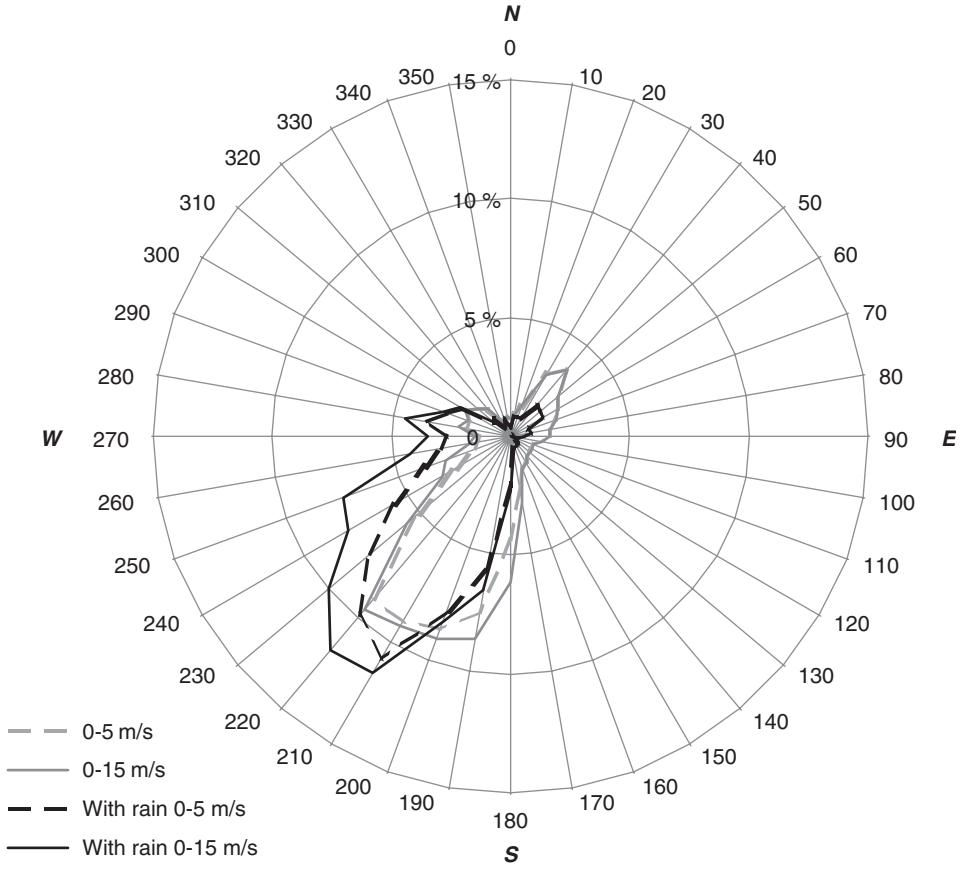

Fig. 11. Wind rose from the hourly values of 2004 measured by the cup anemometer and wind vane on top of the 10 m mast. The rose displays the frequency of occurrence of wind in 10° intervals, for wind data in general and for wind data only during rain (0° = wind from north).

other buildings at the field station for the wind directions during rain. Fig. 12b displays the records of the accumulated WDR coming from the four cardinal directions as measured by the four-way free-standing WDR gauge (Fig. 6a,b). For analysis purposes, also the records of horizontal rainfall and wind direction are given in this figure. Fig. 12c,d show the accumulated WDR by a number of the wall-mounted gauges. Fig. 12e illustrates the distribution of WDR (expressed as the ratio of accumulated WDR to accumulated horizontal rainfall for the rain event) across the west facade as measured by the wall-mounted WDR gauges.

The rain event can be characterised as a succession of light long-duration spells. The mean temperature was 8.7 °C and the total horizontal rainfall was 26.1 mm. The average wind speed was 2.6 m/s at 2 m height and 4.4 m/s at 10 m height. The mean relative humidity was 77% and the wind direction φ_{10} during rain varied mainly between south-west and north-west, with an average value of 252° in general (for the entire event) and also 252° during rain. The free-field WDR amount was 16.6 mm in the west-oriented gauge, 2.7 mm in the north-oriented gauge, 2.6 mm in the south-oriented gauge and no WDR was collected by the east-oriented gauge. The measurements by the wall-mounted gauges allowed discerning a distinct wetting pattern on the west-facing wall (Fig. 12e). Table 3 shows the different error estimates for the WDR measurements by the wall-mounted gauges at the end of the rain event, including the total absolute error E_{TOT} and the relative error $e_{TOT} = E_{TOT}/S_{wdr}$. S_{wdr} is the accumulated WDR for the rain event. The most important errors are the adhesion-water evaporation error and the tipping-bowl error. At those positions where little WDR is registered the errors are quite large (W5 and Wnorth). For all other positions, the errors are acceptable. Note that given the very low wind-speed values, both the splashing error and the wind error are considered negligible.

The observed wetting pattern on the west-facing facade can largely be explained by the wind direction. In this respect, it should be noted that the wind-direction values given above (252°) are not really representative. These averages were obtained based on arithmetic averaging in which an equal weight has been given to all hourly wind-direction values, irrespective of the severity of WDR during that hour. A better indication of the average representative wind direction for the WDR can be obtained by weighted averaging following the method used in [25]:

$$\varphi_{avg} = \frac{\sum U_i S_{hi} \varphi_i}{\sum U_i S_{hi}}. \quad (2)$$

In this equation, the hourly wind-direction values φ_i are averaged with the hourly wind speed U_i (at 10 m height)

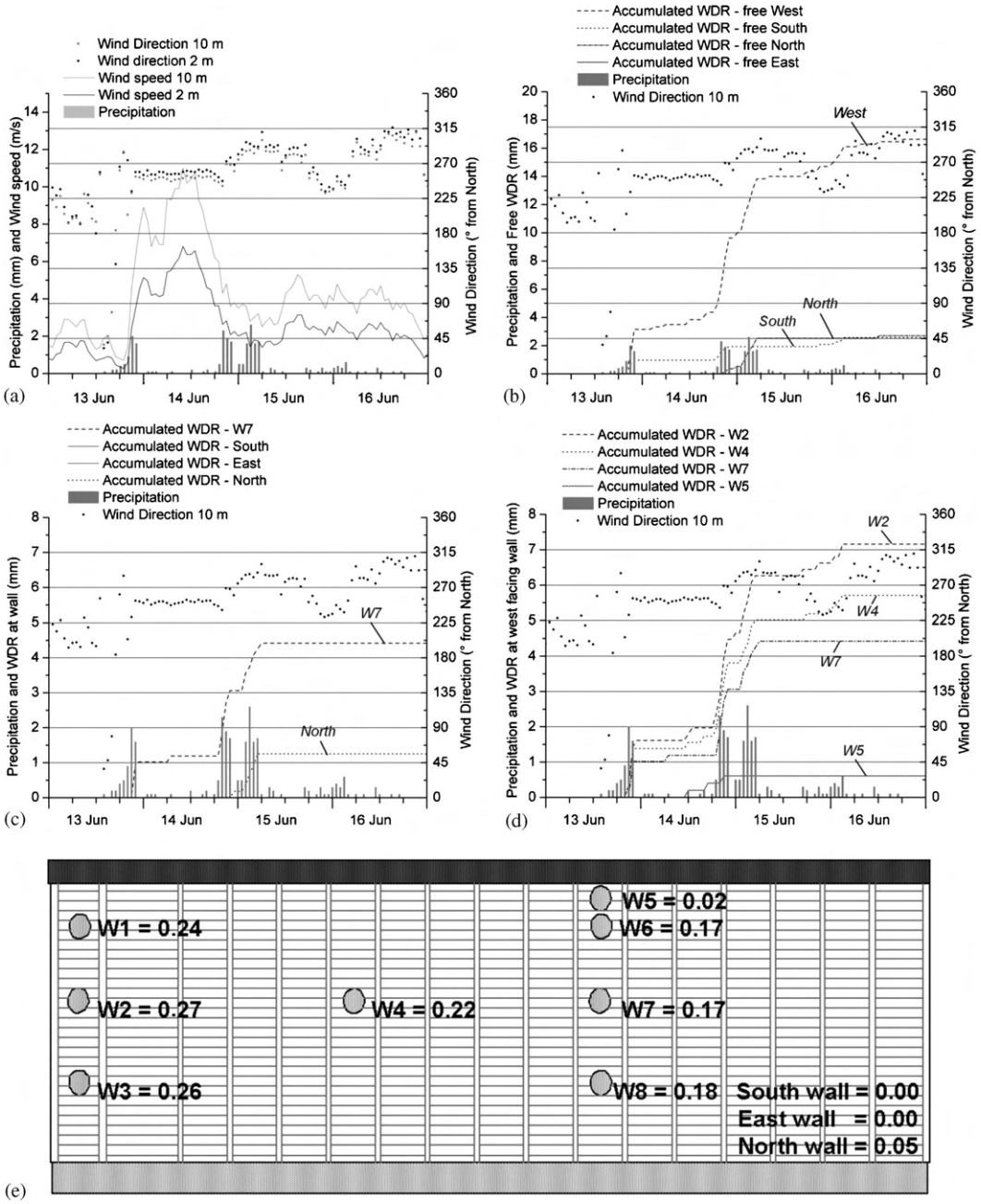

Fig. 12. Results of the rain event during June 13–16, 2004. The total horizontal rainfall amount was 26.1 mm. (a) Wind speed, wind direction and precipitation. (b) Free-field WDR from the cardinal directions: north, south, east and west. (c) WDR caught on the four walls facing the cardinal directions. For the west-facing wall, the measurements by W7 are shown. (d) WDR caught by some of the gauges on the west-facing wall. (e) Wind-driven rain distribution across the facade: ratios of accumulated wind-driven rain to accumulated horizontal rainfall for the rain event (= 26.1 mm).

and the horizontal rainfall S_{hi}, where i is the number of the hourly interval. The summation is taken over all hours in the rain event. This equation yields an average wind direction of 260°. The wind direction is thus almost perpendicular to the west-facing building facade. Therefore, a typical WDR distribution pattern as described for example in [1] was found: the largest amount of WDR was measured by the wall gauges near the facade corner (W1, W2, W3) and less WDR was found closer to the centre of the facade (W4, W6, W7, W8). In typical wetting patterns, the WDR amount increases with the height of the position on the facade. In this case however, the roof overhang partly shelters gauges W1, W5 and W6.

4.2.2. Rain event September 5–8, 2004

Fig. 13 shows the results of the rain event of September 5–8, 2004. The rain event can be characterised as a light almost continuous rainfall. The mean temperature was 11.0 °C and the total horizontal rainfall amount was 44.6 mm. The average wind speed was 1.9 m/s at 2 m height

Table 3
Error estimates for the accumulated wind-driven rain measured at the facades for the rain event June 13–16, 2004

WDR gauge	Number of tips	S_{wdr} (mm)	E_{AW}[a] (mm)	E_{EVAP}[b] (mm)	E_{UC} (mm)	E_{BOWL} (mm)	E_{TOT} (mm)	e_{TOT} (%)
W1	32	6.3	0.280	0.040	0	0.264	0.584	9.3
W2	40	7.2	0.280	0.040	0	0.280	0.600	8.3
W3	39	6.8	0.280	0.040	0	0.278	0.598	8.8
W4	33	5.7	0.280	0.040	0	0.266	0.586	10.3
W5	3	0.6	0.280	0.040	0	0.206	0.526	87.7
W6	22	4.5	0.280	0.040	0	0.244	0.564	12.5
W7	26	4.4	0.280	0.040	0	0.252	0.572	13.0
W8	25	4.6	0.280	0.040	0	0.250	0.570	12.4
South	0	0.0	0	0	0	0	0	—
East	0	0.0	0	0	0	0	0	—
North	7	1.3	0.280	0.040	0	0.214	0.534	41.1

[a]Calculated by multiplication of the adhesion-water error (0.07 mm) for a single occurrence of adhesion-water evaporation with the number of interruptions of the rainfall by dry periods. The number of interruptions is estimated to be 4, taking into account that intermittent interruptions shown in Fig. 12a can be due to the delay of registration by the tipping-bowl mechanism.
[b]Calculated by multiplication of hourly evaporation error with number of hours in the rain event from the start to the end of horizontal rainfall registration: 78 h.

and 3.0 m/s at 10 m height. The mean relative humidity was 82%. The wind direction during rain varied between south and north and the wind-direction fluctuations were significantly more pronounced than in the June rain event. The average value was 226° in general and 237° during rain. The free-field WDR was 28.4 mm in the west-oriented gauge, 6.3 mm in the north-oriented gauge and 4.8 mm in the south-oriented gauge. Nothing was caught in the east-oriented gauge. Fig. 13c,d shows the time distribution of the accumulated WDR caught by a number of the wall-mounted WDR gauges. Fig. 13e illustrates the WDR distribution across the west facade. Table 4 contains the error estimates.

As opposed to the June rain event, the WDR distribution on the west facade is now more uniform: the differences between the values at the north-west edge and the centre of the facade are less pronounced than for the June rain event. This difference can mainly be attributed to two reasons: (1) the difference in "representative wind direction" during rain and (2) the differences in the wind-direction fluctuations between both rain events. Concerning the first reason, the representative wind direction for the September event is 246° versus 260° for the June event. In the former case, most of the WDR was coming to the west facade from a direction that was more oblique. Concerning the second reason, the wind-direction fluctuations during rain for the September event are significantly larger than for the June rain event. Earlier work based on CFD simulations of WDR [14] has shown that the WDR wetting pattern on a building is highly influenced by the wind direction. Due to these large wind-direction variations, quite different wetting patterns corresponding to the different wind directions are superimposed in time, which can yield a final wetting pattern that is quite uniform. Note that, theoretically, because of the wider range of wind directions for the September rain event, the wind error might have some effect here. But because the wind speed values during rain are very low, it is expected to be negligible.

4.3. Dataset

In the previous section, two rain events were selected and discussed. The complete dataset is made available at the following URL: http://www.ivt.ntnu.no/bat/bm/WDR/WDR.htm. Currently, the dataset contains data for 2004. Further data from the ongoing field investigation will be added. The spreadsheets contain hourly data needed for model validation (temperature, relative humidity, wind speed, wind direction, horizontal rainfall, WDR on the facade in space and time and an estimate of the undercooling condensation on the gauge surface). It is important to note that all gathered data have been provided and that they have not been filtered to remove WDR measurements that are less accurate (due to e.g. wind errors, snow). The user of the dataset should ensure that the extracted data are reliable for model validation by performing an error estimation as outlined above and should be aware of the possibility for errors due to splashing and wind errors. Some guidelines for data selection to reduce these errors have been mentioned in this paper and are also provided in [16].

5. Conclusions

This paper has presented a dataset of wind-driven rain (WDR) measurements for a low-rise block-type test building in Trondheim, Norway. It contains a detailed description of the building, its surroundings and the meteorological station. It also contains WDR measurements in free-field conditions and on the building facades, measurements of wind speed, wind direction, horizontal

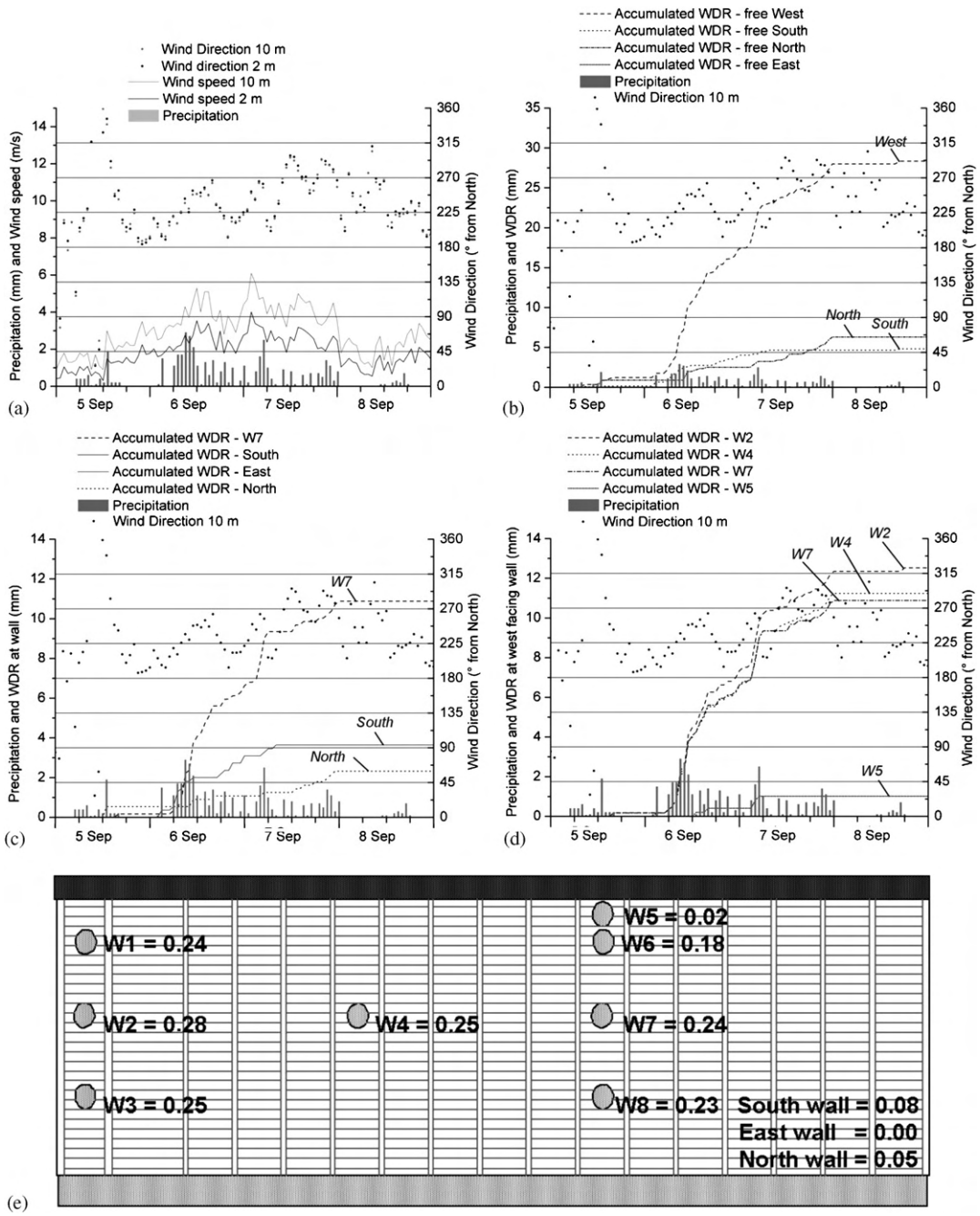

Fig. 13. Results of the rain event during September 5–8, 2004. The total horizontal rainfall amount was 44.6 mm. (a) Wind speed, wind direction and precipitation. (b) Free-field WDR from the cardinal directions: north, south, east and west. (c) WDR caught on the four walls facing the cardinal directions. For the west-facing wall, the measurements by W7 are shown. (d) WDR caught by some of the gauges on the west-facing wall. (e) Wind-driven rain distribution across the facade: ratios of accumulated wind-driven rain to accumulated horizontal rainfall for the rain event (= 44.6 mm).

rainfall intensity, temperature and relative humidity. Finally, the errors associated with the WDR measurements have been estimated. Concerning the latter aspect, the existing approach for error assessment has been extended to include the additional error due to the tipping-bowl registration system. The paper also provides the link to a website from which the full dataset can be downloaded. The paper and dataset are intended to be used for validation of CFD and other WDR models.

Acknowledgements

The wind-driven rain dataset has been established as part of the ongoing SINTEF Byggforsk research & development programme "Climate 2000—Building constructions in a more severe climate" (2000–2006: strategic institute project "Impact of climate change on the built environment"). The support provided by the industrial partners and the Research Council of Norway is gratefully acknowledged.

Table 4
Error estimates for the accumulated wind-driven rain measured at the facades for the rain event September 5–8, 2004

WDR gauge	Number of tips	S_{wdr} (mm)	E_{AW}[a] (mm)	E_{EVAP}[b] (mm)	E_{UC} (mm)	E_{BOWL} (mm)	E_{TOT} (mm)	e_{TOT} (%)
W1	53	10.5	0.210	0.043	0	0.306	0.559	5.3
W2	70	12.5	0.210	0.043	0	0.340	0.593	4.7
W3	65	11.3	0.210	0.043	0	0.330	0.583	5.2
W4	65	11.2	0.210	0.043	0	0.330	0.583	5.2
W5	5	1.0	0.210	0.043	0	0.209	0.462	46.2
W6	40	8.1	0.210	0.043	0	0.280	0.533	6.6
W7	64	10.9	0.210	0.043	0	0.328	0.581	5.3
W8	56	10.4	0.210	0.043	0	0.312	0.565	5.4
South	20	3.6	0.210	0.043	0	0.240	0.493	13.6
East	0	0.0	0	0	0	0	0	—
North	13	2.3	0.210	0.043	0	0.226	0.479	21.2

[a]Calculated by multiplication of the adhesion-water error (0.07 mm) for a single occurrence of adhesion-water evaporation with the number of interruptions of the rainfall by dry periods. The number of interruptions is estimated to be 3, taking into account that intermittent interruptions shown in Fig. 13a can be due to the delay of registration by the tipping-bowl mechanism.
[b]Calculated by multiplication of hourly evaporation error with number of hours in the rain event from the start to the end of horizontal rainfall registration: 84 h.

During the course of this work, the second author has been a post-doctoral research fellow of the FWO-Flanders (= Research Fund-Flanders, Fonds voor Wetenschappelijk Onderzoek-Vlaanderen). The FWO-Flanders supports and stimulates fundamental research in Flanders (Belgium).

The authors wish to express special thanks to Egil Rognvik for his important and creative contributions in planning and operation of the measurements at Voll. We also thank Kristin Lenz, Jon Andreas Ask, Kim Robert Lisø, Ole Aunrønning and Wendy Desadeleer for their kind assistance in the completion of this paper and the associated website.

References

[1] Blocken B, Carmeliet J. A review of wind-driven rain research in building science. Journal of Wind Engineering and Industrial Aerodynamics 2004;92(13):1079–130.
[2] Hoppestad S. Slagregn i Norge (Driving rain in Norway). Report No. 13, Norwegian Building Research Institute; 1955.
[3] Lacy RE. Driving-rain maps and the onslaught of rain on buildings. RILEM/CIB symposium on moisture problems in buildings, rain penetration, Helsinki, vol. 3; 1965. Paper 3–4.
[4] Sanders C. Heat, air and moisture transfer in insulated envelope parts. Final report, vol. 2. Environmental conditions, task 2. Leuven: Acco; 1996.
[5] CEN/TC89. Hygrothermal performance of buildings—climatic data—part 3: calculation of a driving rain index for vertical surfaces from hourly wind and rain data. prEN ISO 15927-3, Standard under approval; 2002.
[6] Rydock JP, Lisø KR, Førland EJ, Nore K, Thue JV. A driving rain exposure index for Norway. Building and Environment 2005;40(11): 1450–8.
[7] Choi ECC. Numerical simulation of wind-driven rain falling onto a 2-D building. Asia Pacific conference on computational mechanics, Hong Kong; 1991. p. 1721–8.
[8] Choi ECC. Simulation of wind-driven rain around a building. Journal of Wind Engineering and Industrial Aerodynamics 1993; 46&47:721–9.
[9] Choi ECC. Determination of wind-driven rain intensity on building faces. Journal of Wind Engineering and Industrial Aerodynamics 1994;51:55–69.
[10] Karagiozis A, Hadjisophocleous G, Cao S. Wind-driven rain distributions on two buildings. Journal of Wind Engineering and Industrial Aerodynamics 1997;67&68:559–72.
[11] Van Mook FJR. Measurements and simulations of driving rain on the main building of the TUE. Fifth symposium on building physics in the Nordic countries, Göteborg, Sweden; 24–26 August, 1999. p. 377–84.
[12] Van Mook FJR. Driving rain on building envelopes. PhD thesis, Building Physics Group (FAGO), Eindhoven University of Technology. Eindhoven University Press, Eindhoven, The Netherlands; 2002. 198pp.
[13] Blocken B, Carmeliet J. Spatial and temporal distribution of driving rain on a low-rise building. Wind and Structures 2002;5(5):441–62.
[14] Blocken B, Carmeliet J. On the validity of the cosine projection in wind-driven rain calculations on buildings. Building and Environment 2006;41:1182–9.
[15] Blocken B, Carmeliet J. The influence of the wind-blocking effect by a building on its wind-driven rain exposure. Journal of Wind Engineering and Industrial Aerodynamics 2006;94(2):101–27.
[16] Blocken B, Carmeliet J. High-resolution wind-driven rain measurements on a low-rise building—experimental data for model development and model validation. Journal of Wind Engineering and Industrial Aerodynamics 2005;93(12):905–28.
[17] Blocken B, Carmeliet J. On the accuracy of wind-driven rain measurements on buildings. Building and Environment; 2005, in press (doi:10.1016/j.buildenv.2005.07.022).
[18] Lisø KR, Kvande T, Thue JV. Climate 2000—building enclosure performance in a more severe climate. Seventh Nordic symposium on building physics, Reykjavik, Iceland; June 13–15, 2005. p. 211–8.
[19] Holmgren J. Husbygging (House construction), vol. 1. Oslo; 1946. p. 119–28.
[20] Isaksen T. Driving rain in Bergen. Report F4625-TI/RJ.6.6.75, Norwegian Building Research Institute; 1975.
[21] Nore K, Thue JV, Time B, Rognvik E. Ventilated wooden claddings—a field investigation. Seventh symposium on building physics in the Nordic countries; June 12–15, 2005, Reykjavik, Iceland. p. 617–24.
[22] Rydock JP. Validation of a present weather observation method for driving rain mapping. Building and Environment; 2005, in press (doi:10.1016/j.buildenv.2005.09.017).

[23] Lyberg, M. Results from driving rain measurements on a tall apartment building 1969–1978. Proceedings of the CIB Working Group W61 joints in exterior walls 1979, Danish Building Research Institute; 1980.
[24] Högberg AB, Kragh MK, van Mook, FJR. A comparison of driving rain measurements with different gauges. Proceedings of the fifth symposium of building physics in the Nordic countries, Gothenburg; 1999. p. 361–8.
[25] Blocken B, Roels S, Carmeliet J. A combined CFD-HAM approach for wind-driven rain on building facades. Journal of Wind Engineering and Industrial Aerodynamics; 2006, in review.

Paper II: Evaluation of Moisture Pins for Measuring Moisture Variations in Wood Cladding

Evaluation of Moisture Pins for Measuring Moisture Variations in Wood Claddings

Kristine Nore, Research Fellow,
SINTEF Building and Infrastructure
Department of Civil and Transport Engineering, Norwegian University of Science and Technology (NTNU)
Kristine.Nore@sintef.no

Jan Vincent Thue, Professor,
Department of Civil and Transport Engineering, Norwegian University of Science and Technology (NTNU)
Jan.Thue@ntnu.no

KEYWORDS: Moisture pins; moisture content; measurements; moisture profile; accuracy; wood moisture.

SUMMARY:
The wood moisture content (MC) is vital for the wood performance and durability in external applications. Moisture pin sensors are widely used for measuring the MC of wood materials by measuring the electrical resistance of the material. They are durable and respond quickly to changes in the moisture conditions in the wood.

This paper presents a laboratory study of moisture pins used in an extensive field investigation on wood cladding. In this project wood moisture is logged by measuring resistance between two steel pins. Attempts were made to use moisture pins for monitoring the moisture profile in the cladding boards. The quality of these measurements are examined and compared with gravimetric measurements. The paper also discusses the accuracy of moisture pin measurements.

The quality of continuous electrical resistance measurement series as well as the ability to define the current moisture profile of the cladding board by moisture pins is discussed. The free field measurements conclude that measurements in external applications should be continuous measurement series in order to control the rapid MC fluctuations resulting from the wood cladding response to the ambient climate. The laboratory measurements conclude that measuring the moisture profile was not possible for coated wood cladding.

1. Introduction

In order to have durable wood constructions the moisture content (MC) must be kept below the level of risk for rot. Rot and stain fungi need high MC to be able to decompose the wood substrate. Also wood swell and shrink according to its MC. Hence, limiting the wood MC is vital for the wood performance and durability in external applications.

MC in wood claddings is usually between 12 and 25 % by weight, depending of its location (Geving et al. 2006). The work in this project is linked to performance of wood cladding. Esping, Salin and Brander (2005) present Swedish requirements for delivery of outer cladding boards, where the MC may not exceed 18 % with a tolerance of ± 2 %. Norwegian requirements for planed timber are 17 % with a tolerance of ± 5 % (NS 3180). A risk for rot is often set to a limit of 20 % MC.

The MC can be found by several methods. Most commonly used is gravimetric, electrical resistance or capacitive measurements. Moisture pins, often in steel, measure the resistance in the wood material. The correlation between resistance and moisture content is used to calculate the wood moisture content (MC). This measurement method is fast and effective and quite accurate, which makes it widely used in the wood industry, construction industry and also when evaluating causes of failures in building constructions that contain wood.

SINTEF Building and Infrastructure is using wood moisture pins in an extensive field investigation on the performance of wooden claddings. The MC fluctuations of treated and untreated wood in external climate are

tracked carefully. In addition to examining the wood MC in different cladding types and assemblies, we have attempted to measure the moisture profile in the cladding boards. This was in order to study and to verify calculations of moisture transport in the cladding. This paper presents laboratory tests that study the moisture profile measurements and discuss the accuracy of moisture pin measurements.

2. Background

The reference method for measuring wood MC is gravimetric measurements (EN 13183-1). This is done by weighing the wood material, drying it at 103 °C and then weighing the dried material. This is the most exact way to measure the moisture content in wood, but it is time-consuming and often destructive.

Said (2007) presents a literature review on methods of moisture measurements in building envelopes. His opinion is that resistance and voltage methods are most suitable for continuous monitoring of building envelope performance. By voltage measurements he refers to monitoring the surface time-of-wetness (TOW).

In our project, wood MC is monitored by measuring resistance as described in EN 13183-2. There is a correlation between resistance and wood moisture content; when the MC increase the resistance decreases. This correlation is not linear, as seen in Figure 1. The initial mathematical model that describes this correlation was derived in the 1920's (Apneset and Hay, 1992). Resistance measurements must be adjusted according to material temperature, wood density and wood species. Wood species contain different amounts and types of salts, resulting in different conductive properties. Above fibre saturation point the resistance increases slowly, but exact measurements above this point are most often not of interest because the critical risk for rot MC value is already exceeded. Another relating fact is that the accuracy decrease when the moisture content increase. This is also seen in Figure 1.

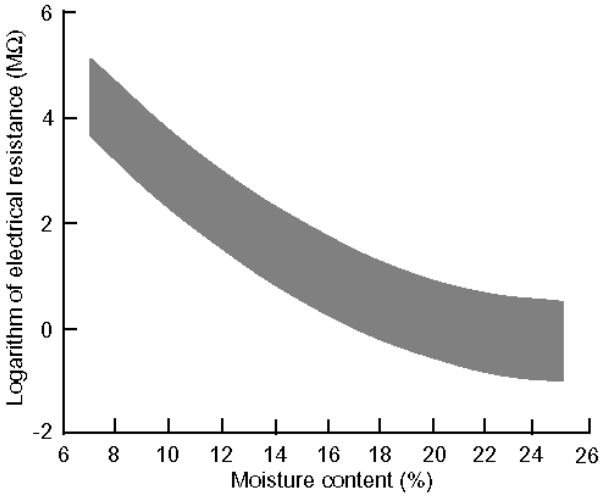

Figure 1. Wood Moisture Content (MC) versus the logarithm of electrical resistance measured at 27°C. The shaded area includes the 90% percentil. (U.S. FPL 1982).

When measuring continually the current is switched in each measurement to avoid polarization of the poles, in what follows from the electrolysis of the water and wood fluids. In addition, when the current is switching and MC value is recorded immediately, the dielectric constant of the wood is not affecting the measurement.

Nordtest 420 is a standard for measuring MC using wood probes with embedded electrodes, some with thermocouple integrated. They are meant for continuous measuring, but may have a delay and larger tolerances, due to the surface transfers between the dowel and the material of interest.

The most exact MC meters measure resistance only at the tip of the two steel pins, with 2-5 mm not insulated. If the entire pin has no insulation there is a risk of measuring surface moisture (Nordtest 302) and according to D 4444-84 the highest MC in contact with the pins will be measured.

When the pins are insulated one may measure a profile (Apneset and Hay 1992). The ASTM standard D 4444-84 presents four special problems that should be considered when doing moisture profile measurements;

(1) nonisolated pins, (2) nonparabolic gradients, (3) surface moisture on electrode and (4) high surface MC on sample.

The distance between the steel pins are normally about 25 mm, but according to Forsén and Tarvainen (2000) the distance have no significant effect on moisture content measured with resistance MC meters. Measuring in the end section of the wood is not correct according to EN 13183-2. Forsén and Tarvainen (2000) found that the measured wood MC was not influenced by whether the measuring was done perpendicular or parallel to the wood grain. In general measuring parallel to the grain is recommended.

Forsén and Tarvainen (2000) state that wood density has no influence on moisture readings, but Nordtest 302 describe that the moisture content is read too low in fast grown wood, due to higher resistance in less wood substrate. Measurements on impregnated wood increase the MC reading about 2 – 4 % (Esping, Salin and Brander 2005). D 4444-84 also reports that preservatives and adhesives may cause abnormal readings – usually higher. Small concentrations of salt may impact the resistance measurements.

Forsén and Tarvainen (2000) state that resistance measurements are most accurate within a MC range of 8-20 %. Apneset and Hay (1992) report the range of 7-25 % MC as reliable.

The standards D 4444-84 and Nordtest 302 both present the relative error of moisture pins within this measurement range, after temperature and type of wood is taken into consideration. They state that the error is 7 % in a 95 % confidence interval (0.5 - 2 % MC). Esping, Salin and Brander (2005), however, reduce the accuracy to 15 % in a 95% confidence interval (1 - 4 % MC). If the tolerance must be below 1 % MC one may increase the number of measurements to 5 (Apneset and Hay 1992).

Forsén and Tarvainen (2000) differentiate between systematic and rest error. Systematic error gives the same value at every reading and includes hysteresis, design of moisture sensors, measuring in the end grained wood, wrong measurement calculation, wrong temperature and if the wood is impregnated. The rest error is variable even when measurements are done exactly the same way and includes inaccuracy in the display, uncertainty in the calibration, variation in the calibration resistance, uncertainty in the preparing of the calculation curve, variation of the electrical resistance of the wood, different measurement depths and the variation of the moisture profile in the wood. Table 1 gives the systematic and rest error of hand held wood MC meters.

Table 1. Systematic error and rest error, in % MC, at different MC levels (Forsén and Tarvainen 2000).

	10 % MC	15 % MC	20 % MC
Systematic error	1.4	2.2	2.5
Rest error	0.1	0.4	1.0

3. Method

In our wood cladding field investigation at Voll, Trondheim, 102 MC sensors are mounted. The project is described in Geving et al. (2006). In this project all sensors are mounted measuring perpendicular to the grain. The distance between the electrodes is 25 mm. Most MC sensors are measuring “total moisture content”, see Figure 2. This means that the entire steel pin is pressed 16 mm into the wood.

When initiating the project, one part of the work was to monitor the moisture movement in the wood cladding boards. Measuring the local MC was intended when mounting moisture pins in different depths. Figure 2 shows the measurement set up with moisture pins in three different depths. These pins are insulated with heat-shrinkable tubing, except for a length of 3 mm at the tip. The pins for measuring the total MC were uninsulated in full length.

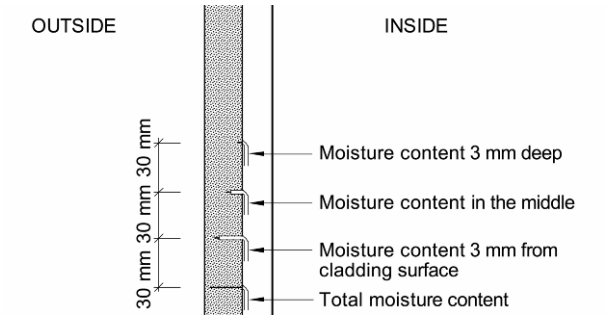

Figure 2. The set up of the moisture profile measurement. The cladding board thickness is 19 mm and the outside is coated. Temperature is measured at the inner surface of the cladding board.

The steel pins used are 2 mm in diameter. Every MC sensor is set in a predrilled hole of 1.9 mm in diameter for the measuring contact area and 2.5 mm in diameter where the insulated pin is lowered into the wood.

At the field investigation all measurement sensors are read every 10th minute and an average hourly value is stored. This cladding experiment has continued since January 2004.

In order to ensure the quality of our measurements a gravimetric study of the wood moisture pins mounted at the test façade was carried out in October 2006, after three years in service. Gravimetric measurements were in this case a destructive method, stripping down some of the field test instrumentation. Two instrumented boards, from the same full length board, fast grown wood, primed and coated with alkyd paint, were chosen. The boards had full instrumentation with both total and profile MC sensors. The cladding boards were removed from the wall and cut into four pieces. Two of these four pieces were split into outer, middle and inner part. The paint was scraped off. All board pieces were weighed directly after stripping down and again after drying. The two end section parts of each test board were used for measuring the total moisture content. This way the split parts, used to measure the moisture profile had no original end grained wood.

Corresponding tests were done in the previous investigation at the Voll test house, “Moisture condition in timber frame roof and wall structures”. The moisture pins corresponded well to the moisture pins in the range 10 - 18 % MC, and satisfactory in the span 18 – 25 % MC (Geving and Uvsløkk 2000).

To study whether it was possible to measure the moisture profile with moisture pins, new identical cladding boards were instrumented for laboratory tests. These were conditioned in two relative humidities (RH), 50 % and 75 %, in several months, making sure no moisture profiles were present. In this test we did not use heat-shrinkable tubing on the MC pins.

4. Results of Free Field Moisture Pins

With the large amount of MC data from the continuous time series, collected for four years, the systematic error is minimal; implying that the variations found in one measurement point is true variations. Correlating the measurement series to the ambient climate gives explicit comparison for the direct response. The measurements for one typical moisture pin for ten days, one month and three years are presented in Figure 3, showing averaged hourly, twenty-four hour and monthly values.

Studying the hourly data of the resistance sensor in Figure 3a we find that the variations during a twenty-four hour period may reach 2 % MC. During a month the twenty-four hour average values in Figure 3b show a span of about 4 % MC. The span of the 3 year period with averaged monthly values, shown in Figure 3c, reaches about 6 % MC. Continuous hourly measurements are useful to avoid the error of twenty-four hour fluctuations in non-conditioned investigations.

When using continuously measured data to compare different wood cladding designs, the true data variation, e.g. the degree of slope of the linear regression (trend), give valuable information regarding the performance of the different cladding designs.

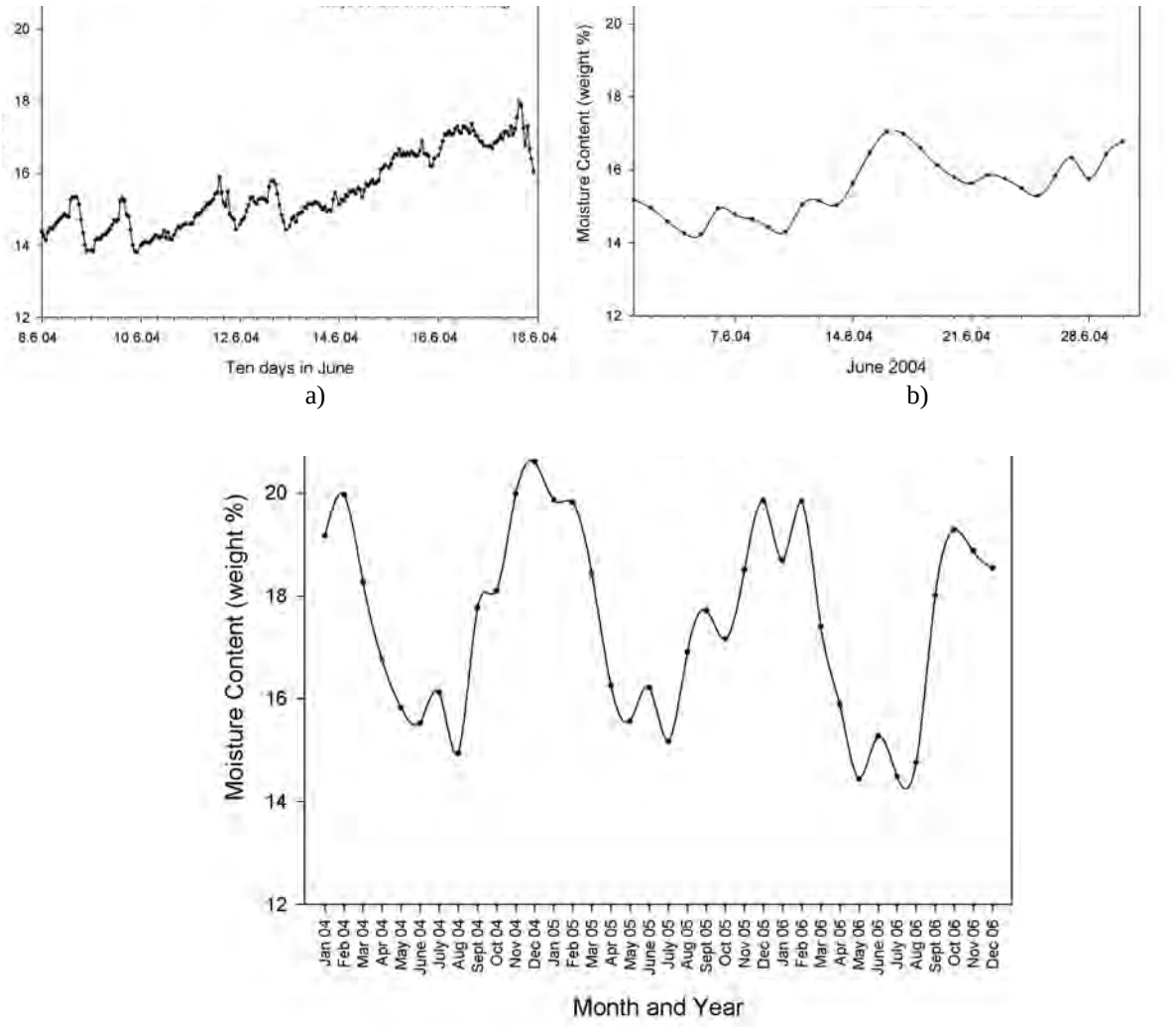

Figure 3. MC fluctuations of one randomly chosen resistance sensor. a) Variation in the hourly average, given for a ten day period. b) Averaged twenty-four hour values given for one month. c) Monthly averaged values given for three years.

The results of the MC measurements revealed that moisture pin measurements of the moisture profile in the cladding board did not correspond to gravimetric measurement, see Figure 4.

The readings from the moisture pins gave an apparent moisture profile; the outer part wetter than the inner part, indicating a moisture transport towards the inside of the cladding board. The gravimetric measurements however, are more reliable and show that the middle parts of the boards were the wettest. 25 hours had passed since last rain fall when stripping down the instrumented boards. The moisture distributions found by the gravimetric measurements are more accurate. Even though the s_d value of the alkyd coating on fast grown wood was 2.5 m one year earlier; the drying out through the coating layer is obviously considerable.

The highest electrical resistance MC value is found in the outer part, but the "total measurement" value is always higher. This is discussed in section 5

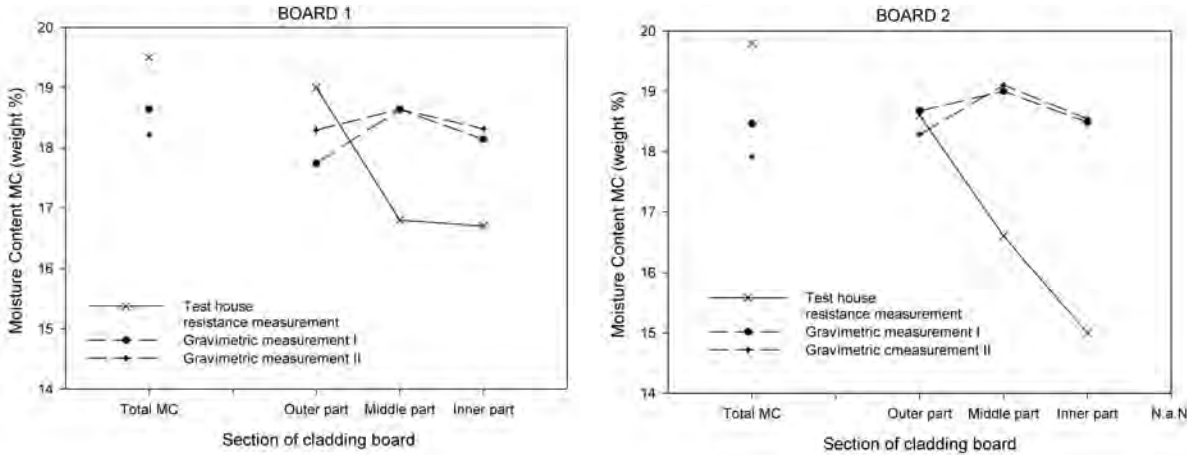

Figure 4. Gravimetric and electrical resistance measurements of cladding (fast grown bards with alkyd paint). Resistance measurements present moisture profiles with the wettest part close to the coated side. Gravimetric measurements give a moisture profile showing the wettest part is in the middle of the board.

5. Results of Laboratory Study of Moisture Pins

The results of the laboratory study revealed that electrical resistance measurements also read a "profile" in the wood cladding board, even though no moisture profiles were present – the boards were conditioned for several months and measured in controlled environment. One should have read identical MCs for each RH and not the span of about 3% at 50 % RH and 4% at 75 % RH, as shown in Figure 5. The deviation increases with higher RH, which corresponds to Figure 1.

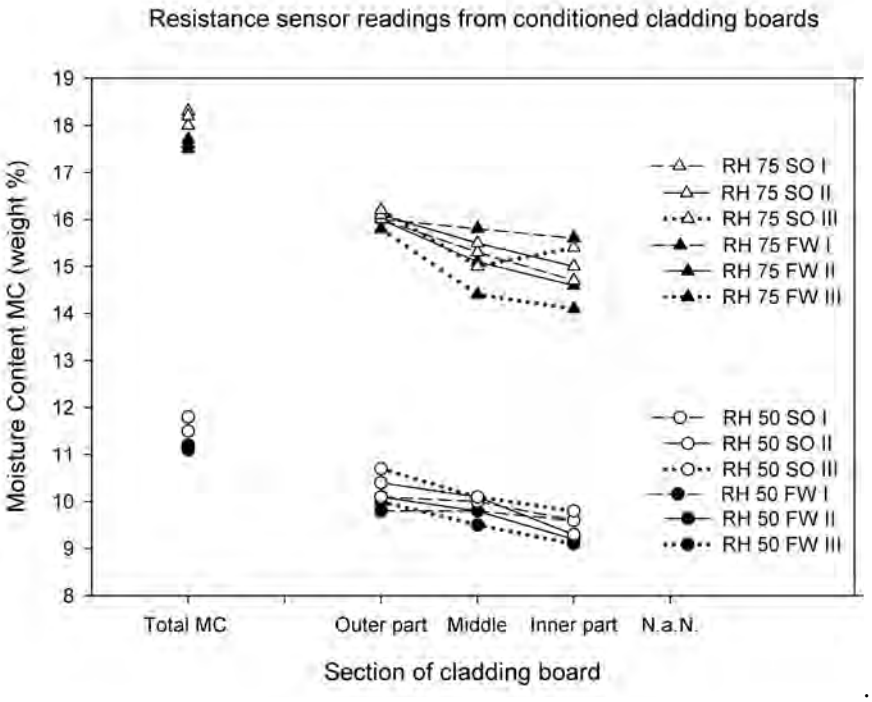

Figure 5. Electrical resistance measurements of wood cladding conditioned in the laboratory. Six cladding sections are tested, FW – fast grown with water (acryl) based paint and SO – slow grown with oil (alkyd) based paint.

Figure 5 also indicate a difference in the reading of fast and slow grown wood. The fast grown wood gives lower moisture readings. This support the theory of Apneset and Hay (1992) mentioned in section 2; the wood density does influence the moisture readings, presenting too low MC values for less dense wood. Or the calibration curve is not correct for both densities.

According to D 4444 – 84 the highest value should be read by the noninsulated pin. Both free field and laboratory results present higher values for the "total" pin, not equal to the outer part, which has the highest value of the 3 mm electrodes. This might suggest that the "Total" sensor reads higher MC than the actual highest MC Assessing the nonisolated pins as parallel couplings may explain this. In an electrical field all paths will contribute to the total reading. Consequently, the "total" reading with the noninsulated pins, providing the largest contact area, will always give a higher MC value than the highest local MC, see Figure 6.

This analogy may also explain the reason for the reading of the apparent moisture profile. The electrical fields in the different depths are unequal, see Figure 6. The inner pins, mounted on the back side of the cladding have the smallest electrical field, and the middle pins have the largest. The pins closest to the treated surface have a cross, but the surface treatment may give a shortening in case of conduction, adhesives in the primer or paint. In this case the highest reading is found in the outer part pins implying that the surface treatment does affect the electrical properties. Similar points of view have not been found in any literature studied by the authors.

The cladding thickness is usually not more than 23 mm. This is not enough to measure full electrical fields in different depths.

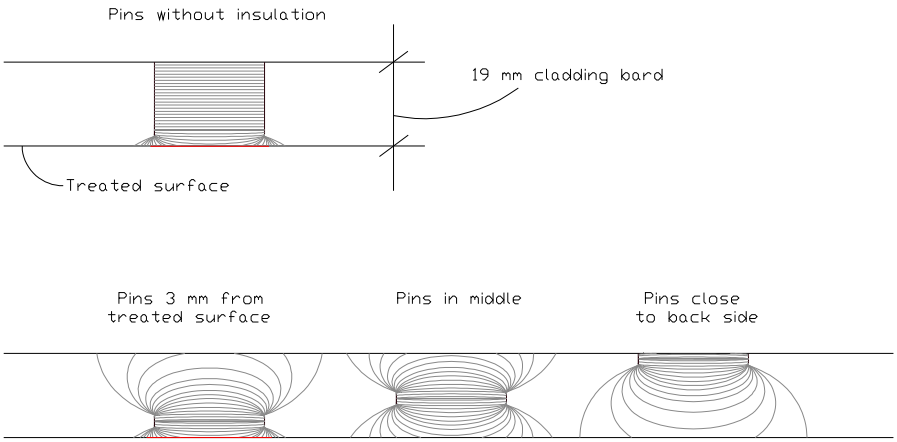

Figure 6. Electrical field lines in the four different moisture pins set up.

Unfortunately moisture profile measurements on untreated cladding boards have been conducted neither in free field nor in the lab tests. The laboratory test intended to include removal of the paint layer and repeating the measurements, but due to a break-down of a climate chamber the test could not proceed. The authors hope to be able to include these results in the last version of this paper, after the review.

6. Conclusions

Using electrical resistance is an effective way to read the moisture content (MC) in wood materials. But MC meters must be operated by qualified personnel and ambient climate data must be recorded in order to ensure high quality measurement data.

Twenty-four hour fluctuations in external applications are relatively large. Randomly collected data gives low data output, e.g. making one measurement a day. Monitoring and averaging the MC over a period of time provides a good conception of the moisture fluctuation in the test boards.

Analyses of the correlation of continuous time series with measured wood cladding MC and ambient climate gives valuable data. Narrowing down to e.g. analysing and comparing the degree of slope of the regression line of the MC in different periods, further decreases the tolerance and increases the data output.

Measuring the moisture profile with moisture pins in wood cladding is not recommended. Three relations influence the moisture pin measurements:

- length of the electrode – equivalent to the contact area;
- distance to the surface and;
- surface treatment

7. Acknowledgements

This paper has been written within the NBI Research & Development program "Climate 2000 –Building Constructions in a More Severe Climate" (2000 – 2006), strategic institute project "Impact of climate change on the built environment". The authors gratefully acknowledge all construction industry partners and the Research Council of Norway.

8. References

Apneseth, T. and Hay, M. 1992. Test of hand held electircal moisture meters (In Norwegian). Work report. NTI Norwegian Wood Technology Institute. Oslo.

D 4444-84. Standard Test Methods for Use and Calibration of Hand-Held Moisture Meters. ASTM American Society for Testing and Materials.

Esping, B., Salin, J.G. and Brander, P. 2005. Moisture in wood for the building construction industry – moisture properties, demands, use and measurements. (In Swedish). SP INFO 2005:24, SP Trätek.

European standard EN 13183-1, 2002. Moisture content of a piece of sawn timber - Part 1: Determination by oven dry method. European Committee for Standardization. Brussels.

European standard EN 13183-2, 2002. Moisture content of a piece of sawn timber - Part 2: Estimation by electrical resistance method. European Committee for Standardization. Brussels.

Forsén, H and Tarvainen, V. 2000. Accuracy and functionality of hand held wood moisture content meters. Technical Reesearch Centre of Finland, VTT Publications 420.

Geving, S., Erichsen, T.H, Nore, K. and Time, B. 2006. Hygothermal conditions in wooden claddings – Test house measurements. Project report 407. Norwegian Building Research Institute. Trondheim

Geving, S. and Uvsløkk, S. 2000 Moisture condition in timber frame roofs and wall sturctures. Project report 273. Norwegian Building Research Institute, Trondheim.

Nordtest Method NT BUILD 302 Building materials, wood: Moisture content. Approved 1986-09. Helsingfors Finland

Nordtest Method NT BUILD 420 Building materials, wood: Moisture content. Approved 1993-05. Helsingfors Finland

NS 3180. 1976. Quality specifications for planed timber. Pronorm, Norway.

Said, M. N. 2007. Measurement methods of moisture in building envelopes – a literature review. International Journal of Architectural Heritage. Vol 1, no.3. pp. 293-310.

U.S. Forest Product Laboratory (FPL). 1982. Wood Engineering Handbook. Englewood Cliffs, NJ: Prentice Hall, Inc.

Paper III: A comparison of time-of-wetness and wind-driven rain measurements on wooden cladding

A COMPARISON OF TIME-OF-WETNESS AND WIND-DRIVEN RAIN MEASUREMENTS ON WOODEN CLADDING

Kristine Nore[1, 2], Jan Vincent Thue[2] and James P. Rydock[1, 2]

1. Norwegian Building Research Institute (NBI)
Høgskoleringen 7B, 7591Trondheim, Norway,
e-mail: kristine.nore@byggforsk.no, james.rydock@byggforsk.no
2. Department of Civil and Transport Engineering, Norwegian University of Science and Technology (NTNU), Trondheim, Norway,
e-mail: jan.thue@ntnu.no

Keywords: Moisture, time of wetness (TOW), wind-driven rain (WDR), condensation, wooden cladding, ventilated façade

ABSTRACT

When determining service life of building materials, the stresses induced on the material must be defined. Assessment of the climatic stresses on a building envelope is generally based on meteorological records. During the years, considerable research efforts have been made in order to convert meteorological data into a moisture load imposed on a building. Wind-driven rain (WDR) gives data on the impact of rain on a vertical surface. Time of wetness (TOW) is a parameter describing the period when there is a water film on the surface, which includes liquid water both from WDR and condensation. This paper, which presents results from an extensive field investigation of wooden claddings in Trondheim, Norway, includes ambient climate data, TOW and WDR measurements on the façade surface. Preliminary results of parallel measurements of WDR and TOW are presented and discussed. The results show, as expected, longer TOW than the WDR measurements indicate, presumably due to surface condensation and the drying out period after the moistening from the WDR or condensation incidents. The paper suggests that the TOW parameter can give valuable supplemental information in addition to WDR when assessing the design moisture stresses on façades.

INTRODUCTION

When determining service life of building materials, the stresses induced on the material must be defined. The main parameter regarding wooden cladding deterioration is moisture, which, as time goes by, leads to germination and growth of algae and fungi. Inorganic façade materials may also, due to surface moisture, have algae growth that reduces the esthetical quality of the façade. The moisture influence on a façade is determined by the ambient climate, e.g. relative humidity (RH), temperature (T), wind-driven rain (WDR) – amount of rain caught on the façade, condensation, or time of wetness (TOW) – the period when the surface is covered with a water film.
This paper presents the appearance of the parameters TOW, WDR and condensation on wooden claddings and discusses their influence. The relation between the parameters can be as displayed in equation (1).

$$t_{TOW} = t_{WDR} + t_{condensation} + t_{drying\ out\ period} \quad (1)$$

where t = the period the condition occurs summed in hours

Assessment of the climatic stresses on a building envelope is generally based on meteorological records. In the past, considerable research efforts have been made to convert meteorological data on wind and precipitation into a moisture load imposed on a building. WDR, the impact from rain on a vertical surface, can be calculated from the pre-standard ISO/CD 15927-3 (2005). The pre-standard gives a semi-empirical method for calculating the WDR impacting a designated wall, according to precipitation and wind data in addition to orientation, geometrical properties of the wall and the topography of the surroundings. More semi-empirical and numerical methods exist to calculate the quantity of WDR caught on a façade, and even though detailed determination about the spatial and temporal WDR exposure can be found (Blocken and Carmeliet, 2004), there are still challenges to explore the effects of the WDR load. How does the wall respond when the rain hits the façade; e.g. the amount of runoff, the influence of the wind speed and wind direction, how are different façade materials and surfaces reacting to the WDR distribution or what is the drying out period?
Condensation periods can be calculated from the dew point temperature of the air and the surface temperature. Becker and Putterman (2002) found that mould and algae growth on façades in Israel was due to condensation. Condensation on a render façade did not lead to a water film, but higher moisture content in the capillary active render. They also found that condensation has a bigger influence on well-insulated dwellings. Zillig et al. (2003) discuss condensation load on façades based on different construction types and façade colors. It was shown that by using an IR coating with a lower emissivity, the condensation rate was lower.
TOW is a parameter which is less explored both due to the fact that it is harder to calculate, because of the multiple parameters involved, and it is more difficult to measure. The EU project “Wood Assess” that addressed durability of wooden cultural heritage buildings, performed TOW measurements in addition to the wooden moisture content, in order to provide detailed information of the wooden rotting risk (Haagenrud et al., 2001). It was found that the method gave a more accurate rotting risk index than e.g. Scheffers index, which takes RH and temperature into account (Scheffer, 1971),.
The duration of the drying out period depends on the ambient microclimate of the wall, i.e. the energy balance; air temperature and convection, radiation and heat conduction through the wall, and the moisture balance; moisture content in the façade material, the air RH and the liquid moisture influence. Calculating the duration of the drying out period is therefore complicated.
This paper is based on an extensive wooden cladding investigation at the field station of NBI (Norwegian Building Research Institute) and NTNU (Norwegian University of Science and Technology), which includes measurements of TOW, WDR and surface temperatures of the cladding. The results of these measurements are presented in order to find the relation to other parameters, the validity of TOW and to explore the possible use of TOW.

THE FIELD STATION AND MEASURING METHODOLOGY

The field station

The field station of NBI and NTNU is located in an open field at Voll in Trondheim, shown in Figure 1a. The claddings have different build ups of the air gap opening, two wood qualities and different paint systems. A detailed set up of the cladding investigation is described in Nore et al. (2005a). The meteorological station of Trondheim is located 17 meters to the south of the test house. The test house has almost identical test claddings on its east and west facing side. In total, 246 temperature and moisture sensors including WDR and other meteorological parameters are measured hourly at the test station. The inside of the house has a controlled temperature of 20ºC. Southwest is the prevailing wind direction for rain in Trondheim and thus the dominant direction for WDR. This leads to an east facing wall with small WDR influence and a heavily WDR influenced west-facing wall. Thus according to the WDR parameter the east facing wall should not be influenced by liquid water. Measurement results from 2004 are analyzed in this paper.

a. **b.**

Figure 1. a) The Voll test field of NBI and NTNU with the two test houses and the meteorological mast. b) West facing façade. Wetness and temperature sensors are located close to the WDR gauges in the painted areas.

WDR measurements

Wind-driven rain (WDR) is measured in the free field and on the test house walls at the test station. It is measured with tipping bowls, each tip representing 0.2 mm/m^2/tip. The west facing wall has the highest WDR intensity and therefore also the most WDR gauges in order to find the WDR dispersion on the wall, see Figure 1b. The test house has totally eleven WDR gauges. The results from nine WDR gauges, one at the east facing wall and eight at the west facing wall, are presented in this work.

Condensation calculations

Condensation occurs when the temperature of the façade surface (T_{CS}) falls below the dew point temperature of the air. The dew point temperature is calculated from RH_{air} and T_{air}. The surface temperature of the wooden cladding is measured close to the TOW sensors, with a thermo couple with a 1 cm^2 copper plate sensor coated with one paint layer. Figure 2 illustrates how the condensation periods are found. Condensation occurs in the night time. As the temperature sensor has a different surface and a tolerance of ± 0.5°C, more condensation might have taken place as the dew point temperature approaches the surface temperatures as seen Sept. 19th and 20th in Figure 2.

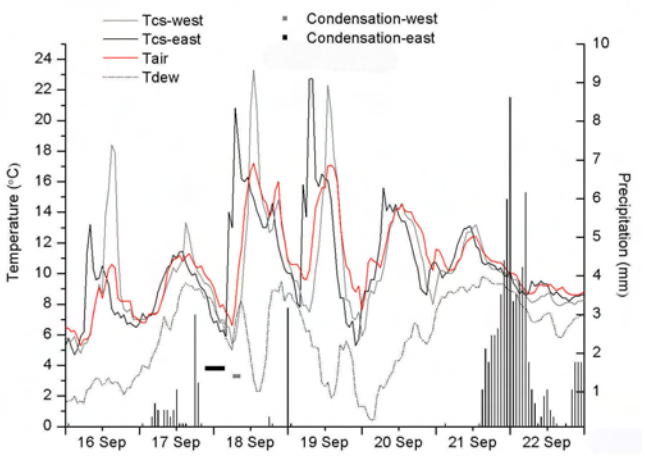

Figure 2. A selected period, September 16th to 22nd 2004, shows when condensation occurs. The surface temperatures (Tcs) of the west and east facing sides are compared to the air temperature (Tair) and the dew point temperature (Tdew). Precipitation is shown with columns and registered condensation hours are shown with dots. In this graph data from the lowest measurement sensors of the cladding sections with 4 mm air gap opening are presented. The location is shown in Figure 5 and 6.

TOW measurements

Time of wetness (TOW) is measured with wood moisture pins fastened on the paint surface as shown in Figure 3 a & b. Moisture pins to record the wood moisture content (MC) are mounted in the same board behind the TOW sensor, measuring the moisture content in the full length to 3 mm from the cladding board surface. The TOW pins were mounted after the priming and the first paint layer was applied to the wooden boards. The second paint layer ensured contact of the pins and the paint surface. The measured impedance signals are transformed the same way for both sensors, into wood moisture content in weight%. One hour of TOW is registered when the measurements exceed the wood MC measured in the same board, see equation (2).

$$\begin{aligned} TOW &= 1 \quad | \; MC_{TOW} = MC_{WOOD} \\ TOW &= 0 \quad | \; MC_{TOW} < MC_{WOOD} \end{aligned} \tag{2}$$

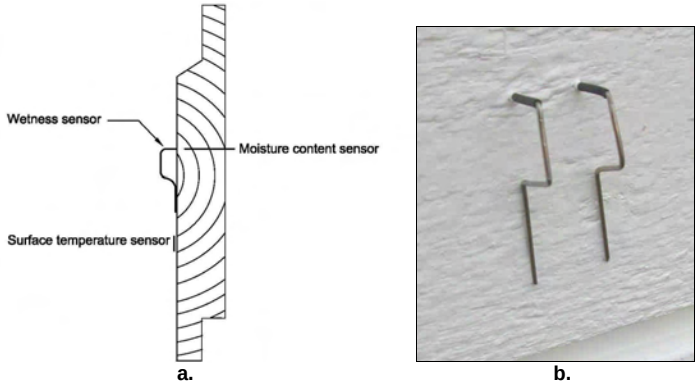

a. b.

Figure 3. a) Sketch drawing of cladding board with mounted wetness, moisture content (MC) and surface temperature sensors. b) Photo of the TOW sensor which measures the actual water film on the surface.

Figure 4 illustrates the function of the TOW sensor. One can see that the MC_{WOOD} increase when TOW is measured. There are eleven TOW sensors mounted on the test house, eight on the west facing side and three on the east facing side.

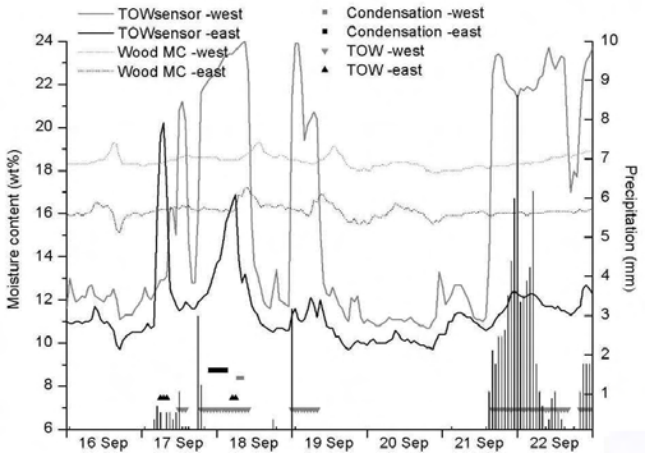

Figure 4. Results from the TOW sensor with the wood MC, condensation periods and precipitation measured September 16th to 22nd, 2004. The TOW has good correlation with the measured climate parameters. This graph presents the same sensor locations as in Figure 2.

RESULTS

The results are displayed with the summed hours of the different moisture influences during 2004. 2004 had 8784 hours in total. In 1657 of these hours, or 18.9 %, horizontal precipitation (rain and snow) was registered. Free field WDR from the west was registered in 814 hours, which amounts to 9.3 %. The number of hours with the two moisture influences on the façades, WDR and condensation, are presented in Figure 5. The measurement sensors are located where the numbers are displayed. The blue numbers give the hours with WDR. Only 14 hours of WDR were registered on the east facing wall, indicating a low liquid water influence on this façade. However, when looking at the green numbers, displaying the condensation period, one can see that condensation appears more frequent on the east facing side. The lower part of the walls also had longer condensation periods. The dispersion of WDR is also indicated in the presented WDR periods. The roof overhang protects the top WDR gauge, resulting in less hours of WDR. The corner of the test house has the highest WDR influence and the lower areas on the wall receive more WDR than the WDR gauges above.

When looking at the hours with registered TOW, as shown in Figure 6, the amount of hours exceeds the sum of the WDR measured and condensation period calculated. This might be, as indicated in equation 1, due to the drying out period following the moistening, when the wall still has a moisture film.

The build up of the cladding sections presented in this paper has 4 mm and 23 mm air gap openings, i.e. sparse versus full ventilation of the cladding backside. One can observe longer condensation periods and TOW for the cladding sections with full ventilation (23 mm).

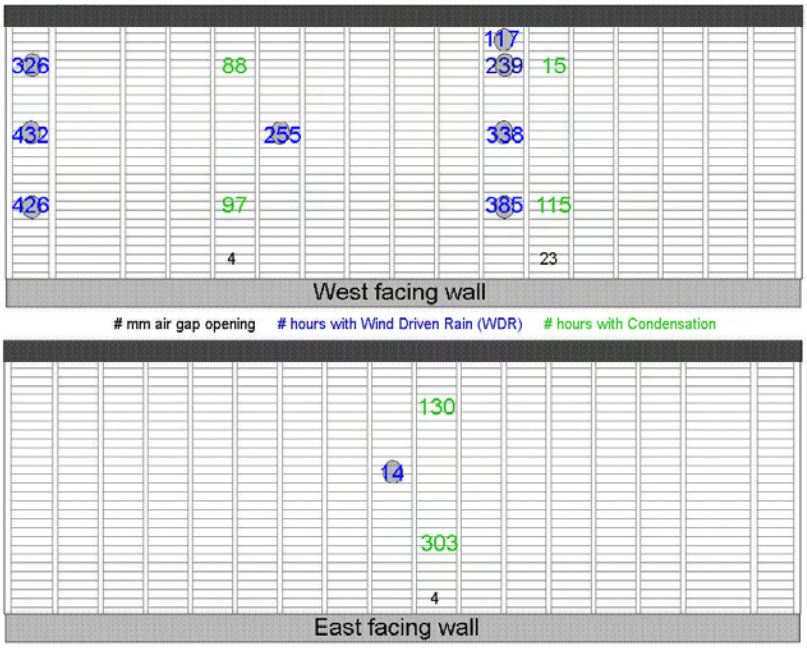

Figure 5. Accumulated hours with WDR (blue) and calculated condensation (green) on the test house, 2004.

Figure 6. Accumulated hours with TOW on the test house, 2004.

In order to show the change of the measured values, the monthly variation of 2004 is presented in Figure 7 a & b. 2004 was a wetter year than normal with annual precipitation of 956 mm compared to 885 mm/year for the reference 30-year period 1961-90. The springtime was relatively dry and the autumn was wet. Figure 7 shows the TOW period as the middle column with the WDR column to the left and the calculated condensation column to the right. Mean air temperature (Tair), Relative Humidity (RHair) and the responding wood MC are also displayed. The measurements from the middle part of the wall are used, but the calculated condensation periods are for the bottom part.
The long TOW periods on the east facing wall are mainly in the winter and autumn season. The condensation is also mostly found in these periods. One can see a correlation of the TOW periods and the corresponding wood MC.

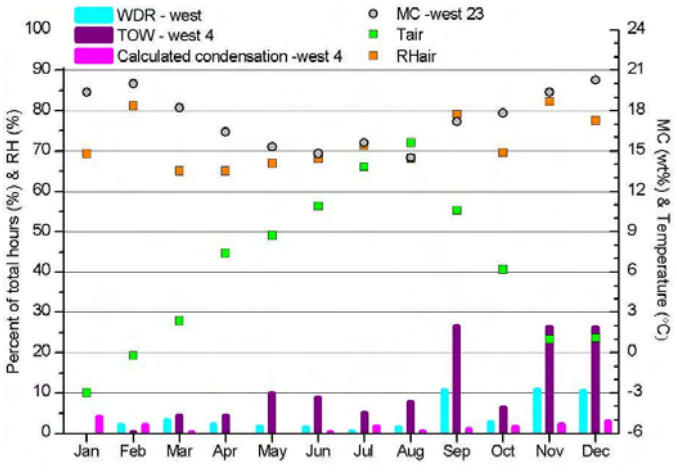

a.

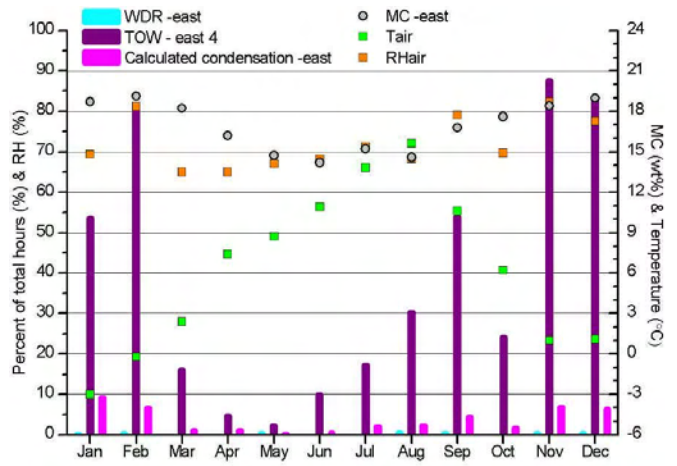

b.

Figure 7. The monthly accumulated number of hours with the moisture loads WDR, TOW and condensation at the a) west and b) east facing side. Condensation is calculated, WDR and TOW are measured. Mean air temperature (Tair), Relative Humidity (RHair) and wood moisture content are displayed with dots. Both sides have a 4 mm air gap opening.

DISCUSSION

The results display WDR, condensation and TOW periods generally in agreement with expectations. In this discussion section each parameter is evaluated, followed by concluding remarks about the validity and the possible use of the TOW parameter.

WDR is a simple parameter to measure, but the tipping bowl mechanism requires at least 0.2 mm/m^2 in order to tip, which means that there might be hours with a lower WDR amount that has not been counted, but has given the surface a water film. An error analysis of the WDR investigation at Voll is given in Nore et al. (2005b). The WDR gauge might also register condensation, i.e. if enough dew runs from the collection area into the tipping bowl. However, as mentioned earlier, the WDR periods registered correspond well with the expected values due to the building geometry and prevailing wind direction.

The inaccuracy of the temperature sensors might have a great influence on the calculated condensation periods. The different materials of the temperature sensor and the cladding might also lead to inaccurate values due to their different properties, e.g. when solar radiation is high the response of the copperplate is more rapid than the wooden cladding. RH_{air} and T_{air} are measured at 2 meters height 17 meters from the house, which might give incorrect values for the dew point temperature closer to the house. However the proportion of the calculated condensation periods seems to be correct. The longer condensation periods are expected on the lower part of the walls due to less sheltering from the roof overhang, which implies more long wave radiation loss from the bottom part of the wall. A higher temperature in the top of the wall is also expected due to the rise of warm air in the air gap that heats these areas. A higher condensation rate at the east facing wall is also expected due the lower net flux of solar radiation compared to the west facing façade. The east side is partly sheltered by a hill and another test house to the southeast of the test house. The shading effect of the house and the hill dominates during the cold season when the sun elevation is lower.

Even though the benefit of the simplicity of measuring TOW by using this methodology is evident, it represents a challenge to read the measured values correctly in order to determine whether a water film exists or not. The TOW values found on the east facing wall seem to be misinterpreted; the step from 616 to more than 3000 hours does not seem likely (see Figure 6). Most of these hours are in the winter period (as seen in Figure 7b). In laboratory testing of the TOW sensor it is found that it does not register frost crystals, which is also a reason for questioning the readings of the two top sensors on the east facing side that gives TOW mainly in the winter period. The electrical conductivity of the paint layer might rise when the temperature decreases, and for the east facing side with lower wood MC in the top of the walls this may have given disproportionate TOW readings. This effect is not found on the west facing side, where the TOW periods seem reasonable. The west facing side has longer TOW periods for the bottom part of the wall, which also receives more WDR and has longer condensation periods. Longer TOW periods are also found for the cladding design with the fully ventilated air gap (23 mm). The fully ventilated section also has longer condensation periods and therefore lower surface temperatures, due to less radiation flux from the warmer back wall, which also implies longer drying out periods. This is consistent with observations in recent years, which shows that due to better insulated walls the problem with biological growth on façades is increasing.

More reliable readings from this TOW sensor are necessary. However, the authors believe that this sensor type is better than the commercially available RH and TOW chips because it measures the actual surface wetness of the façade material.

The fact that for each sensor the hourly values are averaged 10 minute values also might lead to an error. There might have been some of the 10 minute values which show that condensation has occurred, but these condensation conditions might get lost when the values are averaged for the hour. This effect might also influence the TOW parameter.

The TOW sensor gave reliable results according to the measured WDR and condensation periods, which suggest that the TOW parameter can improve the determination of the moisture stresses on wooden cladding. When designing wooden cladding, TOW may be a more important parameter than the WDR.

However, WDR includes wind pressure that can press water into board joints of the cladding. This might be of importance in some circumstances. The consequences of WDR versus TOW must be further investigated.
Numerical calculations can be used to determine TOW, but until now sufficient methods have not existed to calculate liquid "storage" – dew, on the façade surface and thereby the responding drying out period. A calculation tool that could be validated with the TOW sensor described in this work would be a step forward in order to calculate the risk for algae growth and germination on façades.

CONCLUSION

The results indicate a reasonable connection between the wind-driven rain (WDR) periods, calculated condensation periods and time of wetness (TOW) periods. The TOW parameter can be measured and yields valuable supplemental information in addition to WDR when assessing the design moisture stresses on façades. In the future, a methodology should be developed to identify the total moisture load influence on building components.

ACKNOWLEDGEMENTS

This paper has been written within the ongoing NBI Research & Development program "Climate 2000 – Building Constructions in a More Severe Climate" (2000 – 2006), strategic institute project "Impact of climate change on the built environment". The authors gratefully acknowledge all construction industry partners and the Research Council of Norway and also the EU Northern Periphery Program, project "External Timber Cladding in Maritime Conditions".

REFRENCES

Becker, R. and Putterman, M., 2002, Patterned Mold Growth on Rendered Facades in Israel – A Consequence of Substrate Thermal Insulation, Proceedings of the 6th Symposium on Building Physics in the Nordic Countries, pp 667-674.

Blocken, B. and Carmeliet, J., 2004, A review of wind-driven rain research in building science, Journal of Wind Engineering and Industrial Aerodynamics, vol. 92, pp 1079-1130.

Haagenrud, S., Veit, J., Eriksson, B., Henriksen, J.F. and Krigsvoll, G., 2001, Wood assess project – systems and methods for assessing conservation state and environmental risk for outer wooden parts of cultural buildings- research project, No. 12. EUR 19439, ISBN 92-894-0796-4.

ISO/CD 15927, 2005, Hygrothermal performance of buildings - Climatic data - Part 3: Calculation of a driving rain index for vertical surfaces from hourly wind and rain data, ISO TC 163/SC 2/WG. Under Approval.

Nore, K., Thue, J.V., Time, B. and Rognvik, E., 2005a, Ventilated wooden claddings - A field investigation, Proceedings of the 7th Symposium on Building Physics in the Nordic Countries, pp 617-624.

Nore, K., Blocken, B., Jelle, B.P., Thue, J.V. and Carmeliet, J., 2005b, A database of wind-driven rain measurements on a low-rise test building in Norway, Building and Environment, submitted.

Zillig, W., Lenz, K., Sedlbauer, K. and Krus, M., 2003, Condensation on façades – influence of construction type and orientation, Proceedings in the 2nd International Building Physics Conference, pp 437-444.

Scheffer, T.C., 1971, A Climate Index for Estimating Potential for Decay in Wood Structures above Ground, Forest Products Journal, vol. 21, no. 10, pp 25-31.

Paper IV: Statistical analysis of wooden cladding moisture response to climate parameters

Is not included due to copyright

Paper V: Climate adapted wooden cladding design – field investigation and numerical validation

Is not included due to copyright

Paper VI: On CFD simulation of wind-induced airflow in narrow ventilated façade cavities: coupled and decoupled simulations and modelling limitations

Accepted for publication in *Building and Environment*, February 15, 2010

On CFD simulation of wind-induced airflow in narrow ventilated facade cavities: coupled and decoupled simulations and modelling limitations

K. Nore [a,b], B. Blocken [c] *, J.V. Thue [a]

(a) Department of Civil and Transport Engineering, Norwegian University of Science and Technology (NTNU), Høgskoleringen 7A, 7491 Trondheim, Norway
(b) SINTEF Building and Infrastructure, 7465 Trondheim, Norway
(c) Building Physics and Systems, Eindhoven University of Technology, P.O. box 513, 5600 MB Eindhoven, The Netherlands

Abstract

Heat and mass transfer modelling in building facades with ventilated cavities requires information on the cavity air change rates, which can be a complex function of the building geometry and meteorological conditions. This paper applies Reynolds-averaged Navier-Stokes (RANS) CFD to study wind-induced airflow in the narrow (23 mm) ventilated facade cavities of a low-rise building by coupled and decoupled simulations. In the coupled simulations, the wind-flow pattern around the building and the resulting air flow in the cavities are calculated simultaneously and within the same computational domain. In the decoupled simulations, two separate CFD simulations are conducted: a simulation of the wind flow around the building (with closed cavities) to determine the surface pressures at the cavity inlet and outlet openings, and a simulation of the cavity airflow, driven by these surface pressures. CFD validation is performed for the external and internal (cavity) flows. It shows that while both laminar and turbulent cavity airflow can be accurately reproduced with low-Reynolds number modelling, this method fails in the transitional regime. The valid CFD results (outside the transitional regime) are analysed in terms of cavity air flow patterns and air change rates per hour (ACH) for different cavity positions, wind speeds and wind directions. The CFD results of cavity air speed and ACH compare favourably with values from previous experimental studies. The coupled and decoupled simulation results provide an indication of the local losses. Future work should focus on adapting RANS CFD low-Re-number models to accurately model cavity flow in the transitional regime.

Keywords: Cavity ventilation; Building envelope; Computational Fluid Dynamics; Numerical simulation; Pressure loss

Nomenclature

C	local loss coefficient
C_p	pressure coefficient
C_S	roughness constant
C_μ	variable in realizable k-ε model
d	cavity depth (m)
D_h	hydraulic diameter (m)
f	friction factor
k	turbulent kinetic energy (m²/s²)
$k_{non\text{-}c}$	correction factor for non-circular cross-sections
k_S	equivalent sand-grain roughness height (m)
L, W, H	length, width, height (m)
n	air change rate (1/h)
P	pressure (Pa)
Re	cavity Reynolds number
Re_z	wall-distance based Reynolds number
u*	friction velocity (m/s)
u^*_{ABL}	friction velocity associated with the inlet profiles of U, k and ε (m/s)
U	streamwise component of the mean wind-velocity vector (m/s)
U_H	wind speed in upstream undisturbed flow at building height (m/s)

* Corresponding author: Bert Blocken, Building Physics and Systems, Eindhoven University of Technology, P.O.Box 513, 5600 MB Eindhoven, the Netherlands. Tel.: +31 (0)40 247 2138, Fax +31 (0)40 243 8595
E-mail address: b.j.e.blocken@tue.nl

U_{10}	reference wind speed at 10 m height in the upstream undisturbed flow (m/s)
W	vertical component of the mean wind-velocity vector (m/s)
x	coordinate along building facade (m)
z	height (m)
z_P	distance between the centre point P of the wall-adjacent cell and the wall (m)
z_0	aerodynamic roughness length (m)
z^+	dimensionless wall unit
z*	dimensionless wall unit

Greek symbols

Δ	difference
ε	turbulence dissipation rate (m^2/s^3)
θ	angle between the reference wind direction and the normal to the facade (°)
κ	von Karman constant (≈ 0.42)
ν	kinematic viscosity (m^2/s)
ρ	air density (kg/m^3)

Abbreviations

ABL	Atmospheric Boundary Layer
ACH	Air change rate per hour
CFD	Computational Fluid Dynamics
RANS	Reynolds-averaged Navier-Stokes
SIMPLE	Semi-Implicit Method for Pressure Linked Equations

Subscripts

avg	averaged
D	computational domain
P	centre point of the wall-adjacent cell

1. Introduction

Analysis of the hygrothermal behaviour of ventilated cavity walls requires information on the cavity air change rates as a function of the influencing parameters. Cavity ventilation can be driven by wind (forced convection) or by local density differences due to buoyancy (natural convection). The resulting pressure differences can drive airflow through the cavity when they can overcome the local losses and the friction losses in the cavity. The local losses consist of the entrance and exit losses. Wind pressure on a windward building facade generally increases from bottom to top, and will cause a downward cavity flow. Buoyancy on the other hand will generally cause an upward flow. The resulting flow direction and cavity ventilation rate will depend on the interaction between both driving forces.

In general, the cavity air change rate per hour (ACH) depends on a wide range of parameters including building geometry, environment topography, position and size of the cavity openings in the facade, cavity dimensions, cavity wall roughness, permeability of the cladding, wind speed, wind direction, temperature and cavity Reynolds number. Numerical heat-air-moisture (HAM) transfer models for building facades with ventilated cavities require detailed information on cavity air flow to calculate the transfer of heat and moisture to and from the inside cavity wall surfaces [1-4]. This type of information can be obtained from full-scale measurements [5-12], theoretical models [10-11,13] or numerical simulations with Computational Fluid Dynamics (CFD) [1,3,11]. While much work has been done on natural and forced ventilation of buildings (indoor) and of wide ventilated cavities (e.g., double-skin facades), much less effort has been devoted to the ventilation of narrow facade cavities such as those found in a rainscreen-type wall. Most previous work on ventilation for this type of walls has been experimental and theoretical, and CFD studies are very scarce. A literature review of cavity wall ventilation studies, up to 2004, has been provided by Straube et al. [10].

In the past, a number of full-scale measurements of cavity air speed and/or ACH and of the corresponding exterior wind speed, wind direction and surface pressures and exterior-interior temperature differences have been performed both on site, for real buildings [5-10], and in laboratory conditions, on wall specimens [10-12]. They have indicated the importance of both wind and buoyancy as driving forces for cavity ventilation and they have also provided information on the ACH and cavity air speeds for those specific building and cavity geometries. However, both on-site measurements and laboratory tests have a number of important disadvantages. The interpretation of on-site measurement results is complicated by the uncontrolled meteorological conditions during the measurements and the possibility of combined occurrence of wind and

buoyancy, which can counteract each other. This makes it hard to analyse the influence of each individual parameter and to draw general conclusions. Laboratory measurements allow a much larger control of the influencing parameters, but the inlet and outlet conditions for the cavity flow are generally strongly simplified, and the complexity of the wind-flow pattern around the building is not taken into account.

Cavity airflow rates can also be assessed by theoretical equations such as the Darcy-Weisbach equation that relates pressure differences to airflow rates, and in which a distinction is made between friction losses and local losses, such as entrance and exit losses [14,15]. For wind-induced ventilation, the wind pressures at the positions of the cavity openings are needed as input to this equation. They are either measured on site or in reduced-scale wind tunnel experiments, or extracted from existing databases or analytical equations (for a review on pressure coefficient data in building simulation, see [16]). There are two main problems associated with this approach. First, detailed pressure coefficient (C_p) data in databases are often only available for buildings with a simplified geometry that can be very different from the actual building under study. Second, the entrance and exit losses are generally not known. Although hydraulic resistance data sets [e.g., 14,15]. provide standard values for simplified inlet and outlet geometries, they often do not provide values for the actual inlet and outlet geometries of building wall cavities. They generally also do not provide information on the variation of the local losses with wind direction.

Apart from measurements and theoretical equations, cavity ventilation can also be studied by CFD. Up to now, only a few efforts have been made in this direction [1,3,11]. CFD simulations can be performed in a coupled or a decoupled way. In the coupled simulations, the atmospheric boundary layer wind-flow pattern around the building and the resulting air flow in the cavities are calculated simultaneously and within the same computational domain. In the decoupled simulations, two separate CFD simulations are made: a simulation of the outdoor wind flow around the building (with closed cavities) to determine the surface pressures at the position of the cavity inlet and outlet openings, and a simulation of the cavity air flow, driven by these surface pressures. Pinon et al. [11] performed isothermal CFD simulations of the air flow in different types of cavities and with different inlet conditions. The simulations were made in a decoupled way, i.e. excluding simulation of the wind flow around the building. Stovall and Karagiozis [1] conducted thermal CFD simulations in different cavities and with different wind speed and temperature differences. To some extent, these simulations were coupled with the outdoor wind flow, however only a relatively small outdoor air volume (L x W x H = 0.5 x 0.36 x 2.43 m³) was considered, and the specific features of wind flow around the building were not included. Gnoth et al. [3] have recently extended a HAM model with CFD to analyse "cavity fluid dynamics (CaFD)", allowing simulation of laminar convective heat and moisture transfer in cavities. Also in these simulations, the outdoor wind flow was not considered.

At present, there are a number of open issues concerning cavity ventilation in general and CFD simulations of cavity ventilation in particular. There is very little information about cavity ACH and air flow patterns. Up to now, to the knowledge of the authors, fully coupled CFD simulations of the atmospheric boundary layer wind-flow pattern around buildings and the resulting air flow in the cavities have not yet been performed. This type of studies is required for detailed and systematic investigations of cavity ACH and air flow patterns as a function of influencing parameters. There is also very little information on local losses for facade cavities. An investigation of the local losses in cavities requires the combination of both coupled and decoupled simulations. However, first and foremost, the accuracy and reliability of CFD for cavity ventilation studies should be investigated. As such studies can encompass laminar, transitional and turbulent cavity flow, it should be examined to what extent RANS CFD can accurately reproduce these flow regimes.

This paper presents a CFD investigation of wind-induced air flow in the narrow (23 mm) ventilated facade cavities of an isolated low-rise building, based on coupled and decoupled simulations. CFD validation is performed for the building surface pressures and for the interior cavity flow. The results of the study are presented in terms of cavity air flow patterns and cavity ACH for different cavity positions, wind speed and wind directions. The coupled and decoupled simulations are compared to provide an indication of the local losses. Based on the validation studies, some CFD modelling limitations for this type of studies can be identified**.**

The paper consists of 9 sections. In section 2, the geometry of the low-rise building model is described. Section 3 contains some considerations for coupled outdoor wind flow and cavity airflow simulations. Section 4 presents the validation studies. In section 5, the coupled and decoupled simulations are outlined. Section 6 presents the simulation results. In section 7, the CFD results are compared with results from previous experimental studies. Sections 8 (discussion) and 9 (summary and conclusions) conclude the paper.

2. Building model

The geometry of the building model is for a large part based on that of the low-rise rectangular test building of SINTEF Building and Infrastructure and the Norwegian University of Science and Technology

(NTNU) in Voll, Trondheim, Norway. It has dimensions L x W x H = 11.3 x 4.8 x 4.3 m³ and a roof overhang with a length of 0.34 m and a height of 0.3 m (Fig. 1). The long front and back facades each consist of 17 ventilated cavities. Each cavity has a height of 3.495 m and a horizontal linear inlet and outlet slot over the entire width of the cavity (Fig. 1). The cavities are separated from each other by vertical wooden battens, some of which have different cross-sectional dimensions. A wooden cladding of 19 mm thickness separates the cavities from the outdoor environment. In this study, the cavity depth is 23 mm and the cladding itself is assumed airtight. The building is considered to be isolated (no surrounding buildings, trees, etc.) and positioned on flat, uniformly rough terrain covered with short grass (aerodynamic roughness length $z_0 = 0.03$ m [17]). Fig. 1c is a detailed view of the vertical cross-section of the top and bottom of the cavity. The bottom cavity opening is 400 mm above ground level, and the top opening is 35 mm below the roof overhang. The vertical batten also starts at 400 mm below ground level, but extends all the way up to the roof overhang. This configuration represents the computational geometry for the "fully coupled" approach (configuration A). For the decoupled approach, this configuration is decomposed into two separate configurations: configuration B, in which the cavity is closed, and configuration C, which only represents the cavity (Fig. 2).

3. Considerations for coupled outdoor wind flow and cavity airflow simulations

For the specific geometry of the cavity openings of the building (opening just below roof overhang and opening adjacent to wall at a certain distance from the ground surface), no standard values for local loss coefficients could be found in hydraulic resistance data sets [e.g. 14,15]. This motivates the coupled CFD approach.

The flow around the building is fully turbulent, apart from the small viscosity-affected regions in the boundary layer near the building surfaces and ground surfaces in the domain. The flow in the cavities however can be laminar, transitional or turbulent, depending on the cavity Reynolds number and on wall roughness and entrance effects. The coupled simulations need to consider the possibility of these different flow regimes occurring within the same computational domain.

The commonly used approach in wind engineering for building aerodynamics is based on the Reynolds-averaged Navier-Stokes (RANS) equations [18,19]. The turbulence models used in this approach, such as the k-ε models and the Reynolds Stress model, are generally high-Reynolds number models that are only valid in the turbulent region of the flow. For the boundary layer region, which contains the inner layer including the thin viscous sublayer, the buffer layer and the logarithmic layer, modelling adjustments need to be made. The two main options are low-Reynolds number modelling and wall-function modelling. Low-Re number modelling refers to resolving the whole boundary layer by placing cells in each part of it. Wall functions are semi-empirical formulae that bridge the region between the wall and the logarithmic layer, and that provide an approximation of the effect of the wall on the mean wind speed and turbulence quantities in the logarithmic layer. Low-Reynolds number modelling requires much finer grids than wall-function modelling. The near-wall grid resolution can be expressed by the z* value: $z^* = u^* z_p/\nu$ [20,21], where u^* ($= C_\mu^{1/4} k_p^{1/2}$) is the friction velocity, z_P is the distance from the centre point P of the wall-adjacent cell to the wall, and ν is the kinematic viscosity. The friction velocity is based on the turbulent kinetic energy k_P in the point P and on C_μ. Note that in many commercial CFD codes, z* is used instead of the traditional wall unit z^+, because of reasons explained in [20,22]. Appropriate grids for low-Re number modelling have a z* value below 4 or 5 to ensure that the point P is situated in the viscous sublayer. Preferably, z* = 1 to have at least a few cells inside the viscous sublayer [18,20,21]. Wall-function grids should have a z* above 20-30 and below 300-500 to ensure that P is situated in the logarithmic layer [18,20,21].

Modelling the wind flow around buildings is typically performed by combining a high-Re number model with wall functions [18,19]. Modelling the flow in the narrow facade cavities however requires low-Re number modelling. In the commercial CFD code Fluent 6.3.26 used in this study [21], low-Re number modelling refers to a two-layer zonal approach, that divides the computational domain into two regions: the viscosity-affected region and the fully-turbulent region. The demarcation between both regions is determined by the wall-distance based turbulent Reynolds number, $Re_z = zk^{1/2}/\nu$, where z is the normal distance from the wall at the cell centres and k is the turbulent kinetic energy. Where $Re_z > 200$, the high-Re number model is used. Where $Re_z < 200$, the one-equation Wolfhstein model [23] is employed.

For the coupled simulations in this study, the combination of the high-Re number realizable k-ε model [24] with the so-called "enhanced wall treatment" [21] will be employed. Enhanced wall treatment refers to the approach in which the two-layer zonal model is combined with enhanced wall functions. This approach is identical to the two-layer zonal approach when the grid is fine enough (typically z* = 1), and provides improved accuracy for those regions where the grid is not fine enough. The aim in generating the grid for the coupled simulation is to have z* < 1 in the cavity and near the cavity entrance and exit. For the remainder of the walls in the computational domain, such as the exterior building surfaces, along which higher wind

velocities are present, keeping $z^* < 1$ would lead to an unnecessary and excessively fine grid with cell sizes down to a few hundred micrometers [25].

4. CFD validation

Different options could be pursued for CFD validation. The most straightforward option would be to use experimental data of wind speed around the building, surface pressures on the facade, and cavity air speed and ACH for the building under study. However, because of several practical reasons, this was not an option. The most important are (1) the fact that the geometry of the cavities is variable in time (as new test walls with different cavity geometries are regularly installed) and (2) the fact that even at a given moment in time, the cavities have different geometries. Therefore, the building in the present study is a simplified version of the real building, in which all cavities have the same depth and height and the same type of inlet and outlet openings. This limits the number of variables involved and allows an analysis of the ACH as a function of cavity position in the facade, without the results being obscured by additional geometrical parameters.

Instead, it was chosen to perform generic sub-configuration validation [18,26]. This method implies decomposition of the actual problem or configuration into simpler, generic problems or configurations, which contain at least part of the features of the flow in the actual configuration. Validation is then performed for the generic sub-configurations, for which often high-quality experimental data are available in the literature. If the numerical model performs well for these configurations, it can reasonably be assumed that it will also provide reliable predictions for the more complex building configuration. An advantage of the sub-configuration validation is that it allows a step-by-step analysis of the performance of CFD, which will allow to clearly identify modelling limitations.

The sub-configuration validation consists of three parts: (1) wind velocity pattern around a cubic building; (2) wind pressure distributions on the surfaces of a cubic building; and (3) laminar, transitional and turbulent flow in a channel. Focusing on the cubic building is justified because the flow around this basic type of bluff body contains the salient features of the flow that will also occur around the building model in Fig. 1. Because the first part of the validation study has been reported in detail in an earlier paper [25], in which a good qualitative and quantitative agreement was found, it is not repeated here, and only the two other parts are described below.

4.1. Mean surface pressures

Wind tunnel measurements of pressure distributions on the surfaces of a cubic (0.15 m) building model were reported by Richards et al. [27]. The tests were conducted in the University of Auckland boundary layer wind tunnel, at a scale of 1:40 and for different wind directions. The maximum blockage ratio is 1.6 %. The boundary layer up to two building heights was well matched by a log law with $z_0 = 0.42$ mm (= 16.8 mm in full scale). Mean wind speed at cube height, U_H, was 6.4 m/s, yielding a building Reynolds number of about 65,000, which is well above the limit 11,000 for Reynolds number independent flow [28]. The undisturbed vertical profiles of mean wind speed and turbulence were measured in the empty wind tunnel (with roughness elements but without building present). The exact measurement location at the turntable however is not known. Ideally, this location should be that at which the building will be positioned. Recent research has shown that reference measurements further upstream can to some extent lack representativeness due to the development of an internal boundary layer over the smooth surface of wind tunnel turntable [29]. The pressure measurements were made along the intersection of the cube with the vertical centre plane and with a horizontal plane at half the cube height ($z = H/2$), among other positions. More information on the experiments can be found in Richards et al. [27].

3D steady RANS simulations are performed at model scale. The computational domain has dimensions L_D x W_D x H_D = 21H x 21H x 10H. The building model is placed at 5H from the inlet, yielding a downstream distance of 15H. A structured grid is used with grid resolution determined by grid-sensitivity analysis on three different grids with a refinement factor $\sqrt{2}$. The resulting grid has 207,980 cells (Fig. 3). 24 cells are used along the building edges. Both for the building walls and the bottom of the domain, the distance z_P is 0.005H, yielding z^* values in the range 30-90, apart from the intersection of the building surfaces with the bottom of the domain, where z^* is lower than 30. Fluent 6.3.26 is used to solve the 3D RANS equations and the realizable k-ε model equations [24]. Pressure-velocity coupling is taken care of by the SIMPLE algorithm. Standard pressure interpolation is used. Second order discretization schemes are used for both the convection terms and the viscous terms of the governing equations.

Simulations are made for two wind directions: $\theta = 0°$ (wind direction perpendicular to the surface) and 45° (Fig. 3). The vertical boundary planes of the domain have different types of boundary conditions depending on the wind direction (Fig. 3). In the case of $\theta = 0°$, plane 1 is the inlet plane, plane 3 the outlet plane and

planes 2 and 4 are the side planes. For $\theta = 45°$, planes 1 and 2 are the inlet planes and planes 3 and 4 are the outlet planes. The side planes (for $\theta = 0°$) and the top of the computational domain are modelled as slip walls (zero normal velocity and zero normal gradients of all variables). At the outlet(s), zero static pressure is specified. At the inlet plane(s), the vertical profiles of mean wind speed, turbulent kinetic energy k and turbulence dissipation rate ε are imposed. The vertical inlet profile of mean wind speed is equal to the measured one [27]. The turbulent kinetic energy profile was obtained from the measured turbulence intensities, and turbulence dissipation rate $\varepsilon = (u^*_{ABL})^3/\kappa(z+z_0)$ with $u^*_{ABL} = 0.46$ m/s. For the ground boundary condition, the standard wall functions by Launder and Spalding [30] with roughness modifications by Cebeci and Bradshaw [31] are used. The values of the equivalent sand-grain roughness height k_S and roughness constant C_S needed in these wall functions are obtained based on the aerodynamic roughness length z_0 (= 0.42 mm) by the function derived by Blocken et al. [32] for Fluent 6 (up to at least version 6.3):

$$k_S = \frac{9.793\, z_0}{C_S} \tag{1}$$

The values used are $k_S = 0.0008$ m and $C_S = 5$. Note that for fully aerodynamically rough walls, only the value of the product $C_S k_S$, and not the values of the individual parameters, determine the wall function values [21,32].

Fig. 4 displays measured and simulated pressure coefficients C_p, for $\theta = 0°$ and 45°, along the intersections of the cube surfaces with a vertical centre plane and the horizontal plane at $z = H/2$. The pressure coefficients are calculated with reference wind speed $U_H = 6.4$ m/s. Figs. 4a and c each show two sets of measurement data. The difference between both sets is caused by the effect of the pressure tappings in one roof corner (quarter of the roof), see [27]. Richards et al. [27] also mention that the model was slightly misaligned in the wind tunnel, causing some asymmetry in the results, as shown in Figs. 4b and d. Comparing the CFD results with the wind tunnel data shows that:

(1) Fig. 4a: C_p at the upper part of the windward facade is predicted very well, while at the lower part, underestimations go up to a maximum of 25%. On the roof, the absolute value near the upwind edge is overestimated (15%), but larger errors (underestimations) are found for the rest of the roof (up to 100%). Values at the leeward facade are about half those of the measurements.
(2) Fig. 4b: The agreement between simulated and measured C_p at the windward facade is very good. Large underestimations however are found at the side and leeward faces (up to 100%).
(3) Fig. 4c: Again, the agreement at the windward facade is very good. On the roof, a 40% underestimation is present at the upwind edge, but a significantly better agreement is found for the rest of the roof. A quite good agreement is also seen at the leeward facades (max. deviation is 20%).
(4) Fig. 4d: A good overall agreement is observed at both windward and leeward facades. The deviation along line "01" is partly due to misalignment of the model. Deviations at the leeward facades are lower than 25%.

The deviations at the roof, the side facades and the leeward facade are for a large part attributed to the fact that steady RANS is not capable of modelling the inherently transient nature of separation, recirculation and of vortex shedding in the wake. Therefore, calculation results in these regions are generally deficient [33,34]. However, both the validation study in [25] and the validation study in this paper show that steady RANS with the realizable k-ε model seems to provide quite accurate results for the windward facade. Note that the focus will be on the windward facade and on wind directions 0° and 22.5°only. Results for e.g. $\theta = 67.5°$ and 90°, when this facade is (partly) in the region of separated flow, are not considered reliable.

4.2. Laminar, transitional and turbulent channel flow

A distinction is made between developing and fully-developed channel flow. For fully-developed flow, detailed experimental data are reported in the literature, often in terms of friction coefficients as a function of channel Reynolds number and wall roughness. For developing flow however, unambiguous quantitative information about entrance lengths for laminar and turbulent flow is not available; different sources provide either very different entrance length equations, or provide very wide ranges of possible entrance lengths [14,15,35-37]. The reason for this can be the sensitivity of the entrance length to the inlet conditions (inlet geometry, flow profile, turbulence intensity), wall roughness, etc. For this reason, the validation study here only focuses on fully-developed channel flow.

The pressure loss in fully-developed channel flow (i.e. due to friction) is given by the Darcy-Weisbach equation [14,15]:

$$\Delta P_F = f \frac{L}{D_h} \left(\frac{\rho W_{avg}^2}{2} \right) \quad (2)$$

where f is the Darcy-Weisbach friction factor, L is the length of the channel, D_h is its hydraulic diameter, ρ is the fluid density and W_{avg} is the average fluid speed in the cross-section. For fully-developed laminar flow in a pipe with circular cross-section, f is equal to 64/Re. For fully-developed turbulent flow, the friction loss depends not only on the Reynolds number, but also on the roughness of the pipe. For smooth walls and for Reynolds numbers below 10^5, the turbulent friction factor is well described by the Blasius equation for smooth pipes with circular cross-section: $f = 0.3164/Re^{0.25}$ [14,35]. This equation is a curve fit to experimental smooth-wall data collected in 1913.

For a channel of non-circular cross-section, generally, Eq. (2) is used with the appropriate hydraulic diameter D_h. This, however, is only allowed when the thickness of the boundary layer is very small over the entire or almost the entire perimeter of the cross-section compared with the dimensions of the cross-section [14]. Idelchik [14] provides correction factors k_{non-c} for the friction factor f for non-circular channels. For laminar flow in a plane slot, $k_{non-c} = 1.5$, yielding $f = 96/Re$. For turbulent flow in a plane slot, $k_{non-c} = 1.1$, yielding $f = 0.3480/ Re^{0.25}$.

The validation study focuses on the reproduction of the friction losses for fully-developed laminar, transitional and turbulent flow in a smooth pipe with circular cross-section and in a plane slot. The pipe has a diameter of 0.046 m, and the plane slot has a depth of 0.023 m, corresponding to a hydraulic diameter of 0.046 m. The CFD simulations are performed with the RANS equations, the realizable k-ε model and enhanced wall treatment, i.e. the same combination that will be used for the actual coupled and decoupled simulations in the next section. The simulations are conducted in 2D, because of axial symmetry (for the pipe) and the 2D character of the plane slot (infinite width). The grids are based on grid-sensitivity analysis. Simulations are made for Re ranging from 100 to 10^5. The results for the friction coefficient f are presented in a double-logarithmic graph in Fig. 5a, and also in a semi-logarithmic graph in Fig. 5b to allow a better quantitative assessment of the deviations. The following observations are made:

(1) The simulations correctly predict the friction factor differences (correction factors 1.5 and 1.1) between pipe flow and plane slot flow for low Re (< 500) and high Re (> 10000);
(2) A close agreement is found between CFD simulations and theoretical/empirical expressions for the friction factors for low Re (< 500) and high Re (> 10000);
(3) Large deviations however occur in the intermediate Re numbers, which are larger than 25% for Re = 1000-3500, indicating an important modelling discrepancy here. For this reason, in the next section, only results for which the cavity Re numbers are outside this range will be reported.

5. CFD application

CFD simulations are performed for the coupled case (case A) and the decoupled cases (case B and C), see Fig. 2.

5.1. Coupled simulations

5.1.1. Geometry and computational grid

Due to the relatively complex geometry of the building with cavities, battens and roof overhang, and the large difference between the smallest (0.023 m) and the largest (about 100 m) length scales in the domain, generating a computational grid with good quality for the coupled simulation is not straightforward. The quality of the grid in the immediate vicinity of the building and in the cavities is considered very important for the coupled simulation. Standard automatic or semi-automatic generation of an unstructured grid allows insufficient control of local grid resolution, grid stretching, control volume skewness and aspect ratio. To allow full control over the grid quality and resolution, the grid is constructed using the grid generation procedure presented by van Hooff and Blocken [38]. This procedure allows to efficiently and simultaneously generate the geometry and the computational grid. It consists of a series of extrusion operations, i.e. creating the geometry and the grid based on geometrical translation operations of pre-meshed 2D cross-sections. In this case, the ground plane of the computational domain is constructed and meshed first, after which it is extruded vertically to generate the 3D geometry and grid. For more details, the reader is referred to ref. [38]. This procedure allows modelling complex geometries with full control over grid quality and grid resolution. This is considered very important here, because the grid resolution near the cavity openings and inside the cavities should be adjusted for low-Reynolds number modelling, as explained in section 3.

The resulting computational domain has dimensions L_D x W_D x H_D = 110 x 110 x 50 m³. The building is situated in the corner of the domain, at 5H from both inlet planes (Fig. 6a). Fig. 6b shows the model geometry, including the roof overhang, the individual cavities and the vertical battens separating the cavities. The grid that has been constructed is a hybrid grid, which is fully structured (hexahedral cells) in the cavities and in the immediate vicinity of the building model, and unstructured (prismatic cells) at a larger distance from the building. The grid resolution was determined based on grid-sensitivity analysis, yielding about 2.6×10^6 cells with 20 cells across the depth and a minimum of 8 cells along the width of each cavity. In all cavities and for all simulations that will be reported, z* was lower than 1. Fig. 6c displays the grid on the surfaces of the building, and Fig. 6d is a detail of the surface grid near the top frontal corner, in which the top cavity openings and the battens can be seen.

5.1.2. Solution characteristics and settings

The 3D RANS equations and the equations of the realizable k-ε model are solved. Pressure-velocity coupling is taken care of by the SIMPLE algorithm. Pressure interpolation is standard. Second order discretization schemes are used for both the convection terms and the viscous terms of the governing equations. The inlet profiles for mean wind speed, turbulent kinetic energy and turbulence dissipation rate are those by Richards and Hoxey [39], corresponding to z_0 = 0.03 m. Simulations are performed for different reference wind speed U_{10} and wind directions. The boundary condition settings for outlet, sides and top of the domain are identical to those in section 4.1. For the walls, enhanced wall treatment is applied. It is important to note that "enhanced wall treatment" in Fluent 6.3 implies that all walls are considered smooth (roughness height k_S = 0 m), also those where the enhanced wall functions are used. The bottom of the computational domain therefore also has zero roughness height, instead of the proper value given by Eq. (1). As a result, there is an inconsistency between the roughness of the inlet profiles (z_0 = 0.03 m) and the ground roughness in the computational domain, which will lead to a non-horizontally homogeneous atmospheric boundary layer in the simulations [32,40]. This means that streamwise gradients will occur in the vertical inlet profiles of mean wind speed and turbulence quantities. The incident profiles (at the location where the building would be positioned) are therefore different from the inlet profiles. The occurrence of these gradients was tested by a simulation in an empty 2D domain (Fig. 7). They are pronounced for each of the three variables. This does not compromise the value of the simulations, but it should be considered that the results are representative of the incident profiles of the simulation, rather than the inlet profiles.

5.2. Decoupled simulations

The decoupled simulations consist of two parts: (1) simulations for the building with closed cavities (case B) and (2) simulations for the cavities (case C) (Fig. 2). The grids are constructed in the same way as explained in section 5.1.1. All solution characteristics and settings are the same as for case A. For case C, two sets of simulations are performed: C1 and C2. In case C1, the pressures at the inlet and outlet openings of the closed cavities (case B) are used as boundary conditions for the simulations in the geometry of case C, leading to a developing flow in the cavity, downstream of the inlet. In case C2, fully-developed velocity profiles are used as inlet boundary conditions for the geometry of case C. Therefore, in case C1, both the friction losses and part of the local losses are included. Case C2 on the other hand only includes friction losses. The results are presented in the next section.

6. CFD results

6.1. Coupled simulations

Fig. 8 provides an overall view of the flow inside the cavities for θ = 0° by illustrating streamlines. The overall flow in the cavities is from top to bottom. A clear flow separation and recirculation occur at the top inlet of the four cavities that are situated closest to the edges. This is attributed to the fact that the velocity vector near this opening has a relatively strong lateral component, i.e. parallel to the windward facade.

Vertical profiles of the ratio W/U_{10} at the top and bottom of each cavity, for U_{10} = 10 m/s and θ = 0° and 22.5° are shown in Fig. 9. Results for more oblique wind directions are not shown because for these directions, the cavity Reynolds numbers dropped into the transitional regime. Fig. 9a (and Fig. 1c) show the positions of the two lines along which the profiles are taken. They are located at the top and bottom cavity opening and in the middle of the cavity depth. Negative velocity ratios indicate downflow. Fig. 9b shows that for θ = 0°, both the largest velocities and the largest velocity gradients are found at the edge cavities, in which a highly non-uniform flow occurs. In these edge cavities, a diagonal flow takes place, as indicated by the shift

of the velocity peaks from one cavity edge to the other as the flow moves from top to bottom. At the top opening of these cavities, a small region with upflow occurs. The flow is most uniform in the cavities in the middle of the facade, where the stagnation point at the facade occurs and where the lateral velocities (in x direction) are smallest. Fig. 9c shows that for $\theta = 22.5°$, apart from the edge cavities, also most cavities in the middle region demonstrate non-uniform and diagonal flow. Flow non-uniformity appears least pronounced between x = 1 and 2 m (cavity nr. 5), which approximately corresponds to the shifted stagnation point.

Fig. 10 shows profiles of the ratio W/U_{10} across the depth of the middle cavity (nr. 19) for $\theta = 0°$, and for U_{10} = 2 and 10 m/s. For these values of U_{10}, the cavity Re numbers, based on the average cavity speed, are all below 1000 or above 3500. The values in Fig. 10 are taken in the middle of cavity nr. 19. At the entrance (point A), the profile is skewed towards the inner cavity surface. Travelling downwards, the profile reaches an approximate equilibrium shape (point D), which is maintained until at least point F. At the outlet, the profile is slightly skewed towards the outer cavity surface. The results show a near-parabolic profile (between points D and F) characteristic of laminar flow for U_{10} = 2 m/s and a more uniform (flattened) profile typical for turbulent flow for U_{10} = 10 m/s (also between D and F).

Fig. 11a displays the ratio of the air change rate per hour (ACH) n (1/h) and U_{10}, for U_{10} = 2 and 10 m/s. The decrease of this ratio with decreasing U_{10} is a direct result of the change in cavity flow regime from turbulent to laminar, as shown by the corresponding Re numbers in Fig. 11b. Fig. 11c shows the ratio n/U_{10} for U_{10} = 10 m/s and for $\theta = 0°$ and 22.5°. Fig. 11d shows the corresponding Re numbers. As the wind direction becomes more oblique to the facade, the ratio n/U_{10} shows a general decrease. However, for the cavity at the upwind edge, the value for 22.5° is larger than that for 0°. Similar observations of maxima occurring for slightly oblique instead of perpendicular angles were made in the past concerning pedestrian-level wind conditions around buildings [29,41] and wind-driven rain deposition on building facades [42,43]. These observations could be attributed to changes in the upstream wind-flow pattern, i.e. the so-called wind-blocking effect [29,44,45], due to the changed stagnation region.

6.2. Decoupled simulations

The wind-flow simulations for case B yield the static pressures P at the position of the inlet and outlet openings. These values can be converted to pressure coefficients by $C_p = (P-P_0)/0.5\rho U_{10}^2$, where P_0 is the reference pressure and ρ the air density (1.225 kg/m³). Fig. 12a displays C_p for the top (highest value) and bottom (lowest value) of every cavity, and for the two wind directions. The C_p distribution at the top is quite uniform along the length for $\theta = 0°$, while for $\theta = 22.5°$, C_p shows a pronounced maximum for the cavity at the upwind edge.

The pressures from case B are used to calculate cavity flow rates for case C1. The decoupled simulations for case B+C1 provide significant overestimations of the ACH compared to the coupled simulations of case A (Fig. 12b). The overestimations range from 26% to 40% for $\theta = 0°$ and from 34 to 57% for $\theta = 22.5°$. They are caused by the important simplifications associated with decoupled simulations. In these simulations, the only information transferred from case B to case C1 are the pressure coefficients. The simulations in case C1 do not take into account the actual local direction of the wind velocity vectors near and in the openings and the occasional flow separation and recirculation in the cavities. Instead, only vertical cavity air flow is considered along the entire cavity. As a result, case B+C1 only partly reproduces the local losses that are simulated in case A.

6.3. Local pressure losses

As mentioned in the introduction, one of the open issues in cavity ventilation is that there is very little information on local losses for facade cavities. Hydraulic resistance data sets often do not cover the geometrical complexity of actual inlet and outlet openings of building wall cavities. In particular, for the present building, loss coefficients could not be found in such data sets. The combination of coupled and decoupled (case C2) simulations allows obtaining an estimate of the local pressure losses for the cavity flow. Note that case C2 only includes the friction losses, and not the local losses. The Darcy-Weisbach equation that includes both friction losses and local losses is:

$$\Delta P = \left(\frac{fL}{D_h} + \sum C \right) \left(\frac{\rho W_{avg}^{\ 2}}{2} \right) \tag{3}$$

where ΣC is the sum of the local loss coefficients. Note that, while the friction losses refer to the losses associated with fully-developed flow, the local losses are those due to developing flow conditions. As such,

the local losses include the entrance and exit losses. These losses are generally considered to be localised at the entrance and exit, although in reality they always occur over a certain distance in the flow direction. Substituting $\Delta P = \Delta C_P(0.5\rho U_{10}^2)$ in Eq. (3) and solving for the sum of the local loss coefficients yields:

$$\sum C = \Delta C_P \left(\frac{U_{10}}{W_{avg}} \right)^2 - \frac{fL}{D_h} \quad (4)$$

Application of Eq. (4) for U_{10} = 10 m/s yields values of ΣC from 4.5 (middle cavities) to 5.7 (edge cavities) for θ = 0°, and from 4.9 (middle) to 7.1 (edge) for θ = 22.5°, indicating a clear increase for the oblique wind direction. The ratio of local losses to total losses is quite constant: between 0.56 (middle) and 0.64 (edge) for θ = 0° and between 0.59 (middle) and 0.65 (edge) for θ = 22.5°.

7. Comparison with experimental results from previous studies

The CFD results for ACH and cavity air speed in this study seem quite large: ACH/U_{10} ranges between 120 and almost 250 s/mh for θ = 0°, and the corresponding dimensionless average cavity air speed W_{avg}/U_{10} ranges between 0.21 m/s for the edge cavities and 0.12 m/s for the middle cavities. These large values are attributed to the fact the opening areas are equal to the cavity cross-section. One could interpret this as the reference wind speed U_{10} being converted into a cavity air speed which is 5 to 10 times smaller. Although previous experimental studies were generally conducted for quite different building geometries, a comparison can be made between the CFD results and values from those experiments that most resemble the present situation.

Schwarz [5] measured air speed in a 40 mm cavity behind a 1.25 x 1.35 m² cladding panel with 8 mm thickness on a 18-storey building. As in the present study, the cavity had linear horizontal inlet and outlet openings spanning the entire width of the cavity. The measured cavity air speed W ranged from 0.2 to 0.6 m/s for a reference wind speed U_{ref} from 0 to 8 m/s, which corresponds to ACH values of about 500 to 1500 h^{-1}. For U_{ref} = 8 m/s, wind-induced cavity airflow is expected to dominate. In this situation, Schwartz's values are W/U_{ref} = 0.075 and ACH/U_{ref} = 200 s/mh. Note that U_{ref} is a reference wind speed which can not be directly related to U_{10} due to insufficient information about its measurement location.

Künzel and Mayer [7] reported measurements of air speed in different cavity geometries on a 3-storey building. The cavities were created by one or three consecutive 1.2 x 1.8 m² cladding panels with 10 mm thickness, yielding cavities of 1.8 or 5.4 m height. As in the present study, the cavities had horizontal openings spanning the entire cavity width. For a cavity depth of 20 mm and for U_{ref} > 3 m/s and no solar radiation, they measured similar maximum values for both cavity heights: W up to 0.6 m/s, which corresponds to ACH values of 400 and 1200. The ratio W_{avg}/U_{ref} is 0.2 m/s and the corresponding values of ACH/U_{ref} are 133 and 400 s/mh.

The experimental values by Schwartz [5] and Künzel and Mayer [7] are actually very close to the CFD results in this study. Note that several other experimental studies have been published, but that in many cases the cavity opening geometry is (very) different, e.g. not horizontal openings spanning the entire cavity width but much smaller openings.

8. Discussion

The CFD approach used in this paper, with low-Re number modelling based on the Wolfhstein model, cannot accurately reproduce friction coefficients (and therefore also cavity flow) in the transitional regime. For 1000 < Re < 3500, errors in the predicted friction coefficients are larger than 25%. This imposed a strong limitation on the amount of reliable information that could be extracted from the CFD simulations: only results for which the cavity Re numbers were below 1000 or above 3500 were analysed. Re < 1000 (in all cavities) occurred for U_{10} = 2 m/s and θ = 0°, while Re > 3500 (in all cavities) occurred for U_{10} = 10 m/s and θ = 0° and 22.5°. It is important to note that in reality, U_{10} will often be in the 2-10 m/s range. This stresses the importance for improved low-Re number modelling that can accurately reproduce not only the laminar and turbulent but also the transitional flow regime in narrow facade cavities.

The CFD simulations in this paper were performed for smooth cavity walls, which is the only option in the presently used low-Re number modelling approach. While the friction coefficients are invariable with wall roughness for laminar cavity flow, they considerably increase with wall roughness for turbulent flow [14,15]. Rough walls will therefore cause lower cavity ventilation rates.

The present study only considered wind-induced airflow in the cavities. Future work should consider buoyancy-driven ventilation as well as the combination of wind-driven and buoyancy-driven ventilation. The

present study was limited to averaged wind speed and ACH. Future studies can include the effects of wind gusts and pulsating flow in the cavity. In addition, attention should be given to the problem of horizontal inhomogeneity of the atmospheric boundary layer in CFD simulations [32], in particular related to its effects on the wind pressure distribution on building facades.

The CFD simulations in this study were conducted following the best practice guidelines guidelines for CFD in the outdoor environment [18,19,20,32]. High-resolution computational grids were constructed based on grid-sensitivity analysis, with hexahedral cells adjacent to all wall boundaries and with adequate z* values. Second-order discretisation schemes were used for all simulations. Validation with experimental data was performed for three different sub-configurations. The CFD results of cavity air speed and ACH were compared with those of previous experimental studies, indicating a favourable agreement. For future CFD validation studies, it would be beneficial to establish full-scale experimental data sets containing wind speed around the building, wind pressure coefficients at the facades and cavity air speed, accompanied by detailed measurements and reports of all influencing geometrical and meteorological parameters.

9. Summary and conclusions

This paper focused on coupled and decoupled RANS CFD simulations of wind-induced air flow in the narrow (23 mm) ventilated facade cavities of an isolated low-rise building. Accurately modelling the coupled wind flow and narrow cavity air flow is challenging because of the large differences in length scales and the resulting differences in flow behaviour: high-Re number turbulent flow around the building and low-Re number laminar, transitional and/or turbulent flow in the cavities. The CFD simulations were performed with the intention to identify the potential limitations of CFD for this type of application. This identification was supported by performing generic sub-configuration validation, which implies the decomposition of the actual problem or configuration into simpler, generic problems or configurations, which contain at least part of the features of the flow in the actual configuration. This validation study indicated that the wind velocities upstream of the building facade and the surface pressures on the windward facade can be predicted with good accuracy by steady RANS modelling with the realizable k-ε model, while this is not the case for the wind velocities and surface pressures downstream of the windward facade, due to the specific deficiencies of steady RANS modelling. The validation study showed that low-Re number modelling with the two-layer zonal approach and the one-equation Wolfhstein model can reproduce cavity flow that is either clearly laminar ($Re < 1000$) or turbulent ($Re > 3500$), while it is deficient in the transitional regime: for $1000 < Re < 3500$, errors in the predicted friction coefficients are larger than 25%.

Results of the coupled simulations were analysed for those situations with cavity Re numbers outside the range 1000-3500. Distinct flow patterns and ACH variations were found along the windward facade. For a high reference wind speed U_{10} of 10 m/s and for wind perpendicular to the facade, the ratio ACH/U_{10} ranges between 120 and almost 250. These values compared favourably with those from past experimental studies. Comparing the results from the coupled and decoupled simulations allowed to assess the local losses (entrance and exit losses) of the cavities. The sum of the entrance and exit loss coefficients for $\theta = 0°$ ranges between 4.5 (middle cavities) and 5.7 (edge cavities), and for $\theta = 22.5°$ between 4.9 and 7.1.

While this study has shown that the RANS low-Re number modelling approach used is capable of reproducing both the laminar and turbulent flow in narrow ventilated facade cavities. Future work should focus on adapting this approach to accurately model cavity flow in the transitional regime.

Acknowledgements

The authors want to express their gratitude to Dr. Hartwig Künzel, head of the Hygrothermal Unit of the Fraunhofer-Institut für Bauphysik in Holzkirchen, Germany, for providing valuable literature information that was hard to find. Gratitude is also expressed to the Finn Krogstads Fund for travelling funds that allowed the international collaboration.

References

[1] T.K. Stovall, A.N. Karagiozis, Airflow in the ventilation space behind a rain screen wall, in: Proceedings of Thermal Performance of the Exterior Envelopes of Buildings IX, ASHRAE Buildings IX, Clearwater Beach, FL, USA, 2004.

[2] D. Davidovic, J. Srebric, E.F.P. Burnett, Modeling convective drying of ventilated wall chambers in building enclosures, International Journal of Thermal Sciences 45 (2006) 180-189.

[3] S. Gnoth, P. Häupl, H. Fechner, New aero-thermohygric behaviour of building structures with open and closed cavities, in: Proceedings of Building Physics Conference, Laboratory of Building Physics, Katholieke Universiteit Leuven, Leuven, Belgium, 2008, pp. 29-32.
[4] H.M. Künzel, A.N. Karagiozis, M. Kehrer, Assessing the benefits of cavity ventilation by hygrothermal simulation, in: Proceedings of Building Physics Conference, Laboratory of Building Physics, Katholieke Universiteit Leuven, Leuven, Belgium, 2008, pp. 17-21.
[5] B. Schwarz, Witterungsbeansphruchung von Hochhausfassaden (in German), HLH (Heizung, Lüftung/Klimatechnik, Haustechnik) 24(12) (1973) 376–384.
[6] W. Popp, E. Mayer, H. Künzel, Untersuchungen über die Belüftung des Luftraumes hinter vorgesetzten Fassadenbekleidung aus kleinformatigen Elementen, Fraunhofer Institut für Bauphysik, Forschungsbericht BHo 22/80, April, 1980.
[7] H. Künzel, E. Mayer, Untersuchung über die notwendige Hinterlüftung an Außenwandbekeidung aus großformatigen Bauteilen, Schriftenreihe Bundesminister für Raumordnung, Bauwesen, und Städtebau, 3/1983.
[8] K. Sandin, Cavity wall moisture and temperature conditions (In Swedish), R43, Statens råd för byggnadsforskning, Stockholm, Sweden, 1981.
[9] C. Gudum, Moisture transport and convection in building envelopes – ventilation in light weight outer walls, PhD thesis, Technical University of Denmark, Copenhagen, Denmark, 2003.
[10] J. Straube, R. VanStraaten, E. Burnett, C. Schumacher, Review of literature and theory, Report #1, ASHRAE 1091 – Development of Design Strategies for Rainscreen and Sheathing Membrane Performance in Wood Frame Walls, Building Engineering Group, University of Waterloo, 2004.
[11] J.P. Piñon, D. Davidovic, E. Burnett, J. Srebric, Ventilated cavities in screen-type enclosure wall systems (RP 1091), In: Proceedings of Thermal Performance of the Exterior Envelopes of Buildings IX, ASHRAE Buildings IX, Clearwater, FL, USA, 2004.
[12] C. Schumacher, S. Xing, E. Burnett, Ventilation drying in screen-type wall systems: a physical demonstration, Report #3, ASHRAE 1091 – Development of Design Strategies for Rainscreen and Sheathing Membrane Performance in Wood Frame Walls, Building Engineering Group, University of Waterloo, 2004.
[13] E.F.P. Burnett, J.F. Straube, Vents, ventilation, drying and pressure moderation, Research Report. Canada Mortgage and Housing Corporation, 1995.
[14] I.E. Idelchik, Handbook of Hydraulic Resistance, third ed., CRC Press Inc., 1994.
[15] ASHRAE. Handbook of Fundamentals, American Society of Heating, Refrigerating and Airconditioning Engineers, 2009.
[16] D. Costola, B. Blocken, J.L.M. Hensen, Overview of pressure coefficient data in building energy simulation and airflow network programs, Building and Environment 44(10) (2009) 2027-2036.
[17] J. Wieringa, Updating the Davenport roughness classification, Journal of Wind Engineering and Industrial Aerodynamics 41-44 (1992) 357-368.
[18] J. Franke, A. Hellsten, H. Schlünzen, B. Carissimo, Best practice guideline for the CFD simulation of flows in the urban environment, COST Action 732: Quality Assurance and Improvement of Microscale Meteorological Models, 2007.
[19] Y. Tominaga, A. Mochida, R. Yoshie, H. Kataoka, T. Nozu, M. Yoshikawa, T. Shirasawa, AIJ guidelines for practical applications of CFD to pedestrian wind environment around buildings, Journal of Wind Engineering and Industrial Aerodynamics 96(10,11) (2008) 1749–1761.
[20] M. Casey, T. Wintergerste, ERCOFTAC Best Practice Guidelines, Special Interest Group on Quality and Trust in Industrial CFD, 2000.
[21] Fluent Inc. Fluent 6.3 User's Guide. Lebanon, US, 2006.
[22] T. Defraeye, B. Blocken, J. Carmeliet, CFD analysis of convective heat transfer at the surfaces of a cube immersed in a turbulent boundary layer, International Journal of Heat and Mass Transfer, (2010) 53(1-3): 297-308.
[23] M. Wolfhstein, The velocity and temperature distribution of one-dimensional flow with turbulence augmentation and pressure gradient, International Journal of Heat and Mass Transfer 12 (1969) 301-318.
[24] T.H. Shih, W.W. Liou, A. Shabbir, J. Zhu, A new k-ε eddy-viscosity model for high Reynolds number turbulent flows – model development and validation, Computers and Fluids 24(3) (1995) 227-238.
[25] B. Blocken B, T. Defraeye, D. Derome, J. Carmeliet, High-resolution CFD simulations of forced convective heat transfer coefficients at the facade of a low-rise building, Building and Environment 44(12) (2009) 2396-2412.
[26] B. Blocken, J. Carmeliet, Pedestrian wind conditions at outdoor platforms in a high-rise apartment building: generic sub-configuration validation, wind comfort assessment and uncertainty issues, Wind and Structures 11(1) (2008) 51-70.

[27] P.J. Richards, R.P. Hoxey, B.D. Connell, D.P. Lander, Wind-tunnel modelling of the Silsoe Cube, Journal of Wind Engineering and Industrial Aerodynamics 95(9-11) (2007) 1384-1399.
[28] W.H. Snyder, Guideline for fluid modeling of atmospheric diffusion, US Environmental Protection Agency Report EPA-600/8-81-009, 1981.
[29] B. Blocken, T. Stathopoulos, J. Carmeliet, Wind environmental conditions in passages between two long narrow perpendicular buildings, Journal of Aerospace Engineering – ASCE 21(4) (2008) 280-287.
[30] B.E. Launder, D.B. Spalding, The numerical computation of turbulent flows, Computer Methods in Applied Mechanics and Engineering 3 (1974) 269-289.
[31] T. Cebeci, P. Bradshaw, Momentum Transfer in Boundary Layers, Hemisphere Publishing Corporation, New York, 1977.
[32] B. Blocken, T. Stathopoulos, J. Carmeliet, CFD simulation of the atmospheric boundary layer: wall function problems, Atmospheric Environment 41(2) (2007) 238-252.
[33] S. Murakami, Comparison of various turbulence models applied to a bluff body, Journal of Wind Engineering and Industrial Aerodynamics 46&47 (1993) 21-36.
[34] Y. Tominaga, A. Mochida, S. Murakami, S. Sawaki, Comparison of various revised k–ε models and LES applied to flow around a high-rise building model with 1:1:2 shape placed within the surface boundary layer, Journal of Wind Engineering and Industrial Aerodynamics 96(4) (2008) 389-411.
[35] F.M. White, Viscous Fluid Flow, third ed., McGraw-Hill, 1974.
[36] F.P. Incropera, D.P. DeWitt, Fundamentals of Heat and Mass Transfer, fifth ed., Chichester, Wiley, 2001.
[37] H. Schlichting, Boundary-layer Theory, seventh ed., McGraw-Hill, London, 1979.
[38] T. van Hooff, B. Blocken, Coupled urban wind flow and indoor natural ventilation modelling on a high-resolution grid: A case study for the Amsterdam ArenA stadium, Environmental Modelling & Software 25(1) (2010) 51-65.
[39] P.J. Richards, R.P. Hoxey, Appropriate boundary conditions for computational wind engineering models using the k-ε turbulence model, Journal of Wind Engineering and Industrial Aerodynamics 46&47 (1993) 145-153.
[40] B. Blocken, J. Carmeliet, T. Stathopoulos, CFD evaluation of the wind speed conditions in passages between buildings – effect of wall-function roughness modifications on the atmospheric boundary layer flow, Journal of Wind Engineering and Industrial Aerodynamics 95(9-11) (2007) 941-962.
[41] T. Stathopoulos, R. Storms, Wind environmental conditions in passages between buildings, Journal of Wind Engineering and Industrial Aerodynamics 24 (1986) 19–31.
[42] B. Blocken, J. Carmeliet, On the validity of the cosine projection in wind-driven rain calculations on buildings, Building and Environment 41(9) (2006) 1182–1189.
[43] M. Abuku, B. Blocken, K. Nore, J.V. Thue, J. Carmeliet, S. Roels, On the validity of numerical wind-driven rain simulation on a rectangular low-rise building under various oblique winds, Building and Environment 44(3) (2009) 621-632.
[44] B. Blocken, P. Moonen, T. Stathopoulos, J. Carmeliet, A numerical study on the existence of the Venturi-effect in passages between perpendicular buildings, Journal of Engineering Mechanics – ASCE 134(12) (2008) 1021-1028.
[45] B. Blocken, J. Carmeliet, The influence of the wind-blocking effect by a building on its wind-driven rain exposure, Journal of Wind Engineering and Industrial Aerodynamics 94(2) (2006) 101-127.

Figures

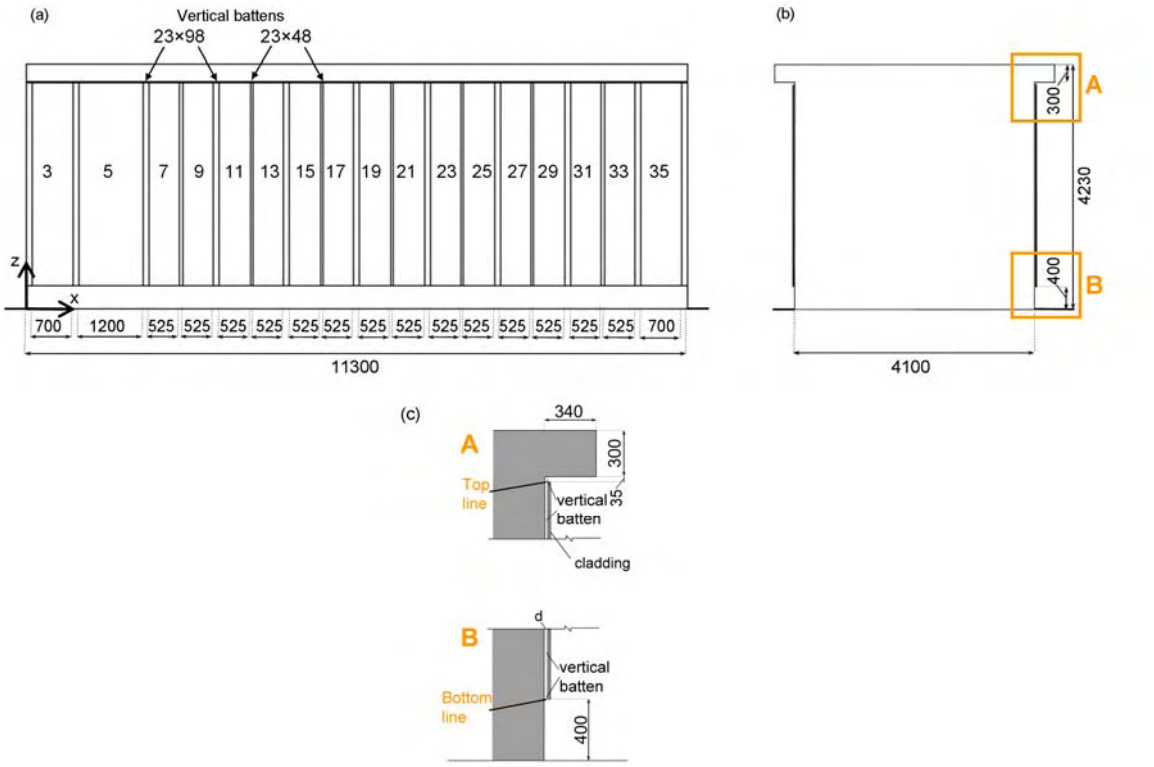

Fig. 1. (a) West facade of the low-rise building model. The numbers and the width of the individual cavities are indicated, as well as the cross-sectional dimensions of the vertical battens. (b) North facade with indication of two details A and B. (c) Details A and B of cross-section at top and bottom of cavity. The position of two horizontal lines (top line and bottom line, along the length of the facade) along which results will be presented, are indicated. Dimensions in mm.

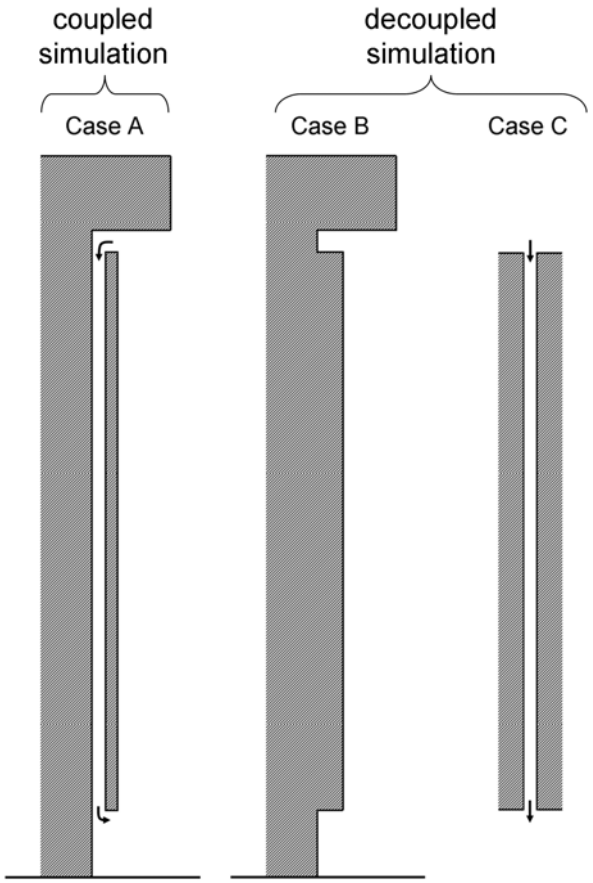

Fig. 2. Schematic representation of cavity configurations for coupled (A) and decoupled (B+C) simulations.

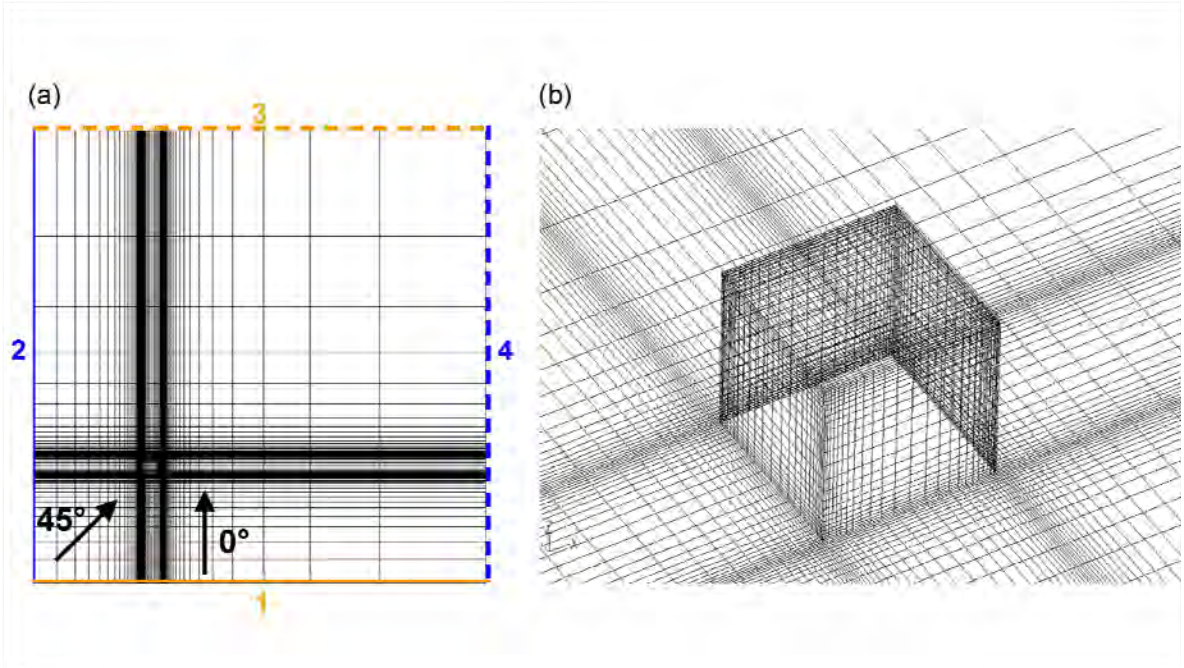

Fig. 3. (a) Grid at the bottom of the computational domain, and indication of the vertical boundary planes (1-4) of the domain. (b) Grid at the surfaces of the building and part of the ground surface.

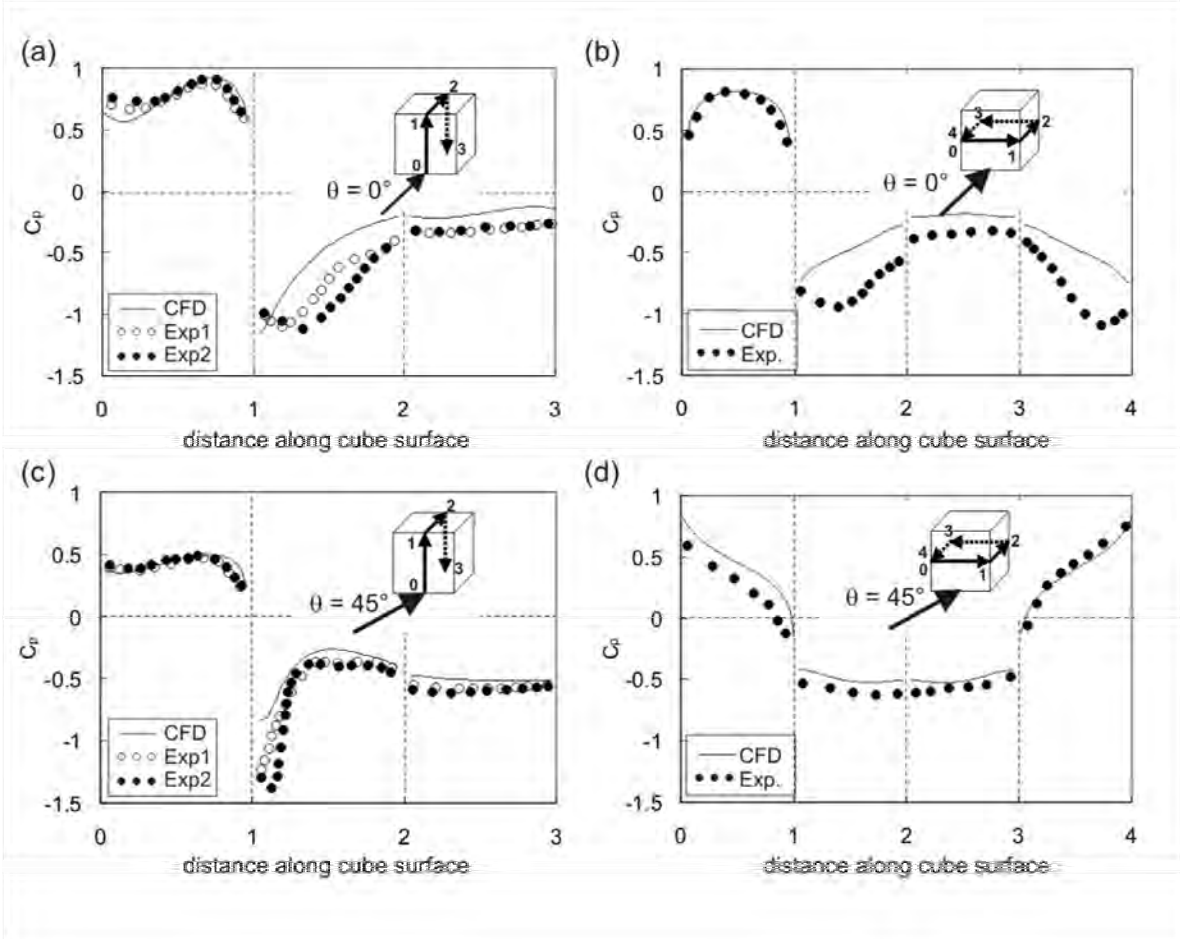

Fig. 4. Comparison between experiments and CFD results for cubic building: mean pressure coefficient C_p along (a) vertical trajectory 0-1-2-3 for θ = 0°; (b) horizontal trajectory 0-1-2-3-4 for θ = 0°; (c) same as (a) but for θ = 45°; (d) same as (b) but for θ = 45°.

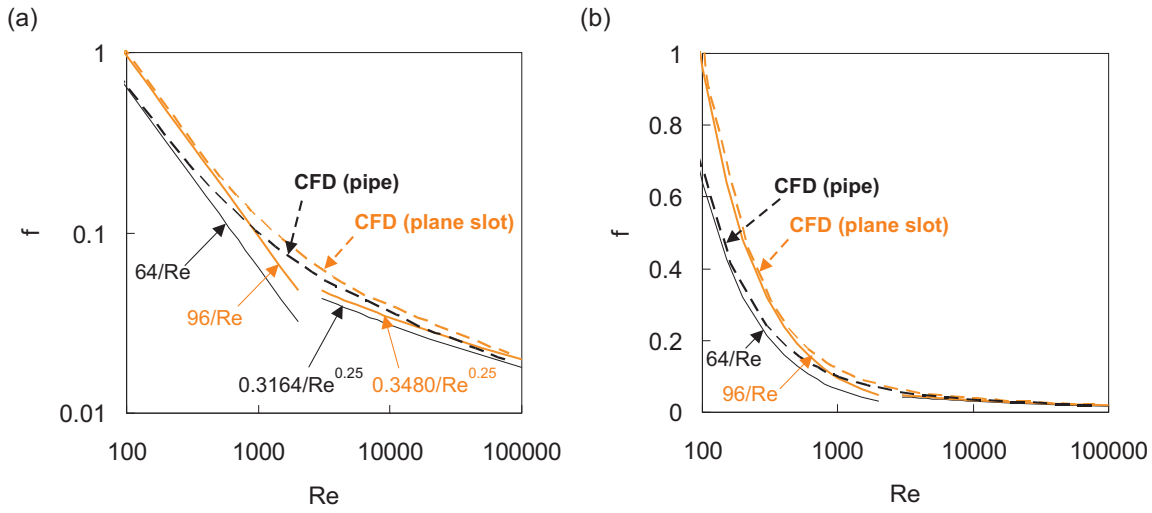

Fig. 5. Friction factors for fully-developed pipe and plane slot flow: comparison between CFD and theoretical/empirical expressions. (a) Double-logarithmic graph; (b) semi-logarithmic graph.

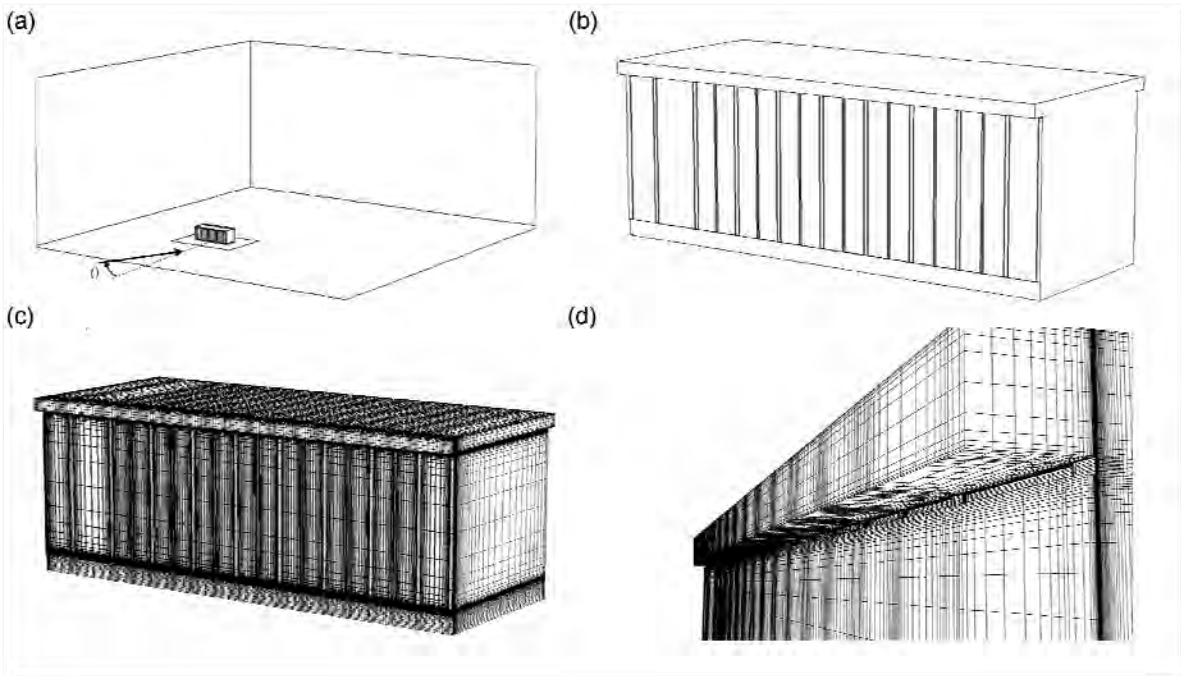

Fig. 6. (a) Building model in computational domain. (b) Building model with details of roof overhang and individual cavities separated by battens. (c) Computational grid on the building surfaces. (d) Detail of computational grid near the upper part of the cavities. The vertical battens, separating the cavities, are visible just below the roof overhang.

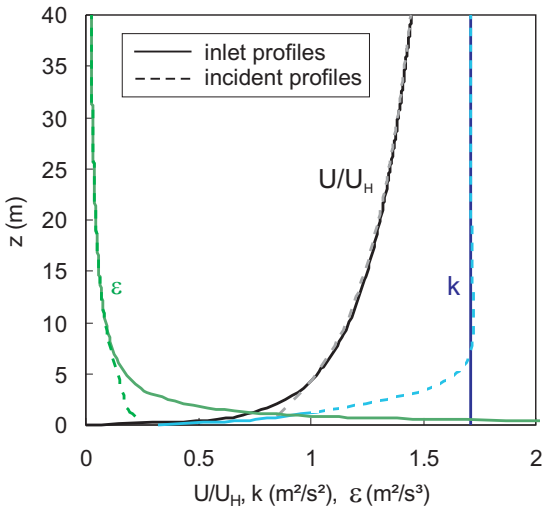

Fig. 7. Comparison between inlet and incident vertical profiles of dimensionless mean wind speed U/U_H, turbulent kinetic energy k and turbulence dissipation rate ε.

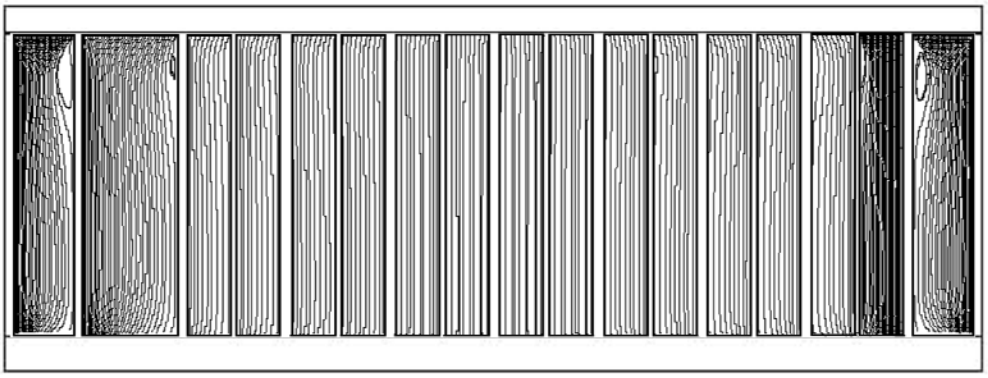

Fig. 8. Streamlines in the mid-planes of the cavities for θ = 0°. Overall cavity flow is from top to bottom.

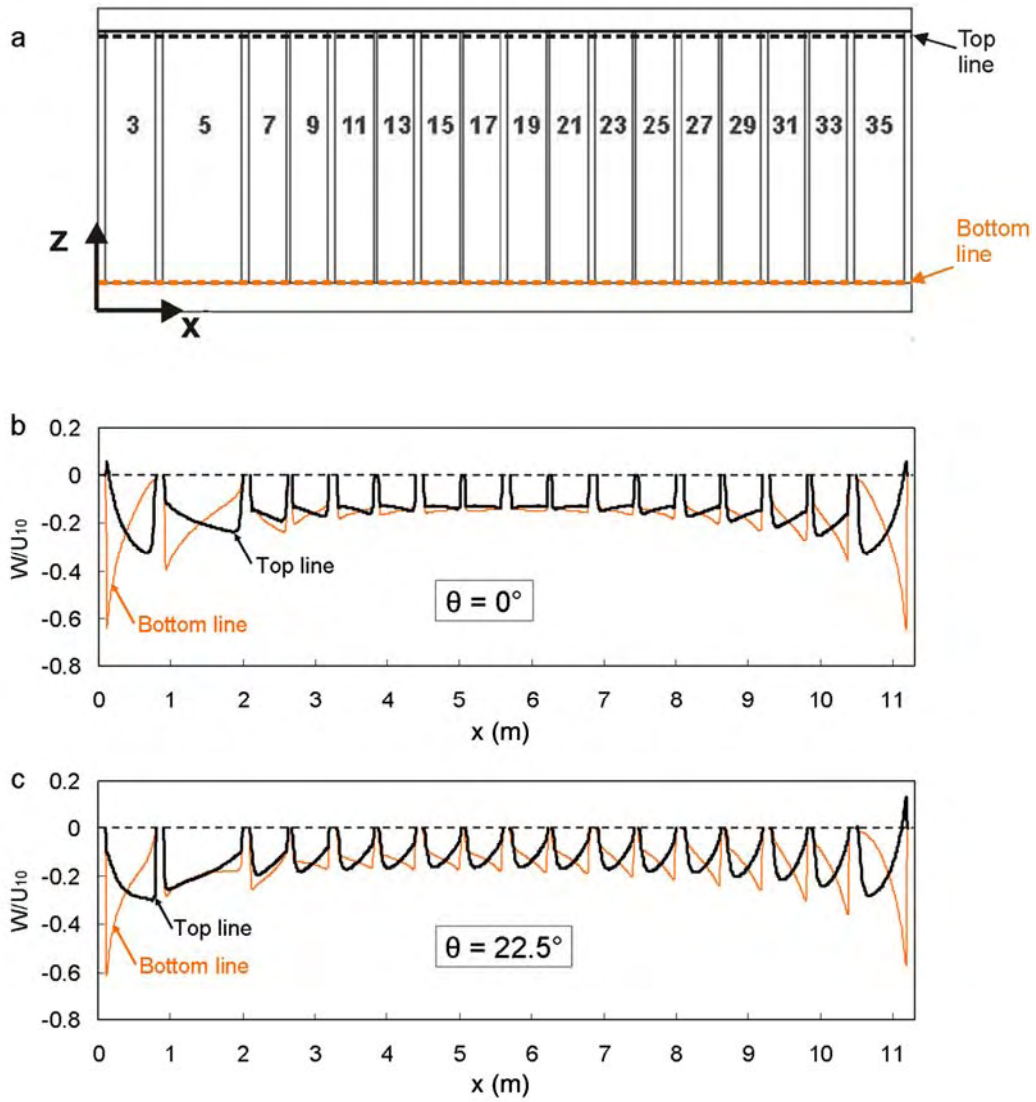

Fig. 9. (a) Building facade with cavities. (b-d) Ratio of vertical velocity component W to reference wind speed U_{10} for each cavity (top and bottom), for U_{10} = 10 m/s and for θ = 0° and 22.5°.

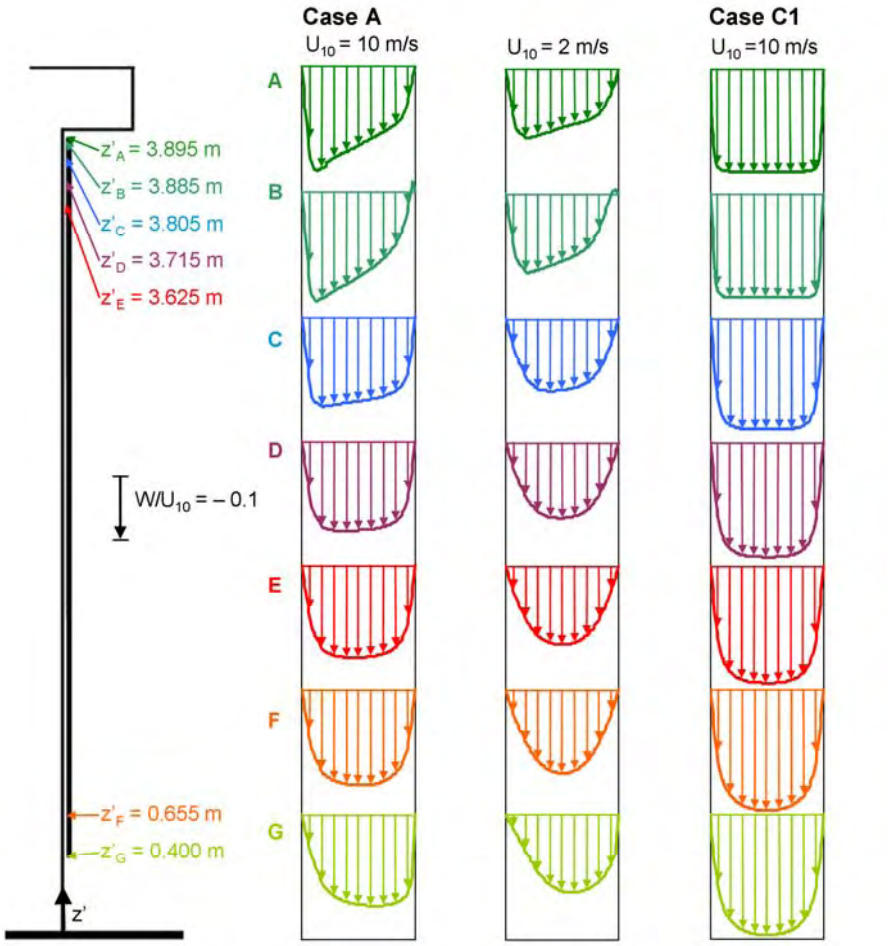

Fig. 10. Profiles of the ratio W/U_{10} across the cavity depth for coupled (case A, for U_{10} = 10 and 2 m/s) and decoupled (case C1, for U_{10} = 10 m/s) simulation, for the middle cavity (nr. 19, see Fig. 1a) and for $\theta = 0°$.

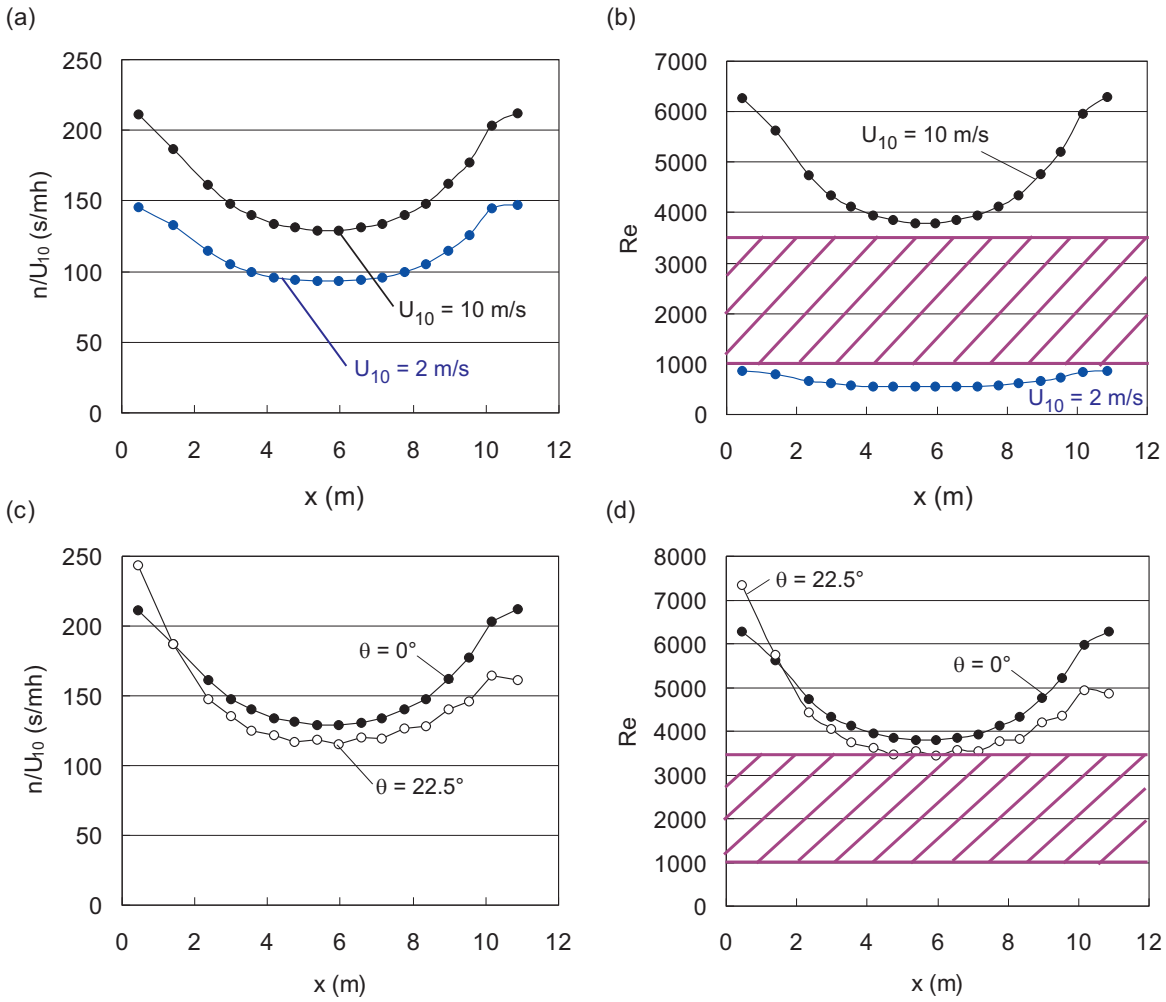

Fig. 11. (a) Ratio of cavity air change rate n and reference wind speed U_{10}, for θ = 0° and U_{10} = 2 and 10 m/s. (b) Cavity Reynolds numbers for same θ and U_{10}. The hatched area indicates the transitional Re number region in which low-Re number modelling fails. (c) Same as (a), but for U_{10} = 10 m/s and θ = 0° and 22.5°. (d) Same as (b), but for U_{10} = 10 m/s and θ = 0° and 22.5°.

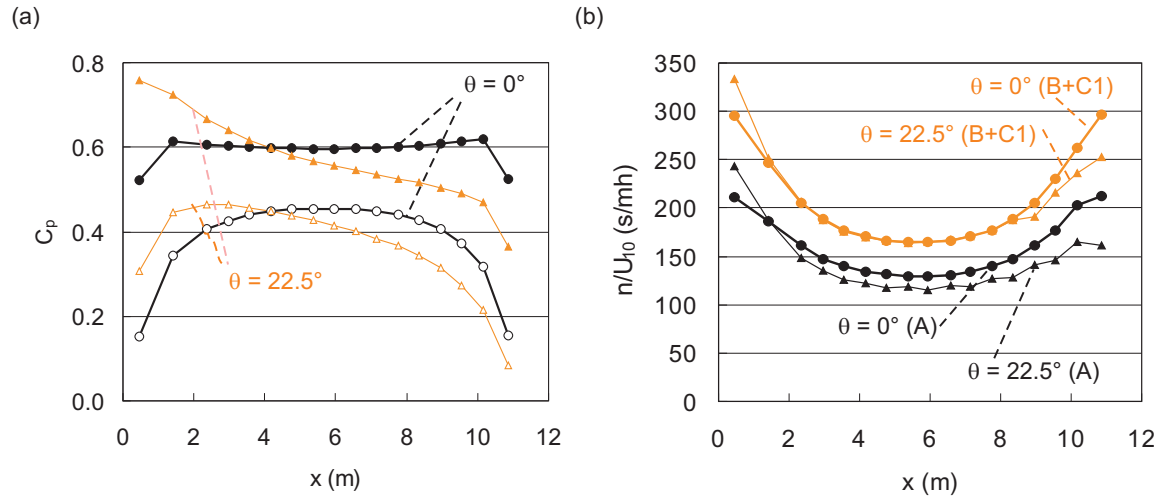

Fig. 12. (a) Pressure coefficient C_p from decoupled simulations, at the position of the top and bottom openings, for U_{10} = 10 m/s and θ = 0° and 22.5°. (b) Comparison of n/U_{10} obtained from the coupled (A) versus decoupled (B+C1) simulations, for U_{10} = 10 m/s and θ = 0 and 22.5°.

Additional publications based on Voll ventilated cladding test house data

A.1 Nore et al. 2005. Proceedings NSB, Iceland

Nore, K., Thue, J.V., Time, B. & Rognvik, E. (2005) Ventilated wooden claddings - A field investigation, *Proceedings of the 7th Symposium on Building Physics in the Nordic Countries.* Reykjavik, Iceland. p. 617-624.

This paper presents the setup and some preliminary results of measurements on different wooden claddings on a test house at Voll. This is in chapter 3 in this Thesis.

Some preliminary measurement results from the first year of measurements was given in the paper. The measured moisture content (MC) in the wood claddings demonstrates the influence of ventilation gap design. When the cladding is heavily exposed to driving rain, full air gap openings give the lowest MC in the cladding, whereas in a dry climate situation closed air gap openings give the driest wood cladding.

A.2 Lauter and Time 2005 Proceedings NSB, Iceland

Lauter, P. & Time, B. (2005) A method to assess the effects of climate and material parameters on the moisture conditions of a wooden façade. *Proceedings of the 7th Symposium on Building Physics in the Nordic Countries.* Reykjavik, Iceland. p. 749-756

This paper presents the Voll data in a service life prediction setting. Service life is "period of time after installation during which a building or its parts meets or exceeds the performance requirements" (ISO 15686).

MC_{FD} measurements of 2004 is used to create a non-dimensional factor describing the divergence of the parameters:

- Local location – reflecting the orientation of the cladding (east / west)
- Surface treatment (oil / water / untreated)
- Material quality (fast grown / slow grown)
- Micro location (top / bottom of cladding)

Monthly average and standard deviation is calculated for each monitoring point. The non-dimensional factor is calculated dividing one parameter on another, resulting in a factor illustrating the difference of the parameters.

With only one year of data few clear differences are apparent. The paper refers to the ageing process which has just started, but may not be detected in this early stage.

The results show that the main difference is found for the local location, which is the orientation of the cladding. The values indicate 16 % higher MC on the west facing wall and up to 94 % larger variation compared to the east facing wall. Surface treatment also give significant results displaying water based paint to be 8 % higher than the oil based paint. The variation is also greater for the water based surface treatment. When evaluating the untreated surfaces the MC content is not different to the treated surface, but the standard variation is significantly greater for the untreated materials.

Material quality and micro location gave no significant results. Material quality results hints that the MC variation is higher for fast grown wood. The micro location referring to the top and bottom of the cladding, gives slightly higher MC and variation for the bottom sensor point. This is logical due to the roof overhang.

It was too early to conclude how MC variations are influencing the service life prediction value.

A.3 Geving et al. 2006 Project report

Geving, S., Erichsen T.H., Nore K. and Time B. 2006. *Hygothermal conditions in wooden claddings – Test house measurements.* Project report 407. Oslo: Norwegian Building Research Institute.

This report is a part of the programme R&D *Climate 2000 – Building constructions in a more severe climate* and closes the project "Requirements for façade systems in relation to driving rain loads". The report is based on the field investigation objective "to increase our understanding of the relation between microclimatic conditions and the responding performance of wooden claddings according to orientation, design of ventilation gap and wood qualities".

The parameters interpreted are:

- Driving rain exposure (orientation)
- Ventilation gap opening at top and bottom of cladding
- Surface treatment of the cladding
- Growth rate of wood

Reducing the orientation aspect to "driving rain exposure" is very simplified. According to the results of Paper IV this short-cut is not correct. Other climate parameters; temperature, radiation and wind speed turned out to be superior to WDR (driving rain).

Measurement data from 2004 and 2005 are basis for the analysis in this report. The results display and discuss graphs of averaged weekly data of:

- Climate; air temperature, air relative humidity, horizontal precipitation, number of minutes with precipitation, directional free field driving rain, driving rain on wall.
- Cladding measurements; MC – all western and eastern sections, MC – effect of ventilation gap openings on east and west wall, MC – variation of height of wall (top/bottom), MC – effect of surface treatment, MC – effect of driving rain with different air gap openings, MC – variation in different depths of on cladding section, RH in air gaps and outdoor air showing effect of ventilation, and MC – effect of removing air gap east and west wall.

The report also has 10-day graphs of hourly data; MC – treated/untreated, corresponding driving rain and relative humidity. Also averaged data of the years, the summer and winter seasons and max and mean weekly seasonal values are calculated and analysed.

In addition the cladding sections are compared by the calculated mould growth potential, called MAX – days. The calculation is based on the results of Viitanen and Ritchkoff (1991).

The report provides insight in the vast data set of Voll, but does not present any rigid future recommendations.

In general ventilated cladding has always been recommended in Norway. The conclusion in the report is that the ventilation gap should be equal to a continuous gap of 4 mm, but the ventilation gap itself does not have to be continuous. The importance of well performed drainage details is accentuated.

Surface treatment differentiation is not straight forward, and no significant variance is found. The results suggest that alkyd paint perform better when the cladding is ventilated (4 mm or full opening), and acryl paint perform best when no ventilation gap is present. Untreated cladding has a higher risk of decay and mould growth, but not significantly higher.

The growth rate of wood show little difference and no conclusion can be made for the wood density interval investigated in this study (385 kg/m^3 and 460 kg/m^3)

A.4 Johansen 2007 Master Thesis, NTNU

Johansen Ø. S. 2007 *Stochastic analyse of rot potential of house cladding. (In Norwegian).* Master Thesis. Norwegian University of Science and Technology (NTNU). Trondheim, Norway.

With basis in the Voll measurements this master thesis is examining how to reduce the rot potential in wood cladding by choosing the best design variables wood quality, air gap opening and surface treatment. The rot potential was calculated from the empirical model of Viitanen and Ritchkoff (1991), using material relative humidity (RH) and temperature. Material RH is calculated from MC using the sorption curve in Tveit (1966). The MC data used from Voll was the MC_{FD} pin.

One problem is that the measurement data, the analyse values, are not linearly independent due to the changing climate influence. This is called multicollinearity. A second problem is that the set up was not balanced – which could have been done by randomizing the cladding parameters in each orientation. The third problem is that three test cladding sections with untreated cladding are too few to conclude on this parameter.

The rot potential of different cladding designs was compared by ordinary regression, generalized least squares method and by ridge regression. The two latter reduces the error of multicollinearity. Climate parameters are not used as response variables. The climate provides non-adjustable variables which have a major influence on the adjustable variables (the design parameters).

The analyse was performed in three parts.
Model 1: Using the values of the test station – representative for the Voll climate.
Model 2: Cladding performance with light exposure of rot growth
Model 3: Cladding performance with high exposure of rot growth

Model 2. and 3. were simulated by subtracting the average rot-growth-potential from the measured rot potential. The average minimum and maximum monthly level were used in respectively model 2 and 3. The results of these models provides more general results of the Voll data.

The results are summarised in Table A3.1. The results of the regression analysis reveal major differences in response between model 2 and 3. This implies that one should differentiate cladding design according to climate impact. Concerning wood quality the growth rate the rot-growth-potential is minimized for fast grown wood. However, this result might not be concise when slow grown wood might tolerate a higher rot-growth-potential. The recommendation of the air gap opening is full opening at the west facing side – this is assumed to be due to the wind exposure at this position, and with the high dry out potential. The east facing side is less exposed to wind and has two recommendations related to different climates. Model 2, with the least rot potential, is best with no air gap opening, while Model 1 and 3 are favourable with 4 mm air gap opening. Full opening will probably accumulate moisture on the east facing wall. Surface treatment B, acryl paint, is preferred for the east facing side in model 1 and 2, but for high exposure to rot paint A, alkyd, is preferred. Alkyd paint provides the best water-repellent properties, but also hinders drying out through the paint layer. For dry, wind exposed locations the surface treatment have no effect on the rot-growth-potential.

Table A.2.1 Recommended wood cladding designs to reduce the rot potential

		West facing wall		**East facing**	
		Treatment	Air gap opening	Treatment	Air gap opening
Model 1	Fast grown	B – acryl	4	B– acryl	4
	Slow grown	B– acryl	23	B– acryl	4
Model 2 Light exposure	Fast grown	U – untr.	23	B– acryl	0
	Slow grown	U – untr.	23	B– acryl	0
Model 3 High exposure	Fast grown	A - alkyd	23	A- alkyd	4
	Slow grown	A	23	A	4

A.5 Akubu et al. 2008 Building and Environment

Abuku, M., Blocken, B., Nore, K., Thue, J.V., Carmeliet, J., Roels, S. (2009). On the validity of numerical wind-driven rain simulation on a rectangular low-rise building under various oblique winds. *Building and Environment* 44(3): 621-632.

This paper uses the WDR measurements at Voll for validation of CFD on WDR at oblique winds. The three rain events investigated show increasing errors as the wind turns more oblique to the wall. The wall measurements are unfortunately not made on the upwind side of the oblique wind, south on the west facing wall, WDR incidents from north-west are not measured.